Insights into the myristoylated
c-Src N-terminal Regulatory Element

Irrem Laareb Mohammad Jabeen

Insights into the myristoylated c-Src N-terminal Regulatory Element
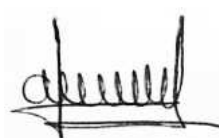
Irrem Laareb Mohammad Jabeen

**Thesis submitted for the degree of
PhD in Organic Chemistry**

**Supervised by:
Prof. Miquel Pons**

**Inorganic and Organic Chemistry Department
Faculty of Chemistry**

UNIVERSITAT DE BARCELONA

Barcelona, 2021.

It is all a matter of perspective.

Abstract

c-Src is a non-receptor tyrosine kinase that controls numerous cellular signaling pathways. c-Src implication in human cancers was brought into the attention in the 1980s. Since its discovery, unveiling of c-Src structural architecture and subsequent regulatory function focused on the folded domains cassette SH3-SH2-SH1(kinase), while the remaining N-terminal intrinsically disordered myristoylated SH4 and Unique domains were assumed to have a membrane-connecting function.

c-Src membrane binding has been well-characterized as a two-prong association requiring the burial of its myristoyl moiety and the electrostatic interaction of the cluster of basic residues in the SH4 domain to the anionic lipids. Membrane binding of c-Src is mostly reversible, however accumulated evidence shows clustering and irreversible binding of a small fraction of c-Src molecules upon membrane anchoring. All the elements required for c-Src self-association are found in the N-terminal myristoylated SH4 domain. However, self-association through the strongly positively charged SH4 domain (+5 net charge) is counterintuitive. The structural basis of this self-association has been investigated in this thesis using Surface Plasmon Resonance. Performing individual mutations, we have determined that the alternate lysine residues at positions 5, 7 and 9 in the myristoylated SH4 domain enables c-Src self-association upon membrane binding. Further analysis reveals that the positive charge of the lysine residues is essential for clustering and thus a role of the lipids in the membrane as mediators of the c-Src self-association is proposed.

Recently, it was shown that the (non-myristoylated) N-terminal region comprising the intrinsically disordered SH4-Unique domains and the adjacent globular SH3 domain formed a novel regulatory unit designated as the c-Src N-terminal Regulatory Element (SNRE). The (non-myristoylated) SNRE features an interdomain fuzzy complex, where the Intrinsically Disordered Regions: SH4 and Unique domains (IDR) maintain multiple weak contacts with the SH3 domain. The unavoidable question is whether the nature of this fuzzy complex is altered when the SH4 domain is in its native myristoylated form. In this thesis, characterization of the myristoylated SNRE has been performed using Nuclear Magnetic Resonance and various constructs of the SNRE in the myristoylated and non-myristoylated forms. We show that the myristoyl moiety increases the local concentration of the intrinsically disordered SH4 and Unique domains in the proximity of the SH3 domain by cooperatively favoring the intramolecular interactions that define the fuzzy complex. When c-Src is not bound to the membrane, the myristoyl moiety is harbored in the fuzzy interdomain complex through multiple binding sites in the SH3 domain.

Finally, a preliminary characterization of the SNRE with the adjacent SH2 domain has revealed that the interface region connecting the SH3-SH2 could also be a key component of the SNRE.

Acknowledgements

In the abstract matter, the memories left define the essence of a journey.
I am grateful to all the people that participate in the memories
of this PhD journey.

To my thesis supervisor, Prof. Miquel Pons, I am grateful for the opportunity to have been able to work on this challenging project. For the advice, insightful discussions, and all the time you dedicated to me. You definitely had an impact on the early-stage of this scientific career.

Miguel Arbesú, thank you for introducing me to the practical aspects of molecular biology. Your organized and careful approaches have shaped the way I have worked in the laboratory. Thanks for sharing your knowledge and thoughts, there was always something interesting to learn. And thanks for hosting me at the FMP in Berlin (it was great to see your transition as a postdoc!).

Marga Gairí, besides your NMR expertise, this journey would have not been the same without your valuable advice. You have helped me to get through those days where clarity was shrouded by only the hurdles. You have influenced me not only as a scientist, but as a person. Your kindness and human quality are inspiring. For all that, I will always be grateful.

Anabel-Lise Le Roux, I am grateful for all the time you spend answering questions, doubts and giving me advice on experimental design since my very first SPR experiment.

Marta Taulés, thank you for all the technical help with the SPR experiments. For sharing your experience and knowledge. I am also thankful that you shared your artistic side with me, my best wishes for that project!

Thanks to all the members of the Pons lab, that made a great environment in laboratory. Special words go to João MC Teixeira thanks for sharing your knowledge and thoughts, and Isabel Latorre thanks for all the technical help in the lab. To all the Bsc and Msc students that I had the opportunity to supervise during my time in the lab, you helped me to develop and grow mentorship skills, special mention to Iker Zapirain, Estefania Rusca, and Francisco-Javier Carvajal, it was nice to work with you, good luck with your future projects!

Betlem Mezquita and Montserrat Pau, thank you for sharing your Western Blotting expertise with me. (I enjoyed that short stay at your lab!)

To Prof. Lukáš Žídek, thank you for hosting me at the Central European Institute of Technology (CEITEC) - Masaryk University in Brno and making my internship so fruitful and enjoyable. I am grateful to Dr. Pavel Kadeřávek and Prof. Lukáš Žídek for all the time they dedicated to me and shared their NMR expertise. Thanks to all the members of the laboratory there for the worthwhile internship, specially Zuzana Trošanová.

To my thesis committee, Dr. Anna Grandas, Dr. Maria Antonia Busquets, and Dr. Francesc Rabanal, I am thankful for the discussions and advice during our annual meetings.

I am grateful to Professors Lola Rivera and Antonio Arregui, who gave me the first foundations to take this scientific path.

And the most important acknowledgments:

To my parents, my sister and brothers that encouraged me and gave me unconditional support all these years. Your hard-work, strength and values have always been my guiding light.

To Jessica, Deisy, Patricia and Brenda, that shared this experience from the very first moment and always been there for me. I am grateful for your support, love, and care.

Thank you.

Contents

Abbreviations

ACF	Autocorrelation function
ATP	Adenosine triphosphate
BSA	Bovine Serum Albumine
CHAPS	3-((3-Cholamidopropyl)dimethylammonio)-1-propanesulfonate
CMC	Critical Micelle Concentration
CSP	Chemical Shift Perturbation
ddwater	Double distilled water
DMSO	Dimethyl sulfoxide
DOPA	1,2-dioleyl-sn-glycero-3-phosphate phosphatidic acid
DOPC	1,2-dioleoyl-sn-glycero-3-phosphocholine
DOPG	1,2-dioleoyl-sn-glycero-3-phospho-10-rac-glycerol
EDC·HCl	1-ethyl-3-(3-dimethylaminopropyl) carbodiimide hydrochloride
EDTA	Ethylenediaminetetraacetic acid
FC	Flow Cell
FCS	Fluorescence Correlation Spectroscopy
GFP	Green Fluorescent Protein
HMQC	Heteronuclear Multiple Quantum Coherence
HSQC	Heteronuclear Single Quantum Coherence
IDPs	Intrinsically Disordered Proteins
IDRs	Intrinsically Disordered Regions
laurUSH3	Lauroylated SH4, Unique and SH3 domains of c-Src
LissRho-DOPE	1,2-dioleoyl-sn-glycero-3-phosphoethanolamine-N-lissamine rhodamine B sulfonyl
LUVs	Large Unilamellar Vesicles
MS	Mass Spectrometry
myrSH4	Myristoylated SH4 domain of c-Src
myrUGFP	Myristoylated SH4 and Unique domains of c-Src fused to the Green Fluorescent Protein
myrUSH3	Myristoylated SH4, Unique and SH3 domains of c-Src
NCS	Neuronal Calcium Sensors
NHS	Hydroxysuccinimide
NMR	Nuclear Magnetic Resonance
NMT	N-Myristoyltransferase
NUS	Non-Uniform Sampling

PBC	Polybasic Cluster (i.e. cluster of positively charged residues)
PDB	Protein Data Bank
PIC	Protease Inhibitor Cocktail
PKA	Protein Kinase A
PPII	Polyproline type II helix
PxxP	Polyproline motif
RDCs	Residual dipolar couplings
RTKs	Receptor tyrosine kinases
SAXS	Small Angle X-ray Scattering
SD	Standard Deviation
SDS	Sodium Dodecyl Sulfate
SDS-PAGE	Sodium Dodecyl Sulfate PolyAcrylamide Gel Electrophoresis
SEC	Size Exclusion Chromatography
SFKs	Src Family of Tyrosine Kinases
SH#	Src Homologie # domain
SNRE	c-Src N-Terminal Regulatory Element
SNRE	Src N-terminal Regulatory Element
SPR	Surface plasmon Resonance
TEV	Tobacco Etch Virus
UD	Unique Domain
ULBR	Unique Lipid Binding Region
ULBR	Unique Lipid Binding Region
USH3	SH4, Unique and SH3 domains of c-Src

PART (I) Introduction and Objectives
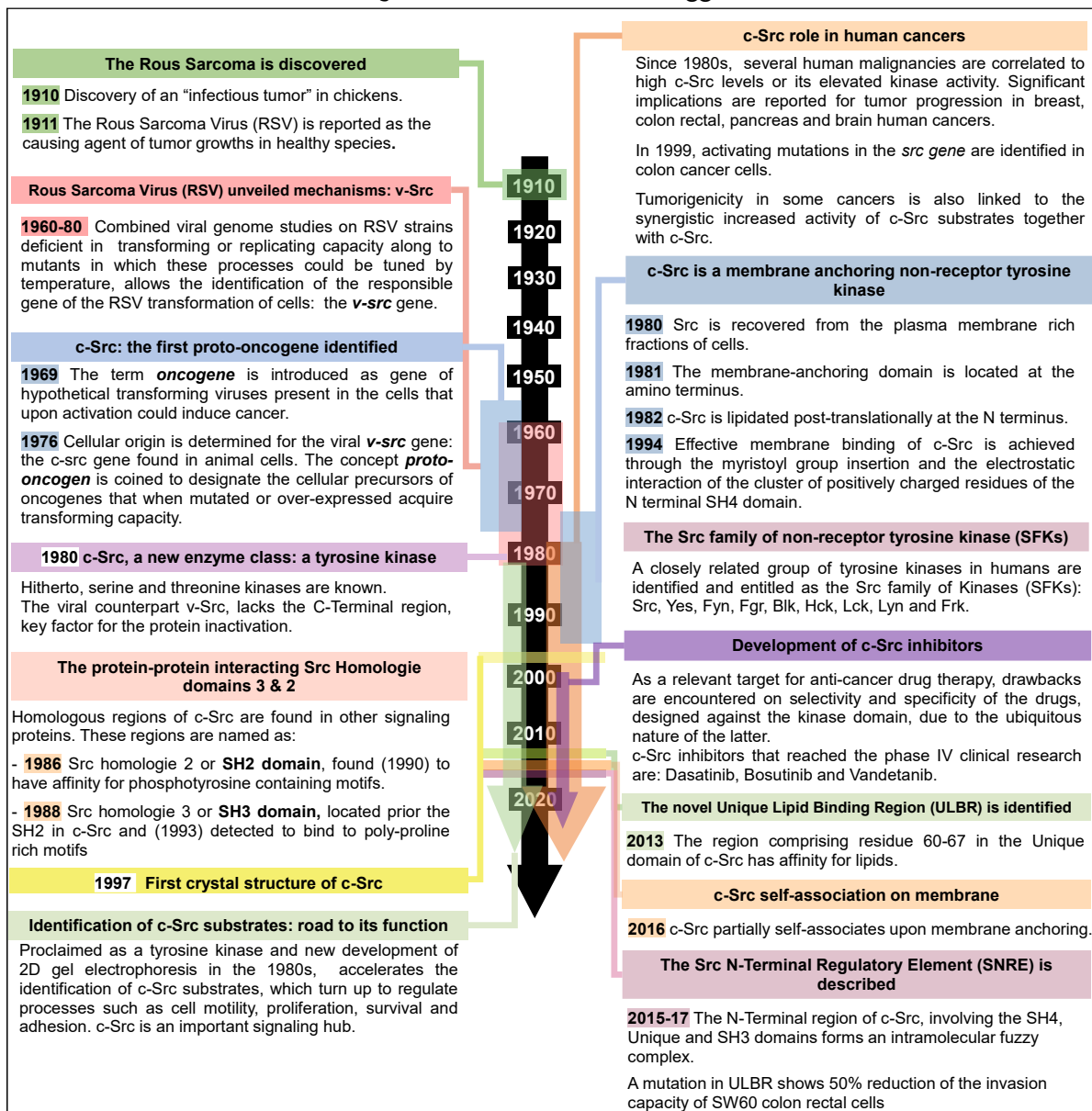
Chapter 1

About c-Src and membrane anchoring

1.1. The non-receptor tyrosine kinase c-Src

c-Src, a non-receptor protein tyrosine kinase, entered the spotlight of cancer research since the discovery of the Rous Sarcoma Virus (RSV) in 1911 by Peyton Rous. The *src* gene was the first proto-oncogene to be discovered that enlightened the path of a complete novel research era, focusing on the importance of a signaling proteins in cancer and in particular tyrosine phosphorylation.

I invite the reader to skim through *Figure 1.1.* for a very short condensed historical overview of the long c-Src prolific research, strongly active up to date.

Figure 1.1. c-Src historical nuggets.

The Rous Sarcoma is discovered

1910 Discovery of an "infectious tumor" in chickens.

1911 The Rous Sarcoma Virus (RSV) is reported as the causing agent of tumor growths in healthy species.

Rous Sarcoma Virus (RSV) unveiled mechanisms: v-Src

1960-80 Combined viral genome studies on RSV strains deficient in transforming or replicating capacity along to mutants in which these processes could be tuned by temperature, allows the identification of the responsible gene of the RSV transformation of cells: the *v-src* gene.

c-Src: the first proto-oncogene identified

1969 The term *oncogene* is introduced as gene of hypothetical transforming viruses present in the cells that upon activation could induce cancer.

1976 Cellular origin is determined for the viral *v-src* gene: the c-src gene found in animal cells. The concept *proto-oncogen* is coined to designate the cellular precursors of oncogenes that when mutated or over-expressed acquire transforming capacity.

1980 c-Src, a new enzyme class: a tyrosine kinase

Hitherto, serine and threonine kinases are known.
The viral counterpart v-Src, lacks the C-Terminal region, key factor for the protein inactivation.

The protein-protein interacting Src Homologie domains 3 & 2

Homologous regions of c-Src are found in other signaling proteins. These regions are named as:

- **1986** Src homologie 2 or **SH2 domain**, found (1990) to have affinity for phosphotyrosine containing motifs.

- **1988** Src homologie 3 or **SH3 domain,** located prior the SH2 in c-Src and (1993) detected to bind to poly-proline rich motifs

1997 First crystal structure of c-Src

Identification of c-Src substrates: road to its function

Proclaimed as a tyrosine kinase and new development of 2D gel electrophoresis in the 1980s, accelerates the identification of c-Src substrates, which turn up to regulate processes such as cell motility, proliferation, survival and adhesion. c-Src is an important signaling hub.

c-Src role in human cancers

Since 1980s, several human malignancies are correlated to high c-Src levels or its elevated kinase activity. Significant implications are reported for tumor progression in breast, colon rectal, pancreas and brain human cancers.

In 1999, activating mutations in the *src gene* are identified in colon cancer cells.

Tumorigenicity in some cancers is also linked to the synergistic increased activity of c-Src substrates together with c-Src.

c-Src is a membrane anchoring non-receptor tyrosine kinase

1980 Src is recovered from the plasma membrane rich fractions of cells.

1981 The membrane-anchoring domain is located at the amino terminus.

1982 c-Src is lipidated post-translationally at the N terminus.

1994 Effective membrane binding of c-Src is achieved through the myristoyl group insertion and the electrostatic interaction of the cluster of positively charged residues of the N terminal SH4 domain.

The Src family of non-receptor tyrosine kinase (SFKs)

A closely related group of tyrosine kinases in humans are identified and entitled as the Src family of Kinases (SFKs): Src, Yes, Fyn, Fgr, Blk, Hck, Lck, Lyn and Frk.

Development of c-Src inhibitors

As a relevant target for anti-cancer drug therapy, drawbacks are encountered on selectivity and specificity of the drugs, designed against the kinase domain, due to the ubiquitous nature of the latter.
c-Src inhibitors that reached the phase IV clinical research are: Dasatinib, Bosutinib and Vandetanib.

The novel Unique Lipid Binding Region (ULBR) is identified

2013 The region comprising residue 60-67 in the Unique domain of c-Src has affinity for lipids.

c-Src self-association on membrane

2016 c-Src partially self-associates upon membrane anchoring.

The Src N-Terminal Regulatory Element (SNRE) is described

2015-17 The N-Terminal region of c-Src, involving the SH4, Unique and SH3 domains forms an intramolecular fuzzy complex.

A mutation in ULBR shows 50% reduction of the invasion capacity of SW60 colon rectal cells

*REFERENCES of c-Src historical nuggets *(in alphabetical order)*: (Arbesú et al., 2017; Courtneidge et al., 1980; Huebner and Todaro, 1969; Hunter and Sefton, 1980; Krueger et al., 1980; Levinson et al., 1981; Maffei et al., 2015; Martin, 2001, 2004; Mayer et al., 1988; Moran et al., 1990; Pérez et al., 2009, 2013; Ren

et al., 1993; Rous, 1910, 1911; Le Roux et al., 2016a; Sadowski et al., 1986; Sefton et al., 1982; Sigal et al., 1994; Stehelin et al., 1976a, 1976b; Xu et al., 1997; Yeatman, 2004).

Protein tyrosine kinases are a class of enzymes, which using ATP catalyze the phosphorylation of a tyrosine residue in their selected substrates (*Figure 1.2.*). In cells, the enzymes reversing this post-translational modification are the phosphatases (Hubbard and Till, 2000).

Phosphorylation also occurs on serine and threonine residues by respective kinases. This modification introduces structural changes to the protein conformation, altering its function by promoting or abolishing inter/intra-molecular interactions. Reversibility of this covalent modification provide a simple yet robust *on/off* reading state to the substrates mediating signal transduction through the protein network of the mammalian cells (Cohen, 2002).

Figure 1.2. Phosphorylation/dephosphorylation reaction.
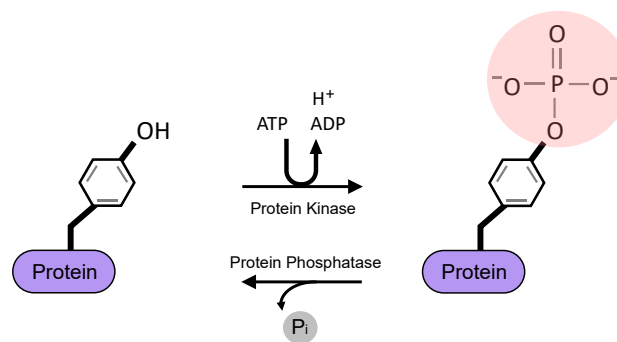
Thence, c-Src controls numerous signaling protein complexes, that regulate important pathways such as cell proliferation, differentiation, adhesion, survival, or motility (Parsons and Parsons, 2004). c-Src itself is regulated by phosphorylation at key residues (*Figure 1.3*). Not surprisingly, deregulation of these protein kinase cascades gives rise to a countless of human diseases, including cancer. The role of c-Src in human cancer is known to be significant. The reader can find a nice overview of c-Src involvement in cancer at Irby and Yeatman (2000).
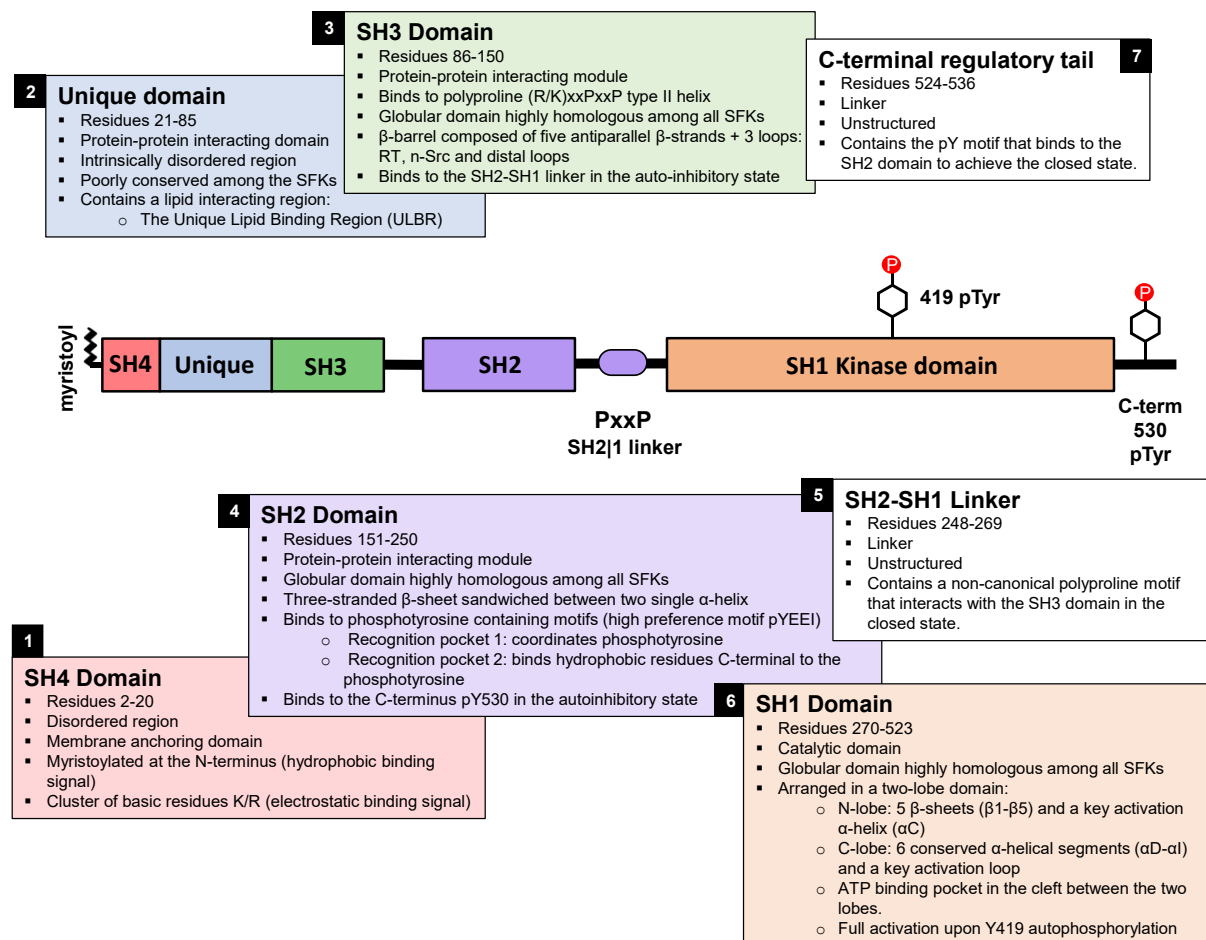
c-Src is expressed ubiquitously in various human tissues, although particular high levels are found in some cell types as neurons, platelets or osteoclasts (Thomas and Brugge, 1997). c-Src localization depends on its regulatory state. It associates to cellular membranes and can be tracked down at the plasma, perinuclear and endosomal membranes (Konitsiotis et al., 2017). Interaction of its non-catalytic domains with other proteins also modulates its subcellular localization, relevant for the specific cell regulatory pathways such as cytoskeletal assembly, induction of mitosis or membrane trafficking (Bjorge et al., 2000). Nonetheless, membrane binding is essential for c-Src effective signal transmission (Brown and Cooper, 1996; Buss et al., 1986).

The human *kinome* includes more than 500 protein kinases. These enzymes are assorted in families collecting sequence similarities of their catalytic domain, domain arrangement

beyond the kinase domain and the recognized biological functions (Manning et al., 2002). Succeeding c-Src, a close related group of tyrosine kinases is identified: c-Yes, Fyn, Fgr, Blk, Hck, Lck, Lyn, Frk and Yrk. Crowned as the Src Family of non-receptor tyrosine Kinases (SFKs), all the siblings share a common domain structure: i) a lipidated N-terminal -SH4 domain[1]-, ii) a disordered region that presents singularity in terms of sequence and length for each member of the SFKs -the Unique domain-, iii) a modular cassette containing SH3 and SH2 protein-protein interacting domains followed by the SH1 catalytic domain[2] and iv) a C-terminal regulatory tail.

Human c-Src is composed by 536 aminoacids. Specific features of its domain arrangement are presented in the *Figure 1.3*.

Figure 1.3. c-Src domain architecture.

3 · SH3 Domain
- Residues 86-150
- Protein-protein interacting module
- Binds to polyproline (R/K)xxPxxP type II helix
- Globular domain highly homologous among all SFKs
- β-barrel composed of five antiparallel β-strands + 3 loops: RT, n-Src and distal loops
- Binds to the SH2-SH1 linker in the auto-inhibitory state

2 · Unique domain
- Residues 21-85
- Protein-protein interacting domain
- Intrinsically disordered region
- Poorly conserved among the SFKs
- Contains a lipid interacting region:
  - The Unique Lipid Binding Region (ULBR)

7 · C-terminal regulatory tail
- Residues 524-536
- Linker
- Unstructured
- Contains the pY motif that binds to the SH2 domain to achieve the closed state.

419 pTyr

myristoyl | SH4 | Unique | SH3 | SH2 | PxxP SH2|1 linker | SH1 Kinase domain | C-term 530 pTyr

4 · SH2 Domain
- Residues 151-250
- Protein-protein interacting module
- Globular domain highly homologous among all SFKs
- Three-stranded β-sheet sandwiched between two single α-helix
- Binds to phosphotyrosine containing motifs (high preference motif pYEEI)
  - Recognition pocket 1: coordinates phosphotyrosine
  - Recognition pocket 2: binds hydrophobic residues C-terminal to the phosphotyrosine
- Binds to the C-terminus pY530 in the autoinhibitory state

5 · SH2-SH1 Linker
- Residues 248-269
- Linker
- Unstructured
- Contains a non-canonical polyproline motif that interacts with the SH3 domain in the closed state.

1 · SH4 Domain
- Residues 2-20
- Disordered region
- Membrane anchoring domain
- Myristoylated at the N-terminus (hydrophobic binding signal)
- Cluster of basic residues K/R (electrostatic binding signal)

6 · SH1 Domain
- Residues 270-523
- Catalytic domain
- Globular domain highly homologous among all SFKs
- Arranged in a two-lobe domain:
  - N-lobe: 5 β-sheets (β1-β5) and a key activation α-helix (αC)
  - C-lobe: 6 conserved α-helical segments (αD-αI) and a key activation loop
  - ATP binding pocket in the cleft between the two lobes.
  - Full activation upon Y419 autophosphorylation

---

[1] Frk is not myristoylated and/or palmitoylated at the N-terminus.

[2] The term SH# stands for Src Homologie domain, as these were originally identified in c-Src and afterwards recognized in other proteins.

Xu and coworkers (1997) contributed the first crystal structure of human c-Src. Successive X-ray structures of the open and closed conformations (Cowan-Jacob et al., 2005; Xu et al., 1999) brought up light on details in the c-Src activation mechanism (Huse and Kuriyan, 2002). The release from the auto-inhibitory state implies a major domain rearrangement, that Harrison (2003) describes as a flow of three main elements: the *latch,* the *clamp,* and the *switch*:

A. Latch: The phosphorylated tyrosine pY530 in the C-terminal tail binds to the SH2 domain and promotes the compact attachment of the SH2 domain opposite to the C-lobe of the SH1 domain. In cells, phosphorylation of Y530 is carried out mainly by Csk and Chk kinases (Okada, 2012; Thomas et al., 1991; Zrihan-Licht et al., 1997). *Unlatching,* i.e. unphosphorylation of pY530, would be steered by phosphatases such as the cytoplasmic PTP-1B or the transmembrane CD45 (Roskoski, 2005).

B. Clamp: The SH3 domain binds to the polyproline motif of the SH2-SH1 linker. Although the latter not presenting a canonical sequence, it conforms a polyproline type II helix. The linker interacts as-well with the SH1 domain N-lobe. Altogether, spur the attachment of the SH3 against the N-lobe of the SH1 domain. The clamp is the tight packing of the SH2 and SH3 domains in the rear of the catalytic SH1 domain. Clamping affects the catalytic region by displacing the key αC helix of the SH1 N-lobe that contains the critical E313 residue which ultimately impedes the ATP binding. The intramolecular binding partners for both SH2 and SH3 present non-canonical sequences and thus low affinity. Availability of external proteins containing high affinity SH2 and SH3 binding motifs readily competes and displaces the intramolecular interactions and eventually *unclamps* the c-Src machinery, detaching the SH3 and SH2 from the SH1 domain.

C. Switch: A *Non-latched, non-clamped* system unblocks the SH1 kinase domain, and the catalytic site rearranges into an open state. The αC helix (N-lobe) and the activation loop (C-lobe) reorients along to a patch of hydrophobic residues from both lobes, forming the so-called regulatory spine (protein substrate pocket) and the catalytic spine (ATP pocket). Further stabilization of the catalytic site, a hallmark to increase ~ 4-fold its kinase activity (Boczek et al., 2019), is achieved through the phosphorylation of the activation loop Y419. This is referred as the *switch* by Harrison (2003). The latter event is recognized to be a self-phosphorylation in *trans*, i.e accomplished by a second c-Src molecule (Smart et al., 1981).

Seemingly, kinase activity of c-Src would be launched by C-termini Y530 dephosphorylation. Nonetheless, mutations in the SH3, SH2 and catalytic domain proved to trigger c-Src high activity, even when those mutants where phosphorylated at Y530 (Cooper and Howell, 1993; Murphy et al., 1993). A SAXS study of an active c-Src mutant (Y530F), revealed that even when the enzyme is in an eternal *unlatched* state, the protein kinase conformation remains at an equilibrium towards the closed form (85%) (Bernadó et al., 2008). The SH3-

SH2 clamp is not completely released. Indeed, cooperatively binding of SH2 and SH3 domains to external ligands of a substrate protein can stimulate c-Src activation (Alexandropoulos et al. 1996). In addition, Fajer et al., (2017) reveals a key role of the SH2-SH1 linker, modulated by the SH3-SH2 tandem, in the activation process. The overarching scenario posits an activated state achieved via an intramolecular allosteric gear transmitted through the SH3-SH2 modules to the kinase domain, being the Y419/Y530 phosphorylations essentials to *lock* the activated (pY419) (Boczek et al., 2019) and repressed (pY530) states (Cooper and Howell, 1993).

Consistently, viral homologue v-Src truncation of the C-terminal (including Y530) and the different amino-acid substitutions in the SH3-SH2 and kinase domains[3] is *raison d'être of its perpetual* active state and consequent transforming capacity (Kato et al., 1986; Tanaka and Fujita, 1986). Substitution of the key Y419 by Phe in the activation loop, severely reduces the biological activity of c-Src. Intriguingly, the same mutation in the highly transforming v-Src has slight effects. The mutation was self-evident to act as a negative regulator in v-Src, thus raises the possibility of other intramolecular alterations liable for the tumorigenesis by v-Src; or the same alterations to be sufficient in *locking* the enzyme activity independent to the phosphorylation of Y419 (Bjorge et al., 2000; Snyder and Michael Bishop, 1984). Presumably, it may account for the several mutations in the non-catalytic and kinase domains of v-Src.

c-Src is normally in a basal dormant state during the cell cycle, yet transient activation occurs upon cellular events such as mitosis, cell growth or neural synaptic transmission among others (Roskoski, 2004). During a mitotic cell division, c-Src is reported to be phosphorylated in the Unique domain at T37 and S75[4] by cyclin-dependent kinase 1 (Cdk1)[5] (Shenoy et al., 1989). These post-traslational modifications set off c-Src activation by altering the self-inhibitory SH2-pY530 interaction, ultimately causing dephosphorylation of the C-terminal tail pY530 by the correspondent phosphatases (Shenoy et al., 1992; Stover et al., 1994).

Mammalian cells harbor a myriad of growth factors able to regulate cellular growth and proliferation, such as the platelet-derived growth factor (PDGF), that binds to the corresponding receptor, i.e. PDGF receptor (PDGFR), eventually triggering the signaling pathways by this receptor tyrosine kinase (RTK). PDGF stimulation of fibroblasts induces enhanced c-Src kinase activity (Ralston and Bishop, 1985). c-Src is phosphorylated at Y215 (Y212 in chicken c-Src) in the SH2 domain by PDGF receptor, which impairs its interaction with the C-terminal regulatory tail and consequently activates c-Src. Nonetheless, pY215 phosphorylation does not affect the interaction of other pTyr binding ligands with c-Src SH2 domain (Stover et al., 1996).

---

[3] Substitutions subjected to the virus strain.

[4] The research was performed with chicken c-Src, thus in the original article, residues are reported as T34 and S72. In the same work the authors also report phosphorylation at T46, which has no correspondence in human c-Src.

[5] Also known as cell division cycle protein 2 homolog (Cdc2).

Broome and Hunter, (1997) reported a second phosphorylation site in c-Src by the PDGF receptor, the SH3 domain Y139. Despite this phosphorylation is not required for PDGF-induced c-Src activation, pY139 reduces the SH3 domain PxxP ligand binding, suggesting an alternative mode for the SH3 domain regulation. Although the biological significance of this c-Src SH3 domain modification remains unclear, phosphorylation of NCK adaptors SH3 domains proved to halt the downstream signalling by these proteins (Dionne et al., 2018). In addition, reciprocal phosphorylation by c-Src to the PDGF β-receptor subunit Y934 (kinase domain), results in the down-regulation of a signal cascade driving motility responses (Hansen et al., 1996).

In neurons, the N-methyl-D-aspartate (NMDA) receptor, a multi-protein complex building an ion channel, has a core role modulating plasticity and synaptic transmission in the central nervous system. Over-stimulation of the NMDA receptors promotes excitotoxicity leading to neuronal death (Carvajal et al., 2016). c-Src is a key up-regulator of the NMDA receptor channel activity. Tyrosine phosphorylations are known to occur within the NMDA receptor 2A and 2B subunits. Yu et al., (1997) revealed that the c-Src - NMDA channel interaction required the region comprising residues 40-58 of the c-Src Unique domain, suggesting a functional role for this IDR, a first evidence that outweighed its assumed anchoring accessory tittle to the date. A more complete picture detailed that the interaction of c-Src Unique domain was mediated by a protein in the NMDA receptor complex, the NADH dehydrogenase subunit 2 (ND2) (Gingrich et al., 2004).

Additional c-Src activity regulation occurs through the interaction with proteins containing polyproline type II and/or phosphotyrosine motifs which bind to SH3 and/or SH2 domains respectively, competing and releasing the self-inhibitory restraints and leading to the activation of the protein kinase. Examples include the focal adhesion kinase (FAK) that activates c-Src by binding to its SH2 domain, whereas p130Cas activates the tyrosine kinase by interacting with both SH3 and SH2 domains (Bjorge et al., 2000).

I have just covered few illustrations of c-Src upstream-downstream regulation. Often, ambiguity shrouds the recognition of c-Src substrates, as the same proteins may also play a role as regulatory partners. The seeking of c-Src substrates as road to its function has been actively engaged from the 1980s since its identity disclosure. In 1987, JT Parsons and colleagues developed a pioneering risky project that led to the identification and characterization of the currently well-known c-Src substrates. Interesting details along the defying uncovering journey of few of the most acclaimed c-Src substrates are given in Reynolds et al., (2014).

Recent collected evidence exposes c-Src modulation under oxidative stress, opening new vista to a non-canonical type of regulation of c-Src. Oxidative stress involves a positive change in the balance of reactive oxygen species (ROS)[6] in the cellular environment, such

---

[6] Reactive oxygen species (ROS) are side product metabolites generated in the mitochondrial respiration, from molecular O_2.

as superoxide anions O_2^-, hydrogen peroxide H_2O_2, hydroxyl radicals $^\bullet OH$ or nitric oxide $NO^\bullet$. Historically, accumulation of ROS species has been linked to cause cellular damage, such as the observed in aging process. In the late years, rediscovered redox regulation heralds a novel role for H_2O_2 as a secondary messenger in cell signaling (Sies, 2014; Sun and Kemble, 2009). This emerged signalling lights up reversible oxidative post-translational modifications, underlining the conserved Cys residues within proteins as redox-prone targets.

Riveting results acknowledge specific cysteine residues in tyrosine kinases implicated in redox-mediated kinase activation, which are also irreversible targets of sought pharmacological inhibitors, e.g. C280 of c-Src (Dustin et al., 2019). c-Src contains nine cysteine residues, considerably conserved among the SFKs and other related kinases. Heppner and coworkers (2018) identified Cys188 (SH2 domain) and Cys280 (SH1 domain) as leading residues undergoing H_2O_2-mediated sulfenylation (Cys-SOH) in c-Src. These oxidations influence directly its self-inhibitory regulatory interactions and consequently promote the kinase activation. C188 sulfenylation destabilizes the down-regulating SH2 domain - pY530 interaction, whereas C280-SOH induces auto-phosphorylation at Y419 by making this residue more accessible (Heppner et al., 2018).

Other targeted positions of c-Src engaged in redox regulation include C501 (SH1 domain) S-nitrosylation that leads c-Src activation upon β-estradiol stimulation of MCF7 breast cancer cells showing important effects on tumorigenesis and invasion (Rahman et al., 2010). Higher c-Src activity during cell adhesion as a result of the oxidation of C248 (SH2 domain) and C490 (SH1 domain). Mutations of these positions reduced cancer cells invasivity and anchorage-independent growth among others (Giannoni et al., 2005).

Although, enhanced activation seems to be the recurring outcome of c-Src oxidation, Kemble and Sun (2009) reported the contrary, demonstrating up to 92% of loss in the c-Src kinase activity upon C280 oxidation and consequent c-Src homodimerization via disulphide bonding. Despite that, all the lines of evidence presented lead to the involvement of c-Src as an important sensor and reciprocal player in the redox signalling. Progressive uncovering of the alternative walk leading to c-Src activation opens up novel prospects for the development of high selective c-Src inhibitors.

Up to this point, we have mind mapped an overview on extrinsic factors causing c-Src activation. Though Y419 phosphorylation is the critical mechanistic switch to fully activate the protein kinase. Recently, Boczek et al. (2019) provided details on the structural rearrangements upon Y419 phosphorylation in the c-Src full length context. Upon pY419 phosphorylation the kinase domain becomes more rigid whereas the regulatory domains (SH4-Unique-SH3-SH2) exhibit significant conformational flexibility, showing the Unique and SH3 domains an enhanced dynamics alteration. Key residues in the active center (K295, E310 & R409) showed different conformations when the phosphorylation occurred in the full-length construct in comparison to the kinase domain alone, suggesting a cross-talk between the kinase domain and the regulatory domains. This idea of cross-

communication between the non-catalytic modules and the kinase domain was already presented by Gonfloni et al., (2000), that suggested a bidireccional regulation.

Therefore, c-Src regulatory module - SH4, Unique, SH3 and SH2 – not only importantly targets specific substrates, granting the kinase a specific subcellular localization, but is also essential to regulate the catalytic domain by transmitting information received through the distinct inputs (e.g. post-translational modifications). The wide range of binding partners from the diverse cellular pathways encompassed by c-Src along the pleiotropic effects of the oncoprotein upon deregulation calls for fine-tuned mechanisms in addition to the canonical interactions, which may also be of relevance on the emerging non-catalytic functions by this protein kinase (García-Martínez et al., 2010).

Considering the stated relevance of the non-catalytic domains of c-Src, the N-terminal Unique domain has remained under-appreciated until the advent of the intrinsically disordered proteins (IDPs) in the beginning of 2000. This poorly conserved domain was assumed to be a linker between the membrane anchoring SH4 domain and the folded cassette, although it has been demonstrated to contain important functional elements (Gingrich et al. 2004; Pérez et al. 2013). The disordered nature of this region hampers structural studies by X-Ray due to inconceivable crystallization of a protein containing an intrinsically disordered region (IDR). Our group has described a novel functional role for the N-terminal region comprising the SH4, Unique and SH3 domains, so that this region is referred as the c-Src N-terminal Regulatory Element (SNRE). In the next subsection, we will review in detail the SNRE and its implications.

1.2. The c-Src N-terminal Regulatory Element (SNRE)

Already in 1980s Nemeth and coworkers (1989) pointed out deletion of residues 15 to 89 would prompt c-Src kinase activation, resulting in increased levels of tyrosine phosphorylated proteins. This region encloses the entire Unique domain. The authors presumed the existence of an N-terminal domain including residues 54 to 90 that would regulate the kinase activity. The discovered regulatory interactions involving the SH3, SH2, SH2-SH1 linker and C-terminal tail would draw the limelight away from the Unique domain, combined to its lack of structure and high sequence divergence among the SFKs, persuaded its entitled assumption of a linker region, until the emergence of the Intrinsically Disordered Regions (IDRs)[7].

The Unique domains of all the SFKs are predicted to be intrinsically disordered regions (Santos and Siltberg-Liberles, 2016). Our group demonstrated this feature for the first time by NMR and Small Angle X-ray Scattering (SAXS) studies (Pérez et al., 2009) in the case of c-Src. Using residual dipolar couplings (RDCs), Pérez et al. (2009) provided accurate estimation of secondary structural elements in c-Src Unique domain. The analysis revealed the presence of a residual helical structure comprising the 60–75 region. Subsequent studies (Pérez et al., 2013) of the Unique domain in the presence of membrane mimics by NMR, revealed affinity to lipids by the residues [60]EPKLFGGF[67] of the partially structured region. Consequently, this region was designated as the Unique Lipid Binding Region (ULBR). In addition to the residual structure of the ULBR, Pérez et al. (2009) suggested that the Unique domain exhibited certain degree of preorganization, given the observed deviation from a random coil behavior, expected for an IDR.

Figure 1.4. Structure of the SH3 domain of c-Src (from PDB: 1Y57).

SH3 domain

---
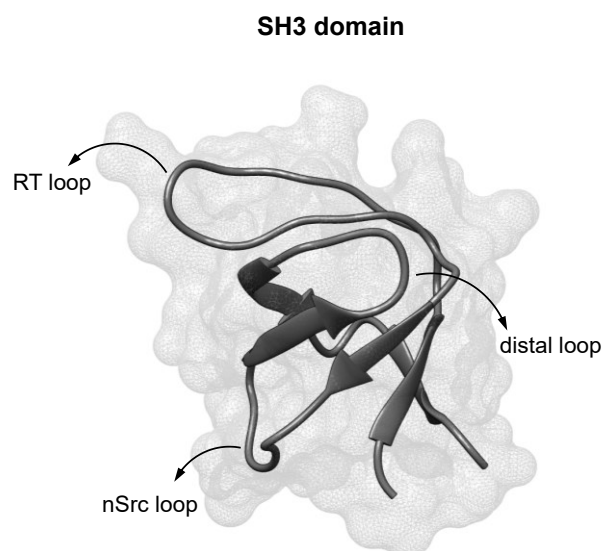
[7] More detailed discussions on the topic of Intrinsically Disordered Proteins (IDPs) and/or Regions (IDRs) are reviewed in Van Der Lee et al., (2014).

The Src Homology 3 domain is an evolutionary conserved protein fold, ubiquitously expressed. *Figure 1.4.* illustrates c-Src SH3 domain, composed of 65 amino-acids, with the signature features of β-barrel consisting of five antiparallel β-strands and three loops: the RT, nSrc and distal loops. It also has a short 3_{10} helix located between strands 4 and 5. The β sheet formed by strands 2, 3 and 4 forms a hydrophobic surface key for the recognition of polyproline II helices (PPII).

Maffei et al., (2015) elucidated novel subdomain interactions that uncovered the role of the SH3 domain as a scaffold for the IDR (SH4 & Unique domains) through multiple weak interactions. Though this would be the first snapshot of an evolution engineered dynamic complex, it was shown that the RT, nSrc, and distal loops of the SH3 domain impacted the conformational space sampled by the disordered SH4 and Unique domains. Upon PxxP ligand:SH3 complex formation, most of the dynamic contacts of the SH3 domain with the IDR would be hampered, except for the SH4-SH3 that remained unaffected and thus kept the Unique domain close to the SH3 domain.

Additionally, to the interaction with the SH4 and Unique domains, the SH3 was proved to interact with lipids via the RT and nSrc loops (Pérez et al., 2013). This contact is lost upon binding of a PxxP ligand (Maffei et al., 2015), however, as the SH4:SH3 domain interaction is retained, and the SH4 domain membrane binding is not affected by the PxxP ligand, the SH3:PxxP complexed domain is maintained close but omitting direct contact to the lipids.

Further interactions were disentangled by Arbesú et al., (2017) demonstrating that in the absence of the SH4 domain, the Unique domain retains the interaction with the SH3 domain. Nonetheless, removing the entire SH4 domain or the first ten residues had opposite effects on the SH3 domain, in the sense of a more isolated-like SH3 domain or adopting a closed state i.e increased interaction with the IDR. Deletion of just the first residues favored the closed state, suggesting that N-terminal part of the SH4 domain may also engage interactions with the Unique domain, competing with the SH3 domain and thus shifting the equilibrium state of the wild type SH4-Unique-SH3 towards a more open-like conformation. This could represent a possible layer of regulation of c-Src, where modulation of SH4 domain by the lipids could be transmitted to the folded cassette through the Unique domain.

Intramolecular interactions within a protein, involve short and/or long-range contacts, which are distinguished based on the chain distance between the two residues, i.e number of amino-acids in between. Long-range intramolecular contacts can provide an idea of the compaction state of the protein. Arbesú et al. (2017) proved that long-range contacts within the Unique domain were similarly maintained in the absence of SH3 domain, suggesting that the IDR is *pre-organized in its disordered state.* Nevertheless, greater contacts were observed between the SH4 and Unique domains in the presence of the SH3 domain, corroborating its scaffolding role (Arbesú et al. 2017; Pérez et al. 2009). Their work proved that compaction of c-Src Unique domain, even in the absence of the SH3 domain, was mainly caused by key features that, surprisingly, were almost conserved within

the different Unique domains of the SFKs. These attributes included occurrence of aromatic residues in analogous positions and distribution of proline residues with respect to these aromatic residues.

c-Src has four phenylalanine residues in the Unique domain (F32, F54, F64 & F67), two of them are located in the ULBR composing the pattern $\Phi_1xx\Phi_2$, where Φ_1 is phenylalanine or tyrosine, x a turn promoting residue (G,S,N) and Φ_2 is an aromatic or a hydrophobic residue. This pattern is conserved in the closely related SFKs members. Mutation of Phe residues in the isolated c-Src Unique domain, resulted in a decrease of long-range interactions and thus compaction of the domain. Whereas, given their allotment, prolines role, was hypothesized to impact local dynamics of the domain chain by nucleating concerted motions of peptide segments. This multiple evidence, suggest that the conformational space sampled by the isolated IDR of c-Src (SH4 plus Unique domains) is constrained yet still diverse. This conformational heterogeneity is retained in the multiple interactions with the SH3 domain, grounding the satisfactory requirement of a fuzzy interaction (Arbesú et al. 2017). In other words, c-Src intramolecular interaction involving the IDR and SH3 domain settles into a dynamic fuzzy interdomain complex. As earlier described, removal of the SH4 domain N-terminal part, resulted in a more closed conformation for the IDR:SH3 interdomain complex. This modulation of the conserved disorder on the binding result, is the distinguishing feature that differentiates a fuzzy complex from a linker non-specifically interacting with a domain (Arbesú et al. 2017). The c-Src N-terminal Regulatory Element (SNRE) is thus designated to the fuzzy complex formed by the SH4, Unique and SH3 domains of c-Src.

Structural enlightenment of the Unique domain of c-Src, brought up gradual insights on its functional relevance. Besides the earlier described role where effective interaction with NMDA receptors required region 40-58 of this disordered domain, Pérez et al. (2013) found anomalous phenotypes in *Xenopus laevis* oocytes when the partially structured ULBR was mutated. Alteration of this region (^{60}EPKLFGGF^{67} → ^{60}EPAAAGGF^{67}) reduced its lipid binding affinity (Pérez et al. 2013). Same mutation in colon rectal cancer cells SW260 where deregulation of c-Src is observed, reduced ~50% the invasive capacity of the cells (Aponte et al., 2021; Arbesú et al., 2017; Maffei et al., 2015). Truncation of c-Src mediated by calpains within the region ^{63}LFGGFNSSDTVTSPQR^{78} containing the ULBR results in neuronal death (Hossain et al., 2013). Calcium-binding calmodulin (CaM), a regulator/effector protein that has key roles in variety of cellular functions, particularly in muscle contraction, was demonstrated to partially interact with the Unique Lipid Binding Region of c-Src (Pérez et al. 2013), modulating some of the intramolecular interactions of the N-terminal c-Src fuzzy complex affecting the SH3 domain. All the latter evidence feed the importance of the ULBR functional role in c-Src regulation.

Several phosphorylations are known to occur within the IDR of c-Src (Amata et al., 2014), prompting additional modes of regulation. Summarized in *Table 1.1*, besides the reported ones, there are several phosphorylations predicted (S12, S39, S43, S51, S69, S70, T72 and T74) which have not been experimentally assessed yet. Of note are T37 and S75 phosphorylations, which have been described to affect the auto-inhibitory SH2-pY530 C-

terminal tail interaction, suggesting a possible cross-talk between the IDR and the SH2 domain. The same phosphorylations have been demonstrated to affect the Unique Lipid Binding Region (ULBR) interactions.

Table 1.1. Reported phosphorylations in the IDR of c-Src.

Phosphorylation sites	Responsible kinase	Functional role	References
S17	PKA cAMP-dependent protein kinase	Protein-protein interactions Cellular location by affecting the polybasic segment of the lipid binding SH4 domain	(Walker et al., 1993) (Pérez et al. 2013)
T37 & S75	Cdk1 cyclin-dependent kinase 1	c-Src activation during mitosis by hampering the self-inhibitory interaction SH2 domain- pY530 C-terminal tail	(Shenoy et al., 1992)
T37 & S75	p25-Cdk5	Modulates the Unique Lipid Binding Region	(Pérez et al. 2013)
S75	p25-Cdk5	Ubiquitin-dependent degradation	(Pan et al., 2011)

The latter described phosphorylation also illustrates the interplay of IDRs sensing external stimuli via post-translational modifications, relaying the information across the folded domains to trigger associated response. As pointed out by Arbesú and Pons (2019), high occurrence of intrinsically disordered segments in the vicinity of SH3 domains of a variety of proteins, may establish a role for this domain as a bonding interface between the IDR sensors and the globular regulatory domain actuators. The c-Src IDR:SH3 fuzzy complex provides an example of this intricated dynamic regulation. Modulation of the SH2 domain binding can be accomplished through the action of phosphatases-kinases, however the way SH3 binding motifs interaction can be regulated is not clear. A straightforward mechanism might be SH3 domain availability, which could be modulated by altering its interaction with the IDR (i.e. by post-traslational modifications) (Shalloway and Taylor, 1997).

The reader may have noticed the regulatory players of c-Src that have not centered the stage yet: the myristoyl moiety plus membrane anchoring. Reported by (Kamps et al., 1985), myristoylation defective v-Src mutant fails to perform transformation of cells. This condition was attributed to the alteration of the cellular location by a decreased membrane association of the non-myristoylated c-Src rather than unsuccessful catalytic activity (Buss et al., 1986), pointing out the requirement of membrane anchorage for an adequate physiological function.

c-Src membrane binding is accomplished through two components: i) hydrophobic insertion of the myristoyl moiety within the lipid bilayer and ii) electrostatic interaction of the positively charged residues (K5, K7, K9 and [14]RRR[16]) of the SH4 (Poly-Basic Cluster (PBC)) with the acidic lipids. Synergistic action of both membrane-binding signals is

necessary for c-Src effective membrane binding, as neither myristoylation nor the PBC individually provide sufficient anchorage to the protein (McLaughlin and Aderem, 1995; Sigal et al., 1994). Several myristoylated proteins have shown to integrate a myristoyl binding site/pocket, to harbor the myristoyl chain when the protein is in the membrane unbound state, as in the case of the kinase c-Abl, whose myristoyl self-docking leads to a conformational change restraining the protein activity. In the case of c-Src, the identification of a myristoyl binding site has remained elusive.

As mentioned earlier, c-Src membrane anchoring requires insertion of the myristoyl moeity within the lipid membrane and electrostatic interaction of the PBC in the SH4 domain. Although c-Src has additional lipid binding regions (ULBR and RT plus nSrc loops of SH3 domain), contribution to membrane anchorage by these secondary elements have not been assessed (Pérez et al. 2013). Membrane tethering is reversible, however, our group reported the presence of a minor fraction of membrane-bound c-Src that is persistently anchored to the lipid bilayer, existing as self-associated species with prevalence of homodimer formation (Le Roux et al., 2016a, 2016b).This self-association requires membrane binding, and the potential dimer interface only involves the myristoylated SH4 domain i.e. all critical residues entailed in the self-association lay within the residues of the SH4 domain (Le Roux et al., 2016a).

While the other members of the SFKs have additional palmitoylation(s) in the N-terminus along with myristoylation providing a more robust anchorage to the membrane, c-Src single myristoyl insertion results in a labile association. Thus, c-Src self-association may represent the alternative regulation mode for a stronger membrane binding. Moreover, the equilibrium with the monomeric species could modulate this persistent signalling point. The structural characterization of self-associated c-Src could unravel its formation mechanism and lead to the critical implications by this new mode of binding.

1.3. Myristoylation and membrane binding

Protein-membrane interaction is a complex event. Broad range of context-dependent factors influence and intervene in this process, that ultimately results in targeting of the protein to specific subcellular locations and the restriction of protein diffusion to two dimensions. This thesis' particular case of study, is a peripheral membrane-protein, lodged in the cytoplasmic milieu (3D space) that eventually migrates to the inner leaflet of the plasma membrane (2D space). *Figure 1.5* summarizes the key components of the multifactorial scenario affecting the protein-membrane binding events.

Figure 1.5. The protein-membrane interaction context. (A) The plasma membrane. (B) Physicochemical properties of the local membrane. (C) Type of attachment by peripheral membrane protein.
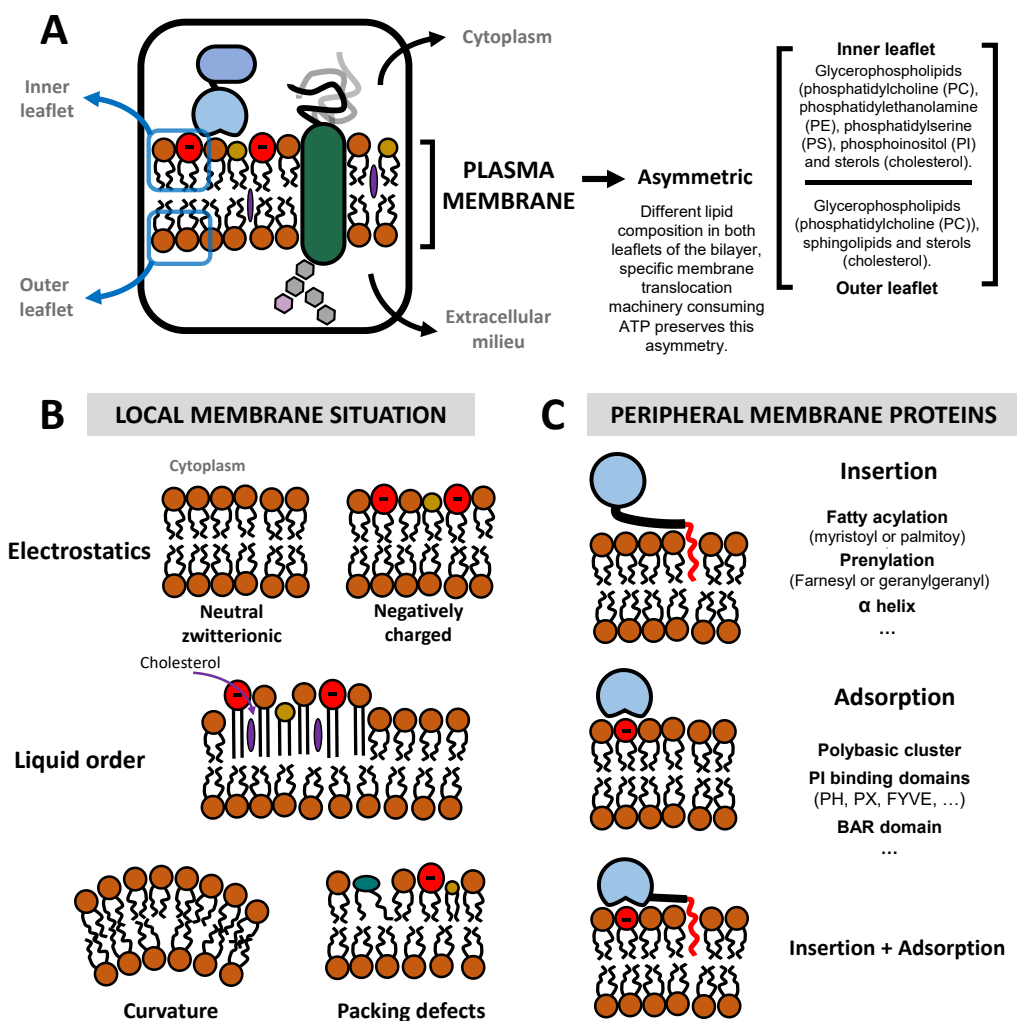
Table 1.2. Overview on major lipid-protein modifications modulating the anchorage on the cytosolic leaflet of the plasma membrane: fatty-acylation and prenylation. Reference: (Pool and Thompson, 1998).

	Fatty acylation		Prenylation	
Lipid moiety	Myristate	Palmitate	Farnesyl	Geranyl-geranyl
Where?	N-terminal Gly[2]	Cys located in the region close to the N or C-terminus	Cys located in the C-terminus	
Fatty acid-protein linkage type	Amide bond	Thio-ester linkage	Thio-ether linkage	
When? By who?	Co-traslationally[3] Enzyme: N-myrystoyltransferase (NMT)	Post-trasllationally Enzyme(s): palmitoyl acyl transferases (PATs)	Post-trasllationally Enzyme: farnesyl transferase (FTase)	Post-trasllationally Enzyme: geranylgeranyl transferase I (GGTase I) [5]
Reversible?	No	Yes Enzyme(s): palmitoyl protein thioesterases	No	
Consensus sequence	M_1-G_2-X_3-X_4-X_5-[S/T]$_6$-[K/R]$_7$ M_1 initiator removed by methionine aminopeptidase X includes most amino acids X_3 is not favored by Pro, aromatic or charged residues X_6 Ser/Thr preference X_7 Lys/Arg preference	Not defined [4]	C-A-A-X C = Cys A = aliphatic amino acid X = Met/Ser → farnesyl X = Leu → geranyl-geranyl	
$\Delta G_u°$ (kcal/mol) neutral membrane binding [1]	-10.6	-12	-9.2	-11
Examples	SFKs, Arf1, c-Abl, MARCKS, BASP-1, retroviral Gag proteins, calcineurin B eNO, Protein kinase A, Protein kinase C, Recoverin, Gα subunits	SFKs, H-Ras, CD4, caveolin-1, β2 adrenergic receptor, Gα subunits, GAP43, eNOS	H-Ras, K-Ras, Lamins	Gγ subunits, Rho family proteins, Rab proteins

[1] Values from literature (Pool and Thompson 1998) for mono-acylated peptides. The experiment was performed using the same peptide scaffold for the four types of lipid moieties, at 37°C and on a neutral phospholipid membrane. The peptide scaffold was BimTA-AC(X)R where BimTA= (S-bimanylthio)acetyl,

A= ala, C= cys, R= arg and X= thioester bond myristoyl or palmitoyl groups; or thioether bond farnesyl or geranylgeranyl groups.

[2] Multiple studies have reported lysine myristoylation in Ras GTPases and tumor necrosis factor α (TNF-α) among others (Jing et al. 2017; Stevenson et al. 1992, 1993)

[3] The pro-apoptotic protein BID is post-traslationally myristoylated after caspase proteolytic cleavage, exposing an internal glycine residue (Zha et al. 2000).

[4] The signal for palmitoylation modification has not been defined yet.

[5] It exists a third class of prenyl transferase that modifies only Rab proteins that terminate with -CC, CXC, CCX or CCXX sequences: Rab GGTase or GGTase II.

Apropos the membrane, the determining factor is the local lipid composition where the binding event occurs. The different lipid combinations ground physical parameters as membrane curvature, packing defects, thickness of the hydrophobic core of the bilayer and charge density distribution, which modulate the lipid-protein interaction (Adhyapak and Kapoor, 2019). Whereas the protein may define the interaction occurrences based on the type of attachment, that for our case, could be divided in three categories: insertion, adsorption or combination of both. As summarized in the *Table 1.2* overview (*page 17*), fatty acylation, i.e. addition of myristic or palmitic fatty acids, is one the major types of protein lipid modification. Other modifications include: prenylation (farnesyl or geranylgeranyl isoprenoids), cholesteroylation (cholesterol molecule) or glypiation (glycosylphosphatidylinositol anchor). Each type of lipid modification endows the protein singular properties, directly leading the location onto particular regions of the membrane (e.g. lipid rafts) (Resh, 2013a). Myristoylation is the common lipidation found in all SFK and the only one present in c-Src.

Evolution has engineered new pathways of regulation in cells, adding extra complexity to proteins through co/post-traslational modifications with acyl moieties (*Table 1.2*), being the final protein product reliant on the availability of the lipid source. Myristic acid, a saturated C14 fatty acid, is a scarce lipid source in cells, accounting for < 1% of the total lipodome. The attachment of this acyl moiety specifically to a N-terminal glycine amino acid in proteins is known as N-myristoylation. The process is catalyzed in cells by the enzyme N-myristoyltransferase (NMT) and occurs in eukaryotes but not in archaea or bacteria prokaryotes (Boutin, 1997). With a limited reservoir in cells, having only emerged in complex organisms that added a cost of a specific enzyme for this post-traslational modification, it may seem reasonable to wonder why myristic acid has been selected as an acyl moiety for lipid modified proteins. A question already reflected by Towler and Gordon (1988):

> "[...] it remains to be explained what properties of the 14-carbon fatty acid led
>   to its unique selection by the cell over other more abundant fatty acids" [...].

However, hitherto the query is still active.

Figure 1.6. Protein myristoylation mechanism. Myristoylation occurs co-traslationally after removal of the initiator methionine M_1. The process is catalyzed by the enzyme N-myristoyltransferase (NMT) and it involves a Bi-Bi reaction mechanism, with myristoyl-CoA binding first to NMT and the nascent peptide second.
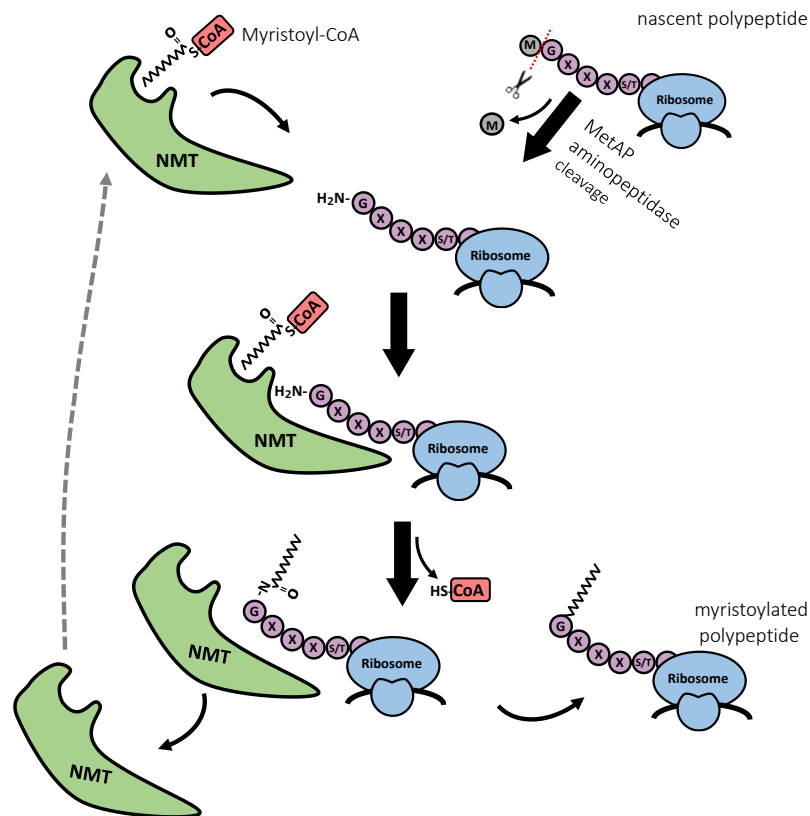
Additional to the condition of a N-terminal Gly residue, NMT recognizes a consensus sequence. However, ubiquity of the NMT among the various Eukarya members, its isoforms and the cell-type-dependent activity, samples for divergent but overlapping substrate specificity among the organisms. Maurer-Stroh et al., (2002) identified generalized features involving the first 17 residues from substrates of various NMT, independently of the taxon, characterizing three substrate regions directly linked to NMT recognition: i) residues (1-6) fit in the NMT binding pocket ii) residues (7-10) interact with the gate of the catalytic region and iii) residues (11-17) constitute a hydrophilic linker. For most proteins, the consensus sequence obeys M^1-G^2-X^3-X^4-X^5-$[S/T]^6$-$[K/R]^7$, where the initiator methionine M^1 is removed and G^2 becomes available; X includes most of the amino acids, position X^3 is not favored by proline aromatic or charged residues and Ser/Thr are preferred at the position X^6 or Lys/Arg at position X^7 (*Figure 1.6.*).

Myristoylated proteins are estimated to comprise 0.5-3% of the total mammalian proteome (Martin et al., 2011). The existence of a fatty moiety boosts the lipophilic surface of the protein granting an optimized association with membranes and/or also facilitating transient interaction with other proteins (i.e. membrane receptors), overall essentially affecting the particular cellular localization of the protein (Sonnenburg and Gordon, 2013). In various

events, myristoylation is also a required signal for further post-translational protein processing, as for the Cys[6] S-palmitoylation and N-terminus lysines methylation of the SFK member Fyn (Liang et al., 2004).

Although myristate increases the hydrophobicity, it does not provide a sufficient anchorage to the membranes (Peitzsch and McLaughlin, 1993). Increasing chain length of the acyl moiety positively enhances the binding degree (Pool and Thompson, 1998). Peitzsch and McLaughlin (1993) reported 0.825 kcal/mol as the free-energy associated to membrane binding per methylene carbon of the fatty group. Thus, apparently palmitoyl and geranyl-geranyl groups would provide a more stable binding than myristoyl and farnesyl. However, Pool and Thompson (1998) estimated that at equilibrium, ~21% of a mono-palmitoylated protein would be found tethered to the membrane (~2% in the case of a single myristoyl chain), suggesting that neither the sole palmitoyl moiety would not provide enough binding energy to trap the protein onto the membrane[8]. Same holds true for the geranyl-geranyl moiety, alone is found not to be sufficient to provide an enduring anchorage (Silvius and l'Heureux, 1994).

The previous scenario calls the need for a second membrane-binding signal, potentially enabling the transition from a labile to a long-lived membrane tethering, when required. Common elements providing this second anchoring signal on the plasma membrane can include:

- **Additional fatty acid moieties:** post-translational attachment of one or more palmitoyl groups on cysteine residues located nearby the first signal (myristoyl, palmitoyl, farnesyl or geranyl-geranyl) of the lipid-modified proteins, boosts the hydrophobic interactions trapping the protein on the phospholipid bilayer. Moreover, palmitoylation/depalmitoylation interplay by transferase/thioesterases enables a reversible membrane targeting (Martin et al., 2011; Shahinian and Silvius, 1995).

- **Cluster of basic residues:** a stretch of basic residues – lysines and arginines - (in this thesis referred as a PolyBasic Cluster (PBC)) provide an additional component to the membrane binding through electrostatic interaction with negatively charged phospholipids, i.e. phosphatidylserine and phosphatidylinositol phosphates which are frequently found in the cytoplasmic side of the plasma membrane.

- **Others:** a domain interacting with a membrane bound protein (Resh, 1999), membrane phosphoinositides (PI) binding domains (PH, PX, FYVE.), an amphipatic helix adjacent to the myristoylation site (e.g. guanidine nucleotide binding protein Arf6 (Gizachew and Oswald, 2006), are other usual elements providing additional membrane anchorage.

---

[8] With the assumption that the binding would solely depend on the acyl chain. Other factors such as the protein conformation would not be considered.

The PBC is the case of c-Src. Its myristoylated SH4 domain contains three lysine plus three arginine residues [5]KSKPKDASQRRR[16] (net charge +5) endowing the protein a two-prong membrane association device, being one component the hydrophobic insertion of the myristoyl group and the second, the electrostatic interaction of the PBC (Sigal et al., 1994; Silverman and Resh, 1992).

Individually, myristoyl anchors to a phospholipid bilayer with a K_d of 10^{-4} M, whereas a non-myristoylated peptide containing five basic residues[9] (net charge +5) binds to a negatively charged membrane[10] with a K_d of 10^{-3} M (Buser et al., 1994; Kim et al., 1991; Peitzsch and McLaughlin, 1993; Sigal et al., 1994). Buser et al. (1994) reported a K_d of 10^{-7} M for the binding of a peptide corresponding to the myristoylated N-terminus of c-Src (net charge +5) with a negatively charged lipid bilayer, suggesting the synergistic contribution of both hydrophobic and electrostatic components. Additionally, Sigal et al. (1994) reported a similar value for full length c-Src binding on negatively charged lipids ($K_d = 6 \times 10^{-7}$ M) and provided evidence that alteration of the PBC in the SH4 domain, reduced binding affinity (*Table 1.3*) on a negatively charged membrane, supporting the needed concurrent action of both hydrophobic and electrostatic components of the myristoylated SH4 domain for an effective membrane binding of c-Src.

Table 1.3. Dissociation constants K_d (M) from literature for full length c-Src constructs upon binding with a negatively charged membrane.

Construct	Comment	Apparent K_d (M) negatively charged membrane[1]	Reference
c-Src	Wild type	6×10^{-7}	
v-Src	Viral counterpart	$\sim 1 \times 10^{-5}$	
Y527F c-Src	Activated mutant	$\sim 1 \times 10^{-5}$	(Sigal et al. 1994)
N5N9 c-Src	Lys 5 and 9 replaced by neutral Asn	2×10^{-5}	
N5N9N14-16 c-Src	Lys 5 & 9 and Arg 14, 15 & 16 replaced by neutral Asn	1×10^{-4}	

[1] Negatively charged membrane composed of PC:PS at ratio (2:1).

Interestingly, their work compared the binding of wild type c-Src to the constitutively active mutant Y530F[11] and its viral counterpart v-Src (*Table 1.3.*). The affinity of Y530F c-Src and v-Src was about ~1 order of magnitude weaker than c-Src, concluding that the lack of the intramolecular regulatory SH2:pY530 interaction in both constructs (Y530F c-Src and

[9] Two studies report the similar value using two distinct peptides with net charge +5, one performed with a peptide comprising the non-myristoylated N-terminus region (residues 2-16) of c-Src (Buser et al. 1994) and the other used a penta(lysine) peptide (J. Kim et al. 1991).

[10] Composed of (2:1) phosphatidylcholine (PC):phosphatidylserine (PS) lipids.

[11] Chicken c-Src was used, in the original paper the construct is referred as Y527F c-Src.

v-Src) led to a different protein conformation, modifying the presentation of the myristoylated SH4 domain to the lipid membrane. The latter suggesting that besides electrostatic interactions, the protein conformation have a determining role on the membrane affinity and suggest that the interaction of the membrane anchoring myristoyl and SH4 groups with other regions of the protein may modulate the strength of the membrane binding interactions.

c-Src anchors to zwitterionic membranes by partial insertion of its N-terminus myristoyl group, as reported by the thermodynamics studies of Buser et al. (1994), 10 of the 14 CH_2 groups are estimated enter into the lipid bilayer. Scheidt and Huster (2009) investigated the dynamics of c-Src[12] myristoyl moiety with respect to the surrounding phospholipids of different membranes. Although expected to have a good hydrophobic match, on zwitterionic DMPC composed membranes, the (14:0) c-Src myristoyl group presented a more extended conformation and a lower mobility (higher lipid order) in comparison to the myristoyl chains of DMPC, the latter not being affected by the peptide binding. This is in contrast to other acylated proteins, whose hydrocarbon moieties packs to adapt the thickness of the enveloping lipid bilayer, such as the Ras palmitoyl group (16:0) that becomes highly flexible upon adopting similar chain length as the surrounding (14:0) DMPC membrane (Scheidt and Huster, 2009; Vogel et al., 2005). In a negatively charged membrane, composed of DMPC/DMPS, the c-Src myristoyl chain was less extended compared to the pure DMPC membrane, but still exhibited significant lipid order versus the membrane lipid groups. Moreover, the peptide binding distorted the upper region of the DPMC/DMPS lipid matrix, as it embeds deeper into the headgroup region due to the electrostatic interactions of the PBC, being DMPC lipids the most affected which could be indicative of lipid demixing (Scheidt and Huster 2009).

Figure 1.7. Alignment of the N-terminal SH4 domains of the SFKs. **X**: myristoylation signal, **X**: palmitoylation sites, **X**: positively charged and **X**: negatively charged residues.

```
        1                  10                        20
Src    M G S N K S K P K D A S Q R R R S L E P
Yes    M G C I K S E N K S P A I K Y R P E N
Fyn    M G C V Q C K D K E A T K L T E E R D G
Lyn    M G C I K S G K D S L S D D G V D L K
Lck    M G C V C S S N P E D D W M E N I D V C
HckA   M G G R S S C E D P G C P R D E E R A P
HckB   M G C M K S F L Q V G G N T F S K T E
Fgr    M G C V C F K K L E P V A T A K E D A G
Yrk    M G C V H C K E K I S G K G Q G G S G T
Blk    M G L V S K K P D K E K P I K E K D K
```

All the SFK members have a N-terminus SH4 domain, whose leading role is anchoring the phosphotransferase to a particular membrane, ensuring the specific sub-cellular localization (Sato et al., 2009) which perhaps motivated the significant sequence divergence of the SFK SH4 domains (*Figure 1.7.*), including different degrees of post-traslational palmitoylations. Evidence for this, is found in the SFK Hck that is expressed as two isoforms

---

[12] Using a peptide derived from the N-terminal region of c-Src residues 2-19.

exclusively differing by 21 residues in the N-terminus (*Figure 1.7.*). While Hck isoform A is solely myristoylated and primarily associated to lysosome membranes, Hck B is myristoylated plus palmitoylated and anchored to the plasma membrane. Curiously, Poincloux et al., (2009) showed that oncogenic activity by Hck relied on combined action by the two isoforms, setting out the hypothesis of tumourigenicity by oncogenes as a result of collaborative action by their different isoforms. In addition to Hck A isoform, c-Src and Blk are the exclusively myristoylated SFKs.

Another interesting case is presented by Dubois et al., (2015) related to c-Yes, which localizes in cholesterol rich lipid-rafts. Their work demonstrated that introduction of a palmitoylation site in the SH4 domain of c-Src was enough to recover oncogenic properties in cancer derived cells in which c-Yes was silenced. Although the latter suggesting overlapping functions redressing the loss of c-Yes, it also showcases the specificity dictated by the SH4 domain.

While palmitoylation is a reversible modification through counteraction of thioesterases, myristoyl and prenyl (farnesyl or geranylgeranyl) moieties are not withdrawn from the modified protein by orchestrated regulatory actions. Some of the latter proteins, in the cytosolic dormant state, sequester the acyl group within a hydrophobic pocket, which can be located within the protein or found in an external partner forming a complex with the myristoylated protein. In addition, exposure of the myristoyl moiety from this pocket, and thus membrane association, can be modulated by conformational changes induced by either extrinsic factors or intermolecular interactions (Resh, 1999, 2013b, 2013a).

Figure 1.8. Types of myristoyl switches.
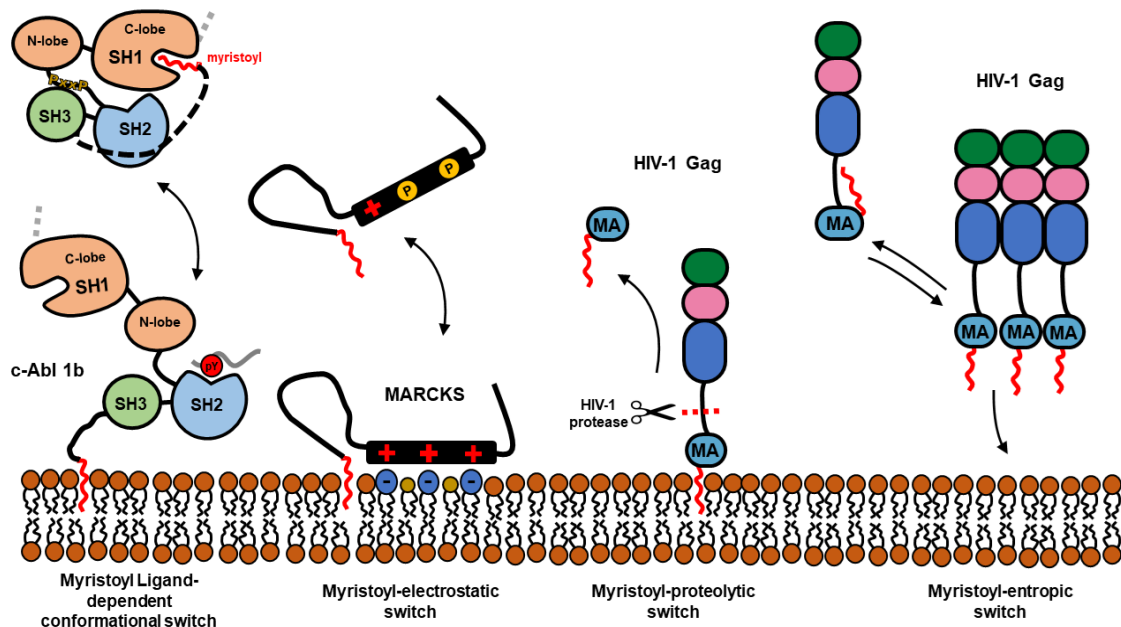
Table 1.4. Type of myristoyl switches. References: (Gaffarogullari et al., 2011; Kim et al., 1994; Resh, 1999, 2006; Tang et al., 2004; Timr et al., 2017; Wang et al., 2006; Wright et al., 2010)

Type	Defining factors	myr-Proteins	Regulatory switch factor
Myristoyl Ligand-dependent conformational switch	Conformational change on the protein upon ligand binding inducing either the myristoyl moiety to *sink in* or *flip out* the hydrophobic pocket.	c-Abl	SH2-phosphoTyr
		ARF GTPase	GTP
		Recoverin	Ca^{2+} binding → myr-out state
Myristoyl-electrostatic switch	Modulation of the polybasic cluster domain additional to the myristoyl group, by phosphorylation on the nearby residue(s) or a ligand binding. Positive modulation may include change in the membrane composition (i.e. accumulation of PIP2)	MARCKS	1) Phosphorylations on serine residues by PKC 2) Calmodulin (CaM) binding
		Gravin (AKAP250)	1) Phosphorylations on serine residues by PKC 2) Calmodulin (CaM) binding
Myristoyl-proteolytic switch	Protease cleavage resulting in a myristoylated fragment with a different affinity for the membrane and/or sequestration of the myristoyl group.	HIV-1 Gag	HIV-1 protease
Myristoyl-entropic switch	The protein in equilibrium between two states, where the myristoyl is exposed in the self-associated state and sequestered in the monomeric state. Additional interactions favoring protein multimerization propel the entropic switch towards the myristoyl exposed state.	HIV-1 Gag	Gag-Gag interactions Self-association

The regulatory process leading modulation of the myristoyl accessibility state in the protein towards the membrane, is widely known as myristoyl switch and depending on the nature of the driving force, they have been sorted into: *ligand-dependent conformational, electrostatic, proteolytic* or *entropic* myristoyl switches. *Table 1.4* summarizes the different known switches with a selected example depicted in *Figure 1.8*.

Some proteins' structure (ARF, recoverin, c-Abl 1b and HIV-1 MA) have been solved for the two state myristoyted conformation (i.e. myr- sequestered/ myr-exposed), elucidating the integrated myristoyl binding pocket that harbors the fatty moiety when the protein is in the membrane unbound state. In the case of the tyrosine kinase c-Abl[13], a close relative of the SFKs, the myristoyl self-docking leads to a conformational change restraining the protein activity. The N-terminal half of the c-Abl (1b) kinase presents the same c-Src domain architecture myr-IDR-SH3-SH2-SH1, being the myristoyl hydrophobic pocket of c-Abl found in the C-lobe of its catalytic SH1 domain. c-Abl intramolecular docking its myristoylated N-terminus, allosterically clamps the SH2-SH3 domain onto the catalytic

---

[13] There are two isoforms of the c-Abl kinase differing in the 26 first N-terminal residues. The isoform 1b is N-terminus myristoylated whereas the 1a not.

SH1 domain, resulting in the autoinhibited form of the kinase (*Figure 1.9 A*). This regulatory interaction is disrupted by binding of phosphotyrosine ligands to the SH2 domain, leading to c-Abl activation (myristoyl ligand-dependent conformational switch) (Hantschel et al., 2003; Nagar et al., 2003).

Figure 1.9. Comparison between c-Abl 1b and c-Src protein structures in the autoinhibited state. (A) c-Abl 1b (PDB: 1OPL).The expansions highlight the myristoyl hydrophobic pocket. In red the myristoyl moiety and in orange the residues involved in the hydrophobic pocket: L359, L360, A386, L448, A452, P484 , E481, F512, I521, V525 and L529. (B) c-Src (PDB: 2SRC). The expansions indicate the putative residues of the predicted myristoyl pocket by Cowan-Jacob et al., (2005): L360, L363, V364, A367, L455, L482, P488, L491 and L512.
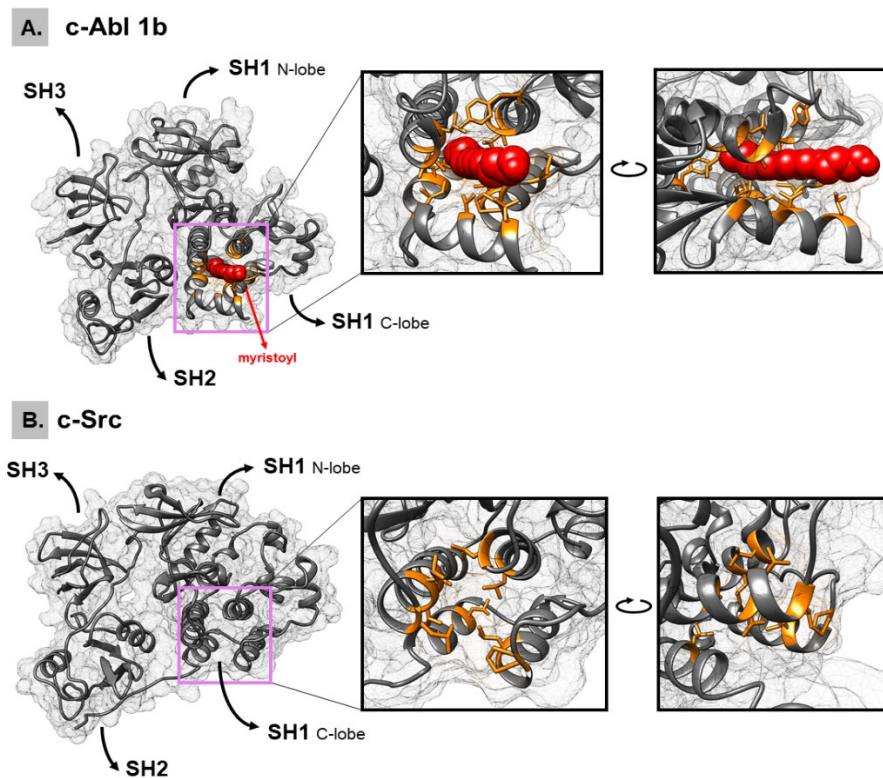
By similarities to the c-Abl kinase structure, Cowan-Jacob and coworkers (2005) predicted a hydrophobic pocket in c-Src, for myristoyl binding, in the C-terminal lobe of the catalytic SH1 domain (*Figure 1.9 B*). Their work reported perturbations in the NMR spectra upon myristate addition only when c-Src was phosphorylated at Y530 (i.e. in the auto-inhibited form), though the precise site was not recognized. Based on these observations, Patwardhan and Resh (2010) explored the critical residues (L360, E486 and T459) in the hypothesized pocket, however alteration of these residues had no effect[14] on the membrane anchorage suggesting absent interaction of the myristoyl moiety with the predicted pocket. Moreover, their work showed that in the kinase-inactive form, 80-90% of c-Src protein was bound to the membrane, suggesting that in this conformation the myristoyl moiety is exposed.

---

[14] T459A resulted in a slight increase of c-Src cytoplasmic fraction, however it was attributed to be induced by this specific mutation, as it would result in an artificial myristoyl pocket.

Recently, Spassov et al. (2018) marked the same SH1 C-terminal lobe hydrophobic pocket as a binding site for a second c-Src molecule through its myristoylated N-terminus. The second c-Src molecule is required to be in the kinase active form (pY419). Even though regulation and biological determinants for this dimerization are not clear, the authors point out increased auto-phosphorylation upon dimerization, although self-phosphorylation is pre-required for dimerization. Nonetheless, identification of a *self-myristoyl binding site* in the individual c-Src remains elusive.

It is clear that c-Src dynamic membrane binding involves the two signal myristoyl plus PBC interaction, however how the protein is *switched off* from the membrane, apparently has not been assigned to a specific mechanism but may be tuned by various PTM or regulatory partners. Phosphorylation of the SH4 domain residue S^{17} by the cAMP-dependent PKA kinase[15], has been associated with c-Src translocation from the plasma membrane to the cytosol (Walker et al., 1993). Murray et al., (1998) demonstrated 10-fold decrease in the membrane binding of a myristoylated peptide corresponding to the c-Src residues 2-19, phosphorylated at S^{17}. This PTM being a myristoyl electrostatic switch like MARCKS protein (myristoylated alanine-rich C kinase substrate), whose serine residues phosphorylation in the basic domain detaches the protein from the membrane. Although enhanced c-Src kinase activity concomitant to S^{17} by PKA has been reported (Schmitt and Stork, 2002), implying that unbinding of c-Src from the plasma membrane does not necessarily involves the kinase inactivation.

Interesting results by Huang et al., (2018) showed that acetylation of the lysine cluster (K^5, K^7, and K^9) in the SH4 domain by the CREB binding protein, results in c-Src dissociation from the cell membrane and translocation to the nuclei, where activates and undergoes complex formation with STAT3 protein, engaging into gene regulation.

Recently, Erwin et al., (2018) reported that the acyl-binding protein UNC119A, involved in the cellular trafficking of fatty-acylated proteins (Zhang et al., 2011), competes with the membrane for the myristoyl moiety of c-Src N-terminus, reducing the kinase membrane anchoring affinity. The myristoyl moiety tucks into the hydrophobic pocket of UNC119A (*c-Src myristoyl ligand-dependent conformational switch*).

Finally, c-Src in known to be sequestered into lipid rafts (Dwivedi et al., 2017; Oneyama et al., 2008), which are ordered membrane microdomains enriched in cholesterol and sphingolipids presenting distinct properties than the bulk membrane phospholipids. Thus, changes in the membrane composition could potentially modulate c-Src lipid binding affinity, as the former is known to regulate the two-signal membrane anchoring of c-Src (Buser et al. 1994; Kim et al. 1991; Peitzsch and McLaughlin 1993; Sigal et al. 1994).

To complete this introduction section, I would like to spotlight the role of myristoylation beyond membrane association. Indeed, multiple studies have noted a function for myristoyl as a stabilizing element of the acylated protein structure and function. As the case of the

---

[15] The cAMP-dependent PKA kinase recognizes the motif RxxS, as in c-Src residue $^{14}RRRS^{17}$ of the SH4 domain

N-terminal myristoylated guanylate cyclase-activating proteins (GCAPs) a group of Ca^{2+}-binding proteins related to the neuronal calcium sensors (NCS) family. Various NCS members, like recoverin, exhibit a calcium myristoyl switch conformation, that exposes the myristoyl group upon binding of Ca^{2+} for membrane engagement. The work by Stephen et al., (2007) provided the crystal structure of myrGCAP1 and demonstrated that myristoyl moiety remained buried in GCAP1 protein in the Ca^{2+}-bound conformation, in contrast to recoverin, suggesting a non-switching myristoyl system, that steadily holds the myristoyl buried in the protein. Structural details of myrGCAP1 revealed that the myristoyl moiety is key clustering element in the hydrophobic core of its structure providing conformational stability and required for full activation of the protein at signaling concentrations of Ca^{2+} (Stephen et al. 2007).

Additional evidences of this myristoyl role include: observation of higher melting temperatures of myristoylated calcineurin compared to the non-acylated form (Kennedy et al., 1996), local structure transition from ordered to disordered state in the recoverin protein upon extrusion of the myristoyl group from its hydrophobic pocket (Ames et al., 1997) and minimization of frustration in protein folding of hisactophilin when the myristoyl is present (Smith et al., 2010). Lastly, Patwardhan and Resh (2010) demonstrated reduced kinase activity in the non-myristoylated c-Src form (G2A mutant) in *in vitro* assays.

It has been demonstrated that increased burial surface of hydrophobic elements in a protein, enhances its stability (Kuhlman and Baker, 2004; Malakauskas and Mayo, 1998). Burial of the myristoyl group within the protein may have evolved to favor this property.

1.4. Objectives

A novel functional role has been identified for the N-terminal region of c-Src comprising the intrinsically disordered SH4, Unique and the SH3 domains, so that this entire region is defined as the c-Src N-terminal Regulatory Element (SNRE). c-Src has also been reported to self-associate upon membrane binding through the myristoylated SNRE. The present thesis aims to further characterize the SNRE to shed light on the intrinsically molecular characteristics that could differentiate c-Src from other close related tyrosine kinases (Src Family of tyrosine Kinases (SFKs)) that have a conserved domain architecture. The main objectives are:

(I)   Characterization of the structural role of c-Src myristoyl moiety in the framework of its N-terminal interdomain IDR:SH3 fuzzy complex.

(II)   Evaluate the contribution of c-Src additional lipid binding regions in the SNRE in terms of membrane binding.

(III)   Identify the structural determinants of the c-Src self-association.

(IV)   Characterize the SNRE with the adjacent SH2 domain.

PART (II) Results and Discussion

Chapter 2

An intramolecular myristoyl binding site in c-Src

2.1. Context

Despite a century of accumulated knowledge on c-Src, there is still long way to fully understand the details of the *design* of this tyrosine kinase. Various efforts (Cowan-Jacob et al., 2005; Patwardhan and Resh 2010) have been placed to uncover the myristoyl-binding pocket of c-Src, nonetheless it is still not clear how c-Src retrieves its myristoyl moiety from the non-favorable aqueous milieu when it is not bound to the membrane.

c-Src membrane binding has been extensively characterized, underlining that membrane anchorage takes place through synergistic action by hydrophobic burial of the myristoyl moiety and electrostatic interaction of the polybasic cluster (PBC) in the SH4 domain (Sigal et al., 1994; Silverman and Resh 1992). However, whether the discovered additional lipid binding regions of c-Src (Pérez et al., 2013), namely ULBR and residues in the RT & nSrc loops of the SH3 domain contribute to this membrane binding, has not been assessed yet. Conversely, phosphorylation on S17 in the SH4 domain is known to reduce membrane binding affinity but has not been structurally characterized in the myristoylated c-Src construct.

Finally, recent work by our group (Maffei et al., 2015; Arbesú et al., 2017) elucidated the structural arrangement of the N-terminal region in which the IDR (SH4 and Unique domains) was shown to form a fuzzy interdomain complex around the SH3 domain through multiple weak contacts. The non-myristoylated version of the SH4 domain, was demonstrated to have a significant contribution in the interdomain fuzzy complex. The unavoidable question is whether the nature of this fuzzy complex is altered when the SH4 domain is in its native myristoylated form.

In this chapter we aim to shed light on these questions.

2.2. Production of myristoylated c-Src constructs

Previously, our group established the methodology (Flamm et al., 2016) to produce the myristoylated N-terminal region (residues 2-150) of c-Src comprising the SH4, Unique and SH3 domains (myrUSH3) using recombinant protein expression in *Escherichia coli*. The approach consisted in co-express the N-myristoyl tranferase (NMT) enzyme, given that bacteria lack the machinery for myristoylation, alongside the USH3 c-Src construct (SH4-Unique-SH3 domains). Both enzyme and substrate were encoded in a single bicistronic vector (pETDuet-1 (Novagen)). To initiate a rapid myristoylation, sodium myristate was added to the bacterial medium complexed to the carrier protein BSA.

However, as indicated in Flamm et al., (2016), one side product obtained was lauroylated protein. The lauroyl group is two carbon atoms shorter than the 14 carbon myristoyl moiety but confers very distinct biochemical properties. Thus, complete elimination of this byproduct is required. N-lauroylation occurs due to the lack of NMT specificity for the shorter acyl group. Since exogenous myristic acid is added to the media, it might trigger the β-oxidation metabolic pathway of the bacteria as an alternative means of energy source, producing lauroyl-Coenzyme A from the myristoyl one that apparently is not discriminated by the NMT. Complete separation of lauroylated protein from the myristoylated is difficult to be accomplished through liquid chromatography (*Figure 2.1.* (left)).

Figure 2.1. Size exclusion chromatography elution profiles of acylated USH3 protein obtained from the different modifications during the expression step. (left) Addition of just myristic acid. (middle) Addition of myristic and palmitic acids (right) Addition of myristic + palmitic acids and glucose 1h after the protein expression induction. *This elution profile corresponds to the mutant ^{63}LFG^{65} → ^{63}AAA^{65} myr/laurUSH3.
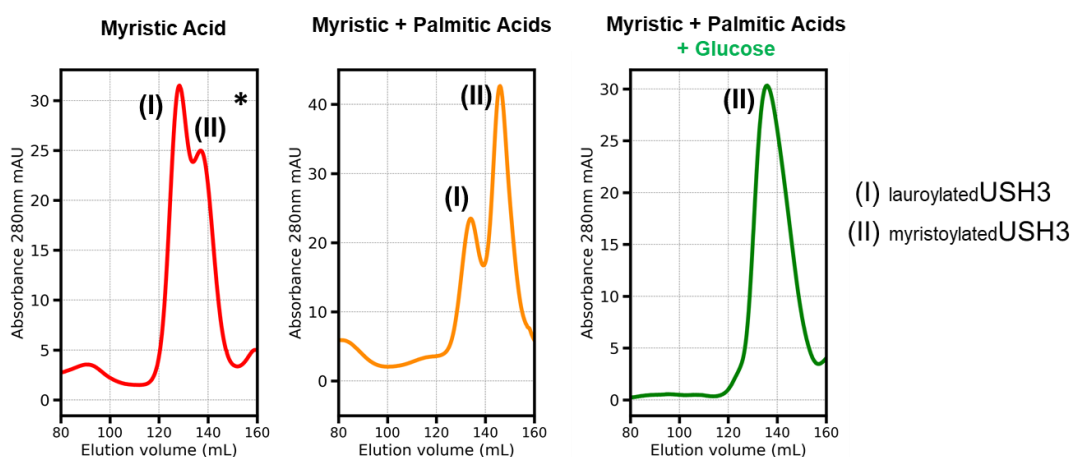
This issue was partially solved by adding a mixture of palmitic (16 carbon fatty acid) and myristic acid (1:1) to the bacterial medium instead of myristic alone, so upon β-oxidation of palmitic specie, the myristic one would be obtained. Although, this approach substantially decreased the lauroylated protein, significant amount of lauroylated was still present (*Figure 2.1.* (middle)), as indicated in the elution profile of the size exclusion

chromatography (last purification step). Thus, to circumvent this problem, I tried adding glucose (6 g/ L of culture) as additional energy source for the bacteria, 1h after the induction of the protein expression had started. This apparently solved the problem, enabling us to obtain a homogeneous myrUSH3 protein sample (*Figure 2.1.* (right)). Further analysis by mass spectrometry confirmed the sample purity.

For NMR studies, the Marley expression method (Marley et al. 2001) was used to prepare isotopic ^{15}N enriched myrUSH3 samples, as described in Flamm et al. (2015). However, when ^{13}C labeling was required, we faced the N-lauroylation problem again. This is because the source ^{13}C is glucose and the amount of this reagent is restricted to the minimum necessary, mainly because it is a very expensive reagent. Thence, to avoid N-lauroylation without adding extra glucose we reduced the amount of the myristic, and palmitic acid added to the bacterial medium from 200 μM (final concentration each) to 50 μM. The final protein obtained was still fully myristoylated.

The next hurdle in the production of myrUSH3 was found in the purification procedure. This protocol had to differ from the standard purification for non-myristoylated USH3 c-Src. Routinely, the bacterial cell suspension is lysed through sonication and subsequently the cell debris is separated through ultracentrifugation (pellet fraction). The non-myristoylated USH3 remains in the supernatant (i.e. solution fraction after ultracentrifugation) and is recovered from the supernatant via a Ni Affinity chromatography, since the construct bears a His$_6$Tag. The last purification step consists in a Size Exclusion Chromatography (SEC).

In the myrUSH3 case, the supernatant besides intact myrUSH3 also contained (1) myrUSH3 complexed to NMT (2) a significant amount of truncated myrUSH3 and (3) a small portion of non-myristoylated USH3. However, it was found that a significant intact myrUSH3 fraction also remained in the cell debris pellet (ultracentrifugation step). Thus, the supernatant was discarded and myrUSH3 was extracted from the pellet fraction by washing multiple times with a buffer containing detergent (1% v/v Triton X100) (*Figure 2.2.*A). The collected re-solubilized myrUSH3 fraction was further purified with Ni affinity chromatography. In this step, all the buffers would not contain the detergent, so that the elution product is detergent free, as required for membrane binding assays. During the Ni affinity chromatography, spontaneous truncation of myrUSH3 occurs which elutes with the intact protein. However, it was found that at a low imidazole concentration (100 mM), while the truncated fragment of myrUSH3 completely eluted, the majority of intact myrUSH3 still remained in the Ni-NTA resin. Therefore, a step gradient Ni affinity chromatography was performed by eluting the truncated fragment with 100 mM imidazole (W(II) step *Figure 2.2.*A and D) and subsequently increasing the amount of imidazole to 400 mM to elute the intact myrUSH3. However, the final elution was also problematic, since large volumes of buffer were required to completely elute myrUSH3. Apparently, the myristoyl moiety would enhance hydrophobic interactions with the resin. We solved this issue by adding Triton X100 at a sub–Critical Micelle Concentration (CMC) (<0.02% v/v), this would ensure that Triton X100 could be removed in the SEC step.

Figure 2.2. Scheme of the purification steps for (A) "Pellet wash" protocol and (B) Supernatant optimized. (C) Size exclusion chromatography elution profiles of the protein obtained from both protocols. (D) SDS-PAGE gel monitoring the purification steps of the Supernatant optimized protocol.

A "Pellet wash" protocol

Sonication

Centrifugation

1st Supernatant discarded

Centrifugation x3 times

Ni Affinity Chromatography

Ni-NTA

1. Load 2nd supernatant
2. Wash (I) 10mM Imid.
3. Wash(II) 100mM Imid.
4. Elution 400mM Imid +0.018%v/v Triton X100

Bacteria cell suspension — Lysate — 1st Supernatant

Pellet resuspeded in buffer with +1%Triton X100

2nd Supernatant

Size exclusion Chromatography

B Optimized protocol

+1%Triton X100

Sonication

Centrifugation

Ni Affinity Chromatography

Ni-NTA

1. Load 2nd supernatant
2. Wash (I) 10mM Imid.
3. Wash(II) 100mM Imid.
4. Elution 400mM Imid +0.018%v/v Triton X100

Bacteria cell suspension — Lysate — Supernatant

Size exclusion Chromatography

C

Supernatant optimized

"Pellet Wash"

D

MK = Protein marker
Lys = Cell lysate (after sonication)
Sup = Supernatant
FT = Flow Through Ni affinity chromatography
W(I) = 1st Wash fraction Ni affinity chromatography
W(II) = 2nd Wash fraction Ni affinity chromatography
E = Elution fraction Ni affinity chromatography

Although the "Pellet Wash" protocol enabled to obtain a pure sample of myrUSH3, the final yield, from 2 L of culture, was very poor (30-50 μM in 1 mL). Since the various techniques used for myrUSH3 characterization required to have a good amount of protein and increasing the number of cultures was unsustainable, I tried to further optimize the

purification procedure. The main issue was that the first discarded supernatant contained a substantial amount of intact myrUSH3 (along the problematic myrUSH3 forms). Thus, I changed the protocol by adding the detergent (1% v/v Triton X100) before the cell lysis with sonication. Now, after the ultracentrifugation the supernatant was more enriched with intact myrUSH3. During the Ni affinity chromatography, the elution volume of the W(II) step with 100 mM was carefully controlled and we were able to separate the non-desired products (myrUSH3:NMT complex, truncated myrUSH3 and non-myr USH3) from myrUSH3, since the latter eluted only at a higher imidazole concentration. The sub-CMC concentration of Triton X100 was also added to the elution buffer. (*Figure 2.2.* D). The subsequent steps were performed as previously. With this method the final yield (from 2 L of culture) increased almost 3 times (*Figure 2.2.*C).

One additional constrain when working with myrUSH3 was that the final concentration of the sample could not exceed 70-80 µM, since spontaneous truncation occurred. Thus, extra caution needs to be taken during the concentration step using the centrifugal concentrator system. The origin of this spontaneous truncation in myrUSH3 remains elusive, although it is certain that this phenomenon only occurs upon myristoylation, since USH3 and laurUSH3 do not exhibit this behavior under the same working conditions. We speculate that the myristoyl moiety confers a certain conformation in myrUSH3 enabling self-proteolysis. The truncation point is found within the Unique Lipid Binding Region between ^{63}L and ^{64}F (in the Unique domain) (^{58}AAAEPKL | FGGFNSS^{70}).

2.3. The fuzzy interdomain IDR:SH3 complex harbors the myristoyl moiety.

This part of the study focuses on the SNRE comprising the myristoylated SH4, Unique and SH3 domains, therefore we have employed c-Src constructs lacking the SH2 and SH1 domains. *Figure 2.3.* presents the schematic overview of the constructs and the nomenclature used in the following sections.

Figure 2.3. c-Src domain architecture with the schematic summary of the constructs used in the work presented in *Chapter 2.*
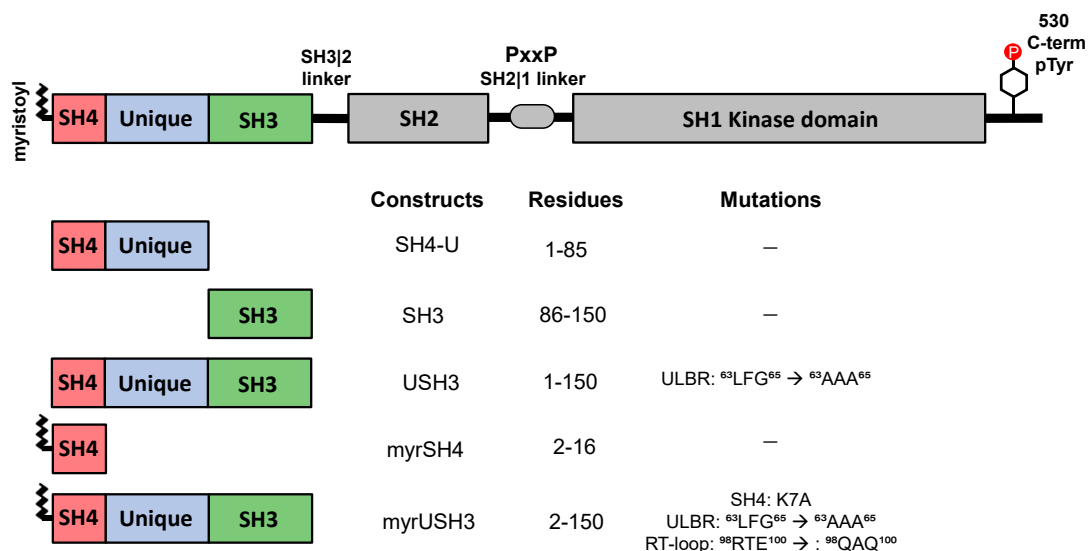
NMR can give us details of the protein at a residue level. Changes in the protein at selected regions can alter intra-molecular interactions, resulting in a new environment for the affected residues. In its *naive essence,* the NMR derived Chemical Shift Perturbation (CSP) analysis takes advantage of the latter.

Figure 2.4. ^1H ^{15}N HSQC spectra of myrUSH3. (A) the SH4 and Unique domains residues signals (spectra acquired at 278 K) and (B) the SH3 domain residues signals (spectra acquired at 298 K).
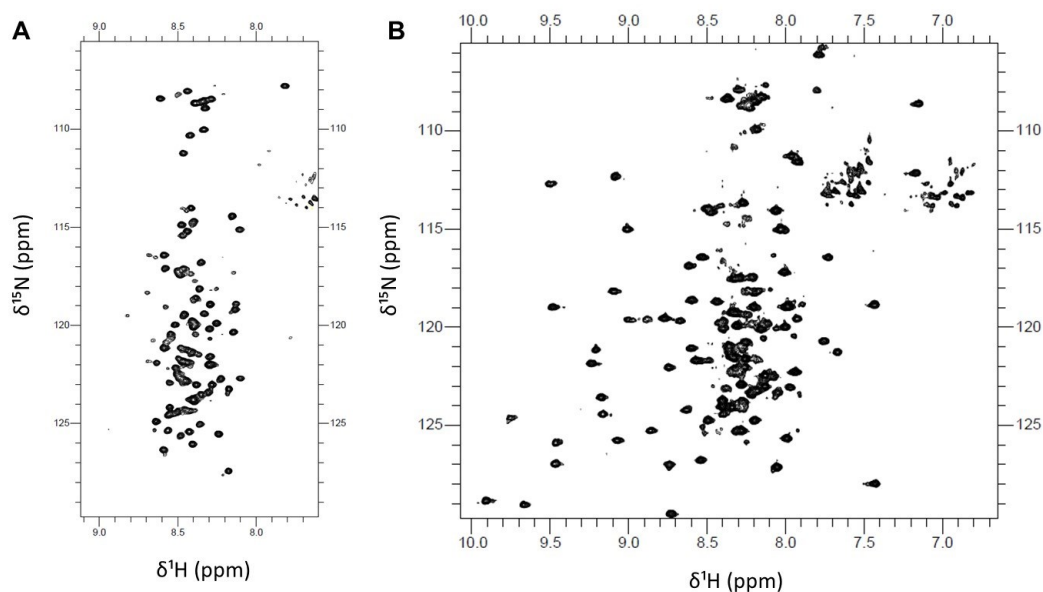
Given its sensitivity, amide backbone H-N is commonly chosen as a reporter of structural alterations in protein NMR and hence the 2D ^{1}H-^{15}N Heteronuclear Single Quantum Coherence (HSQC) has been the NMR experiment that we have exploited the most, which gives a ^{1}H-^{15}N chemical shift correlation peak per protein residue, for all amino acids except prolines. In other words, a ^{1}H-^{15}N HSQC provide us spectra with a unique pattern of signals for a given protein. *Figure 2.4.* shows ^{1}H-^{15}N HSQC spectra of wild type myrUSH3 at two different temperatures.

Our group had already assigned the spectra of the non-myristoylated construct USH3 of c-Src, however as the addition of the 14C myristoyl moiety was likely to affect the neighbor SH4 domain, we first verified the peak assignment for myrUSH3 spectra.

CSP analysis evidences the alterations upon changes in the protein, therefore it is necessary to define the reference state with respect to which the chemical shifts will be compared. The pairs of spectra to be compared differ in specific features whose effect is to be analyzed.

We used combined ^{1}H-^{15}N CSPs, that merges the changes in both ^{1}H and ^{15}N chemical shifts in a weighted manner, see *equation 2.1*.

Equation 2.1.
$$\mathrm{CSP} = \sqrt{\frac{1}{2}(\Delta\delta_H^2 + 0.2 \cdot \Delta\delta_N^2)}$$

CSPs can be viewed as a weighted Cartesian distance between the coordinates of peak in a certain protein state with the reference condition. The weighting used reflects the different sensitivity of proton and nitrogen chemical shifts to environmental changes (Williamson et al. 2013).

2.3.1. The N-terminal myristoyl moiety interacts with the SH3 Domain

We first analyzed the c-Src N-terminal Regulatory Element (SNRE) regions affected by the presence of the myristoyl, taking the non-myristoylated USH3 as the reference state. The combined ^{1}H ^{15}N CSP per residue between myrUSH3 with respect to USH3 are displayed in *Figure 2.5.*

Figure 2.5. Combined ^{1}H ^{15}N CSP of WT myristoylated myrUSH3 versus WT non-myristoylated USH3. Seagreen bars correspond to the CSP of the duplicated signals in the SH3 domain. The red line represents the significant threshold defined as the mean CSP for the lowest decile (μ(lowest decile CSP)) plus five standard deviations (5σ). Prolines are marked with *.
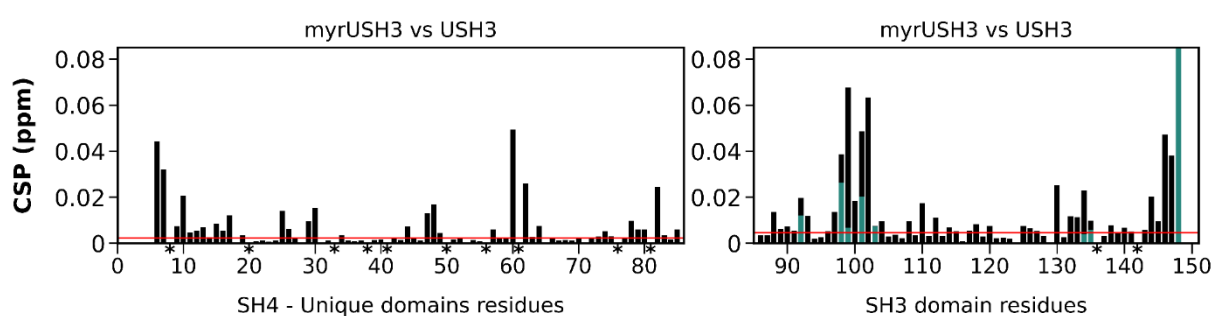
As expected, the CSPs of the SH4 domain indicate that this region is affected due to the myristoyl group attachment, being the N-terminal part the most altered. Residues S^6, K^7, D^{10} and S^{17} exhibit the highest perturbations in the SH4 domain. Large CSPs are observed in residues E^{60} and K^{62} of the ULBR. Other small CSPs in the Unique domain include residues: ^{25}HG^{26}, ^{29}GG^{30}, ^{47}HR^{48} and the segment prior to the hinge region ^{78}RAG^{80}. The hinge region is not significantly affected when the myristoyl moiety is present, with exception of moderately affected L^{82}, suggesting that even though the Unique domain have sensed the presence of the acyl chain (i.e. perturbations observed), the local interactions near the attachment between the two domains have not changed. Together with the small number of perturbations observed in the Unique domain, these results indicate that the fuzzy complex and the network of IDR:SH3 domain interactions existing in absence of the myristoyl group, are presumably maintained in the myristoylated form of the USH3, i.e. the fuzzy interdomain IDR-SH3 complex exists in the native myristoylated c-Src. So, where do the few perturbations in the Unique domain stem from? Before engaging into the latter question, we analyze the SH3 domain.

In the SH3 domain CSP plot of myrUSH3 with respect to USH3 (*Figure 2.5.* (right) and *Figure 2.6*A), we note the myristoyl-dependent chemical shift changes in this domain. High perturbations are observed in the segment ^{97}SRTETDL^{103} of the RT loop and the region in contact with this loop: residue G^{130} (distal loop) and the ^{132}TGYI^{135} segment of the β_4 strand. The C-terminal region of the SH3 domain and the β_1 strand in contact with this

region, are significantly affected when the myristoyl group is present[16]. Interestingly, both regions contain hydrophobic residues as highlighted: [87]TT<u>FV</u>A<u>LY</u>[93] in β_1 strand and [144]DS<u>IQ</u>A<u>EE</u>[150] in the C-terminal region. Minor perturbations are observed in the β_5 strand [140]VAPS[143] preceding the C-terminal region.

Figure 2.6. (A) Combined ^{1}H ^{15}N CSP of WT myrUSH3 versus WT USH3 mapped over the c-Src SH3 crystal structure. (B) c-Src SH3 domain structure highlighting the residues that present duplication of signal in the ^{1}H ^{15}N HSQC spectra. (PDB: 1Y57)
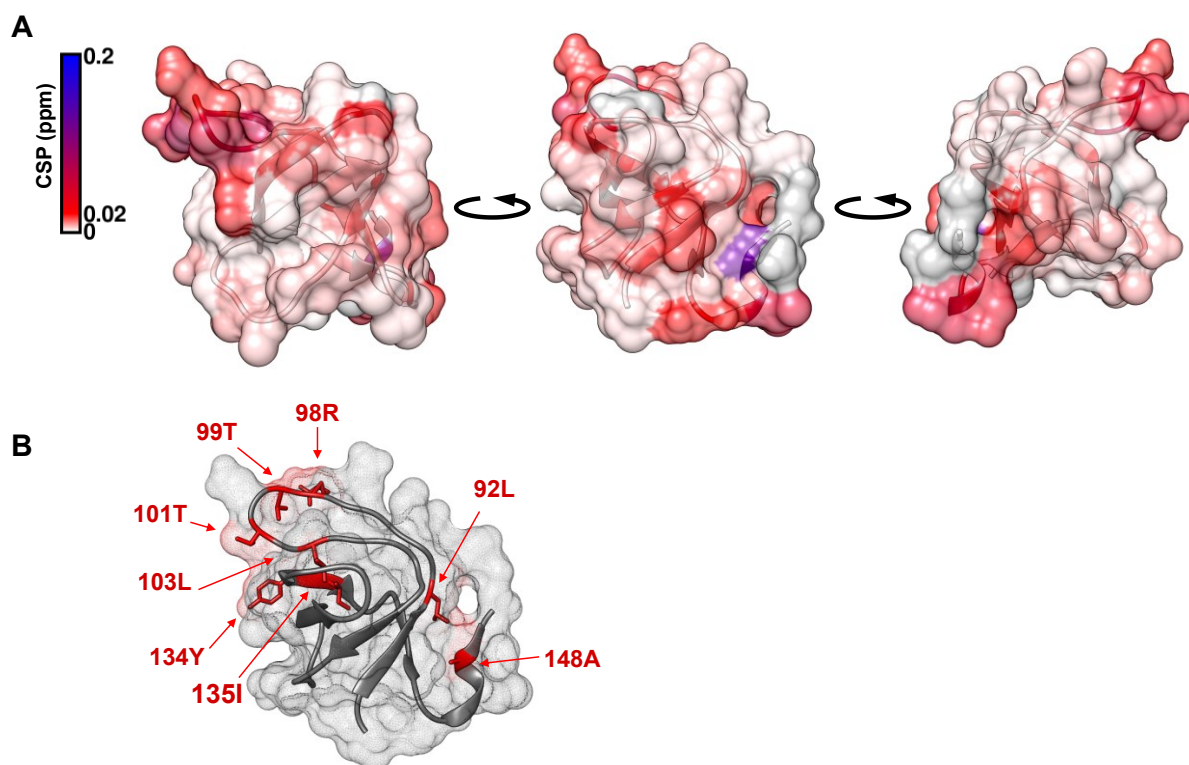
Intriguingly, in the above highlighted regions, duplicated signals were observed for the amino acids: L[92], R[98], T[99], T[101], L[103], Y[134], I[135] and A[148] marked in red in the *Figure 2.6*.B and with corresponding CSP in seagreen in *Figure 2.5.*, using USH3 as reference. Sample purity was carefully assessed; therefore, these duplicated signals probably appear due to a slow exchange between alternative protein conformations. Duplicated signals are not observed in the non-myristoylated USH3 construct. The conformation in myrUSH3 exhibiting the duplicated signals would have a more similar environment to that of USH3, since the CSPs have a lower magnitude (seagreen bars *Figure 2.5.* (right)).

Next, to assess the effect of the myristoyl group on the IDR (SH4 - Unique):SH3 interactions, that exist in absence of the 14C fatty acid, we used separately the isolated SH4-U construct and isolated SH3 domain as references and analyzed the CSPs induced

---

[16] Residues E149 and E150 have been excluded from the analysis due to difference in the C-terminal ends of myrUSH3 and USH3, since myrUSH3 bears a His$_6$Tag at the C-terminus.

on the IDR and SH3 domain of USH3 *Figure 2.7.* (top) and myrUSH3 *Figure 2.7.* (bottom).

Figure 2.7. Combined ^{1}H ^{15}N CSP of WT (top) non-myristoylated USH3 and (bottom) myristoylated myrUSH3 vs the isolated SH4-U (left) and isolated SH3 (right) domains. The red line represents the significant threshold: μ(lowest decile CSP)+5σ. Prolines are marked with *. Regions of interest are highlighted in gray.
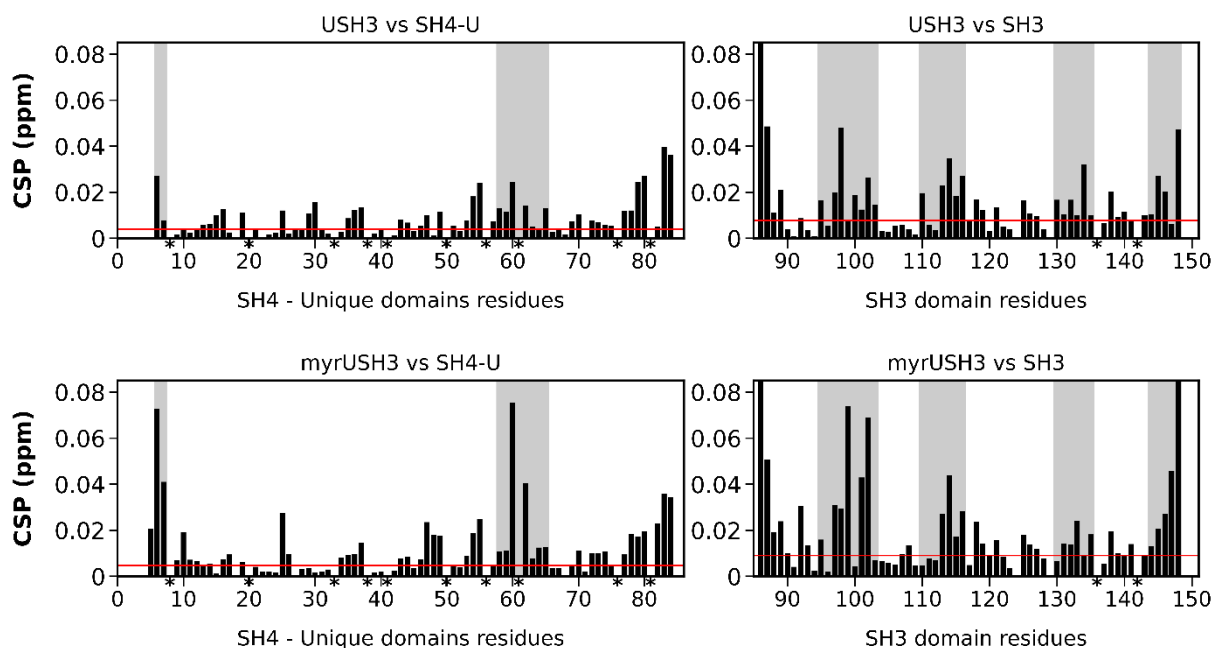
In general, as highlighted in the *Figure 2.7.* the same regions are affected in USH3 and myrUSH3, supporting the idea of the fuzzy IDR:SH3 inter-domain complex *existing* in native myristoylated c-Src. Nonetheless, the pattern of the perturbations is not the same in both constructs. With respect to the IDR, residues ^{6}SK^7, ^{25}HG^{26}, ^{60}EPK^{62}, ^{47}HRG^{49} exhibit large CSPs in myrUSH3. Conversely, residues ^{29}GG^{30} are perturbed in USH3 but not in myrUSH3, suggesting that the presence of the myristoyl group may cause these residues to experience a similar environment as in the isolated non-myristoylated SH4-U c-Src construct. The latter could stem from competing interactions directly or indirectly provoked by the myristoyl moiety against these residues for the SH3 domain or the IDR itself.

Apropos the SH3 domain in myrsUSH3 or USH3 with respect to isolated SH3 domain (*Figure 2.7* right panels), much larger CSPs are observed in the RT loop of myrUSH3 compared to USH3, suggesting that the presence of the myristoyl strongly affects this loop, either through direct interactions with the fatty acid or by redefining the interactions between the SH4 and SH3 domains. Similarly, the C-terminal segment and the spatially close β$_1$ strand of the SH3 domain, both containing hydrophobic residues, are significantly more affected by the presence of the myristoyl group. Residue L^{82} near the IDR-SH3 hinge region, that potentially could be in close contact with β$_1$ strand and the C-terminal region of the SH3 domain, is also affected when the myristoyl moiety is present.

In the first CSP analysis of myrUSH3 vs USH3 (*Figure 2.5.*), the residues [6]SK[7] were considered to be affected due to the presence of myristoyl group, however in view of the broad picture in *Figure 2.7.*, it is also plausible that these perturbations arise from an enhanced interaction of the SH4 domain with the SH3 domain, an interaction that already exists in absence of the myristoyl chain (*Figure 2.7* top-left panel), but the presence of the latter might positively reinforce pre-existing interactions. This might also hold true for the affected residues [60]EPK[62] of the ULBR, the RT loop and the C-terminal region of the SH3 domain, which are also significantly affected in the presence of the 14C acyl moiety. In other words, the myristoyl group could be favoring the interactions of the IDR with the SH3 domain that lead to the fuzzy inter-domain complex formation (Arbesú et al. 2017). To investigate this hypothesis, we use Chemical Shift mapping.

Figure 2.8. Chemical Shift mapping for selected residues peaks of WT myrUSH3 (triangle) and WT USH3 (circle). $\Delta\delta$ ^{1}H (x axes) - $\Delta\delta$ ^{15}N (y axes) are calculated with respect to the isolated non-myristoylated SH4-UD and the isolated SH3 domain residues CS. Green cross represents 0.01 ppm.
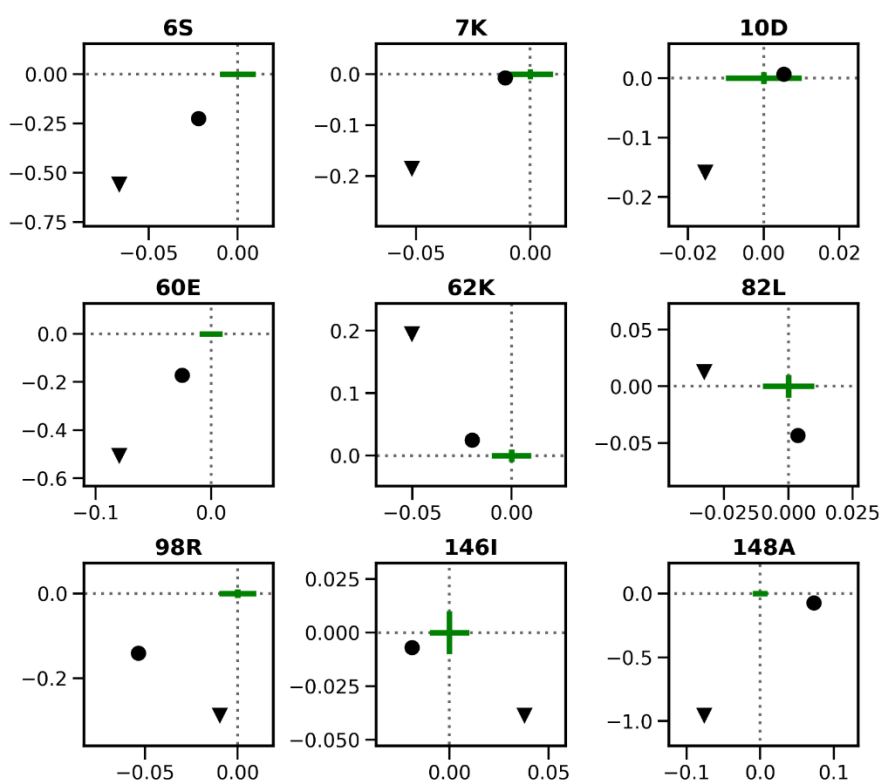
Analysis of combined ^{1}H, ^{15}N CSP, does not allow to distinguish between different chemical environments, in the sense that the same residue in different conformations of the protein can exhibit equal CSP albeit having different chemical shifts. CSP reports the *magnitude of the change* (i.e. distance), but not the nature. However, Chemical Shift mapping by comparing peak positions with respect to a common reference state ($\Delta\delta$ ^{1}H - $\Delta\delta$ ^{15}N plot) (*Figure 2.8.*), possibly enables to differentiate the chemical environments that render a similar CSP. We have used the chemical shifts of the isolated non-myristoylated SH4-UD

construct and the isolated SH3 domain as reference states (= loss of interdomain interactions and myristoylation) and represented the relative position $\Delta\delta\ ^1H - \Delta\delta\ ^{15}N$ for selected residues peaks of WT myrUSH3 (black triangle) and WT USH3 (black circle).

In NMR protein-ligand titration experiments, the free and bound protein forms display distinct chemical shifts. In a fast exchange regime (weak interactions), a continuous change in peak position is observed as the ligand is added. Usually, in a 1:1 interaction the chemical shift position undergoes a linear change from the initial point. Keeping this in mind and that the fuzzy IDR:SH3 complex formation is indeed the interaction between two binding partners (IRD and SH3), we now check (*Figure 2.8.*) the aforementioned residues, whose CSP in the myrUSH3 may arise from an enhanced interaction of the IDR domain with the SH3 domain. As shown in *Figure 2.8.*, residues S^6, K^7, E^{60} and K^{62} display a linear change from the isolated IDR towards USH3 and myrUSH3. In contrast, other residues that presumably interact with the myristoyl group, e.g. L^{82} (near the IDR-SH3 hinge region, potentially in contact with the SH3 C-terminal region), R^{98} (RT loop), I^{146} and A^{148} (SH3 domain C-terminal region) does not exhibit this behavior. Overall, the experiments suggest that the myristoyl moiety increases the local concentration of the IDR in the proximity of the SH3 domain cooperatively favoring the pre-existing interactions in absence of the myristoyl group

The results up to this point, confirm that the c-Src IDR:SH3 interdomain fuzzy complex is conserved in the natively myristoylated form of the protein. Seemingly, the myristoyl moiety would favor the fuzzy complex formation by adding cooperative transient interactions, without altering the overall attributes that define the nature of a fuzzy interaction (i.e. retained disorder by the IDR (SH4-U) featuring multiple low affinity motifs towards the SH3 domain). Additionally, the CSPs analysis and the observed duplicated signals, indicate that the N-terminal myristoyl group interacts with the SH3 domain in the proximity of the RT loop and the groove formed by the C-terminal region and β_1 strand, implying that the myristoyl group is harbored in the fuzzy IDR:SH3 complex by interacting through multiple sites with the latter. Next, we analyzed the effect of myrUSH3 interaction with a negatively charged membrane, as it involves the burial of the myristoyl moiety into the lipid bilayer and the electrostatic interaction of the SH4 domain with the negatively charged phospholipids.

2.3.2. The interdomain IDR:SH3 fuzzy complex is retained in the c-Src membrane bound form

To study the interaction of the c-Src N-terminal region with a lipid membrane, we incubated myrUSH3 with negatively charged Large Unilamellar Vesicles (LUVs) formed by 1,2-dioleoyl-sn-glycero-3-phosphocholine (DOPC) and 1,2-dioleoyl-sn-glycero-3-phospho-10-rac-glycerol (DOPG) in a DOPC:DOPG ratio of (3:1). We used polyunsaturated lipids to ensure that lipid bilayers were in the liquid crystalline state in which proteins and lipids can freely diffuse.

Figure 2.9. Combined ^{1}H ^{15}N CSP of WT myrUSH3 bound to LUVs with respect to free WT myrUSH3. The red line represents the significant threshold: μ(lowest decile CSP)+5σ. Pink bars indicate residues signals that are absent only in one of the conditions compared. Prolines are indicated with *.
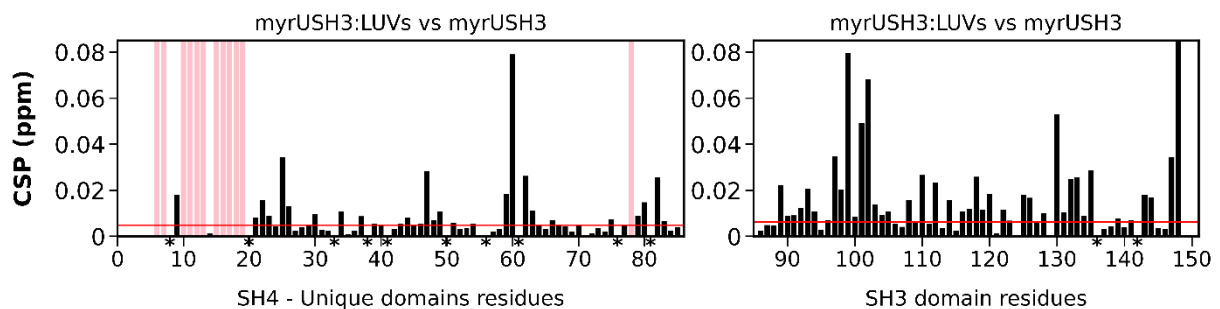
Figure 2.9. displays the CSPs of myrUSH3 bound to the LUVs with respect to free myrUSH3. The SH4 domain residues are broadened beyond detection, consistently with a strong interaction of the positively charged domain with negatively charged LUVs. Interestingly, the most perturbed residues in the Unique domain by the lipid interaction, are the same affected upon myristoylation of USH3. The latter could be interpreted as the intramolecular interactions that established a framework for the myristoyl moiety (i.e. fuzzy IDR:SH3 domain complex) are now in competition with the LUVs for the 14C fatty chain. Likewise, the SH3 domain of the myrUSH3-LUVs bound form (*Figure 2.10.* (right)) is considerably perturbed, also displaying similar regions affected by the myristoyl presence, except for the nSrc loop, that is more affected in the LUVs context.

To disentangle the possible interactions in myrUSH3 that have been lost or gained upon interaction with the lipid membrane, we used the same approach as in the previous section, analyzing the CSPs using separately the isolated non-myristoylated SH4-U construct and the isolated SH3 domain references against myrUSH3:LUVs complex. *Figure 2.10.* displays these results (for a better visualization I include the previous results on the same figure).

Figure 2.10. Combined ^{1}H ^{15}N CSP of WT (top) non-myristoylated USH3 and (middle) myristoylated myrUSH3 (bottom) LUVs bound myrUSH3 vs the isolated SH4-UD (left) and isolated SH3 (right) domains. The red line represents the significant threshold: µ(lowest decile CSP)+5σ. Prolines are marked with *. Regions of interest are highlighted in gray.
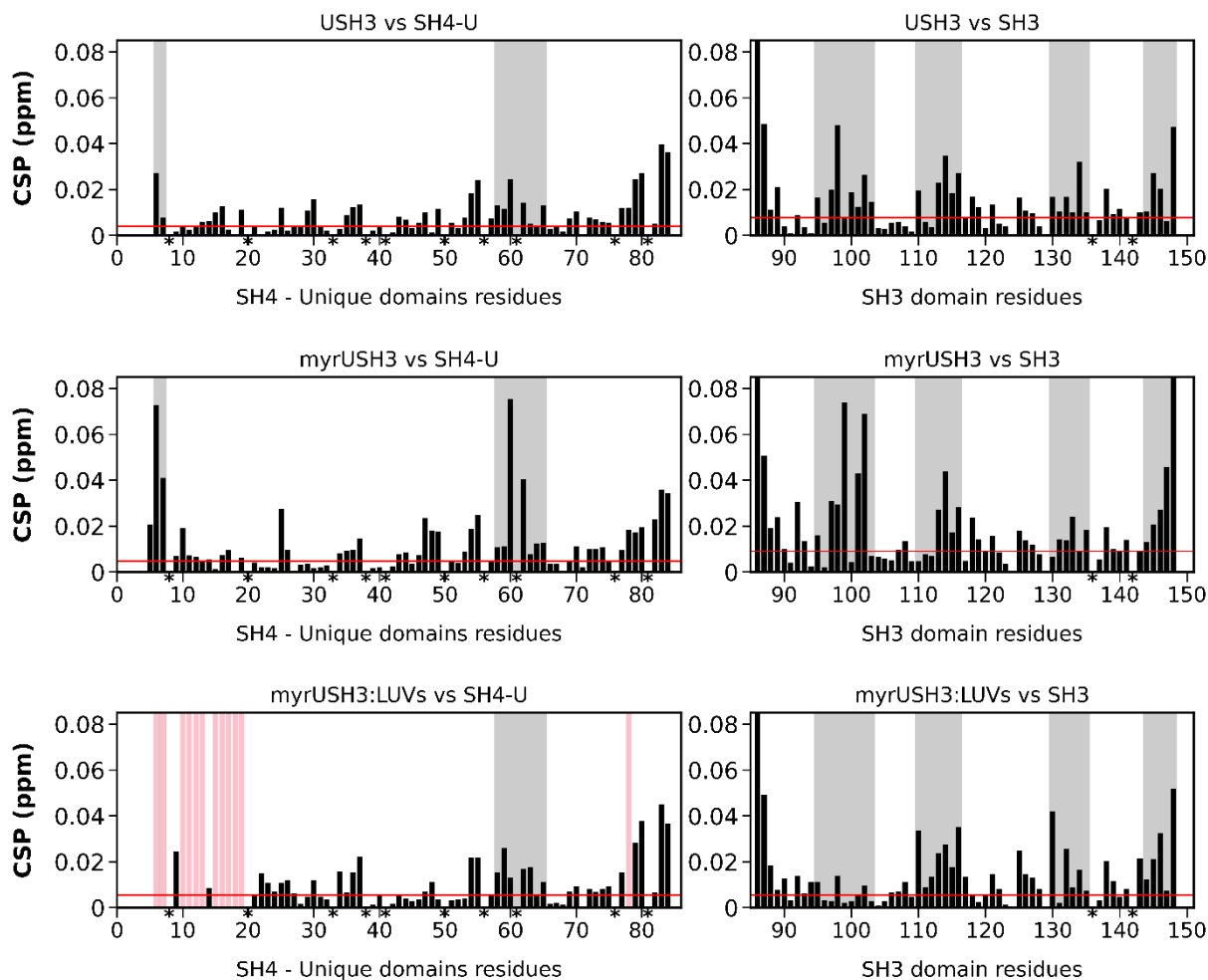
In a first overview (*Figure 2.10.* (bottom-left)), seemingly the SH4-U-SH3 domains in the myrUSH3:LUVs bound form have recovered the interactions as in the non-myristoylated USH3 construct, with the exception of the RT loop of the SH3 domain. In the IDR, residue G^{30} that "lost" interaction in myrUSH3 compared to USH3, is affected again in the myrUSH3:LUVs complex. Residues ^{60}EPK^{62} and L^{82} highly perturbed in myrUSH3, display chemical shifts similar to USH3, implying that the membrane-bound myrUSH3 retains a fuzzy interdomain complex with similar features as the non-myristoylated USH3.

Nonetheless, some of the IDR residues (^{34}ASQT^{37}, A^{59}, L^{63} and ^{79}AG^{80}) are slightly more affected in the membrane bound context compared to USH3, which can be a result of alternative interactions to compensate the less available myristoylated SH4 domain. The latter is also reflected in the CSPs of SH3 domain in the myrUSH3-LUVs context (*Figure 2.10.* (bottom-right)). With the evident exception of the loss of interactions of the RT loop, that adopts chemical shifts typical of an isolated SH3 domain. This is compatible

with the release of the myristoyl + SH4 domain from the RT loop triggered by membrane binding. However, the C-terminal region of the SH3 domain, which is also in contact with the myristoyl group, does not completely lose the interactions as the RT loop, but exhibits comparable CSPs as in non-myristoylated USH3. Likewise, the nSrc and distal loops display, a similar but not identical CSPs pattern as in USH3 (*Figure 2.10.* (top-right) vs (bottom-right)). Overall suggests that the fuzzy interdomain IDR:SH3 complex is preserved in the c-Src membrane-bound form and consequently, the SH3 domain remains close to the membrane surface. The conformational restraints of the myristoylated SH4 domain induced by the lipid anchoring, may hinder the interaction with the RT loop.

Interestingly, the ULBR: ^{60}EPKLFGGF^{67} that in the non-myristoylated USH3 was perturbed on interaction with lipid bicelles (Pérez et al., 2013), does not display significant CSPs in the myrUSH3:LUVs case, except for the N-terminal part of the ULBR ^{60}EPK^{62}, that presumably could be affected due to loss of interaction with the myristoylated SH4 domain, as this segment displayed changes when the myristoyl group was present in the USH3 construct. The ULBR is an amphipathic region, with a *hydrophilic head* ^{60}EPK^{62} and *a hydrophobic tail* ^{63}LFGGF^{67}, like a lipid. If the ULBR does not contribute additionally to lipid anchoring, the unavoidable question is: *which is the targeting "lipid" of this region?* To answer this question, we performed a previously used mutation AAA (^{60}EPK<u>LFG</u>GF^{67}→ ^{60}EPK<u>AAA</u>GF^{67}) in myrUSH3 that abolished the potential lipid binding capacity of the ULBR in the USH3 construct (Pérez et al., 2013).

2.3.3. The ULBR contributes in the myristoyl moiety interaction with the SH3 domain

In order to understand the role of the ULBR, we modified this region by introducing the mutation AAA (^{60}EPK<u>LFG</u>GF^{67}→ ^{60}EPK<u>AAA</u>GF^{67}) in the myrUSH3 construct (AAA myrUSH3) and the in non-myristoylated construct (AAA USH3).

Figure 2.11. Combined ^{1}H ^{15}N CSP of AAA myrUSH3 mutant vs WT myrUSH3. Seagreen bars indicate the mutated residues ^{63}AAA^{65}. The red line represents the significant threshold: µ(lowest decile CSP+5σ. Prolines are marked with *. Pink bars indicate residues that are absent only in one of the conditions compared.
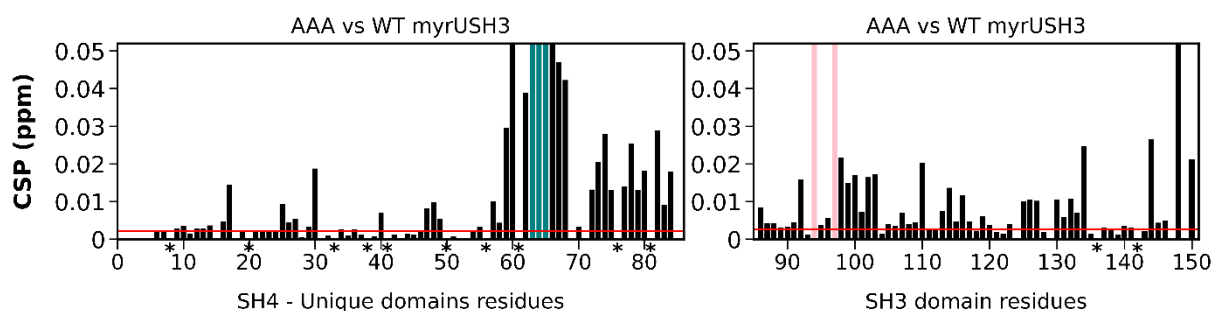
The mutation AAA in myrUSH3 with reference to the WT form (CSPs *Figure 2.11*) does not have any direct effect on the myristoylated SH4 domain as inferred from the CSPs, with exception of the S^{17} that is moderately affected. Besides the trivial perturbations in the regions close to the mutation points in the Unique domain, alterations are observed for G^{30}, the region prior hinge region (^{72}TVTSPQRAG^{80}) and the hinge segment itself (^{82}LAG^{84}). Regarding the SH3 domain of AAA myrUSH3, the mutation had more spread effects along this domain. Significant changes are observed in the RT loop (including the signal loss for residues D^{94} and S^{97}), the segment in contact with this loop (β$_4$ strand plus distal loop) and the C-terminal region. Noteworthy, as previously pointed out, in the WT form the latter regions are sampled by the myristoyl moiety. Other affected regions include the nSrc loop, residue L^{92} (which is in contact with the SH3 domain C-terminal region). So, seemingly the AAA mutation affects the regions known to interact with the myristoyl moiety. Thus, it is reasonable to question whether the ULBR mutation itself directly renders those perturbations or provokes changes in the way the myristoyl moiety interacts with aforementioned regions.

To check how the fuzzy IDR:SH3 domain complex is affected by the AAA mutation when the myristoyl group is not present, we compared the AAA vs WT USH3 CSPs (non-myristoylated context) against above-mentioned results AAA vs WT <u>myr</u>USH3 CSPs (myristoylated context).

Figure 2.12. Combined ^{1}H ^{15}N CSP of (top) myristoylated AAA vs WT myrUSH3 and (bottom) non-myristoylated AAA vs WT USH3. Seagreen bars indicate the mutated residues ^{63}AAA^{65}. Pink bars indicate residues signals that are absent only in one of the conditions compared. The red line represents the significant threshold: μ(lowest decile CSP+5σ. Prolines are marked with *.
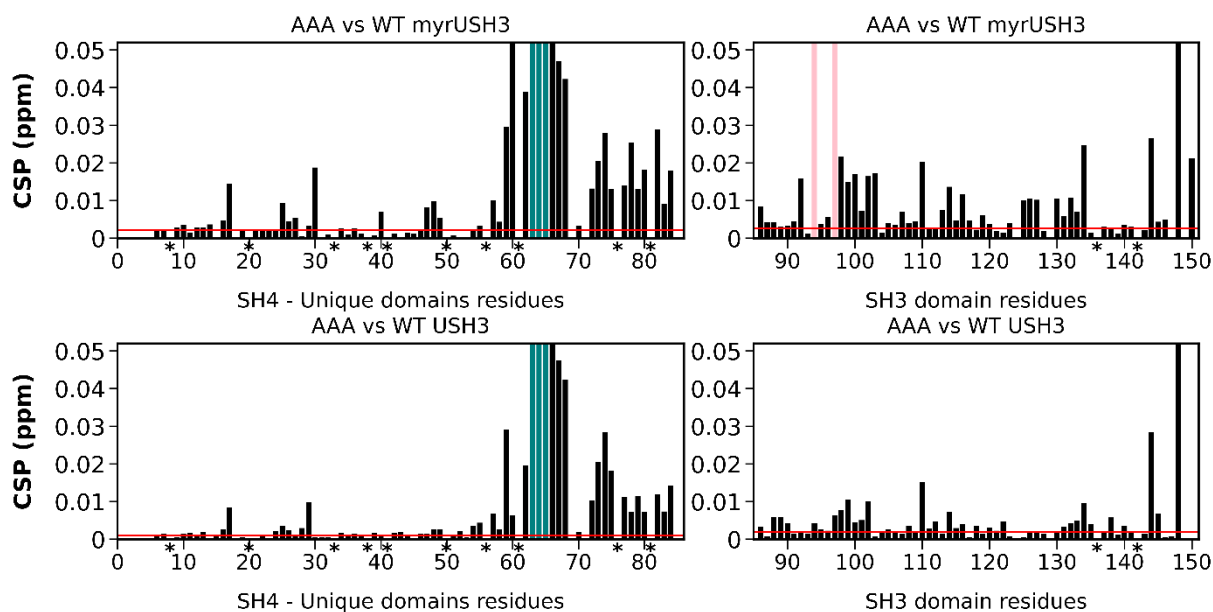
As displayed in *Figure 2.12.* (bottom), the mutation AAA has overall lesser effects in the non-myristoylated USH3 construct, suggesting that the larger perturbations observed in the AAA myrUSH3 construct, are presumably linked to the myristoyl moiety rather than the AAA mutation. This indicates that the ULBR might be important to frame the interactions of the myristoyl group within the fuzzy interdomain complex and thus the introduction of the AAA mutation changes the way the myristoylated SH4 domain interacts with the SH3 domain and thence the higher perturbations observed in the RT loop and the regions in close contact with this loop (*Figure 2.12.* (right panels)). Reinforcing this idea is the fact that no duplicated signals within the SH3 domain residues (attribute of a slow exchange between conformations) were observed in the AAA myrUSH3. To stress, the latter appeared in myrUSH3 but not in the non-myristoylated USH3 construct.

Moreover, whereas the perturbations of residues ^{66}GFN^{68} seems to be a direct consequence of the ^{63}LFG^{65}→ ^{63}AAA^{65} mutation as they are equally affected in AAA myrUSH3 and AAA USH3, changes in the N-terminal part of the ULBR ^{60}EPK^{62} are different in both constructs, being more perturbed in myrUSH3 AAA. Keeping in mind that in both cases the CSPs were calculated with the respective WT form (myrUSH3 or USH3), it may indicate that the combination of myristoyl + AAA mutation provoke the perturbations in ^{60}EPK^{62} of AAA myrUSH3, as these residues are less perturbed in the non-myristoylated AAA form. This could be related to the previous hypothesis, where we posit a different modulation of the myristoyl group by the ULBR due to the AAA mutation and a consequently distinct intramolecular interaction pattern of the myristoylated SH4 domain.

To better understand how the ULBR mutation affects the interactions of the myristoylated SH4 domain within the fuzzy IDR-SH3 inter-domain complex we proceed to the Chemical Shift mapping of the c-Src constructs.

Figure 2.13. (A) Schematic overview of the constructs used in the Chemical Shift mapping. **(B)** Chemical Shift mapping plot guide in the analysis of AAA and WT c-Src constructs.
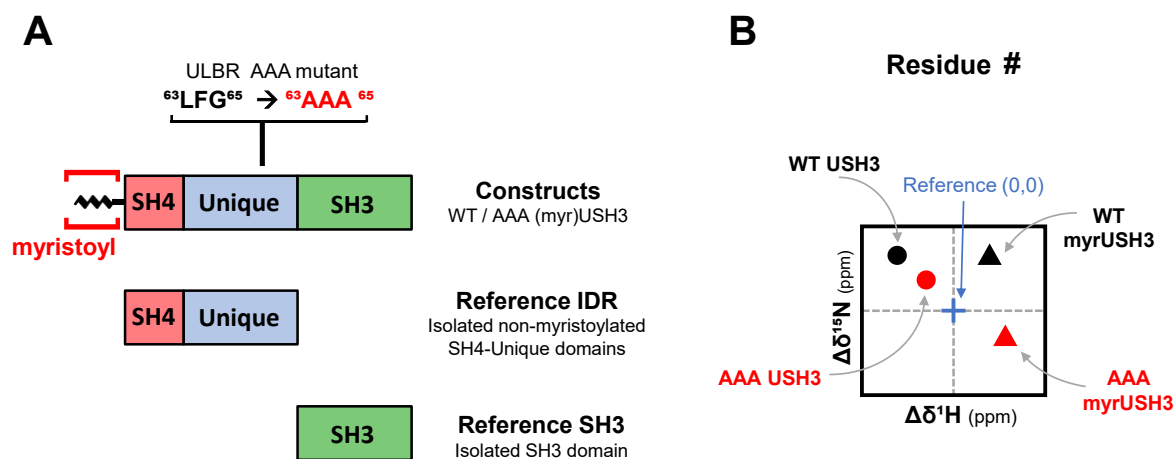
We have used the chemical shifts of the isolated non-myristoylated SH4-U construct and the isolated SH3 domain as reference states (*Figure 2.13.*) and represented the relative position $\Delta\delta$ ^{1}H - $\Delta\delta$ ^{15}N for each residue peak of WT / AAA myrUSH3 and WT / AAA USH3. Simultaneously mapping the $\Delta\delta$ of the four constructs renders a distribution of the positions in the plot, that is concurrently interpreted by pairs:

1. WT USH3 – WT myrUSH3: effect of the myristoyl group presence in the context of WT USH3

2. AAA USH3 – WT USH3: alteration caused by the ULBR mutation in the absence of the myristoyl group.

3. (AAA myrUSH3 – AAA USH3) vs (WT myrUSH3 – WT USH3): relative effect of the myristoyl group in the context of WT or ULBR mutation.

To provide visualization to the latter idea, *Figure. 2.14.* plots the possible encountering scenarios that would support the ULBR – myristoyl modulation hypothesis[17]. Note that close positions would denote a similar chemical environment, ideally the position would overlap.

---

[17] Although much more complex scenarios may also be feasible.

Figure 2.14. Possible encountering scenarios the Chemical Shift mapping analysis of AAA and WT c-Src constructs.
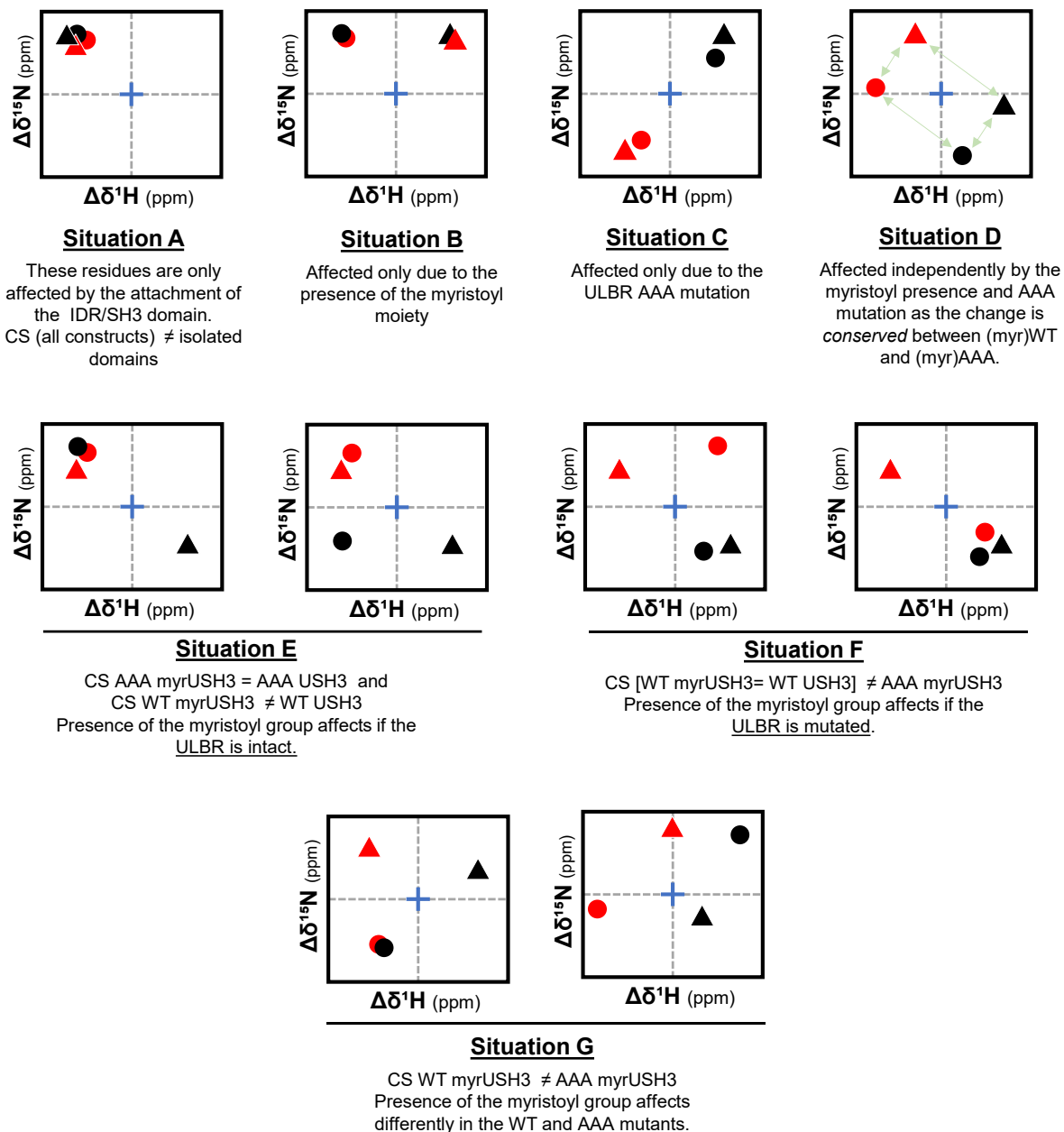
As indicated in the *Figure. 2.14.*, situations A-D would not provide evidence of a ULBR – myristoyl modulation, whereas situation E-G could be indicative of the latter. Although situation D indicates that the residue is affected by both the ULBR mutation and myristoylation, it does not imply a correlative effect among the latter as the change of the Δδ position plus its direction is conserved between the WT (myr)USH3 and the AAA (myr)USH3. Probably, it arises from a change in the protein conformation (indirect effect) that its independent and additive upon introduction of multiple protein alterations (i.e. AAA mutation or myristoyl presence). On the other side, situations E-G would display the cases where the myristoyl moiety presence senses the ULBR mutation, causing a distinct

signals pattern in the myristoylated forms that would be compatible to a ULBR – myristoyl modulation.

As previously stated, the AAA mutation affects the regions known to interact with the myristoyl moiety, which are the RT loop plus the regions in close contact with this loop (β_4 strand and distal loop), the C-terminal region plus the segments flanking this region (β_1 strand and L^{82} near the hinge region of the Unique domain) and as previously commented the N-terminal part of the ULBR $^{60}EPK^{62}$, which despite being near the ULBR mutation segment does not seem to be a direct effect of the latter.

Figure 2.15. shows the Chemical Shift mapping of the region around the ULBR ^{57}AAAEPKLFGGFNSS^{70}, excluding the mutated residues ^{63}LFG^{65}.

Figure 2.15. Chemical Shift mapping for residues in the ULBR of WT (black triangle) and AAA (red triangle) myrUSH3 and WT (black circle) and AAA (red circle) USH3. $\Delta\delta$ ^{1}H (x axes) - $\Delta\delta$ ^{15}N (y axes) are calculated with respect to the isolated non-myristoylated SH4-UD chemical shifts. Green cross represents 0.01 ppm.
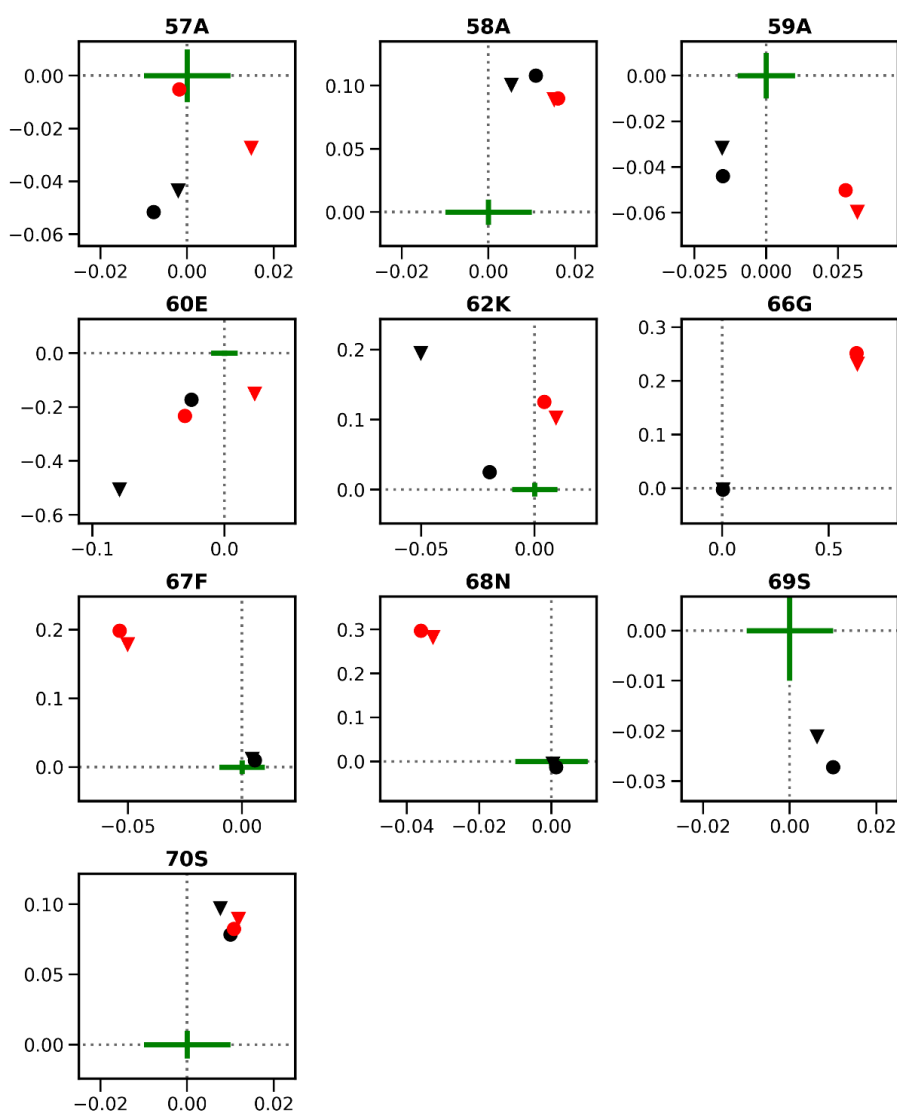
Residues [66]GFN[68] are directly affected by the AAA mutation and the effect is independent of the myristoylation state. Regarding the residue E[60], the AAA mutation has no effect in the absence of the myristoyl group but results in very different chemical shifts when the myristoyl group is present. On the other hand, residue K[62] chemical shifts in the mutated AAA form are independent of the myristoylation state, i.e. myristoylation affects the chemical shift of K[62] only when the ULBR is intact. Both situations support the ULBR-myristoyl modulation hypothesis.

The effect of myristoylation has to be understood as the interactions of the myristoyl moiety plus SH4 domain (myrSH4 elements). We have to keep in mind that neither the CSP nor the CS mapping allow us to recognize specific interactions between two residues. In the next, subsection we will confirm this hypothesis by mutating residue K[7] of the SH4 domain. Now we will complete our analysis focusing on the chemical shift perturbations observed in the SH3 domain.

Figure. 2.16. shows the Chemical Shift mapping for the C-terminal region plus the segments flanking this region (β_1 strand and L[82] near the hinge region of the Unique domain) and *Figure. 2.17.* displays the mapping. of the RT loop residues [96]ESRTETDLSF[105] and the regions in close contact with this loop: G[130] of the distal loop and [131]QTGYI[135] of the β_4 strand.

Figure 2.16. Chemical Shift mapping for residues of the SH3 domain C-terminal region plus the segments flanking this region (β_1 strand and L[82] near the hinge region of the UD) of WT (black triangle) and AAA (red triangle) myrUSH3 and WT (black circle) and AAA (red circle) USH3. $\Delta\delta$ [1]H (x axes) - $\Delta\delta$ [15]N (y axes) are calculated with respect to the isolated non-myristoylated SH4-UD and the isolated SH3 domain residues chemical shifts. Green cross represents 0.01 ppm.
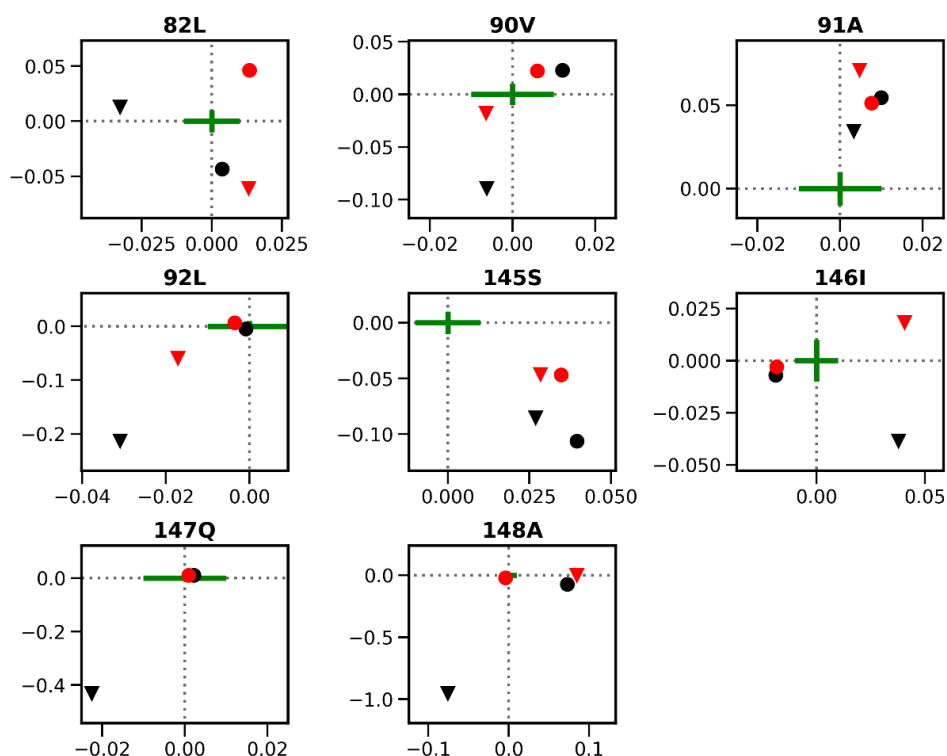
Figure 2.17. Chemical Shift mapping for residues of the SH3 domain RT loop and the residues in close contact with this loop of WT (black triangle) and AAA (red triangle) myrUSH3 and WT (black circle) and AAA (red circle) USH3. $\Delta\delta$ ^{1}H (x axes) - $\Delta\delta$ ^{15}N (y axes) are calculated with respect to the isolated SH3 domain residues chemical shifts. Green cross represents 0.01 ppm.
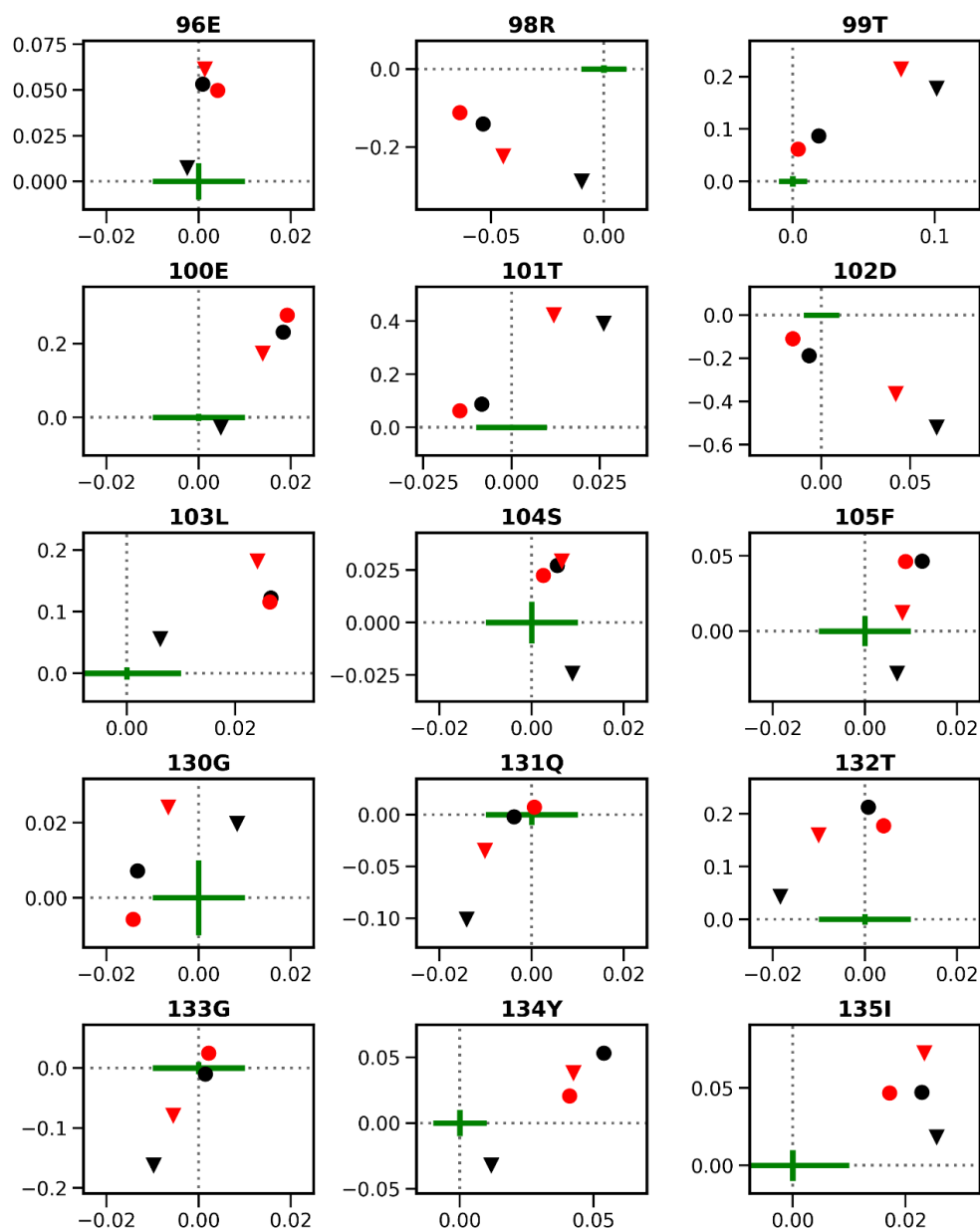
In general, all these regions match the hypothetical scenarios E-G that would support the ULBR – myrSH4 modulation. As displayed in the *Figures 2.16.* and *2.17.*, the effect of myristoylation on the chemical shifts of residues E^{96}, R^{98}, E^{100}, L^{103}, S^{104}, F^{105}, Q^{131}, T^{132}, G^{133}, Y^{134}, V^{90}, L^{92}, A^{148} is larger in the WT myrUSH3 form than in the AAA mutant. The AAA myrUSH3 chemical shifts a more similar to the non-myristoylated forms. The participation of the intact ULBR in the interactions involving the myrSH4 element would explain why duplicated signals in the RT loop and C-terminal region, that are observed in WT myrUSH3, are not observed in the AAA mutant.

During the production of the c-Src constructs, we perform a Size Exclusion Chromatography, a separation method by particle size (from larger to smaller) using a resin. Here we observe that WT myrUSH3 is retained longer in the resin than the non-myristoylated WT USH3, implying that the overall conformation of WT myrUSH3 is much more compact than USH3. From this we deduce that the myristoyl moiety is responsible of this compaction, which is consistent with the NMR results, suggesting that the myristoyl moiety enhance the fuzzy IDR:SH3 complex interactions. However, as inferred from the AAA mutation, an intact ULBR is needed for the proper interaction of the myrSH4 element in the fuzzy complex.

2.3.4. Complementary mutations in the SH4 domain and RT loop of the SH3 domain

In a quest to obtain complementary information about the myristoyl reciprocal modulation by the fuzzy interdomain IDR:SH3 complex we performed additional mutations in the SH4 domain and the RT loop of the SH3 domain. Previous work by our laboratory (Arbesú et al. 2017) showed that in the non-myristoylated USH3, ^{5}KS^6 → ^{5}AA^6 mutation, deletion of the first ten SH4 domain residues (Δ10 SH4) or the entire SH4 domain (Δ20 SH4) would affect the SH3 domain (specially the RT loop), being the effect of the first two c-Src alterations in opposite direction than the latter (Δ20 SH4). ^{5}KS^6 → ^{5}AA^6 mutation or Δ10 SH4 would enhance the IDR interaction with the SH3 domain.

In the myristoylated context (myrUSH3), it is not feasible to perform deletions in the SH4 domain, as it would impair myristoylation by the NMT. We intended to perform the K^5 → A mutation, however K5A myrUSH3 construct production results in a poor yield and low stability upon concentration of the protein sample. Apparently, the spontaneous truncation observed in the WT form is enhanced with the K5A mutation. Therefore, we decided to produce the K7A myrUSH3 mutant, that was produced in better yields compared to the K5A mutant. As already mentioned, non-myristoylated USH3 construct does not exhibit this spontaneous truncation, so somehow myristoyl moiety is linked to the latter.

Likewise, the RT loop mutation that was decided in first place was ^{98}RTE^{100} → ^{98}IHH^{100} a naturally occurring sequence in the SFK member Hck RT loop. However, this mutation also provoked an extensive IHH myrUSH3 truncated form, though in the non-myristoylated USH3 construct the same mutation does not have this effect. Thus, we decided to perform a more structural conservative mutation ^{98}RTE^{100} → ^{98}QAQ^{100}, where the pair of oppositely charged residues was replaced by neutral glutamine, whereas the central residue was mutated to alanine. QAQ myrUSH3 was produced in acceptable yields with no truncation at the working concentration, like WT myrUSH3.

The CSP plot of K7A myrUSH3 with respect to WT myrUSH3 is shown in *Figure 2.18.*

Figure 2.18. Combined ^{1}H ^{15}N CSP of K7A myrUSH3 mutant vs WT myrUSH3. Seagreen bar indicate the mutated residue K7A. The red line represents the significant threshold: μ(lowest decile CSP+5σ. Prolines are marked with *.

54
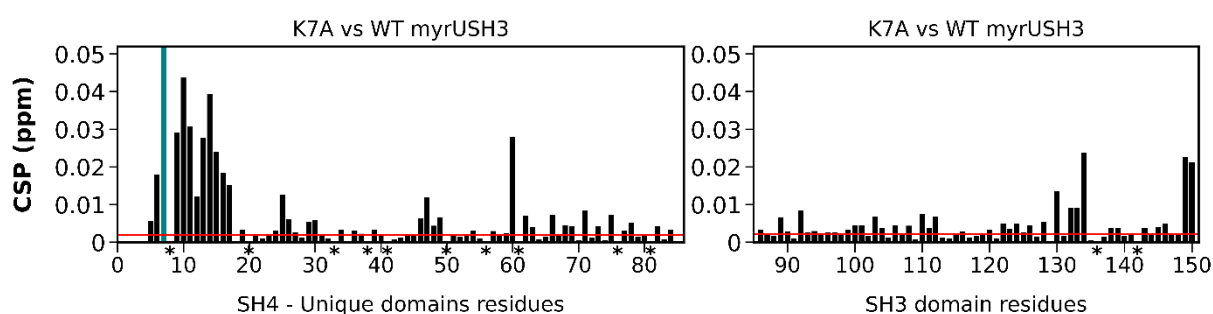
Interestingly, K7A affects the entire SH4 domain. The evident interpretation is that removal of a positive charge upon K7A mutation affects the charge distribution of the SH4 domain myrGSN<u>KS</u>K<u>PKD</u>ASQ<u>RRR</u>SL<u>E</u>P[...]. However, this behavior was not observed by Arbesú et al., 2017 in the K5AS6A USH3 mutant, although the position of the charge can question the argument. To seek alternative perspective, Chemical Shift mapping is used.

Figure 2.19. Chemical Shift mapping for residues in the SH4 domain of WT (black triangle) and K7A (orange triangle) myrUSH3 and WT USH3 (black circle). $\Delta\delta$ ^{1}H (x axes) - $\Delta\delta$ ^{15}N (y axes) are calculated with respect to the isolated non-myristoylated SH4-UD residues chemical shifts. Green cross represents 0.01 ppm.
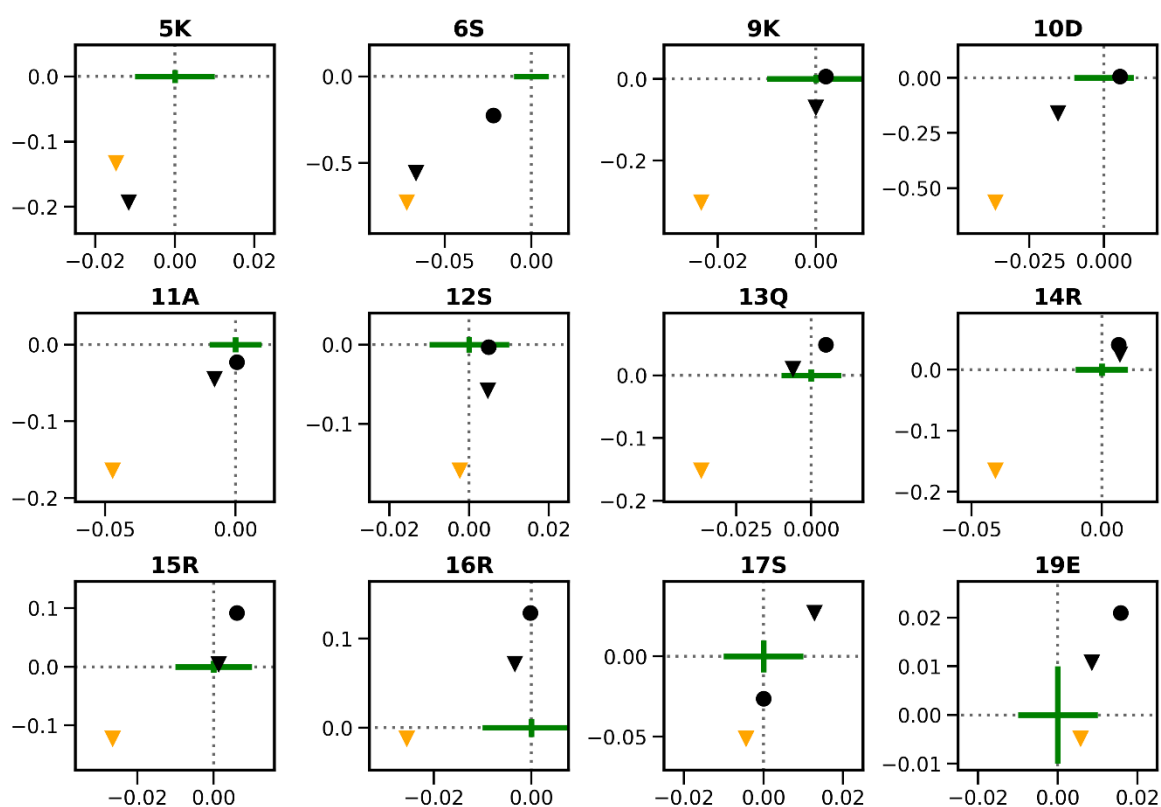
The chemical shift mapping of the SH4 domain is presented in the *Figure 2.19*. Intriguingly, K7A mutation shifts the signal position of the SH4 domain residues after P[8] towards a new state beyond the WT myrUSH3 maintaining the direction. The latter suggesting an enhanced effect on preexisting interactions. This is consistent to the previous results (Arbesú et al., 2017), demonstrating that deletion of the first ten residues or K5AS6A mutation would favor an intimate interaction the IDR and the SH3 domain. From the results presented here, it may seem possible that P[8] would define the boundary of the two regions in the SH4 domain having the opposite interacting behaviors.

Additionally, the CSP analysis (*Figure 2.18.*) show that the K7A mutation perturbs residue E[60] of the ULBR. The same perturbation was observed in Arbesú et al., (2017) Δ10-SH4 non-myristoylated c-Src construct (deletion of the 10 first residues of the SH4 domain), suggesting that the N-terminal part of the SH4 domain interacts with the N-terminal part of the ULBR, also in absence of the myristoyl moiety. Upon myristoylation and consequent

interaction of the fatty group with the C-terminal part of the ULBR ^{63}LFGGF^{67} the SH4 – E^{60} contact might be favored explaining the perturbation observed in the CSP plot of WT myrUSH3 (with USH3 as reference state, *Figure 2.18.*).

Figure 2.20. Chemical Shift mapping for residues in the ULBR of WT (black triangle) and K7A (orange triangle) myrUSH3 and WT USH3 (black circle). Δδ ^{1}H (x axes) - Δδ ^{15}N (y axes) are calculated with respect to the isolated non-myristoylated SH4-UD residues chemical shifts. Green cross represents 0.01 ppm.

The Chemical Shift map of the ULBR (*Figure 2.20.*) shows that in the K7A mutant, the signal from residue E^{60} shifts towards a USH3-like state, supporting the above observation. The reduction of the N-terminal SH4 contact with the N-terminus of the ULBR, may favor the SH4-SH3 domains interactions (i.e. less intramolecular competition). The C-terminal part of the ULBR ^{63}LFGGF^{67} exhibits a small perturbation in K7A myrUSH3 (CSP plot *Figure 2.18.*), which may imply that the myristoyl interaction may be somewhat different. The latter may be reflected on the CSP of the SH3 domain residues (*Figure 2.18.* right panel). Although, the SH3 domain seems to be almost unperturbed upon K7A mutation, it does not exhibit the same duplicated signals pattern, that appeared in WT myrUSH3 (*Figure 2.21.*) and is associated to the existence of alternative protein conformations.

Figure 2.21. c-Src SH3 domain structure highlighting the residues that present signal duplication the ^{1}H ^{15}N HSQC spectra in WT (left) and K7A mutant (right) myrUSH3. (PDB: 1Y57)
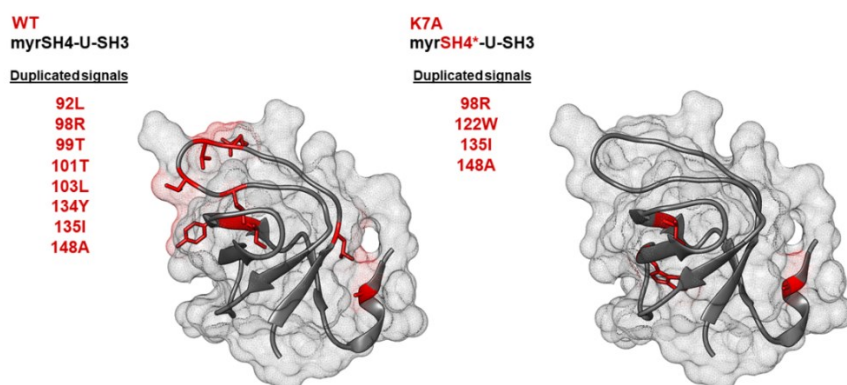
The duplicated signals in WT myrUSH3 exhibited USH3-like chemical shifts, meaning that one of the conformations is similar to the non-myristoylated USH3. In K7A myrUSH3, the resulting enhanced IDR:SH3 interaction may favor the myrUSH3-like conformation and thus not all the USH3-like duplicated signals are observed in this construct. The smaller perturbations observed in the SH3 domain may arise from the slightly different interaction of the myristoyl moiety.

Regarding the SH3 RT loop mutant, QAQ myrUSH3, the CSP analysis with respect to the WT myrUSH3 is presented in the *Figure 2.22.*

Figure 2.22. Combined ^{1}H ^{15}N CSP of QAQ myrUSH3 mutant vs WT myrUSH3. Seagreen bars indicate the mutated residues ^{98}QAQ^{100}. The red line represents the significant threshold: μ(lowest decile CSP+5σ. Prolines are marked with *. Pink bars indicate residues signals that are absent only in one of the conditions compared.
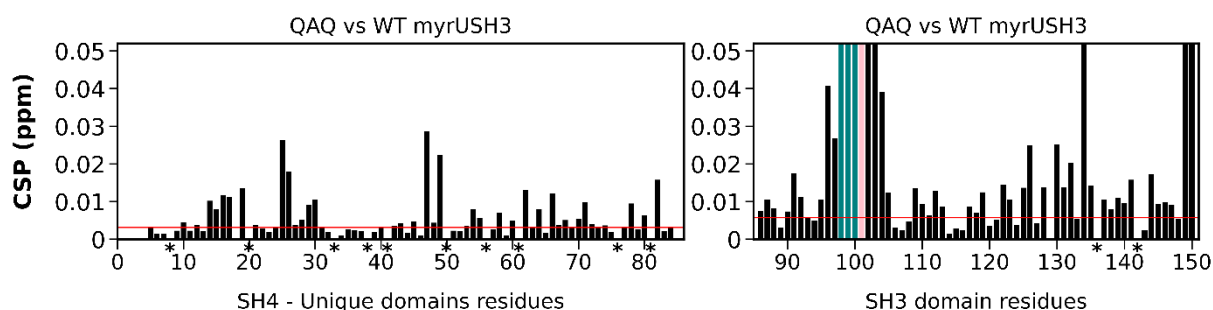
The QAQ mutation in myrUSH3 induce perturbations in the C-terminal part of the SH4 domain, residues 14-20, however, the N-terminal part of the SH4 domain does not exhibit significant CSP as well as the residue E^{60} (ULBR N-terminus) which is in harmony with the previous results. Other changes include residues ^{25}HG^{26}, ^{29}GG^{30}, ^{47}HR^{48}, the ULBR (K^{62}, F^{64}, and G^{66}), D^{71} and L^{82} (earlier stated to potentially interact with the myristoyl moiety). Overall suggesting that the regions known to interact with the myristoyl chain are affected by the RT loop mutation, an expected reciprocal effect due to the myristoyl binding site alteration. Nonetheless, the RT loop has been described as an *interaction hub* (Maffei et al., (2015), Arbesú et al (2017)) clustering most of the interactions with the IDR (SH4 - Unique domains) in absence of the myristoyl group. Therefore, the described perturbations may also arise from affected interactions with the IDR concurrent to the myristoyl ones, which could explain the changes observed in the C-terminal part of the SH4 domain upon RT loop mutation.

With respect to the SH3 domain, evident alterations are observed in the regions near the mutation segment ^{98}RTE^{100} → ^{98}QAQ^{100}, which include E^{96}, S^{97}, T^{101}, D^{102}, L^{103}, S^{128} and G^{130} of the distal loop and the ^{132}TGYI^{135} segment of the β$_4$ strand. Signal duplication of SH3 domain residues in QAQ myrUSH3, is not similar as in the WT myrUSH3 (*Figure 2.23.*), which clearly is a consequence of the mutation as the residues that exhibited signal duplication are now mutated or directly affected by the latter. Nonetheless, signal

duplication of residues E^{96} and I^{135} is observed which may be an indicator of the myristoyl moiety interaction with the SH3 domain but in a different manner.

Figure 2.23. c-Src SH3 domain structure highlighting the residues that present signal duplication the ^{1}H ^{15}N HSQC spectra in WT (left) and QAQ mutant (right) myrUSH3. (PDB: 1Y57)
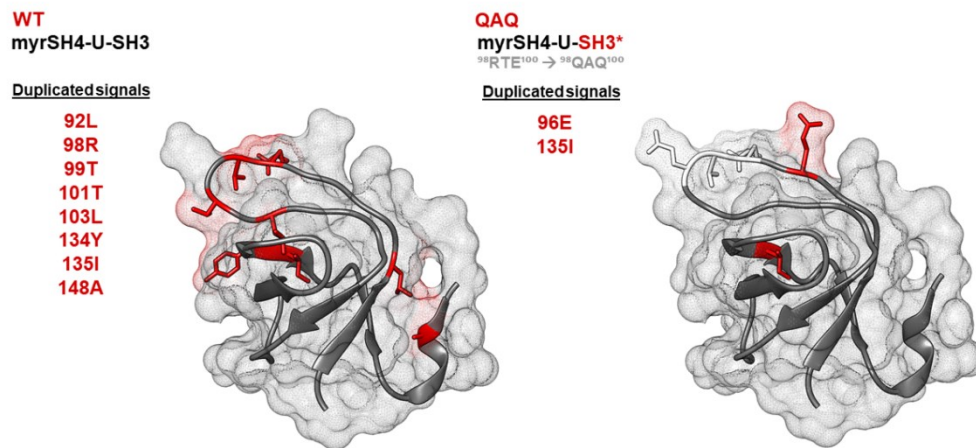

From the NMR results, the a priori additional lipid binding regions (ULBR, RT & nSrc loops of the SH3 domain) appear to interact and modulate the myristoyl acyl chain. To assess the effect of alteration of these additional regions in terms of membrane binding, we have used Surface Plasmon Resonance to measure the binding kinetics and affinities of the myrUSH3 constructs to neutral (DOPC liposomes) and a negatively charged membranes (DOPC:DOPG (3:1) and (2:1) liposomes).

2.4. Modulation of c-Src lipid binding

To evaluate the effect on the myrUSH3 membrane binding upon alteration of the additional lipid binding regions we use Surface Plasmon Resonance (SPR).

Figure 2.24. (top) Surface Plasmon Resonance setup (bottom) the sensorgram obtained during a binding measurement.
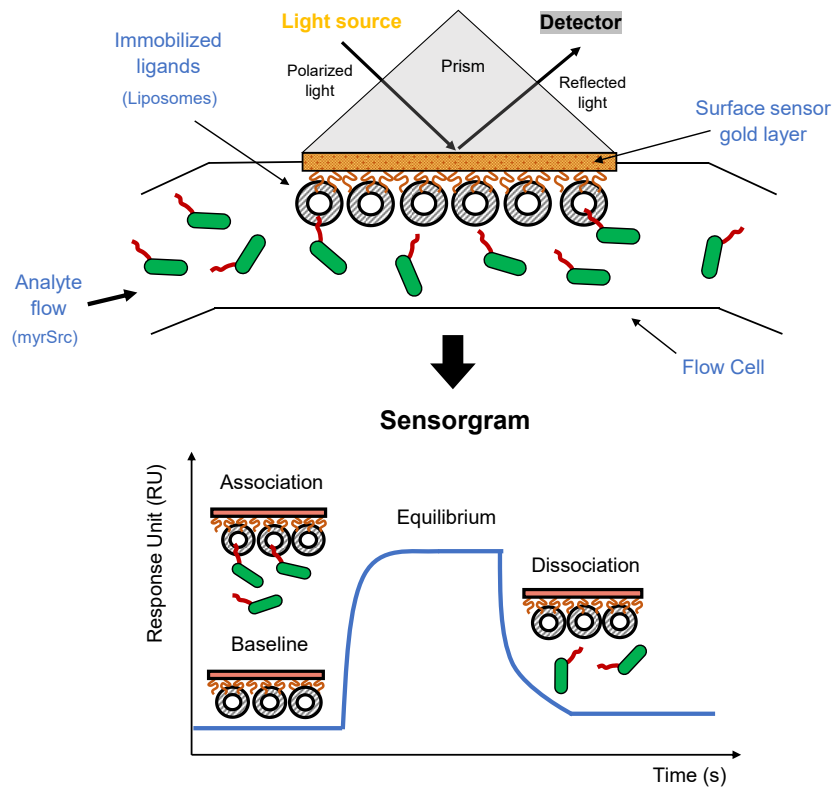
SPR spectroscopy is a label-free technique that allows to monitor molecular interactions taking place close to a gold surface (*Figure 2.24.*), in real time (Bakhtiar, 2013; Homola et al., 1999). One of the components in the binding assay is immobilized on the surface (ligand) while the other component is flowed over (analyte). In our case we deposited liposomes, as membrane mimics, to study the interaction with the myristoylated c-Src constructs. The measured interaction of the myrSrc constructs with the neutral or negatively charged liposomes is obtained in form of sensorgrams, i.e. curves representing the response signal over time and therefore accounting the association and dissociation events. To obtain the kinetics and affinity data, for our system, the sensorgram curves were fitted to the Langmuir model, which describes a simple 1:1 interaction. A more detailed description of the key protocol steps is given in *Chapter 3.*

The role of the additional lipid binding regions of c-Src was investigated using the QAQ, AAA and WT myrUSH3 c-Src constructs and compared to the isolated myristoylated SH4 domain construct (myrSH4) that would only contain the primary anchoring regions

(myristoyl moiety and the PBC of the SH4 domain). The c-Src constructs were tested over neutral DOPC and negatively charged DOPC:DOPG (2:1) or (3:1) liposomes.

Figure 2.25. presents the SPR analysis of the binding of c-Src variants to immobilized neutral and negatively charged liposomes. The main plot presents the association and dissociation rate constants, and the inset presents the affinity constants with an expanded region for the neutral liposomes.

Figure 2.25. SPR analysis of the binding of c-Src variants to immobilized DOPC (neutral), DOPC:DOPG (3:1) and DOPC:DOPG (2:1) (negatively charged) liposomes. The main plot presents the association and dissociation rate constants, and the inset presents the affinity constant. The affinity constants with neutral lipids are also represented in an expanded scale. Data were fitted to a 1:1 Langmuir model. Data expressed as mean ± SD, n = 3. Significant differences in binding constants with respect to WT myrUSH3 are indicated by asterisks (t test: *p < 0.05; **p < 0.01; n.s. not significant).
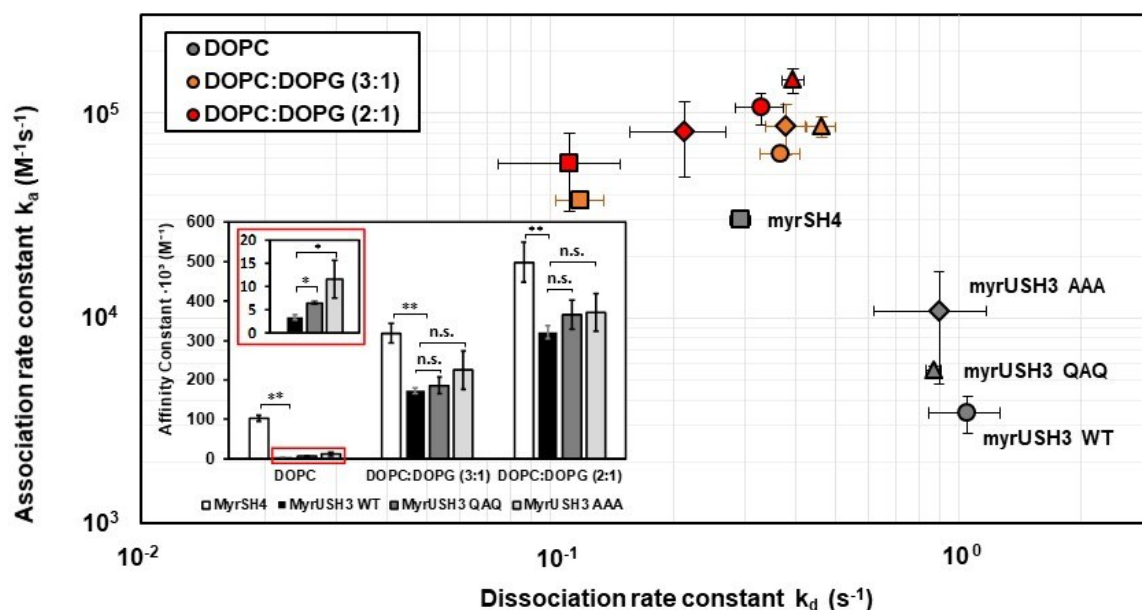
On neutral lipids, membrane anchoring of c-Src is mainly driven through the hydrophobic insertion of the myristoyl moiety, thus the binding affinity could be affected by how exposed the myristoyl group is to the lipids. As shown in the *Figure 2.25.*, the binding affinity of the isolated myristoylated SH4 (myrSH4) domain is nearly 25 times stronger than the variant containing the neighbor Unique and SH3 domains, even though these domains have additional lipid binding regions. The AAA mutation in the ULBR or the QAQ mutation in the SH3 RT loop resulted in increased lipid-binding affinity as a result of a faster association rate, suggesting a higher availability of the myristoyl group upon mutation of the mentioned regions. In contrast, dissociation rates were very similar, suggesting that the mutated sites do not directly interact with the lipid membrane. The lower dissociation rate of the isolated

myristoylated SH4 domain suggest that the neighbor Unique and SH3 domains modulate the way the myr-SH4 domain is anchored to the membrane.

These results are in agreement with the NMR data indicating that the myristoyl group maintain an intramolecular interaction with the SH3 domain assisted by the ULBR and upon alteration of these regions, the myristoyl group becomes more available.

The overall affinity is stronger with the incorporation of negatively charged lipids and the trend is maintained within the myrUSH3 c-Src variants, although the differences are not significative by the fact that now, the membrane anchoring is directed by the polybasic cluster of residues in the SH4 domain. A possible explanation is that in the release of the myristoyl group from intramolecular fuzzy complex is enhanced by the electrostatic interaction of the strongly charged SH4 domain when it is close to the negatively charged membrane. Nonetheless, the isolated myrSH4 domain still exhibits a higher affinity and a lower dissociation rate compared to the myrUSH3 constructs.

2.5. Effects of S^{17} phosphorylation

As presented in the introduction, the biological outcome of c-Src pS^{17}, although significant, remains unclear. This phosphorylation is postulated to contribute on the c-Src performance in different modes: as a binding motif for c-Src substrates or regulatory partners that lead to its activation, since enhanced activity of c-Src has been observed concurrent to the S^{17} phosphorylation[18] by cAMP-dependent PKA kinase (Obara et al., 2004). Also, potentially modulating c-Src subcellular location, as translocation of c-Src from the plasma membrane to the cytosol was detected upon S^{17} phosphorylation (Walker et al., 1993).

Arbesú et al., (2017) studied the structural effects of the S^{17} phosphorylation on the c-Src IDR using a non-myristoylated SH4-U construct. Their work showed that upon pS^{17}, some of the long-range interactions within the IDR were lost whereas other intramolecular contacts were enhanced, in particular the ULBR ^{64}FGGF^{67} segment and the regions around the residues A^{55}, H^{47} and S^{70} to G^{80}. Overall suggesting that pS^{17} could potentially tune the conformational ensemble of the N-terminal fuzzy interdomain complex.

To examine the latter, we performed *in vitro* phosphorylation of S^{17} by PKA in the myristoylated construct of c-Src, myrUSH3 and calculated the CSP with respect to the WT myrUSH3 (*Figure 2.26.*).

Figure 2.26. Combined ^{1}H ^{15}N CSP of pS^{17} myrUSH3 vs WT myrUSH3. Seagreen bars correspond to the CSP of the duplicated signals in the SH3 domain. The red line represents the significant threshold: μ(lowest decile CSP) + 5σ. Prolines are marked with *.
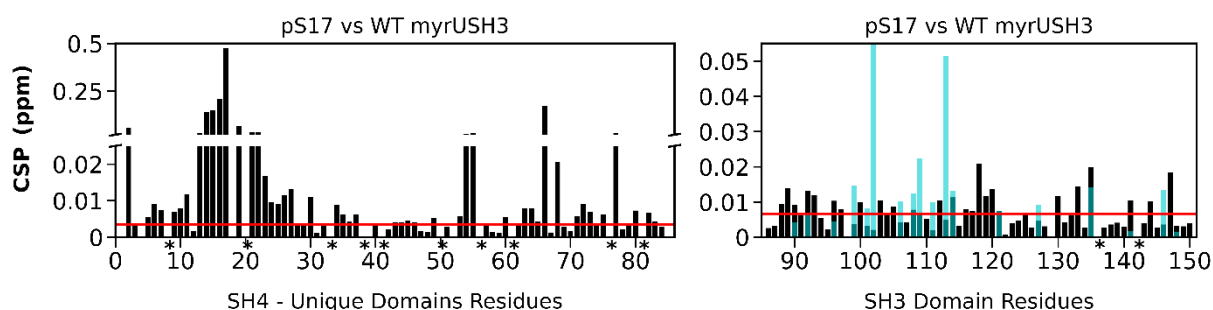

Evident changes in pS^{17} myrUSH3 are observed in the region around the phosphorylated S^{17}, including the ^{14}RRR^{16} arginine patch, which are most likely consequence of the perturbation in the native charge distribution due to the introduction of the phosphate group in the SH4 domain. Curiously, the N-terminal part of the SH4 domain which includes the positive stretch of lysines ^{5}KSKPK^9 sense negligible effects, as well as the ^{60}EPK^{62} segment, supporting the previously stated idea of this region (ULBR N-terminus) maintaining an intimate interaction with N-terminal part of the myr-SH4 domain. The other affected residues in the IDR displaying large CSP with respect to WT myrUSH3, are residues: G^2, F^{54}, A^{55}, G^{66}, N^{68} and Q^{77}. This is consistent with Arbesú et al., (2017)

---

[18] Note that pS^{17} is not an exclusive mode of activation as presented in *subsection 1.2.*

results, that showed enhanced contacts within these regions in the non-myristoylated isolated IDR upon phosphorylation of S[17].

Figure 2.27. Chemical Shift mapping of residue S[17] in the SH4 domain for WT (black triangle) and AAA (red triangle) myrUSH3 and WT (black circle) and AAA (red circle) USH3. $\Delta\delta$ ^{1}H (x axes) - $\Delta\delta$ ^{15}N (y axes) are calculated with respect to the isolated non-myristoylated SH4-UD and the isolated SH3 domain residues chemical shifts. Green cross represents 0.01 ppm.
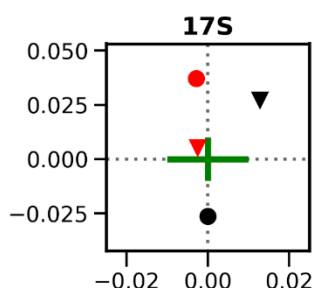
Results in the previous subsections, suggest that residue S[17] interacts with the C-terminal part of the ULBR ^{63}LFGGFN^{68}, as either the presence of the myristoyl group (that interacts with the ULBR) or the AAA mutation in this region, alter chemical shift of this residue (*Figure 2.27.*). Therefore phosphorylation of S[17] and the consequent observed perturbations in G[66] and N[68], are complementary in line with [S[17]]:ULBR interaction. Overall, as proposed by Arbesú et al., (2017), would illustrate an IDR residue playing the sensor role, tuning the outcome of the functional ULBR.

Apropos the SH3 domain in pS17 myrUSH3 (*Figure 2.26.* right) the CSP in the SH3 domain of pS[17] myrUSH3 showed smaller but spread effects along this domain. The spectra of this construct also exhibited duplicated signals additional to the observed in the WT myrUSH3, which are shown in *Figure 2.28.*

Figure 2.28. c-Src SH3 domain structure highlighting the residues that present signal duplication the ^{1}H ^{15}N HSQC spectra in WT (left) and pS17 (right) myrUSH3. (PDB: 1Y57)
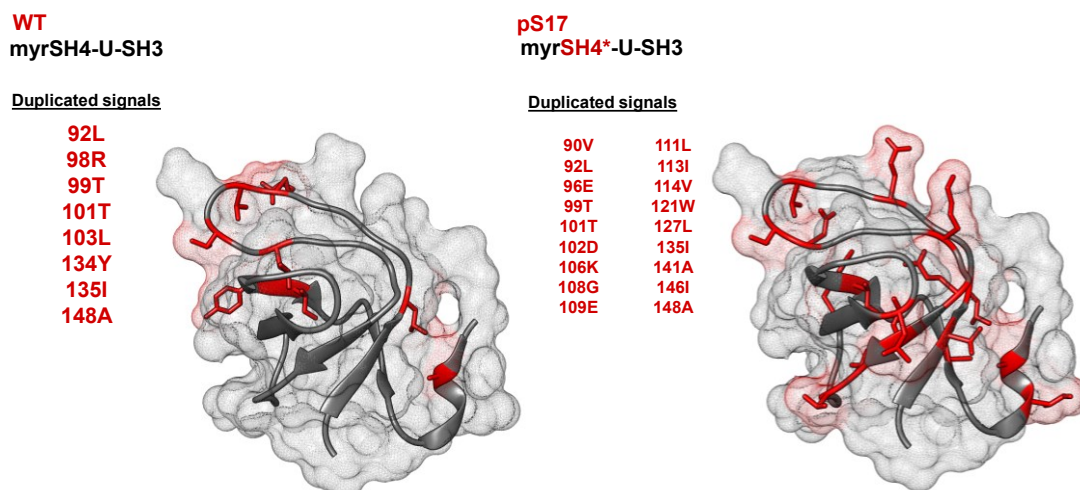
The high number of residues affected suggests a global effect. One hypothesis is that the pS[17] switches the IDR:SH3 conformational ensemble toward a state, where the intra-molecular interactions of the myristoyl group with the SH3 domain are preferred. Therefore, the myristoyl group would be preferentially interacting with the SH3 binding sites.

To gain insight in the latter hypothesis, the membrane binding of pS17 myrUSH3 was qualitatively tested over neutral DOPC and negatively charged DOPC:DOPG (2:1) lipids by checking the binding level using SPR. As indicated earlier, binding on a neutral lipid can indicate how available the myristoyl moiety is for the membrane, since the electrostatic interactions would not contribute. We compared pS[17] binding level to a mutant were K[7] was replaced by alanine, to have a reference as the K7A also decreases the global charge of the SH4 domain.

Figure 2.29. SPR analysis of the binding level of c-Src variants to immobilized DOPC (neutral) and DOPC:DOPG (2:1) (negatively charged) liposomes. The values were compared relative to the response for WT myrUSH3. Data expressed as mean $\pm$ SD, n = 3 (for WT#2 and pS17) n= 5 (for WT#1, K7A).
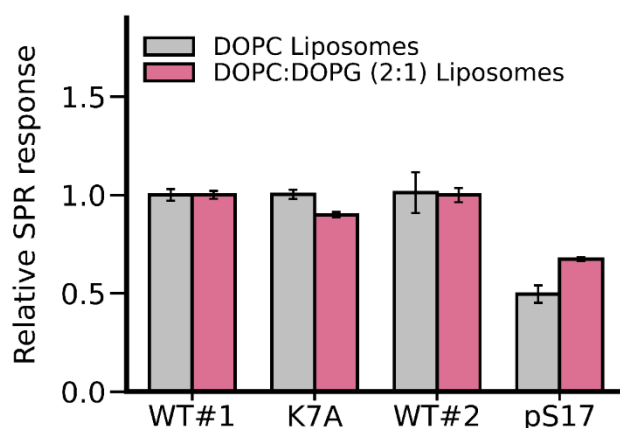
On the electrically neutral DOPC (*Figure 2.29.*) membrane, no difference in the binding level is observed between the K7A mutant and WT myrUSH3, whereas the pS17 myrUSH3 exhibits a ~ 50% reduction in the amount of protein attached to the surface. This result support our hypothesis, as the myristoyl group buried in the fuzzy inter-domain complex would be less accessible to the external lipids. Although this intra-molecular interaction exists in the WT form, as suggested by the NMR results, pS17 might favor the myristoyl buried conformation by changing the dynamics of the overall ensemble.

On the other hand, on negatively charged lipids, the electrostatic contribution to the membrane anchoring by the basic residues of the SH4 domain is present. This is reflected in the higher binding level of pS17 myrUSH3 on DOPC:DOPG (2:1) compared to the neutral DOPC membrane. However, the S[17] phosphorylation can further reduce the membrane anchoring on the negatively charged lipids, due to the presence of additional negative charge in the SH4 domain. Although, contribution in reducing the binding level by competing intramolecular myristoyl interactions cannot be ruled out.

2.6. Discussion

c-Src membrane binding has been characterized as a two-prong association, requiring the burial of its N-terminal myristoyl moiety and the electrostatic interactions of the basic residues cluster in the SH4 domain to the anionic lipids. c-Src membrane anchoring is mostly reversible, although evidence for clustering and irreversible binding of a small fraction of c-Src molecules has been reported (Owen et al., 2010; Le Roux et al., 2016a, 2016b; Smith et al., 2016). Membrane tethering is essential for c-Src activation by a membrane-bound phosphatase (Bagrodia et al., 1993; Buss et al., 1986). However, Donepudi and Resh, (2008) reported that approximately 30% of intracellular c-Src is not bound to membranes. Additionally, phosphorylation of the SH4 domain residue S^{17} by the cAMP-dependent PKA kinase, has been associated with c-Src translocation from the plasma membrane to the cytosol (Walker et al., 1993) and also enhanced c-Src kinase activity observed concomitant to pS17 has been detected (Schmitt and Stork, 2002), suggesting that plasma membrane detachment does not involves the kinase inactivation. This raises the question of possible interactions of the myristoyl group in the non-membrane-bound form of c-Src. The existence of internal myristoyl-binding sites may provide a modulating mechanism. Our results show that the c-Src N-terminal fuzzy IDR (SH4-U):SH3 complex harbours the myristoyl moiety.

The chemical shift perturbations and mapping analysis indicate that the presence of the myristoyl moiety increases the local concentration of the IDR in the proximity of the SH3 domain by cooperatively favoring the preexisting interactions (i.e. observed in USH3). Absence of the myristoyl group (USH3) leads to a more open/lose conformation, while myrUSH3 adopts a more compact conformation, however on average myrUSH3 remains in equilibrium between the open and compact states, as inferred from the signal duplication in the NMR spectra of myrUSH3 (SH3 domain).

Notwithstanding, the integrity of the fuzzy complex is retained in the presence of the myristoyl moiety, since the overall attributes that define the nature of a fuzzy interaction are not altered (i.e. retained disorder by the IDR (SH4-U) featuring multiple low affinity motifs towards the SH3 domain). The results indicate that the myristoyl group interacts with the SH3 domain in the proximity of the RT loop and the groove formed by the C-terminal region and β_1 strand, implying that the myristoyl group is harbored in the fuzzy IDR:SH3 complex through multiple contacts with the latter.

Additionally, a complementary mutational analysis has shown that the key Unique Lipid Binding Region (ULBR) ^{60}EPKLFGGNSS^{69} in the Unique domain is essential to adequately frame the interactions of the myristoyl group plus SH4 domain (myrSH4 elements) within the fuzzy IDR:SH3 complex. Mutation of the C-terminal part of the ULBR (^{60}EPKLFGGF^{67}→ ^{60}EPKAAAGF^{67}, the AAA mutation) highly perturbed the regions known to interact with the myristoyl moiety (SH3 RT loop plus the groove formed by the C-terminal region and β_1 strand). The same AAA mutation in the non-myristoylated USH3 construct had lesser effects in those regions, suggesting that the major alteration in AAA myrUSH3 would not stem from the AAA mutation itself but from changed interactions of

the myristoyl moiety with the SH3 domain. Mutation of the $K^7 \rightarrow A$ in the SH4 domain, affected the residue E^{60} of the N-terminal of the ULBR $^{60}EPK^{62}$. Thus, we hypothesize that the myristoyl moiety may interact with the C-termini hydrophobic part of the ULBR $^{63}LFGGF^{67}$, while the neighbor SH4 domain residues are in close contact with the N-terminal part of the ULBR $^{60}EPK^{62}$. Finally, reciprocal effects were shown upon mutation of the RT loop ($^{98}RTE^{100} \rightarrow ^{98}QAQ^{100}$) in myrUSH3, confirming that this region along the ULBR maintain intramolecular interactions with the myrSH4 terminus.

Upon membrane binding, the intramolecular interactions that established the framework for the myristoyl moiety (i.e. in the fuzzy IDR:SH3 complex) enter in competition with the membrane for the 14C myristoyl chain. The membrane-bound myrUSH3 retains a fuzzy interdomain complex with similar features as the non-myristoylated USH3. However, the SH3 domain RT loop loses all the intramolecular contacts, adopting a state similar to the isolated SH3 domain. The conformational restraints of the myristoylated SH4 domain induced by the lipid anchoring, may hinder the interaction with the RT loop, making this loop available for alternative protein-protein interactions (Arold et al., 1998). Overall, the fuzzy inter-domain IDR-SH3 complex is preserved in the c-Src membrane-bound form and consequently, the SH3 domain remains close to the membrane surface.

Built-in lipid pockets are present in various proteins. The Src related tyrosine kinase c-Abl has a myristoyl-binding pocket in the C-lobe of the kinase domain of c-Abl. Sequestration of the myristoyl N-terminus to this pocket enables the c-Abl inactive state by allosterically clamping the SH2-SH3 domain onto the catalytic SH1 domain (Pluk et al., 2002). Recoverin, a myristoylated Ca^{2+}-binding protein related to the neuronal calcium sensors (NCS), retrieves the myristoyl group within a hydrophobic pocket in the membrane unbound state (Tanaka et al., 1995). Upon binding to Ca^{2+}, recoverin extrudes the myristoyl group for membrane association. Another example is the UNC119, an acyl binding protein, that regulates the subcellular localization of myristoylated proteins by sequestering their acyl group into a hydrophobic pocket (Constantine et al., 2012). The common trait in all these myristoyl-binding sites is that the hydrophobic pocket is "rigid" / well-defined. However, in our c-Src case, the myristoyl group is trapped in a "not defined binding pocket" (i.e. the fuzzy IDR:SH3 complex). What could be the advantages of the "fuzzy pocket"? A "rigid defined pocket" would just allow two states, myr-in or myr-out, whereas a "fuzzy binding pocket" would expose the myristoyl in a tuned manner (e.g. modulation ULBR or SH3 RT loop). Another advantage could be the specificity. The hydrophobic pocket in UNC119 can accommodate lauroyl or myristoyl groups (Constantine et al., 2012). Additionally, neurocalcin (another member of neuronal calcium sensors (NCS)) in absence of Ca^{2+} was able to sequester the N-terminus acyl moiety to its integrated hydrophobic pocket even when the acyl group was a palmitoyl or lauroyl and not the native myristoyl moiety. However, a *fuzzy type* of interaction for the myristoyl moiety in c-Src, could presumably be highly specific (Sharma et al., 2015). In fact, the lauroylated version of c-Src USH3 (laurUSH3), adopted a similar open/lose conformation as the non-myristoylated USH3[19], whereas myrUSH3 presents a more compact conformation. This suggests that the

---

[19] As inferred from the retention time in the size exclusion chromatography.

lauroyl group is not able to maintain the same intramolecular interactions in the fuzzy IDR:SH3 complex as the myristoyl group.

In the *subsection 1.3*, we have reviewed some scenarios where myristoyl moiety had a role beyond the membrane anchoring. Among these roles, it includes to participate in protein-protein associations via interactions between acyl chains. For c-Src, the myristoyl group has been suggested to mediate c-Src dimerization by interaction with a hydrophobic pocket in the kinase domain (Spassov et al., 2018). The hydrophobic pocket in the SH1 domain was the one predicted by Cowan-Jacob and coworkers (2005), however it serves as a binding site for a second c-Src molecule through its myristoylated N-terminus. The second c-Src molecule is required to be in the kinase active form (pY419) and thus the protein would be in the open state. In the light of our results, this suggests that the myristoyl group could be buried in the fuzzy IDR:SH3 complex and competitive interactions may exist for the association of the myristoylated SH4 domain with either the membrane or the SH1 domain hydrophobic pocket of a second c-Src molecule (i.e. SH1 mediated dimerization).

Additional lipid binding regions in the SNRE, namely the ULBR, RT & nSrc loops of the SH3 domain, were shown to interact with lipid bicelles (Pérez et al., 2013) when the c-Src construct was not myristoylated (USH3). However, in the myrUSH3 context, these regions do not contribute to enhancing the c-Src membrane anchoring. The SPR membrane binding measurements revealed that the binding affinity of the isolated myristoylated SH4 (myrSH4) domain is stronger than the variant containing the additional lipid binding regions (myrUSH3) and upon mutation of these regions (ULBR & RT loop mutants) the affinity of myrUSH3 increased. This suggests that the additional lipid interacting regions modulate the myristoyl availability towards the lipid membrane through intramolecular interactions. The latter is consistent with the NMR measurements showing that the ULBR & SH3 RT loop are key to maintain the adequate interactions of the myristoyl moiety within the fuzzy IDR:SH3 complex, particularly the ULBR.

Interestingly, Sigal et al., (1994) compared the membrane binding of inactive WT c-Src to the constitutively active mutant Y530F and the viral counterpart v-Src that lacks the C-terminal regulatory tail. The affinity of Y530F c-Src and v-Src was about ~ 1 order of magnitude weaker than closed/inactive c-Src, suggesting that upon activation the myrSH4 N-terminus becomes less available. This is in agreement to our observations, showing that the myristoylated N-terminal would be buried in the fuzzy IDR:SH3 complex in the open active state[20]. In fact, Patwardhan and Resh (2010) showed that in the kinase-inactive form, 80-90% of c-Src protein was bound to the membrane, suggesting that in this conformation the myristoyl moiety is exposed. A recent work by Ahler et al., (2019), reports that in the autoinhibited form, the SH4 domain interacts with the C-lobe of the kinase domain and the myristoyl is not required for the interaction, supporting that the myristoyl group remains available.

---

[20] Our myrUSH3 construct represents the N-terminal c-Src domains in the open-active state.

As earlier commented, increased catalytic activity (Obara et al., 2004) and translocation of c-Src from the plasma membrane to the cytosol has been observed upon S^{17} phosphorylation by cAMP-dependent PKA kinase (Walker et al., 1993). The latter is expected since pS^{17} alters the native charge distribution of the SH4 domain and thus affecting the electrostatic component of the myrSH4 membrane anchoring. Our NMR results for myrUSH3 suggest that pS^{17} favors the myristoyl buried conformation in the fuzzy complex and this modulation may occur through the ULBR. This is consistent to previous results (Arbesú et al., 2017) showing that upon phosphorylation of S^{17} in a non-myristoylated SH4-U c-Src construct, the IDR intramolecular contacts were enhanced, in particular the ULBR ^{64}FGGF^{67} segment. Thus, presence of the myristoyl group could even favor those effects, since we have shown that the myristoyl interacts with the C-terminal part of the ULBR (^{64}FGGFN^{68}) while the N-terminal part of the SH4 domain would interact with the N-terminal section of the ULBR (^{60}EPK^{62}). Overall, the pS^{17} switches the IDR:SH3 conformational ensemble to the myristoyl harbored state. Additionally, the SPR results of pS^{17} myrUSH3 confirm that the myristoyl group in this construct is less available for interaction with the lipid membrane.

In a nutshell, seemingly the N-terminal myristoyl group in c-Src has a role beyond the membrane binding, it favors the formation of the N-terminal fuzzy IDR:SH3 complex. The myristoyl moiety increases the local concentration of the SH4-U in the proximity of the SH3 domain by cooperatively enhancing the preexisting interactions in absence of the myristoyl group. The key ULBR is essential to frame the intramolecular interactions of the myristoyl group. The overall consequence is multiple binding sites in the SH3 domain to harbor the myristoyl group.

2.7. Material and methods

2.7.1. Myristoylated c-Src variants expression and purification

The myristoylated c-Src variants were obtained by the co-expression of the N-myristoyltransferase enzyme and the USH3 of c-Src substrate in a pETDuet-1 (Novagen) plasmid. The USH3 construct of c-Src, contains the SH4, Unique and SH3 domains, followed by a His_6 purification tag. The mutations were introduced using the QuickChange II XL Site Directed Mutagenesis Kit (Agilent).

Plasmids were transformed in *Escherichia coli* Rosetta[TM] (DE3) pLysS (Novagen) and the bacteria cells were grown in Luria Broth (LB) medium supplemented with chloramphenicol (25 µg/mL) and ampicillin (100 µg/mL) at 37 ºC until an OD_{600nm} of ~0.6 was reached. Before induction with 1mM of isopropyl-β-d-thiogalactopyranoside (Nzytech), a freshly prepared solution of myristic and palmitic acid (Sigma) (200 µM final concentration for each) and fatty acid free Bovine Serum Albumin (BSA) (Sigma) (600 µM final concentration) was added to the cell culture. The lipid solution was prepared by adding one equivalent of NaOH, heating at 65 ºC and adjusting the final pH to 8. The protein expression was performed for 5 h at 28 ºC and 1h after the induction had started 6 g per culture L of glucose were added. For ^{15}N-labeled protein the Marley method was used (Marley et al., 2001). After growing the cells in LB medium as previously described, cultures were harvested by centrifugation at 1000 g for 30 min and resuspended in M9 medium containing 1 g/L ^{15}N NH_4Cl (Cambridge Isotope Laboratories). Before inducing the expression, 3 g/L of glucose and a freshly prepared solution of myristic and palmitic acid (Sigma) at 50 µM final concentration for each, with fatty acid free BSA (Sigma) at 600 µM final concentration, were added to the cell culture. The expression was performed as mentioned above.

Cells were harvested at 4000 rpm for 20 min and resuspended in lysis buffer (20 mM Tris·HCl, 300 mM NaCl, 10 mM Imidazole, pH 8) supplemented with 1% v/v Triton X100, Protein Inhibitor Cocktail (Sigma) and 1 mM PMSF (Sigma), 25µg/mL lysozyme (Sigma) and 5µg/mL DNAse I (Roche). Cells were sonicated on ice and centrifuged at 25000 rpm for 45 min. Subsequently, gradient step Ni-NTA affinity chromatography was performed using a 1 mL-Ni-NTA cartridge (GE Healthcare). In the first elution step, non-desired protein products were eluted with lysis buffer supplemented with 100 mM imidazole. The intact protein was eluted in the second elution step with lysis buffer supplemented with 0.018% v/v Triton X100 and 400 mM imidazole. The final purification step consisted of a size exclusion chromatography in a Superdex 75 26/60 (GE Healthcare), in phosphate buffer (50 mM NaH_2PO_4 /Na_2HPO_4, 150 mM NaCl, 0.2 mM EDTA, pH 7.5). For NMR, samples buffer was exchanged to 50 mM NaH_2PO_4 /Na_2HPO_4, pH 7.0 using a PD10 column (GE Healthcare). The purity of the protein was established by HPLC in a BioSuite pPhenyl 1000RPC 2.0 x 75 mm; 10 µm column coupled to mass spectrometry, confirming the absence of lauroylated protein. The protein was concentrated using Vivaspin 20, 5 kDa

MWCO concentrators (Sigma Aldrich). The myristoylated SH4 domain c-Src construct (myrSH4) was synthesized by SynPeptide Co., Ltd (Shangai, China).

2.7.2. *In vitro* phosphorylation of S17 in myrUSH3 by PKA

The buffer of WT myrUSH3 was exchanged to 100 mM HEPES, pH = 7.5, 100 mM NaCl, 10 mM DTT, 25 mM MgCl$_2$, and 10 mM ATP. The reaction was proceeded by adding 400 units of recombinant PKA catalytic subunit from bovine heart (Sigma Aldrich), incubating 4.5 hours at 30 °C. Then, the phosphorylated product was repurified by SEC in phosphate buffer (50 mM NaH$_2$PO$_4$ /Na$_2$HPO$_4$, 150 mM NaCl, 0.2 mM EDTA, pH 7.5). The final yield was very low with a final concentration of 15 μM.

2.7.3. Preparation of Large Unilamellar vesicles (LUVs)

1,2-dioleoyl-*sn*-glycero-3-phosphocoline (DOPC) (TebuBio) and 1,2-dioleoyl-sn-glycero-3-phospho(1'-rac-glycerol) (sodium salt) (DOPG) (Sigma) were dissolved in chloroform. Three lipid compositions were used: DOPC, DOPC:DOPG (3:1) and DOPC:DOPG (2:1). The organic solvent was evaporated under a nitrogen stream. The lipid films were rehydrated with phosphate buffer (50 mM NaH$_2$PO$_4$ /Na$_2$HPO$_4$, 150 mM NaCl, 0.2 mM EDTA, pH 7.5) with vortexing. LUVs were prepared by extrusion using a Mini-extruder (Avanti Polar Lipids). The lipid suspension was extruded 15 times through a 100 nm-polycarbonate filter. The mean diameter of the LUVs was verified by Dynamic Light Scattering (Zetasizer Nanoseries S, Malvern instruments). LUVs were used within two days to avoid lipid oxidation.

2.7.4 NMR Experiments

For the CSP analysis, 2D ^{1}H-^{15}N BEST-TROSY HSQC or ^{1}H,^{15}N SOFAST-HMQC experiments were acquired at 278K (for the IDR) and 298K (for SH3 domain) in a Bruker 600 MHz Avance III spectrometer equipped with a TCI CryoProbe. The samples contained 0.075-0.2 mM protein concentration in 50 mM NaH$_2$PO$_4$ /Na$_2$HPO$_4$, pH 7.0 with 10 % D$_2$O. The final samples volumes ranged from 250 – 300 μL. 5 mm Shigemi tubes (BMS-005-1T) were used.

NMR data was processed using Topspin 4.0.3. or nmrPipe (Delaglio et al., 1995) and analyzed CCPN Analysis 2.4 (Skinner et al., 2016). The resulting peaklists were exported to Farseer-NMR (Teixeira et al., 2018) for the CSP calculation, according to equation 2.1.

The statistical significant threshold line is defined as the mean CSP for the lowest decile (μ(lowest decile CSP)) plus five standard deviations (5σ). CSP were mapped over the SH3 domain crystal structures using UCSF Chimera (Pettersen et al., 2004).

2.7.5 Surface Plasmon Resonance binding assays

SPR experiments were performed in a Biacore T200 instrument (GE Healthcare). The temperature was set to 25 °C in all the experiments.

The procedure of the surface functionalization will be explained in detail in *Chapter 3*. After surface derivatization, the Flow Cell 1 (FC1) becomes the reference cell, while the other three FCs (2,3 and 4) have been modified by a covalent attachment of phytosphyngosine to allow the capture of liposomes.

Phosphate buffer (50 mM NaH_2PO_4 /Na_2HPO_4, 150 mM NaCl, 0.2 mM EDTA, pH 7.5) was used as running buffer for all the experiments. DOPC, DOPC:DOPG (3:1) and DOPC:DOPG (2:1) LUVs at 1 mM concentration were coated over FC 2, 3 and 4. (maintaining this order to avoid anionic lipid migration towards the neutral LUVs through the flow cells) by a 20 s injection at 10 µL/min. The reference cell FC1 and possible uncovered surface in the LUVs FCs were blocked with 1 mg/ml of BSA at 10 µL/min for 60 s. To minimize mass transport effects, the myristoylated c-Src variants were injected at 50 µL/min. Protein concentration ranged from 1.5 µM to 20 µM. For each c-Src construct three protein concentrations were injected with one in duplicate and in randomized order. The protein was allowed to associate for 60 s while the dissociation lasted 120 s. Triplicate experiments were performed for each c-Src variant. The surface was regenerated with two pulses (30 s at 100 µL/min) of Isopropanol:50 mM NaOH (2:3) solution followed by a 20 mM CHAPS pulse (30 s at 100 µL/min). Each binding experiment started with freshly captured LUVs.

The myristoylated c-Src variants binding to LUVs were analyzed using the Biacore T200 3.0 Evaluation software (GE Healthcare). All data was double referenced: 1) Reference flow cell substraction (i.e. no liposomes coated flow cell) and 2) baseline subtraction (response derived by injecting 0 µM of c-Src construct) and globally fitted using a simple 1:1 Langmuir model. The kinetics of binding and dissociation were measured at three concentrations with one of them duplicated. The curves were fitted globally (see *Appendix Figures A1* to *A3*). Each experiment was repeated three times

Chapter 3
c-Src self-association on the membrane

3.1. Context

3.2. SPR to study the clustered minor fraction of myristoylated c-Src on lipid bilayers.

    3.2.1.   Optimization of the SPR methodology
    3.2.2.   Materials and methods for SPR experiments

3.3. Sequence determinants of c-Src self-association on lipid bilayers.

    3.3.1.   c-Src self-association is modulated by the SH4 domain lysines K^5, K^7 and K^9
    3.3.2.   Positive charge of the lysine residues is essential for clustering
    3.3.3.   The role of lipids in self-association: the membrane interface
    3.3.4.   Could an additional positive charge in the SH4 domain affect the dimerization?
    3.3.5.   A putative β-sheet conformation of the SH4 domain in the c-Src clustered fraction
    3.3.6.   Releasing the c-Src clusters from the membrane

3.4. Lateral diffusion dynamics of the c-Src self-associated species on bilayers

    3.4.1.   Materials and methods for FCS experiments
    3.4.2.   FCS Results

3.5. Discussion

3.1. Context

Protein self-association is a prevailing event in biological systems. However, non-native protein oligomerization can lead to aberrant activity, as observed in amyloid fibril formation associated to human neurodegenerative diseases. About two thirds of human enzymes are found to function as multimers (with homodimer formation predominance) (Marianayagam et al., 2004). A mechanism used by membrane receptor tyrosine kinases (RTKs) is dimerization/oligomerization upon binding of signaling factors to their extracellular domains, provoking structural changes that enables the kinase domain trans-phosphorylation, resulting in the active conformation that triggers downstream signaling. Although it is known that c-Src full activation is also accomplished through trans-phosphorylation by a second c-Src molecule (Smart et al., 1981), c-Src activity has not been stated to require a dimeric state, suggesting that self-association in the activation step is likely to be a transient interaction. However, accumulated evidence in recent reports consistently indicate the formation of stable dimers or large oligomers by c-Src or model proteins including its myristoylated N-terminal region.

Irtegun et al., (2013), detected formation of a minor dimeric fraction of full-length c-Src using analytical ultracentrifugation with fluorescence detection in cell lysates, but further characterization of the mechanism leading this c-Src dimerization was not assessed. In a previous work, Owen et al., (2010) had conducted a super resolution spectroscopy study, where a c-Src chimera comprising the myristoylated N-terminal SH4 domain (residues 2-15) fused to a photoswitchable protein was expressed in HeLa cells. Their study indicated that myrSrc fused proteins formed large clusters on the membrane, although the number of myrSrc entities involved in the clustered formation was not determined. Later on, Smith and coworkers (2016) characterized c-Src mobility on *in vivo* plasma membranes (Cos-7 and Jurkat cells) using photoactivated localization microscopy and fluorescence correlation spectroscopy (FCS). c-Src was expressed as a fusion protein with the myristoylated SH4 domain (residues 2-15) attached to fluorescent proteins. While the predominant species exhibited a high mobility distinctive of the monomeric c-Src form, a small fraction of c-Src fusion molecules presented a slower diffusion. The less mobile species were interpreted to result from c-Src integration into (pre-existing) membrane clusters, though clustering was density-dependent and various c-Src molecules were found in the cluster.

Although, both Owen and Smith works suggested that c-Src clustering could occur on the membrane, being the myristoylated N-terminal region of c-Src (i.e. SH4 domain) sufficient for this purpose, it remained ambiguous that clustering propensity was an intrinsic characteristic of c-Src protein. Otherwise stated, it was not clear whether c-Src molecules self-associated or were recruited by other proteins to form clusters on the membrane, given that within an *in vivo* cellular framework both affirmations might not be exclusive.

Nonetheless, during the same period, Le Roux et al., (2016a) using SPR measurements (*in vitro*), detected a minor irreversible c-Src population formed upon membrane anchoring. The c-Src construct used included the myristoylated SH4, Unique and SH3 domains (residues 2-150). The kinetics characterization of the persistently membrane-bound species

followed a second order law suggesting a dimer formation. This result was explicit in the alternative study (Le Roux et al., 2016b) using Single Molecule Fluorescence, revealing that the self-associated c-Src fraction was predominantly formed by dimers. Overall, provided evidence of the c-Src intrinsic clustering ability upon membrane anchoring. In addition, Le Roux et al. (2016a) also observed formation of large c-Src clusters when a myristoylated SH4 domain peptide was used, suggesting that the domains beyond the SH4 presumably had a role in restricting the large oligomers to dimers. Nevertheless, all the elements required for c-Src self-association were indicated to be in the myristoylated SH4 domain, specifically within the first 9 residues, as subsequently reported by Dwivedi et al., (2017). Although, the latter works surely demonstrate that c-Src membrane clustering is enabled by its myristoylated N-terminal region, c-Src self-association through the strongly positively charged SH4 domain (+5 net charge) is counterintuitive. In this chapter, we investigate the structural basis of this self-association.

Of note, non-membrane dependent c-Src dimerization have also been described. As commented in the *subsection 1.1*, redox regulation is being exposed to additionally modulate c-Src activity, and on this pathway Kemble and Sun (2009) reported *in vitro* c-Src homodimerization via disulphide bonding upon oxidation of Cys280. This dimerization reduced ~ 92% the c-Src kinase activity. Additionally, Spassov et al., (2018) pointed out the N-terminal myristoyl group to mediate c-Src dimerization by interaction with a hydrophobic pocket[21] found in the kinase domain (of the second c-Src molecule). Y419 phosphorylation[22] was required in cis (i.e. in the same molecule containing the myristoyl group). In this case, concomitant to dimerization an increased c-Src autophosphorylation was reported, that accounted for the detection of a higher number of phosphorylated substrates. Although the dimerization reported by Kemble and Sun (2009) can be presumed to occur in the cellular environment, the various modes of c-Src self-association, yet illustrate a conceivable complexity in the regulation of the c-Src kinase activity, with a potential functional competition among those modes of self-association, as each may endow the protein singular characteristics such as origination of novel interfaces or modulation of the binding sites.

---

[21] Apparently, this was the same hydrophobic pocket earlier predicted by Cowan and coworkers (2005), based on similarities to the c-Abl kinase in the enzyme inactive form (i.e. myristoyl-sequestered state). Although several evidence suggest that a c-Abl-like myristoyl sequestration within the kinase domain did not occur in the c-Src monomeric form upon inactivation.

[22] Y419 phosphorylation leads to the full activation of c-Src kinase.

3.2. SPR to study the clustered minor fraction of myristoylated c-Src on lipid bilayers.

Opposed to the initial assumptions, Le Roux et al., (2016a) has evidenced c-Src membrane binding to be a complex phenomenon by the occurrence of two binding modes characterized by a dramatically distinct kinetics, leading the coexistence of monomeric and dimeric c-Src species unequally dwelling on the membrane. While the major monomeric c-Src fraction binds reversibly, the minor dimeric component is permanently anchored on the lipid membrane (*Figure. 3.1*).

Figure 3.1. Illustration of the c-Src membrane binding. A minor fraction of c-Src undergoes clustering upon membrane anchoring in an irreversible manner. The monomeric c-Src species are loosely bound to the membrane and can be readily washed away.
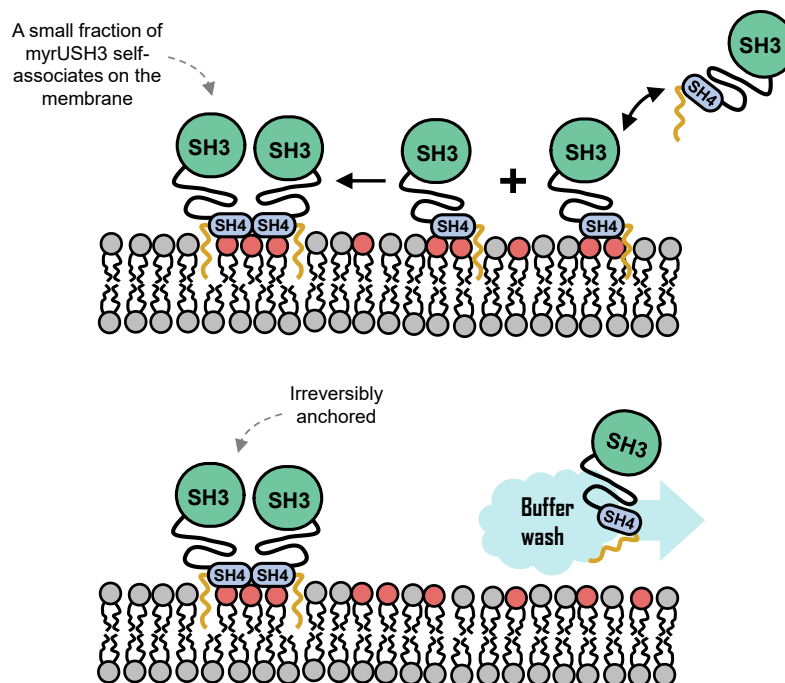
Conventional approaches, such as NMR spectroscopy or X-ray crystallography, which would explicitly provide the structural information of the c-Src dimer, cannot be applied to such a heterogeneous system in which the most interesting species is present as a minor component and the concentration cannot be increased since spontaneous truncation of myrUSH3 occurs at concentrations >80 µM. Nonetheless, as presented in Le Roux et al., (2016a), Surface Plasmon Resonance (SPR) efficiently enables the separate detection of monomeric and dimeric membrane bound c-Src species. However, in this chapter we explore the effect of various mutations in the SH4 domain of c-Src, to shed light on the structural determinants of c-Src dimerization upon membrane anchoring and we will evaluate the mutants' dimerization level against the WT c-Src variant. Thence, accurate comparison requires strict reproducibility from run-to-run and between sensorchips in the SPR assays. Consequently, the first task was to find the SPR conditions that optimize the reproducibility.

3.2.1 Optimization of the SPR based methodology

In any standard SPR assay, the surface has to be functionalized to immobilize one of the components in the binding assay. In our case, we perform the attachment of a lipid anchor to allow immobilization/capture of liposomes on the surface. We use the 2D carboxymethyl dextran coated sensorchip (XanTec bioanalytics GmbH, Germany).

Phytosphingosine is used as the lipid anchor and is covalently immobilized on sensorchip surface using an amine coupling reaction based on EDC-NHS chemistry. We use phytosphingosine due to its lower pKa (between ~ 7-8) compared to other aliphatic amines (pKa about ~ 10-11). This allows the reaction, requiring an unprotonated amine, to proceed at the optimal pH range ~4,5-7,2.

Figure 3.2. The sensorchip surface functionalization is performed with a covalent attachment of phytosphingosine to allow liposome capture. Oversight of the functionalization process can be followed in the SPR sensorgram.
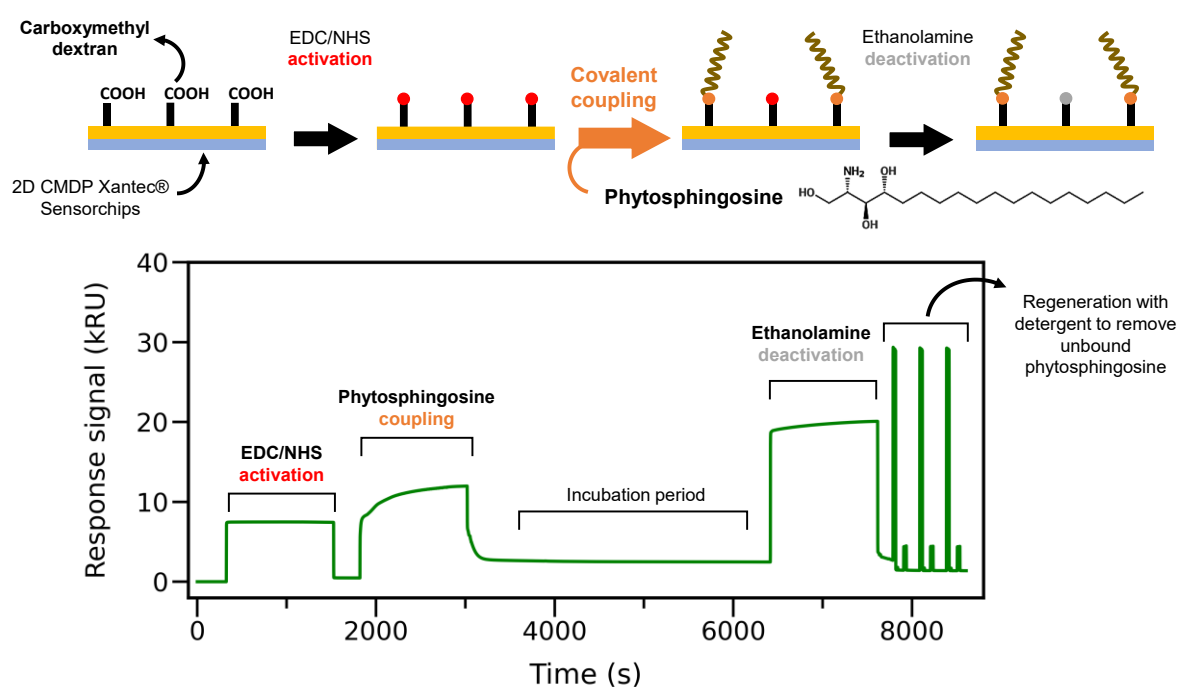
The carboxyls groups on the sensorchip surface are activated using hydroxysuccinimide (NHS) and 1-ethyl-3-(3-dimethylaminopropyl) carbodiimide hydrochloride (EDC·HCl). EDC couples NHS to carboxyls, forming an NHS ester intermediate, that readily allows an efficient conjugation to phytosphingosine. The unreacted NHS esters are quenched/deactivated using ethanolamine (*Figure 3.2.*).

The recommended procedure by the manufacturer was to inject the phytosphingosine on the surface at a 5 mg/mL concentration in 20 mM sodium acetate buffer pH 6 + 50% DMSO. Nonetheless, the chemical resistance of the instrument microfluidics components (Biacore T200, GE Heathcare) does not allow to use such high concentration of DMSO for

long terms. This was partially solved by a 1:10 dilution in 20 mM sodium acetate buffer pH 6, meaning that phytosphingosine was injected at 0,5 mg/mL concentration and 5% of DMSO (agreeing the instrument specificities). However, this protocol was not reproducible, probably because phytosphingosine coating being not homogeneous.

Sasaki et al., (2009) provided a detailed work on sphingosine aggregation with pH and concentration dependence. Extrapolating their results to our phytosphingosine approach, the critical changes were to **adjust the pH to 6.7 after** diluting the phytosphingosine (from 100% DMSO 10mg/mL stock solution) to a concentration of 1mM (~0.03 mg/mL) phytosphingosine in 20 mM sodium acetate buffer, resulting in a residual DMSO concentration of 3.3%, and letting the coupling reaction to proceed for 30-45 min after the phytosphingosine injection, before quenching of remaining NHS ester groups by the ethanolamine injection (*Figure 3.2.*).

Biacore T200 (GE Heathcare) system microfluidics creates 4 Flow Cells (FC) over the sensorchip surface. The first FC is chosen as the Reference cell and thus not modified with phytosphingosine but activated and quenched with EDC/NHS and ethanolamine. The Reference cell will account for the bulk refractive effects or the non-specific binding of the analyte on the sensor surface, though the former effects are minimized by usage of the same running buffer for all the samples, slight mismatches can occur between protein or antibodies stock samples.

Figure 3.3. Multiple captures of liposomes after applying regeneration conditions (A) 1 pulse (30s at 100 µL/min) of 20 mM CHAPS (B) 2 pulses of Isopropanol:50 mM NaOH (2:3) solution + 1 pulse of of 20 mM CHAPS.
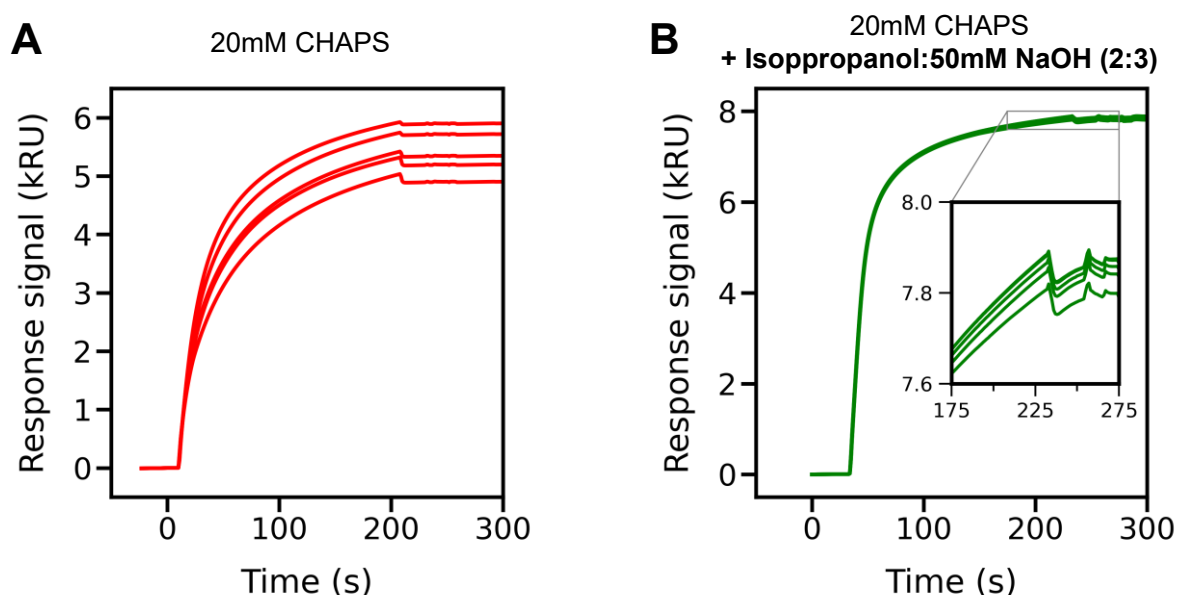
The remaining 3 FCs are modified with phytosphingosine to capture liposomes. The liposomes coating is the first step in all myrSrc binding experiments, thus dictating run-to-run reproducibility of the measurements. Here, it is found that regeneration conditions were critical and significant improvement was achieved by changing a single 20 mM CHAPS

detergent pulse[23] by two pulses of Isopropanol:50 mM NaOH (2:3) solution followed by the 20 mM CHAPS detergent pulse[24]. As shown in *Figure 3.3.*, this led to more reproducible coatings of liposomes.

Figure 3.4. myrUSH3 persistently tethered self-associated fraction detection by SPR. The experiment steps comprise: (0) → (1) Liposomes coating (3) myrUSH3 association (4) myrUSH3 dissociation (5) myrUSH3 persistent fraction detection by anti-Src antibody recognition and (6) surface regeneration.
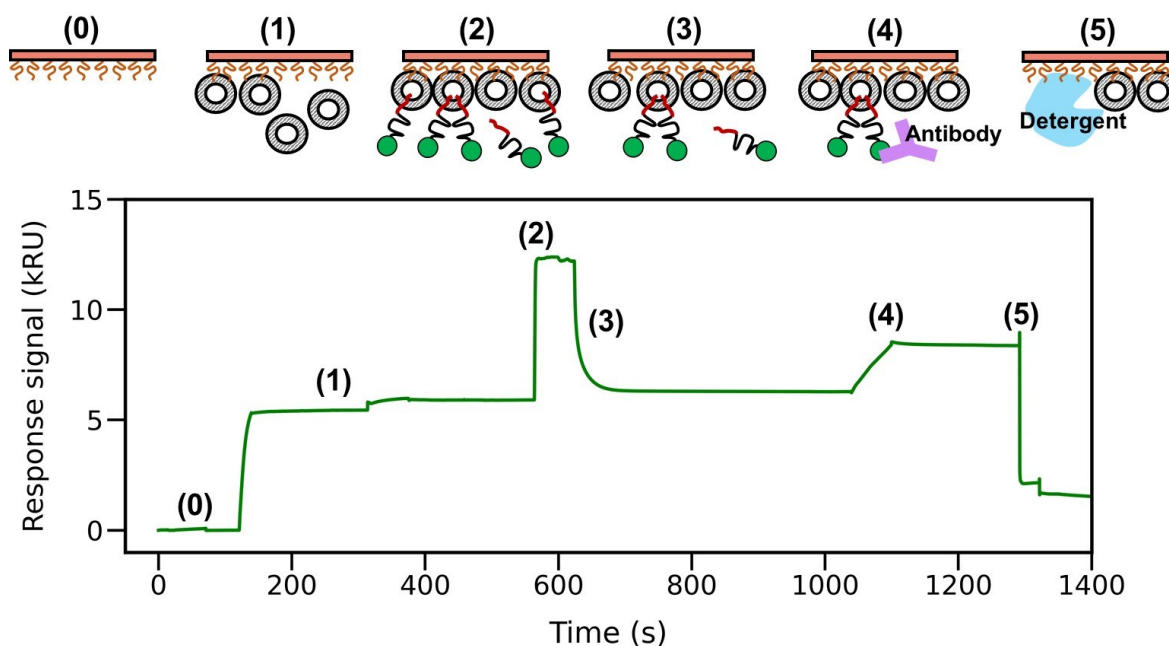
To evaluate myrSrc self-association, the persistent dimeric bound form was detected on immobilized membranes, exploiting the reversibility of the monomeric myrSrc that can be washed away from the bilayer. Specific c-Src antibodies were used to target the myristoylated c-Src dimers irreversibly anchored on the membrane. The steps of each SPR experimental cycle (*Figure 3.4.*) consisted of:

1. Attachment of liposomes (neutral or negatively charged) onto the previously covalently coupled phytosphingosine surface.

2. Injection of c-Src myrUSH3 (association phase).

3. Removal of reversibly bound c-Src myrUSH3 injection by washing with protein-free buffer (monomer dissociation phase).

4. Detection of the persistently bound dimers by specific antibodies.

5. Regeneration of the surface using detergent.

---

[23] Pulse is referred as short injection 30s at high flow rate 100 µL/min.
[24] Using 40mM Octyl-beta-Glucoside detergent instead of 20 mM CHAPS had the same efficacy.

3.2.2 Material and methods for SPR experiments

myrSrc constructs preparation

Myristoylated c-Src myrUSH3 variants were obtained by co-expression of the N-myristoyltransferase (NMT) enzyme along the c-Src USH3-His$_6$Tag construct both encoded in the bicistronic plasmid pETDuet-1 (Novagen) carrying an ampicillin resistance.

The SH4 domain mutations (S3A, N4A, K5A, S6A, K7A, P8A, K9A, D10A and D10R) were introduced in the USH3-His$_6$Tag construct sequence using QuickChange II XL Kit (Agilent) or Q5 High-Fidelity Kit (New England BioLabs) by a standard site- directed mutagenesis procedure. All plasmids were amplified in *E. coli* OmniMAX^{TM}, purified by miniprep procedure using QIAprep Spin Kit (Qiagen) and sequenced by Macrogen Inc. Protein expression and purification was performed as detailed in *subsection 2.7.1*. All the purified mutant protein variants were analyzed by MS to verify correct and complete myristoylation. Myristoylated SH4 domain peptides (myrSH4) were synthesized by SynPeptide Co., Ltd (Shangai, China)

Liposome preparation

1,2-dioleoyl-*sn*-glycero-3-phosphocoline (DOPC) (TebuBio), 1,2-dioleoyl-sn-glycero-3-phospho(1'-rac-glycerol) (sodium salt) (DOPG) (Sigma) and 1,2-dioleyl-sn-glycero-3-phosphate phosphatidic acid (DOPA) (Sigma) were dissolved in chloroform. Lipid compositions used were DOPC, DOPC: DOPG (2:1) and DOPC:DOPA (2:1) at 4mM. The organic solvent was evaporated under a nitrogen stream. Lipid films were rehydrated with vortexing in phosphate buffer 50mM NaH$_2$PO$_4$/Na$_2$HPO$_4$, 150mM NaCl, 0.2mM EDTA, pH 7,5. Large unilamellar vesicles were prepared by extrusion using a Mini-Extruder (Avanti Polar Lipids). The lipid suspension was extruded 15 times through a 100nm polycarbonate filter. The mean diameter of the liposomes was verified by Dynamic Light Scattering (Zetasizer Nanoseries S. Malvern instruments). Liposomes were used within two days to avoid lipid oxidation.

Surface Plasmon Resonance: surface functionalization

All experiments were carried out in a Biacore T200 instrument (GE Healthcare) at 25ºC. A 2D-carboxylmethyldextran sensor chip (Xantec) was used. The running buffer during the surface functionalization was dd H$_2$O. The surface was conditioned 3 min with 1 M NaCl and 0,1 M sodium borate pH 9 at 50 µL/min flow rate. dd H$_2$O was flowed until the baseline was stable. All the flow cells (FC 2, 3 and 4) except for the reference (FC 1), were modified by a covalent attachment of phytosphingosine (TebuBio) to allow the capture of liposomes. The reference FC 1 was activated using 1:1 mixture of 400mM of EDC in dd H$_2$O and 100mM of NHS in 50mM MES pH 5 buffer (both GE Healthcare). The mixture was prepared right before usage and injected for 20 min at 15 µL/min. Afterwards, FC 1 surface was quenched with 1 M ethanolamine pH 8.5 for 20 min at 15 µL/min. FC 2, 3 and 4 surfaces were activated as FC 1 and then, freshly prepared 1 mM of phytosphingosine

in 20mM sodium acetate buffer at pH 6.7 was injected for 20 min at 15 µL/min. dd H2O was flowed for 30-45 min to conclude the amine coupling reaction. The quenching of the remaining NHS ester was proceeded as for FC 1. To remove unbound phytosphingosine, the surface was regenerated with one pulse (30 s at 100 µL/min) of Isopropanol:50 mM NaOH (2:3) solution followed by a 20 mM CHAPS (Sigma) or 40mM Octyl-beta-Glucoside (Sigma) pulse (30 s at 100 µL/min), multiple times (the set of both regeneration injections in this order) until no significant decrease was observed in the baseline.

Surface Plasmon Resonance: myrSrc mutants' analysis

All measurements were carried out at 25°C. The running buffer for all experiments consisted of 50 mM NaH_2PO_4/Na_2HPO, 150 mM NaCl, 0,2 mM EDTA, pH 7,5. The Biacore T200 (GE Healthcare) used was equipped with an integrated buffer degasser, therefore the later procedure was not required previous to each assay. Before each set of runs the surface (i.e. all flow cells) was conditioned with two pulses (30 s at 100 µL/min) of Isopropanol:50 mM NaOH (2:3) solution followed by a 20 mM CHAPS (Sigma) or 40mM Octyl-beta-Glucoside (Sigma) pulse. DOPC, DOPC:DOPG (2:1), DOPC:DOPA (2:1) liposomes at 1 mM concentration were coated over the phytosphingosine modified flow cells by a 20 s injection at 10 µL/min. In case the distinct flow cells contained different types of lipids, the DOPC liposomes were injected in the first available flow cell to avoid anionic lipid migration towards the neutral liposomes through the flow cells. The reference cell and possible uncovered surface on the liposomes flow cells were blocked with 1 mg/ml of BSA at 10 µL/min for 60 s. Mass transport effects were minimized by injecting the myristoylated c-Src variants at 50 µL/min. Protein concentration ranged from 3 µM to 20 µM for the protein density experiments and it was fixed to 20 µM to compare the various mutants. The myrSH4 peptides were injected at 50 µM. The myristoylated proteins or peptides were allowed to associate for 60 s followed by 350 s washing with buffer to ensure complete dissociation of the monomeric species. The antibody (antiHis$_6$Tag or antiSrc antibodies (both SantaCruz Biotechnology)) was injected at 1:5 dilution in running buffer for 60 s at 30 µL/min. n≥3 experiments were performed for the c-Src variants, each time the c-Src constructs injected in randomized order. The surface was regenerated with two pulses (30 s at 100 µL/min) of Isopropanol:50 mM NaOH (2:3) solution followed by a 20 mM CHAPS (Sigma) or 40mM Octyl-beta-Glucoside (Sigma) pulse (30 s at 100 µL/min). Each cycle started with freshly captured liposomes. All data was double referenced: 1) FC1 Reference flow cell substraction (i.e. no liposomes coated flow cell) and 2) baseline subtraction (response derived by injecting 0µM of c-Src construct). The data was analysed using Biacore T200 3.0 Evaluation software (GE Healthcare). Experiments were performed in two sensor chips.

Statistical analysis

All the statistical analysis was performed using the Python scientific library SciPy. If not otherwise stated, all mutants were compared with the WT c-Src construct and statistical significance was assessed using the Mann-Whitney test.

3.3. Sequence determinants of c-Src self-association on lipid bilayers.

Le Roux et al., (2016a) showed that the c-Src construct myrSH4 (comprising residues 2-16) was enough to cause self-association in membranes. A later contribution by Dwivedi et al. (2017) reported that solely the myristoylated N-terminal part of the SH4 domain (i.e. residues 2-9) was sufficient to enable oligomerization on membrane. Therefore, all the sequence determinants of the membrane c-Src clustering are found within the first 9 residues of the SH4 domain. To probe the role of individual residues we introduced mutations in the c-Src N-terminal part of the SH4 domain.

3.3.1. c-Src self-association is modulated by the SH4 domain lysines K^5, K^7 and K^9

The first assays targeted K^5 and S^6 found in the middle of the potential dimer interface region and known to participate in other intra-molecular interactions (Arbesú et al. (2017)). We used synthetic myrSH4 c-Src peptides with individual (K5A and S6A) or combined (K5AS6A) mutations. Dimer formation was tested on neutral (DOPC) and negatively charged (DOPC:DOPG (2:1)) liposomes using an antibody recognizing the N-terminal region of c-Src (antiSrc). Representative binding of the X#A mutants and WT myrSH4 along the antibody detection of the dimer species is shown in *Figure. 3.5*.

Figure 3.5. Representative binding curves of K5A, S6A, K5AS6A and WT mySH4 on negatively charged DOPC:DOPG (2:1) liposomes. The inset expands the antibody response and schematic cartoons represent the scenario at each binding response.

81
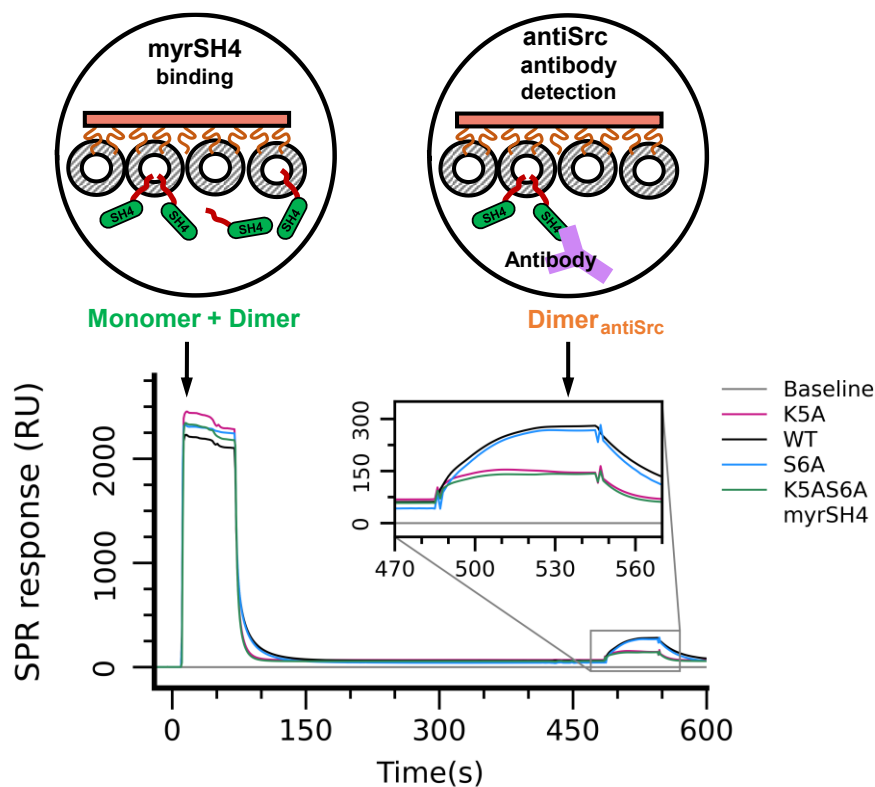
The first binding response represents the coexisting monomeric and dimeric[25] species on the membrane at the equilibrium (steady state), though it is dominated by the monomeric c-Src population and dimer contribution would be negligible, from now on this response is referred as Monomer+Dimer. The second binding response, tagged as Dimer$_{antiSrc}$, corresponds to the irreversible dimeric c-Src specie detected by the antiSrc antibody. The different mutants are compared relatively to WT myrSH4 as indicated per *equations*[26] *3.1* and *3.2*.

Equation 3.1. $\quad$ Relative SPR response Monomer + Dimer $= \dfrac{\left\{\frac{R_{Monomer+Dimer}}{R_{liposomes}}\right\}_{mutant}}{\left\{\frac{R_{Monomer+Dimer}}{R_{liposomes}}\right\}_{average\ WT}}$

Equation 3.2. $\quad$ Relative SPR response Dimer$_{antiSrc}$ $= \dfrac{\left\{\frac{R_{Dimer_{antiSrc}}}{R_{liposomes}}\right\}_{mutant}}{\left\{\frac{R_{Dimer_{antiSrc}}}{R_{liposomes}}\right\}_{average\ WT}}$

Figure 3.6. Monomer+Dimer and Dimer$_{antiSrc}$ relative responses to WT for K5A, S6A and K5AS6A myrSH4 constructs injected at 50 μM over (A) neutral DOPC liposomes and (B) negatively charged DOPC:DOPG (2:1) liposomes. Data expressed as mean ± SD, n = 3 (DOPC) n=6 (DOPC:DOPG (2:1)) . Significant differences in the Dimer$_{antiSrc}$ relative responses with respect to WT myrSH4 are indicated by asterisks (Mann-Whitney test: *p < 0.1; **p < 0.05; ns: not significant, REF: reference).
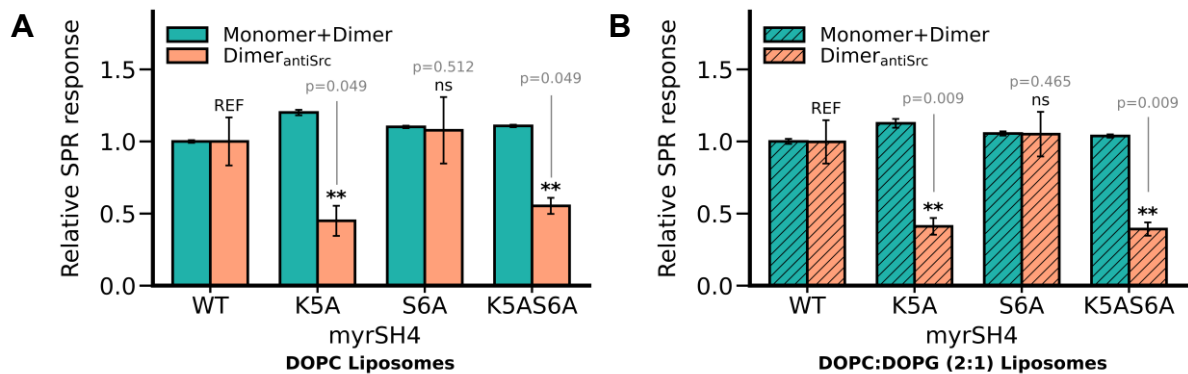
Dimer formation depends on the concentration of myristoylated peptide bound to the lipid bilayer at equilibrium (i.e. monomer density on the membrane) (Le Roux et al., 2016a),

---

[25] As commented, c-Src self-associated fraction, is not constituted exclusively by dimeric species, although the latter is the predominant form. However, for sake of simplicity this nomenclature is used.

[26] The liposomes response term R$_{liposomes}$ is included to correct any variability due to the amount of immobilized liposomes.

thence the aim to evaluate both binding responses to detect possible variations in the myrSH4 steady state response of the various mutants that could translate into a lower or higher dimer population. The results are shown in *Figure 3.6*.

All myrSH4 mutants exhibited a comparable steady state response (Monomer+Dimer) to WT. In both membrane types, K5A mutation clearly reduced ~ 60% the myrSH4 self-associated fraction formation (Dimer$_{antiSrc}$), whereas S6A mutation alone had no effect. The double mutant K5AS6A, exhibited a similar decrease formation of myrSH4 clusters as K5A, confirming the effect of the K^5 mutation and no apparent contribution of residue S^6. Thus, K^5 is a crucial residue in c-Src self-association, as at similar peptide levels attached to the membrane yields a lower dimer population.

Figure 3.7. Monomer+Dimer and Dimer$_{antiHisTag}$ relative responses to WT for the X#A myrUSH3 mutants injected at 20 µM over (A) neutral DOPC liposomes and (B) negatively charged DOPC:DOPG (2:1) liposomes. Data expressed as mean ± SD, n = 3 (DOPC) n=5 (DOPC:DOPG (2:1)). Significant differences in the Dimer$_{antiSrc}$ relative responses with respect to WT myrUSH3 are indicated by asterisks (Mann-Whitney test: *p < 0.1; **p < 0.05; ns: not significant, REF: reference).
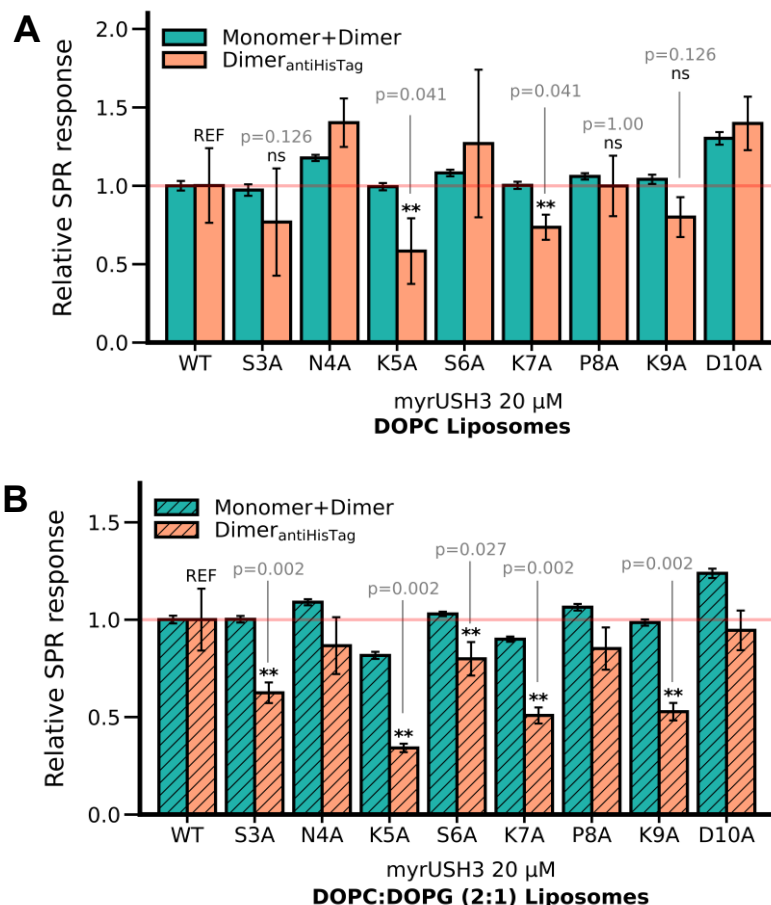
Potential limitations of this initial study were the fact that mutations were performed in the same region as the epitope recognized by the antibody, potentially affecting antiSrc affinity towards myrSH4. Therefore, we decided to introduce mutations in the context of

the 150 residues long SNRE (myrUSH3 c-Src variant), detecting the dimers using an antibody raised against the C-terminal His$_6$Tag[27] (antiHisTag), guarantying the same affinity of the antibody for all the mutants of the SH4 domain. The first ten residues of the SH4 domain were individually replaced by alanine[28]. The results for the X#A mutants and WT myrUSH3 construct are presented in *Figure 3.7*.

The low relative fraction of self-association of the construct bearing the K5A mutation confirmed the results obtained with the synthetic myrSH4 K5A variant. Furthermore, on the negatively charged membrane, mutation of residues K^7 and K^9 also revealed a ~50% reduction in the dimer formation, though differences are less significative on neutral DOPC liposomes. In the latter membrane, the steady state response (Monomer+Dimer) was similar for all mutants to WT myrUSH3, except for N4A and D10A myrUSH3, that showed a slightly higher protein level at equilibrium. This enhancement cannot be explained by a simple electrostatic effect, feasible explanations include the effect of these mutations on the intramolecular interactions with the Unique and SH3 domains or between the charged residues within the SH4 domain, changing the presentation of the myrSH4 domain to the lipids. Consequently, the higher dimer population observed for N4A and D10A mutants could result from the increased protein density on the surface.

On the other hand, changes in the steady state response (Monomer+Dimer) of the myrUSH3 variants observed in negatively charged lipids reflect a small global electrostatic effect (a decrease in the binding with K5A and K7A mutations and an increase in the D10A mutant). Considering the relative effects of individual mutations, there is a clear decreasing trend from K5A to K7A with nearly no effect in K9A (probably due to the neighbor D^{10} residue). This could reflect a preferred orientation/conformation of the myr-GSNKSKPKD segment, stabilized and restricted by the inserted myristoyl group and the electrostatic repulsion of the D^{10} residue to the anionic lipids, justifying the higher binding level (Monomer+Dimer) observed in the D10A mutant case. However, this simple model would not explain the small effects observed for N4A and P8A, thereby pointing out the earlier posited hypothesis on a different presentation of the myrSH4 domain towards the lipids. Although N4A, P8A and D10A myrUSH3 mutants show a higher steady state Monomer+Dimer response, the corresponding Dimer$_{antiHisTag}$ response is not commensurate to the observed enhancement, suggesting that these mutations do affect the c-Src self-association[29].

---

[27] His$_6$Tag is added at the end of the myrUSH3 constructs for purification purposes.

[28] Although mutations were performed in the N-myristoyltransferase (NMT) enzyme recognition site, the mutant constructs were obtained correctly myristoylated, as verified through MS. It has been demonstrated (Liang et al., 2004) that expressing the NMT in excess along the c-Src construct can compensate for point mutations in the NMT recognition signal. Our biscistronic plasmid in E. coli, leads the expression of USH3: NMT in a ratio 2:1.

[29] The statistical analysis of these mutants has been omitted since a direct comparison with the reference WT myrUSH3 cannot be performed, due to the lower steady state response of WT myrUSH3.

Figure 3.8. Dimer$_{antiHisTag}$ relative response in terms of Monomer+Dimer relative response for myrUSH3 WT (blue), K5A (magenta) and K7A (orange). WT myrUSH3 was injected at 3, 6, 10 and 20 µM whereas the mutants were injected at 20 µM. Data used originates from two different sensor chips indicated by the type of marker (circle or triangle). Data expressed as mean $\pm$ SD, n = 3 (circles) n $\geq$ 5 (triangles).
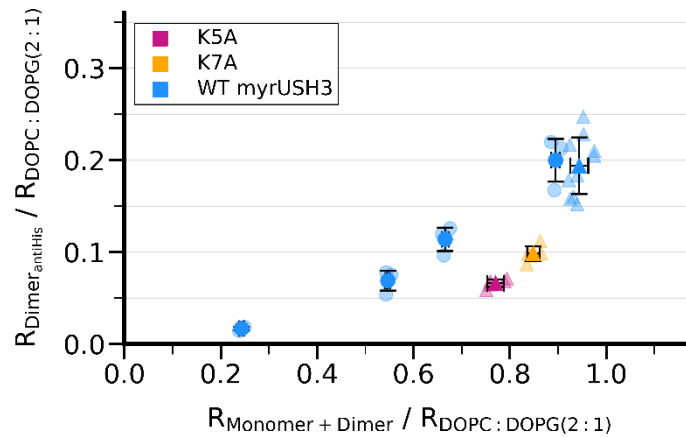

From the latter statement, as observed on the negatively charged membrane, one could argue that dimer formation in K5 and K7 myrUSH3 decreases given the lower protein density on the lipid surface. Even though binding on DOPC liposomes validate the impaired dimer formation by K5 or K7 mutations without affecting the Monomer + Dimer response, we confirmed that in negatively charged DOPC:DOPG (2:1) liposomes, these mutants prevented dimerization beyond the effects that could be attributed to changes in protein density (*Figure 3.8.*).

WT myrUSH3 was injected at different bulk concentrations (3, 6, 10 and 20 µM), modifying the protein density on the surface (*Figure 3.8.* x axis) yielding the corresponding dimer fraction (*Figure 3.8.* y axis). Although the K7A and, even more, the K5A mutants primary binding occurs at a lower density than that of WT myrUSH3 when injected at the same concentration, reflecting the weaker electrostatic interaction with the lipids, the observed density of Monomer+Dimer fraction of the mutants injected at 20 µM is higher than that obtained with WT myrUSH3 at 10 µM, but the dimer response is much lower. Altogether, these results suggest that direct interactions involving K^5, K^7 and K^9 and not simply the overall charge of the basic SH4 domain are the critical determinants of c-Src self-association on the membrane.

3.3.2. Positive charge of the lysine residues is essential for clustering

Self-association of c-Src through its strongly positively charged SH4 domain is counterintuitive, as one would expect that electrostatic repulsion would prevent dimerization. Even more surprising is the apparent role of the positively charged residue K^5, K^7 and K^9 on the effective dimer formation. At this point, we explored whether the positive charge of the lysine residue was the key component by designing two synthetic myrSH4 variants: one in which individually K^5 and K^7 were replaced by acetyllysine (K#Ac), removing the positively charged group of lysine while maintaining its long hydrophobic chain; and a second mutant in which the three lysines K^5, K^7 and K^9 were simultaneously replaced by arginine. In the latter, although the formal charge is conserved, the guanidinium group of arginine may generate more stable interactions through salt-bridges or multiple hydrogen bonding (e.g. bidentate hydrogen bonding) compared to the amino group in the lysine residue. In fact, Musafia et al., (1995) reported arginine residues to be frequently found in complex salt bridges[30], which are abundant at the interface of associated protein subunits, highlighting the preference for arginine over lysine due to a particular geometric structure of the guanidinium group (Musafia et al., 1995).

Figure 3.9. Monomer+Dimer and Dimer$_{antiSrc}$ relative responses to WT for acetylated (K5Ac and K7Ac) and triple arginine (K^5, K^7, K^9)$\rightarrow$(R^5, R^7, R^9) myrSH4 constructs over (A) neutral DOPC liposomes and (B) negatively charged DOPC:DOPG (2:1) liposomes. Data expressed as mean ± SD, n = 3 (DOPC) n=6 (DOPC:DOPG (2:1)). Significant differences in the Dimer$_{antiSrc}$ relative responses with respect to WT myrSH4 are indicated by asterisks (Mann-Whitney test: *p < 0.1; **p < 0.05; ns: not significant).
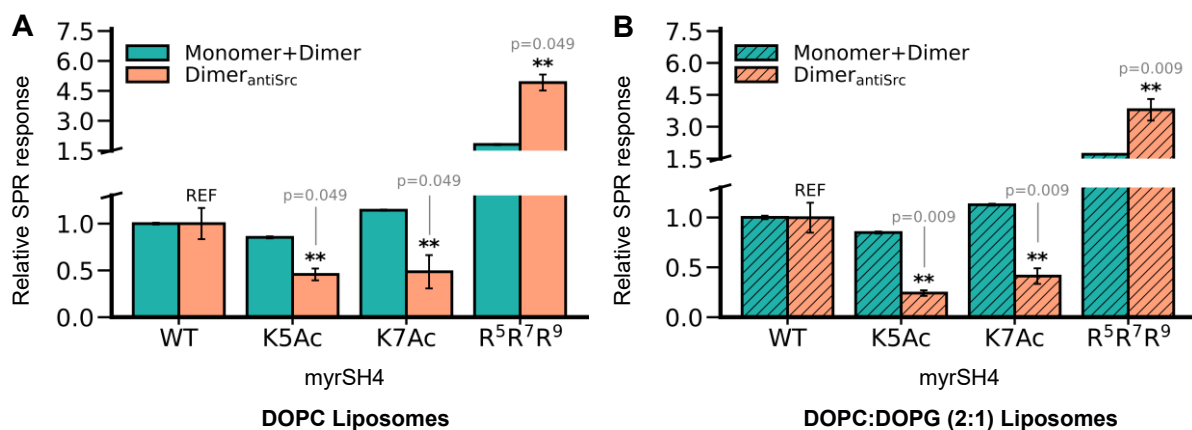

As presented in *Figure 3.9.* acetylation of lysine residues impairs dimer formation, whereas replacement of these residue by arginine, enhances the clustering phenomenon on the membrane. K#Ac mutants exhibited a comparable steady state response

---

[30] Non-bonded or hydrogen-bonded ion-paired interaction joining more than two residues (Musafia et al., 1995).

(Monomer+Dimer) to WT, yet the $Dimer_{antiSrc}$ fraction decreased ~50%, suggesting that the positive charge of the lysine residues is a critical element for self-association.

The $R^5R^7R^9$ myrSH4 mutant steady state fraction (Monomer+Dimer) was ~1.5 times higher than WT myrSH4, setting out a possible different lipid binding affinity by the arginines bearing construct. Although, Robison et al., (2016) using polyArginine Arg_9 and polyLysine Lys_9 peptides, reported a stronger binding to negatively charged membranes by the former, Buser et al., (1994) had reported a similar membrane binding affinity for a shorter $R^5R^7R^9$ myrSH4 variant (residues 2-12) against the native $K^5K^7K^9$ containing construct. In the latter case, the particular conformation of the construct upon membrane tethering due to the myristoyl presence (and/or the singular sequence) might influence the overall binding affinity and thus nature of the basic residue might not be determinant. To confirm the results of Buser et al. (1994) in our system, we measured and obtained a similar binding affinity by $R^5R^7R^9$ myrSH4 (residues 2-16) and WT myrSH4 (*Figure 3.10.*) towards neutral and negatively charged membranes. Then, why the difference in the steady state fraction?

Figure 3.10. (A) Representative SPR binding curves for WT and $R^5R^7R^9$ myrSH4 constructs, injected at concentration ranging between (1.25 – 60 µM) for 30 s (association) on neutral DOPC and negatively charged DOPC:DOPG (2:1) liposomes. Best fit with the 1:1 Langmuir model (black curves) analyzed using the Biacore T200 3.0 Evaluation. (B) K_d values obtained from (A). Data expressed as mean ± SD, n = 4. Significant differences in binding constants with respect to WT myrSH4 are indicated by asterisks (Mann-Whitney test: *p < 0.1; **p < 0.05; ns: not significant).
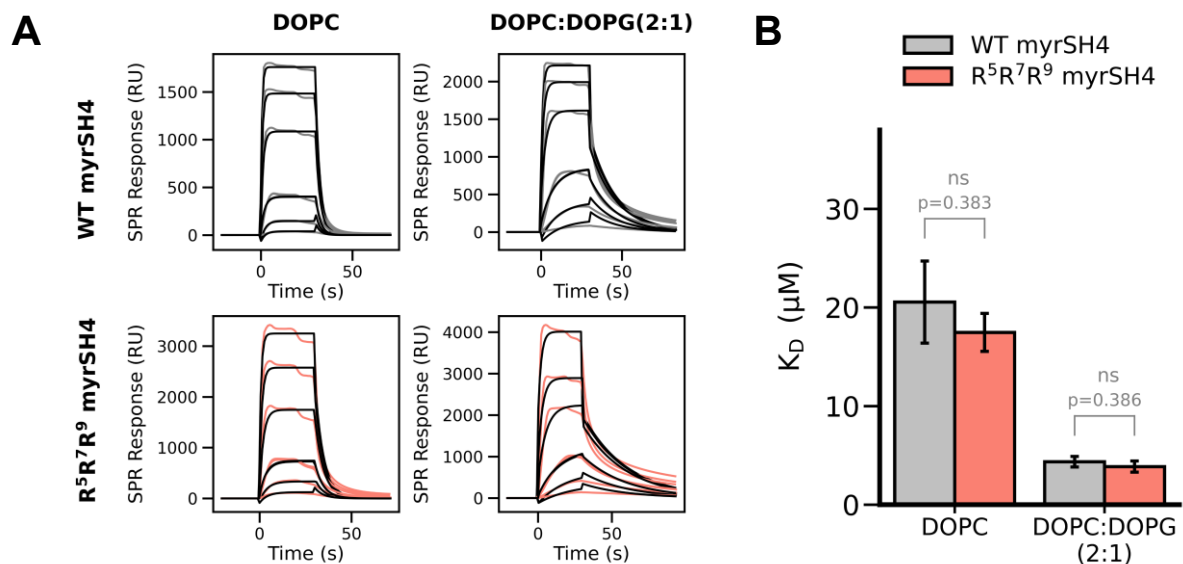
In their study with Arg_9 and Lys_9 peptides, Robison et al., (2016) also observed that lysine Lys_9 peptides adsorbed on the lipid bilayers exhibited strong anticooperative effects due to electrostatic repulsion, whereas arginine Arg_9 showed cooperative interactions leading to an accumulation of the Arg_9 peptides at the membrane surface. This cooperative effect is attributed to the favorable like-charge guanidinium–guanidinium ion pairing, offsetting partially the electrostatic repulsion, adding to the stronger interaction of the guanidinium

moiety with the lipid head groups (Robinson et al. 2016, Vazdar et al. 2018). Thus, these observations might explain the enhanced level of $R^5R^7R^9$ myrSH4 on the membrane surface in our system as well.

While $R^5R^7R^9$ myrSH4 mutant steady state fraction (Monomer+Dimer) was ~1.5 times higher, the Dimer$_{antiSrc}$ fraction was enhanced by a factor of ~4.5 times compared to WT myrSH4, suggesting that K$\rightarrow$R mutations favored dimer formation beyond the enhanced concentration of the myristoylated peptide on the lipid bilayer. This would be in line with the hypothesis of arginine guanidinium group building more stable interactions compared to the native lysine residues in c-Src, raising the question on the interacting partners of these lysine residues (K^5, K^7 and K^9) within the c-Src dimer interface.

3.3.3. The role of lipids in self-association: the membrane interface

The effect of acetyl-lysine and arginine replacements confirm that positive charges are critical for c-Src self-association, suggesting that a negatively charged specie is present, bridging the positively charged residues and alleviating electrostatic repulsion. So far, SH4 domain mediated c-Src self-association has been detected to occur exclusively on the membrane context, thereby phosphate groups of the phospholipids composing, the lipid bilayer as mediators of c-Src self-association, is the utmost plausible scenario. Interestingly, the work of Li et al., (2013), showed a stronger interaction of arginine and the lipid phosphate moieties at the membrane interface compared to lysine, which is in line with our observations.

We tested another negatively charged lipid 1,2-dioleoyl-sn-glycero-3-phosphate (DOPA), using the same molar ratio between anionic and zwitterionic lipids as in the DOPG experiments.

Figure 3.11. (A) Representative SPR binding curves for WT myrUSH3, injected at 20 µM on neutral DOPC, negatively charged DOPC:DOPG (2:1) and DOPC:DOPA (2:1) liposomes. (B) Monomer+Dimer and Dimer$_{antiSrc}$ relative responses on the different types of liposomes. Data expressed as mean ± SD, n = 3. Significant differences are indicated by asterisks (Mann-Whitney test: *p < 0.1; **p < 0.05; ns: not significant).
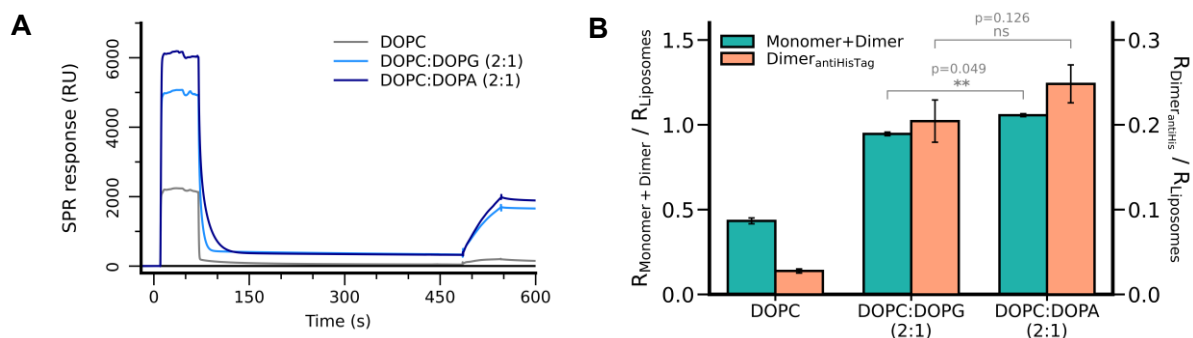

Changing the type of anionic lipid, DOPA instead of DOPG, did not cause a significant effect in the observed dimer formation (*Figure 3.11.*). Indeed, the slight enhancement could be attributed to the increased steady state Monomer+Dimer fraction of myrUSH3 WT. Although a generalization may be tentative but incorrect, whether c-Src dimerization is promoted on a specific lipid availability remains to be explored.

DOPA has a net charge of -1.3 at pH 7.4, thus the negative charge over the surface increases 10% (compared to DOPG), justifying for the slightly slower dissociation observed for monomeric myrUSH3 (*Figure 3.11.* A), which could imply a stronger affinity. Therefore, one highlighting observation from this assay, is that a higher negative charged density on the membrane surface leading an apparent stronger binding of the monomeric c-Src, does not modulate the dimer formation, beyond influencing the total amount of myrUSH3 on the surface. In fact, switching from a neutral DOPC to a negatively charge DOPC:DOPG (2:1) membrane, increases the affinity and consequently the amount of protein on the

surface, thus does it means that if the protein amount on DOPC membrane would be comparable to DOPC:DOPG (2:1) membrane, then Dimer$_{antiSrc/antiHis}$ fraction would be similar?

To answer this question, we examine the dependency of the relative dimer formation in terms of the protein density on the neutral DOPC and negatively charged DOPC:DOPG (2:1) membranes (*Figure 3.12.*).

Figure 3.12. Dimer$_{antiSrc}$ relative response in terms of Monomer+Dimer relative response for myrUSH3 WT injected at concentrations in the range of 3 - 20 µM on neutral DOPC liposomes (gray circles) and negatively charged DOPC:DOPG (2:1) (blue circles). Data expressed as mean ± SD, n = 3.
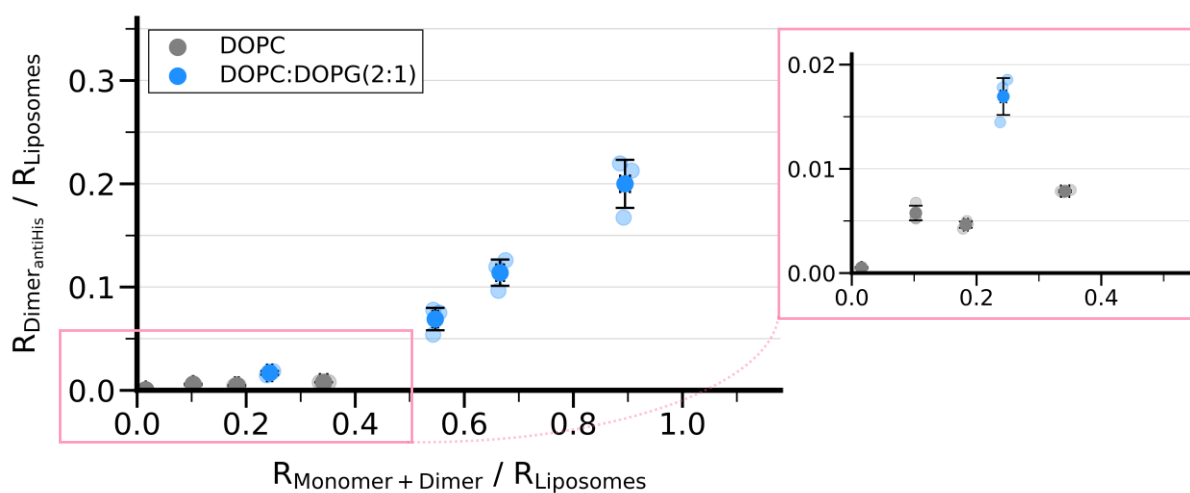
In *Figure 3.12.*, the X axis can be interpreted as the protein density on the surface (as previously commented, R$_{Monomer+Dimer}$ ≈ R$_{Monomer}$ since the dimeric fraction is negligible compared to the monomer population) while the Y axis would be the dimer population observed. Dimer detected on DOPC bilayers is one order of magnitude lower compared to negatively charged membranes and similar "protein densities" (e.g. 0.25 − 0.4 X axis) do not yield same level of dimer formed, indicating that an increased density of c-Src on the membrane surface just not provoke the self-association (i.e. not protein-protein interaction dependent) but depends on the interaction of the K-motif (K^5, K^7 and K^9) with the phosphate groups of lipids at the membrane interface (i.e. lipid headgroup region). As previously mentioned, Scheidt and Huster, (2009) using combined NMR and thermodynamics measurements, demonstrated that on the negatively charged membrane (DMPC:DMPG (2:1)) the SH4 domain inserted deeper into the membrane interface distorting the headgroup region due to interaction of the charged amino acids. Whereas on neutral DMPC membranes the low electrostatic contribution[31] and the need to attenuate Born repulsion localizes the peptide backbone (SH4 domain) farther from the membrane.

---

[31] The membrane lipid headgroups can be characterized as permanent electric dipoles adding a very small contribution to attractive electrostatic forces (Scheidt and Huster, 2009).

These observations arguably illuminate the underlying reason on the different dimerization levels detected in our system on both types of membrane.

Likewise, thinking in terms of receptors with multipl*e* ligand binding sites (visualizing the membrane as a receptor) the neutral DOPC lipid bilayers, potentially having a same number of "c-Src dimers binding sites" as in DOPC:DOPG (2:1), the dimer formation reaches an *early* saturation stage, which could be indicative of negative cooperativity. So, within this assumed framework, why on the zwitterionic DOPC membrane one myrSH4 molecule is hindering the binding of an adjacent myrSH4? Probably due to the crowding of positively charged residues on each SH4 domain repeating other myrSrc molecules, whereas this could be partially compensated by the negative charge on the DOPC:DOPG (2:1) lipid bilayers. This assumption might open one pathway to understand why the c-Src self-associated fraction is such a minor portion compared to monomeric form. Although the scenario seems to be very intricated to be addressed it through a simple model accounting for all the Coulombic and non-Coulombic intrinsic interactions (i.e. hydrophobic, short-range electrostatic contributions, etc.) (Scheidt and Huster, 2009), we can presume a hypothetical mechanism for the dimer formation (*Figure 3.13.*).

Figure 3.13. Putative c-Src dimer formation mechanism. In green background is the monomer binding, specie (II) membrane binding would be driven predominantly by the myristoyl group (i.e. neutral DOPC membrane), specie (III) binding depends on the concurrent hydrophobic burial of the myristoyl group and the electrostatic interaction of polybasic cluster in the SH4 domain (i.e. negatively charged DOPC:DOPG (2:1) membrane). In orange background, the intermediate specie formation (IV) emerged from the hydrogen bond formation with the phosphate groups of the membrane lipids. In red background the self-associated specie (V).
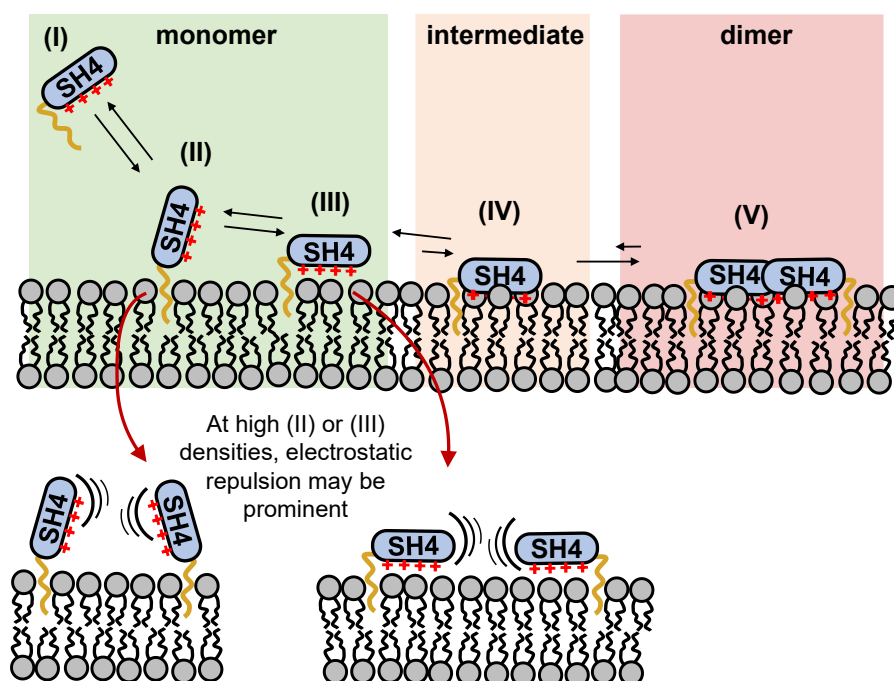
In this hypothetical scenario (*Figure 3.13.*), on the neutral DOPC membrane formation of the intermediate specie (IV) would be less favored and probably the most abundant myrSrc specie would be (II), whereas on the negatively charged DOPC:DOPG (2:1) transition from (I) to (III) would be straightforward due to the presence of the negative charged lipids.

In a nutshell, the results above presented suggest that the position of the K-motif: K^5, K^7 and K^9 of the SH4 domain on the membrane interface seems to be determinant for c-Src self-association, which is in agreement with the statement of c-Src dimerization mediated by the lipids headgroups (i.e. phosphate moieties). The inherent mutual repulsion between myrSrc molecules through the strongly positively charged SH4 domain could influence its penetration toward the lipid headgroup region (membrane interface) consequently regulating the overall amount of dimer formed.

3.3.4. Could an additional positive charge in the SH4 domain affect the dimerization?

The K-motif ([5]KxKxK[9]) in the SH4 domain plays multiple roles in the c-Src membrane binding, it provides an enhanced binding to negatively charged lipids and independently, as confirmed from the neutral lipid bilayers measurements and the point mutations on the SH4 domain, it is responsible for c-Src self-association upon membrane anchoring. c-Src clustering is, presumably, mediated by the phospholipids in the membrane and thereby an effective insertion of the K-motif towards the membrane interface (i.e. lipid headgroup region) could be a crucial step (e.g. (IV) in *Figure 3.13.*). According to Scheidt and Huster, (2009), the presence of anionic lipids promotes a deeper inclusion of the SH4 domain to the membrane interface owing to the electrostatic interactions with the positively charged residues. They concluded that the interaction of myrSH4 with phosphatidyl serine lipids involves short-range (non-Coulombic) electrostatic interactions between the peptide and phospholipid headgroups, which are not accounted by Gouy-Chapman theory. However, increasing the negative charge over the surface apparently just influences on the density of the monomer at the surface but not directly impacts on the amount of dimer formed, although the monomeric form seemingly features a stronger binding. So, what if the SH4 domain was "upgraded" with an extra positive charged residue? The affinity towards the negatively charged membrane would increase, but would it impact on the dimer formation?

We explored these questions by mutating residue D^{10} to R in the myrUSH3 c-Src construct. This modification eliminates a negative charge and introduces an additional positive charge, being an arginine, which has been shown to boost the dimer formation. The SH4 domain of the D10R myrUSH3 mutant would have a +7 net charge. As previously presented in the *subsection 3.3.1*, mutation D^{10} to A, which formally increases the net charge of SH4 domain (residues 2-16) to +6, although this mutation provoked a slight increase in the Monomer+Dimer fraction, it did not enhance the dimerization of the D10A myrUSH3 beyond the expected for WT at the same surface density. In fact, on the negatively charged membrane, the dimer formation of D10A myrUSH3 was even lower. Moreover, while the increase of the Monomer+Dimer fraction of D10A myrUSH3 on the negatively charged membrane could be explained by an increased electrostatic interaction (i.e. +6 net charge), the higher density of D10A myrUSH3 detected on the neutral membrane was not clear. It was hypothesized that D10A could provoked a different presentation of the SH4 domain towards the neutral bilayer by altered intra-molecular interactions. The results of D10R myrUSH3 measurements on neutral (DOPC) and negatively charged liposomes are shown in *Figure 3.14.* (I also include the previous results obtained for the D10A mutation for a better comparison (in a blurred fashion)).

Figure 3.14. Monomer+Dimer and Dimer$_{antiSrc}$ relative responses to WT for D10A and D10R myrUSH3 constructs over (A) neutral DOPC liposomes and (B) negatively charged DOPC:DOPG (2:1) liposomes. Data expressed as mean ± SD, n=3.
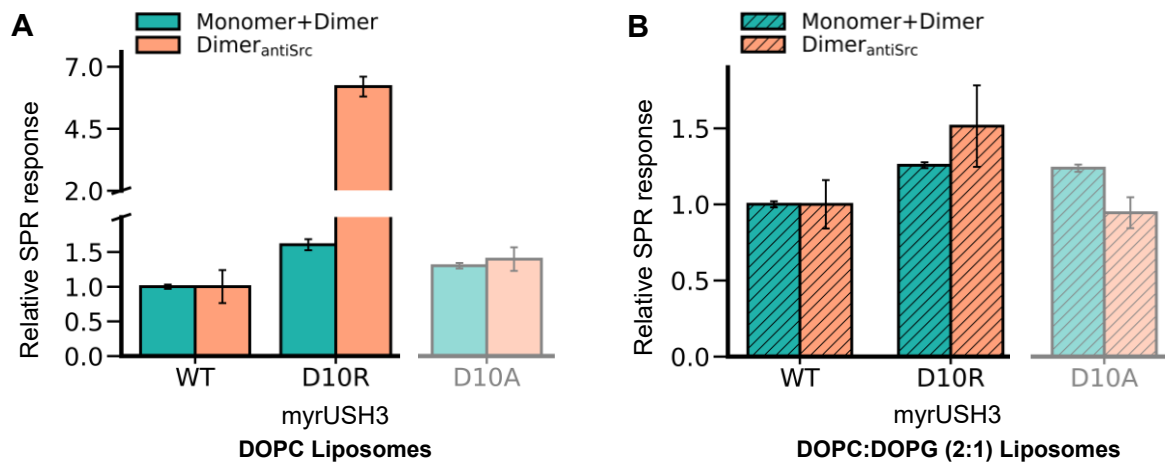

The D10R mutation has a much large impact on the dimer formation (Dimer$_{antiHis}$) on the neutral DOPC membrane compared to the negatively charged DOPC:DOPG (2:1) lipid bilayer. Surprisingly, on the neutral DOPC lipid bilayer the D10R mutation enhances almost ~7 fold the Dimer$_{antiHis}$ fraction while the Monomer+Dimer fraction just increased ~1.5 times compared to WT myrUSH3. Since the D10A myrUSH3 mutant displayed dimer formation levels "proportional" to WT myrUSH3 on the same lipid bilayer, this enhancement must be caused by the arginine mutation. A possible explanation for this observation could be the direct interaction of the guanidinium group with lipid phosphate and glycerol groups of the DOPC in the lipid bilayer, that was predicted to occur by Wu et al., (2013) using atomistic simulations on a similar neutral membrane, resulting in a deeper insertion of the arginine side chain in the polar region of the neutral lipid bilayer. Thence, a direct interaction of R[10] with the membrane lipids may restrain the orientation of SH4 domain, favoring the contact of K[5], K[7] and K[9] with the phosphate groups of the lipids and consequently enhancing the dimerization. In our hypothetical mechanism in *Figure 3.13.*, this mutation may favor the intermediate species (IV). A complementary explanation may be that the D10R mutation could introduce intramolecular electrostatic repulsion reorienting the lysine side chains and favoring dimerization.

Conversely, on the negatively charged DOPC:DOPG (2:1) membrane D10R mutation provokes a slight increase in the Dimer$_{antiHis}$ fraction (compared to the neutral membrane), however this could be readily ascribed to the slightly enhanced Monomer+Dimer D10R myrUSH3 fraction. In terms of dimer formation, D10R myrUSH3 neither yields the same impaired levels as for D10A mutation nor dramatically changes dimer formation as on DOPC liposomes, rather D10R myrUSH3 behaves like WT (on the negatively charged membrane), thought the affinity is unarguably stronger. This result suggests that: i) c-Src self-association does not results from non-specific electrostatic interactions with the lipid bilayer ii) an intact K-motif is enough for an effective c-Src self-association iii) the arginine stretch [14]RRR[16] in the SH4 domain most likely is not required for c-Src self- association, although it may provide additional electrostatic interactions for binding to acidic lipids,

increasing c-Src density at the membrane, indirectly favoring c-Src clustering. Consistently, c-Src oligomerization was observed by Dwivedi et al., (2017) using myristoylated SH4 peptides containing only residues 2-9.

Other explanations justifying the undramatic change in the D10R myrUSH3 dimeric fraction on the negatively charged lipid bilayers as observed on the neutral membrane, could include an increased electrostatic repulsion between myrUSH3 D10R molecules due to greater net charge (keeping in mind the hypothetical mechanism (*Figure 3.13.*). This possible effect of intermolecular electrostatic repulsion was further investigated by using DOPC:DOPA (2:1) liposomes that have ~10% greater net negative charge on the surface compared to DOPC:DOPG (2:1). The results are shown in *Figure 3.15.*

Figure 3.15. (A) Representative SPR binding curves for WT myrUSH3 and D10R myrUSH3, injected at 20 μM on DOPC:DOPA (2:1) liposomes. (B) Monomer+Dimer and Dimer$_{antiSrc}$ relative responses to WT on DOPC:DOPA (2:1) liposomes. Data expressed as mean ± SD, n = 3.
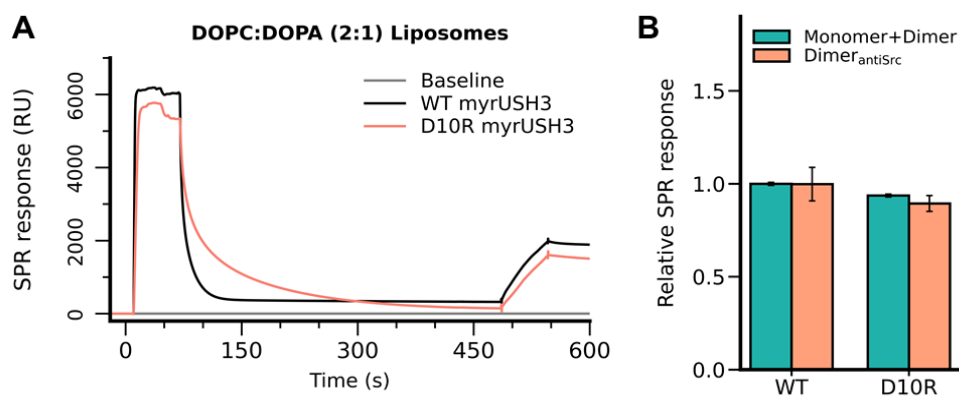
In contrast to WT myrUSH3, a decrease in the total quantity of D10R myrUSH3 bound at equilibrium (Monomer+Dimer) is detected (*Figure 3.15.*B) on DOPC:DOPA (2:1) membrane, however the dissociation was much slower compared to WT myrUSH3 on DOPA containing membranes, indicative of a stronger binding. These results are consistent with an increased electrostatic interaction of the D10R mutant with DOPC:DOPA (2:1) membrane that entails a higher intermolecular (myrUSH3-myrUSH3) electrostatic repulsion.

The decrease Monomer+Dimer fraction of D10R myrUSH3 on DOPC:DOPA (2:1) (*Figure 3.15.A*) is probably due to the accumulation of the highly positively charged D10R myrUSH3 near the membrane surface (charge condensation) ultimately limiting the total amount of protein over the surface. The slower dissociation by D10R myUSH3 makes explicit the stronger binding, however the D10R myrUSH3 dimeric fraction is proportional to the overall protein bound on the membrane (*Figure 3.15.*B), supporting that self-association is an independent phenomenon following membrane anchoring. In the next section, we will discuss a hypothesis that could also clarify the underlying reason of the not enhanced D10R myrUSH3 dimer fraction on the negatively charged membrane.

3.3.5. A putative β-sheet conformation of the SH4 domain in the c-Src clustered fraction

The results presented so far, highlight the role of the alternating lysine residues ($^5KxKxK^9$) in SH4 driven c-Src dimerization. The alternating pattern of the residues whose mutation to alanine hinders dimerization is best observed in DOPC:DOPG (2:1) liposomes and interestingly, in this membrane the alternating pattern extends to S^3.

In the neutral pure DOPC liposomes, K5A and K7A caused significant dimerization impairment but the effect of K9A and S3A mutations on dimerization was not statistically significant. Additionally, on this neutral membrane, mutation to alanine of the alternating residues N^4, S^6, and D^{10} showed a statistically significant increase in the primary (Monomer+Dimer) (*Figure 3.16.*) binding and consequently a similar tendency of increased dimer formation (Dimer$_{antiHis}$)[32]. On the negatively charged membrane, a slight increased (Monomer+Dimer) fraction for those even-sequence-position residues (i.e. N4, S6 and D10) was also observed, but dimer formation was reduced in all the SH4 domain myrUSH3 mutants. In a nutshell, single mutations of residues S^3-x-K^5-x-K^7-x-K^9-x affect the dimerization significantly, while residues in the remaining positions x-N^4-x-S^6-x-P^8-x-D^{10} when mutated do not provoke the same effect.

Figure 3.16. Monomer+Dimer and Dimer$_{antiSrc}$ relative responses to WT for the X#A myrUSH3 mutants injected at 20 μM over (A) neutral DOPC liposomes and (B) negatively charged DOPC:DOPG (2:1) liposomes. Data expressed as mean ± SD, n = 3 (DOPC) n=5 (DOPC:DOPG (2:1)). Significant differences in the relative responses with respect to WT myrUSH3 are indicated by asterisks (Mann-Whitney test: *p < 0.1; **p < 0.05; ns: not significant, REF: reference).
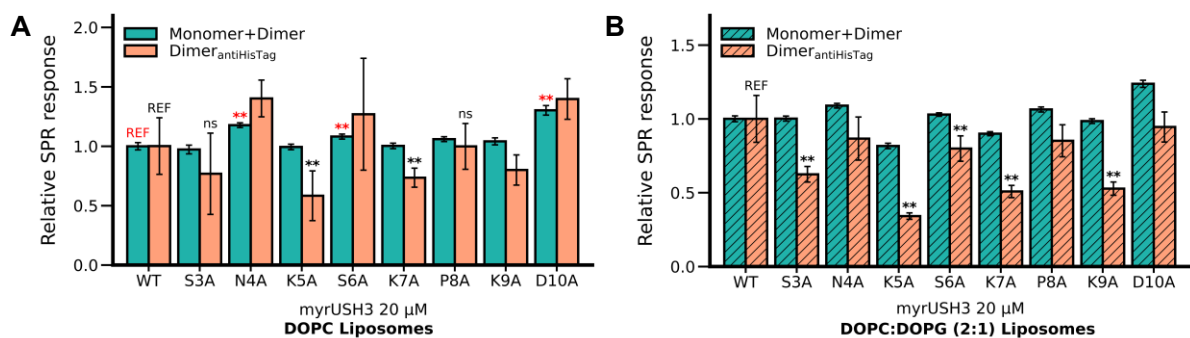

The different effects upon perturbation of alternate positions i.e. S^3-X-K^5-X-K^7-X-K^9-X and X-N^4-X-S^6-X-P^8-X-D^{10} suggests an extended structure, as found in β-strands, with the side chains of alternating residues pointing to opposite directions perpendicular to the direction of the main chain. In this arrangement, the residues shown to be important for c-

---

[32] The statistical analysis of Dimer$_{antiHis}$ of these mutants has been omitted since a direct comparison with the reference WT myrUSH3 might not be accurate, as the Monomer+Dimer response of WT myrUSH3 in lower.

Src dimerization would be pointing to the same direction (*Figure 3.17.*), presumably towards the lipid headgroups. It should be noted that the phosphate groups of all phospholipids are negatively charged, independently of the fact that the overall charge is negative (as in DOPG) or neutral (in DOPC).

**Figure 3.17.** c-Src SH4 domain structure represented in an extended conformation.
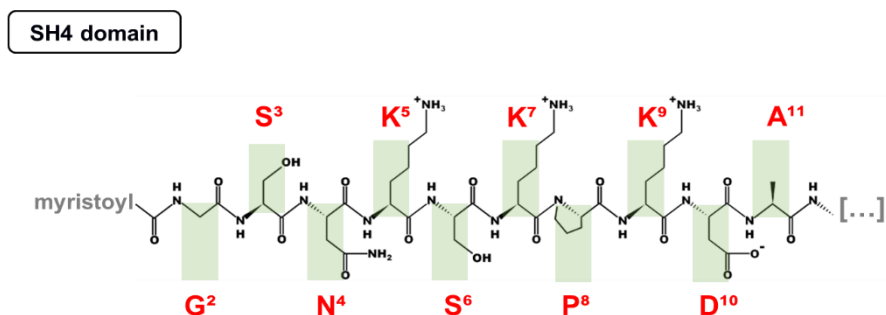
So far, we know that positive charges (^{5}KxKxK^7) are critical for c-Src self-association and thus presumably the negatively charge phosphate moieties of the phospholipids participate in this dimerization to alleviate the electrostatic repulsion. But this (^{5}KxKxK^7) – lipid interaction can also occur in the c-Src monomeric state, so what triggers the "switch" from monomer to a dimer? It could result that (*Figure 3.13.*) in the c-Src intermediate species (IV) the positioning of the K-motif residues by the lipid phosphate groups confers the SH4 domain a particular conformation (i.e. β-strand) and upon encounter of two SH4 domains (with β-strand conformation) both SH4 domain backbone chains hydrogen bond and form a β-sheet (2 strands). This mechanism could potentially give rise to higher order oligomers with a β-sheet structure (*Figure 3.18.*). Additionally, this conformation of the SH4 domain would also justify why the D10R mutation on the negatively charged membrane[33] behaved like WT and not further enhanced the dimer formation, since the R^{10} would not be positioned towards the lipid headgroup region and thus presumably not contributing to the interaction with lipids (*Figure 3.18.*). The latter also suggests that the specific distribution (i.e. altering pattern) of the lysine residues (K-motif) in the SH4 domain is important for the dimer formation, given that the D10R mutation (^{5}KSKPKDA^{11} → ^{5}KSKPKRA^{11}) has not enhanced clustering on the negatively charged membrane.

Hädicke and Blume, (2017) observed the formation of anti-parallel β-sheet by model cationic peptides with alternating lysine and not charged residues ((KX)$_4$K) bound to anionic lipid bilayers, highly supporting our theory. The secondary structure was found to depend on the nature of the lipid head group and was lost above the lipid phase transition. The K-motif in c-Src contains a similar alternating sequence of charged residues, although

---

[33] In contrast to DOPC membrane, in the negatively charged lipid bilayer insertion towards the lipid headgroup region is favored, given the electrostatic contribution of the positively charged residues in the SH4 domain.

is shorter than in the model $(KX)_4K$ peptides. It is followed by additional arginine residues that would probably also favor antiparallel pairing of adjacent chains. An additional difference is that the peptides studied by Hädicke and Blume, (2017) were not myristoylated. An even more significant difference is the presence of the Unique and SH3 domains in myrUSH3. The SH4 domain is known to participate in the fuzzy complex nucleated around the SH3 domain (Arbesú et al., 2017).

Figure 3.18. Hypothesized scenario from our observations and the distinct degree and abundance of c-Src clustering reported upon membrane binding.
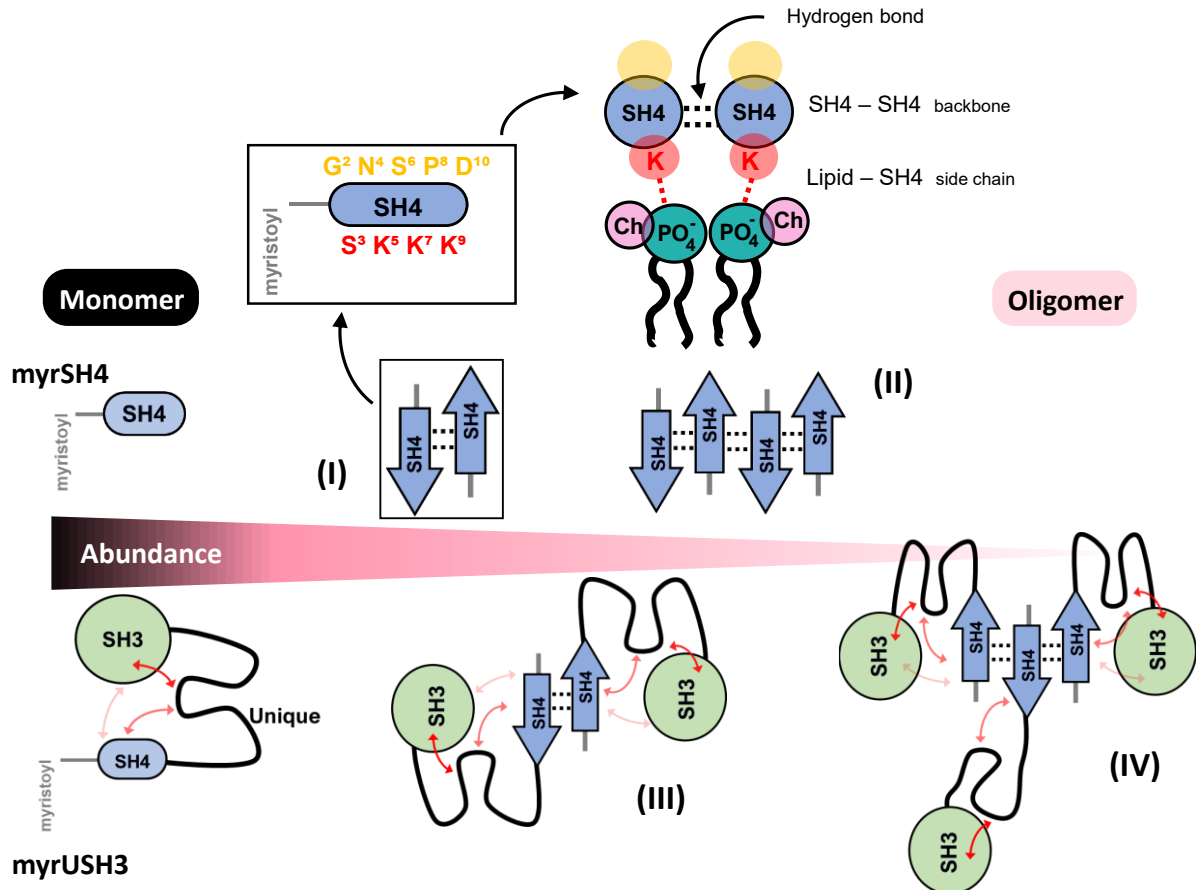

Short myristoylated peptides with the initial 16 residues (Le Roux et al., 2016a) or 9 residues (Dwivedi et al., 2017) of c-Src form large clusters, while the aggregates formed by the longer c-Src constructs (c-Src residues 2-150) are mainly dimers. c-Src constructs containing large fluorescent proteins attached to the myristoylated SH4 domain (residues 2-16) also form large oligomers (Owen et al., 2010). Thus, the almost exclusive formation of discrete dimers, is not simply due to steric hindrance. Our hypothesis is that intra-molecular interactions of the SH4 domain with the adjacent Unique and SH3 domains, described in *Chapter 2*, could restrict the growth of the protein clusters (e.g. β-sheet elongation) beyond dimers or at most trimers as observed by Le Roux et al. (2016a, 2016b). Our current working hypothesis is depicted in *Figure 3.18.*, assuming an anti-parallel SH4 domain conformation in the dimer, bearing in mind the observations by Hädicke and Blume, (2017).

3.3.6. Releasing the c-Src clusters from the membrane

Self-association is known to be a physiological relevant event for c-Src: its full-activation is achieved through trans-phosphorylation by a second c-Src molecule (Smart et al., 1981), although this interaction is assumed to be transient. Nonetheless, membrane mediated dimerization could be a potential activation mechanism for c-Src triggered by the accumulation of charged lipids. Our results show that a fraction of c-Src can form stable dimers, which probably will cross-phosphorylate. However, the inherent capacity of trans-phosphorylation exists as long as the dimer conformation remains, which could translate into a relentless kinase activity if dimerization is not subjected to regulation. In this section, we address this question.

Huang et al., (2018) described acetylation of the SH4 domain lysine cluster (K^5, K^7, and K^9) by CREB binding protein, resulting in the release of c-Src from the cell membrane. As summarized once again in *Figure 3.19.*, we have already explored this post-translational modification in our synthetic myrSH4 c-Src peptides, resulting in a lower c-Src self-association, even in the neutral DOPC membranes. Thence, the SH4 domain acetylation might be one pathway to regulate c-Src clustering.

Figure 3.19 Monomer+Dimer − Dimer$_{antiSrc}$ relative responses to WT for acetylated (K5Ac and K7Ac) myrSH4 constructs over (A) neutral DOPC liposomes and (B) negatively charged DOPC:DOPG (2:1) liposomes. Data expressed as mean ± SD, n = 3 (DOPC) n=6 (DOPC: DOPG (2:1)). Significant differences in the Dimer$_{antiSrc}$ relative responses with respect to WT myrSH4 are indicated by asterisks (Mann-Whitney test: *p < 0.1; **p < 0.05; ns: not significant).
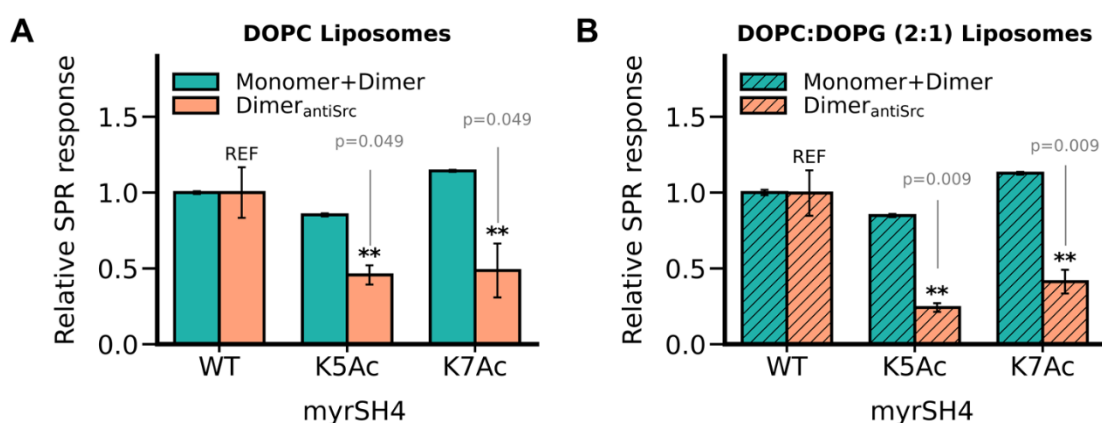
In *Chapter 2*, we learned that phosphorylation of S^{17} by PKA decreases myrUSH3 binding on lipid membranes, due to favored intra-molecular interactions of the myristoyl moiety with the inter-domain IDR-SH3 fuzzy complex. Thence, we assessed whether phosphorylation of S^{17} also affected c-Src self-association capacity. We performed *in vitro* phosphorylation of S^{17} by PKA in the myristoylated construct of c-Src myrUSH3 and performed the analysis by SPR on neutral DOPC lipid bilayers (*Figure 3.20.*).

Figure 3.20. (A) Monomer+Dimer − Dimer$_{antiSrc}$ relative responses to WT for pS17 myrUSH3 construct on neutral DOPC liposomes. (B) Dimer$_{antiSrc}$ relative response in terms of Monomer+Dimer relative response for myrUSH3 WT (gray) and phosphorylated S17 myrUSH3 construct (magenta). WT myrUSH3 was injected at in the range of 3 - 20 μM whereas the pS17 construct at 8.5 μM. Data used originates from two different sensorchips indicated by the type of marker (circle or triangle). Data expressed as mean ± SD, n = 3.
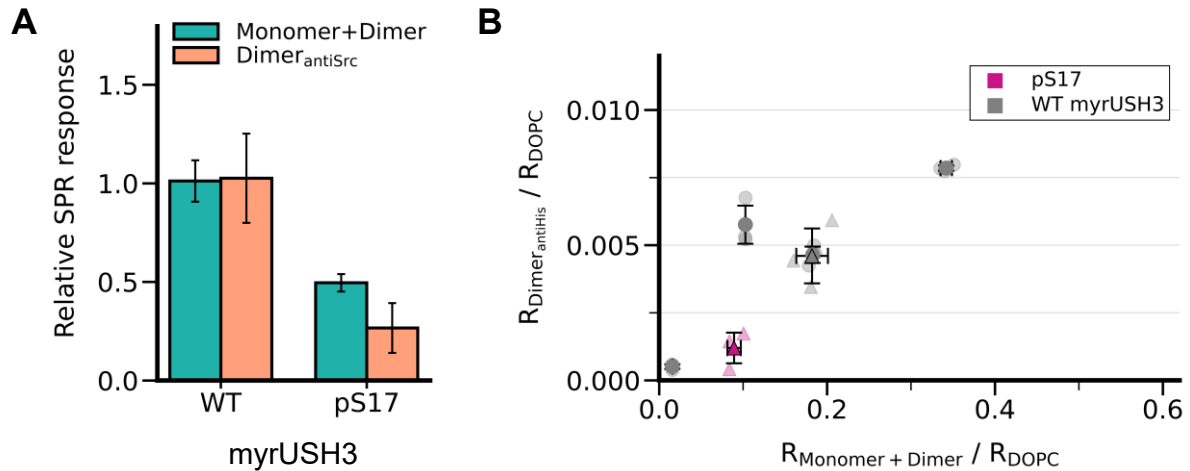

Although Monomer+Dimer fraction of pS^{17} myrUSH3 is lower than WT myrUSH3 (*Figure 3.20.*A), as presented in *Figure 3.20.*B phosphorylation of S^{17} clearly reduces dimer formation as compared to the unphosphorylated protein at the same surface concentration, confirming that this phosphorylation has a direct effect on c-Src self-association. A possible explanation would be the competition between the phosphate group attached at position 17 with the phosphate groups of the phospholipid head groups, as well as the overall net charge decrease of the SH4 domain in the phosphorylated protein, also reducing the fraction of bound monomer. Additional effects, such as changes in the orientation of the SH4 domain, for example by the interaction of the arginine cluster ^{14}RRR^{16} with pS^{17}, cannot be ruled out. All things considered, the biological significance of S^{17} phosphorylation in c-Src might be expanded to include a role to modulate c-Src self-association.

3.4. Lateral diffusion dynamics of the c-Src self-associated species on bilayers

<u>Contribution statement:</u> Sample preparation was done in collaboration with Francisco Javier Carvajal as part of his Bsc. thesis under my practical supervision. I acknowledge Dr. Anabel-Lise Le Roux for the initial help in the supported lipid bilayers design and preparation.

Protein self-association should have an impact on lateral diffusion in the lipid bilayer. We decided to characterize the diffusion dynamics of the c-Src self-associated population on membrane using Fluorescence Correlation Spectroscopy (FCS). FCS is based on the analysis of fluorescence intensity fluctuations over time, as a result of fluorescent molecules diffusing into and out of a microscopic detection volume defined by focused laser beam (confocal excitation volume) (Enderlein et al. 2005). Rapidly diffusing molecules will produce rapidly fluctuating intensity patterns, whereas larger species will remain for longer periods in the confocal volume yielding slower fluctuations. Fluorescence fluctuations are measured for long times (seconds) and analyzed to extract the temporal autocorrelation function (ACF; self-similarity over a lag time τ) (*Figure 3.21.*). In our system, the excitation volume is adjusted to measure the translational diffusion occurring on a scale of milliseconds to seconds.

Figure 3.21. Scheme of the Fluorescence Correlation Spectroscopy analysis.
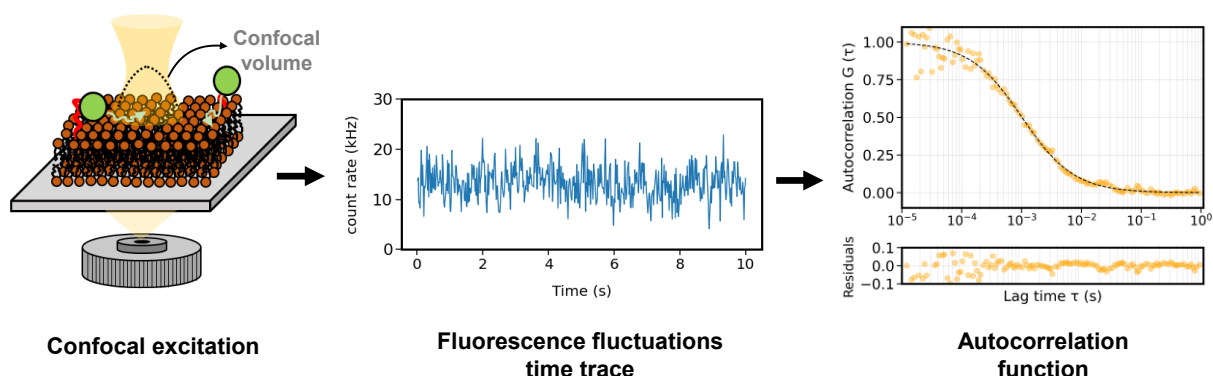
As a fluorescent probe is required for FCS analysis, we used a construct of the myristoylated N-terminal region of c-Src (SH4 and Unique domains) directly fused to the fluorescent protein GFP (referred as myrUGFP) or a variant containing also the SH3 domain with an additional cysteine residue close to the C-terminus that could be derivatized with a fluorescent Alexa dye. To accurately position the focusing illumination spot and to verify the integrity of the lipid bilayer on the glass cover-slip (referred as the supported lipid bilayer (SLB), we added a fluorescent lipid probe (1,2-dioleoyl-sn-glycero-3-phosphoethanolamine-N-lissamine rhodamine B sulfonyl LissRho-DOPE) in the negatively charged membrane composed of DOPC:DOPG (2:1) (+ 0.001% molar ratio LissRho-DOPE). The subsequent section describes the set-up for these experiments.

3.4.1. Materials and methods for FCS experiments

myrSrc constructs preparation

myrUGFP was expressed and purified as detailed in *subsection 2.7.1*. To prepare the myrUSH3-Alexa[555] conjugate, we used a myrUSH3 construct with a cysteine at the C-terminus and Alexa Fluor [555] maleimide (Thermo Fisher Scientific). The conjugation reaction was proceeded as per manufacturer protocol. The coupling efficiency was checked as indicated by Kim et al., (2008).

Supported Lipid Bilayers preparation

Glass cover slips (thickness 0.17 mm, Menzel Gläser) were cleaned in ddwater/NH_3 (30% w/w)/H_2O_2 (30% w/w) at volume ratio 5:1:1 bath heated at 65°C for 20 min. Afterwards, the coverslips were gently washed with double distilled water, dried using N_2 stream and placed overnight in an oven at 65°C for complete drying.

PDMS rings (4 mm interior diameter, ~3-4 mm thickness) were used to create a chamber on the coverslips. Bonding of the PDMS rings on the glass coverslips and complete cleaning of the chamber was proceeded using a Plasma Cleaner (O_2 plasma, Harrick, Model: PCD-002-CE). Lipid bilayer formation was proceeded immediately after plasma cleaning, liposomes diluted 1:6 in buffer 10 mM Tris, 300 mM NaCl, 10 mM $MgCl_2$ at pH 7.4 were deposited in the chamber and incubated for 1h at room temperature. After incubation the chamber was rinsed 20 times with 50 µL of dd water and 10 times with 50 µL of the working buffer (50 mM NaH_2PO_4/Na_2HPO_4, 150 mM NaCl, 0.2 mM EDTA, pH 7.5) and kept in buffer.

The myrSrc constructs (myrUGFP/ myrUSH3-Alexa[555]) were added to the bilayer containing chambers by rinsing 2 times with 50 µL of the protein solution and incubated for 30 min (minimum). After protein incubation, to minimize the myrSrc monomer fraction, the SLBs were washed 20 times with 50µL of working buffer.

Fluorescence Correlation Spectroscopy measurements and data analysis

All measurements were performed at 23°C using a Zeiss LSM-780 confocal microscope consisting of an inverted microscope (XYZ motorized Zeiss Axio Observer Z1) equipped with water immersion objective 40x NA1.2 C-Apochromat/VIS-IR/ Korr FCS/Korr 0.13-0.17. The excitation laser power was kept in the range of 0,1-1%, the signals were filtered by a 1 Airy unit pinhole, detected using a gallium arsenide phosphide photon-counting detector and processed with LSM Software ZEN 2.1 to obtain the autocorrelation analysis.

The integrity of the lipid bilayer was verified with trace amounts of LissRho-PE. Time traces were acquired for 10s, 10 times/spot in three different spots.

The autocorrelation functions were analyzed with PyCorrFit software (Müller et al., 2014) applying a fitting model of a single component 2D diffusion with a Gaussian laser profile using the Levenberg-Marquardt algorithm. Fitted curves with higher fitting errors were discarded.

3.4.2. FCS Results

The persistent c-Src dimers formed on the membrane coexist with the reversible monomeric form, however adding higher quantities of total c-Src protein increases the clustered form (as observed in the SPR results). Additionally, to minimize the reversible monomeric fraction, after incubation of the myrUGFP protein on the SLB, the sample was rinsed with protein-free buffer 20 times with equivalent sample volume. The performed FCS analysis at increasing myrUGFP concentration with corresponding auto-correlations obtained is shown in *Figure 3.22.*

Figure 3.22. A) Representative normalized auto-correlation (ACF) curves of myrUFGP at different concentration. The highest concentration analyses 1000nM yield an anomalous ACF. B) Residence times (τ_{diff}) at the different myrUGFP concentration extracted from the ACF fitting to a single component 2D diffusion model. Data is represented as a boxplot n>10. Green line represents the mean and red line the median.
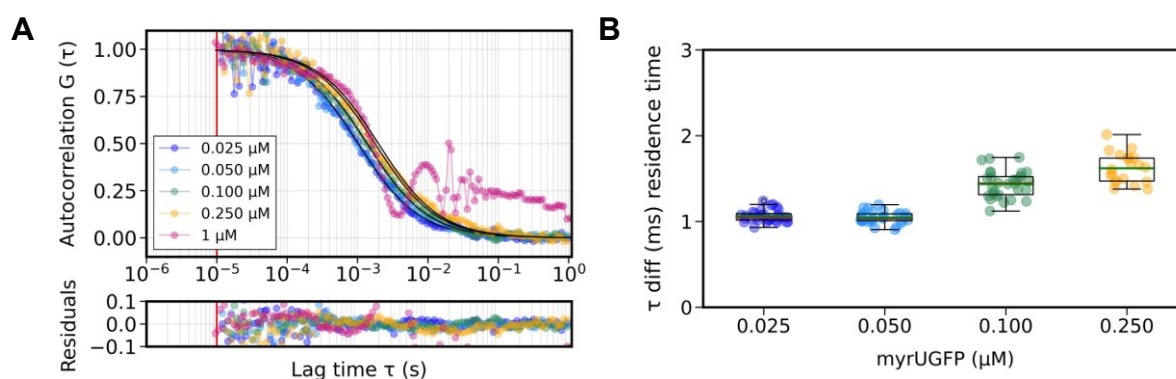
Although evidence from other techniques demonstrates the coexistence of monomeric and self-associated species, the auto-correlations obtained were best fitted using a single component 2D diffusion model, giving an apparent residence time for the predominant species. As the concentration of myrUGFP was increased, the apparent residence time showed a small increase, suggesting slower diffusion. This effect could originate by the unresolved contribution of self-associated species, i.e. those that have diffusion coefficients not distinct enough to warrant modeling as a separate species, or to crowding effects (Houser et al., 2016), affecting the diffusion of myrUGFP monomers. As reported by Houser et al., (2016), the crowding effects would reach a saturation at certain protein concentration. Nonetheless, as shown in *Figure 3.22.* at 1µM of myrUGFP, receiver saturation and/or GFP photobleaching derived in anomalous time traces, not enabling to increase the quantity of self-associated form on the membrane.

To overcome the concentration limit, we fixed the amount of fluorescent labeled c-Src construct and added non-labeled myrUSH3 c-Src at higher concentrations. We used a derivatized form of c-Src construct, bearing an Alexa[555] dye attached to the SH3 domain. Using a low and constant concentration of fluorescently labeled myrUSH3-Alexa[555] at 0.1 μM enabled to increase the total concentration of myristoylated protein up to 4 μM by adding unlabeled myrUSH3, attenuating the monomeric specie contribution while favoring dimer formation with an enhanced protein concentration. The higher brightness of Alexa and lower sensitivity to photobleaching allowed to work even at "diluted protein" conditions. The increase in the residence time (decrease in the apparent diffusion coefficient) with myrUSH3 concentration was evident using this approach (*Figure 3.23*).

Figure 3.23. A) Representative normalized auto-correlation (ACF) curves of the myrUSH3 + myrUSH3-Alexa[555] mixtures. Concentrations indicated correspond to non-labeled myrUSH3 added to 100 nM myrUSH3-Alexa[555]. B) Residence times (τ_{diff}) extracted from the ACF fitting to a single component 2D diffusion model. Data is represented as a boxplot n ≥ 8. Green line represents the mean and red line correspond to the median.
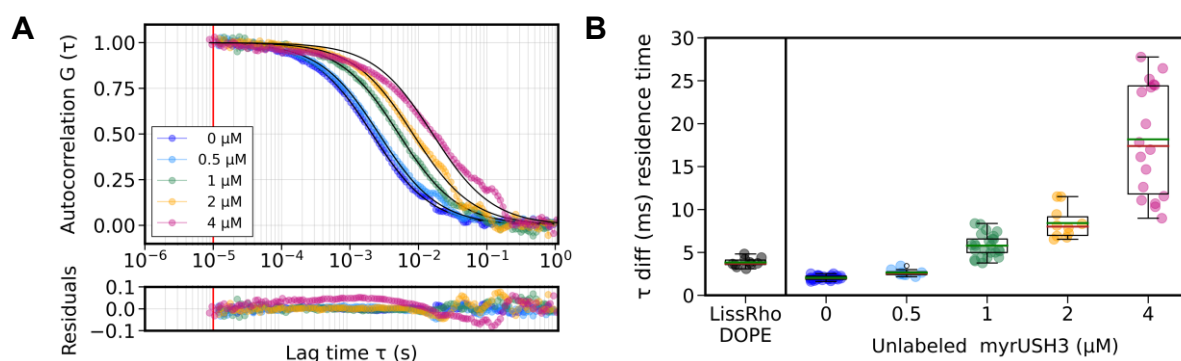
Although crowding effects cannot be ruled out, the remarkable changes observed in the residence times are most probably attributed to myrUSH3 self-association on the lipid bilayer. Of note is that clustered c-Src myrUSH3 mobility would be lower as compared to LyssRho-DOPE in the similar lipid bilayer[34] whereas monomeric (dominant specie in the samples <1000nM) myrUSH3 would display a diffusion coefficient similar to LyssRho-DOPE in the fluid membrane, in agreement with the idea that the lateral diffusion of monomeric myrUSH3 in membranes is dominated by the inserted myristoyl group, i.e. similar to the one observed in lipids. Our SPR results suggest discrete phospholipid-peptide complexes containing two c-Src molecules interacting through the K-motif ([5]KxKxK[9]) with the phosphate of the lipids' headgroup, hence the c-Src dimer diffusion within the membrane would not only depend on the two c-Src proteins but also for restricted mobility of the lipids mediating c-Src self-association, which could enable the recruitment of additional lipids in the surroundings to compensate the defect.

---

[34] The lipid bilayers used with myrUSH3-Alexa[555] would not contain LyssRho-DOPE (Ex/Em 560/583), as the later would interfere with myrUSH3-Alexa[555] (Ex/Em 556/572).

At a 10 μM myrUSH3 concentration, the lipid bilayer was immediately disrupted. This was observed by a reduction of fluorescence at the plane of the membrane and the appearance of rapidly diffusing species in the surrounding fluid. At lower concentrations (2 − 4 μM myrUSH3) membrane disruption was also observed but at a lower rate. The low stability of the membrane in the presence of 4 μM myrUSH3 probably explains the large variability observed in these samples. One explanation might be that as membrane c-Src clustering reaches a thermodynamic equilibrium, the higher accumulation of irreversibly bound myrUSH3 would increase the steric pressure that is alleviated through membrane bending (Stachowiak et al., 2012) eventually disrupting the lipid bilayer. Moreover, Busch et al., (2015) has recently demonstrated the important role that disordered segments play in membrane curvature formation, pointing out the Unique domain as a contributing factor. FCS analysis illustrates the clustering of c-Src myrUSH3 on fluid bilayers and unexpectedly unraveled the membrane disruption at apparently high density of c-Src clustered fraction, conveying that dimerization will not only affect c-Src function but might avenue signal transduction through altering the membrane biophysics.

3.5 Discussion

Membrane proteins continuously undergo homo or hetero-oligomeric complex formation. The lipid milieu exerts key roles in the recruitment, interactions and properties of the complex components (Gahbauer and Böckmann, 2016; Škerle et al., 2020). A growing number of structural elucidated membrane proteins unveil details on the regulatory roles of membrane lipids (Yeagle, 2014). Herein I report that self-association upon membrane binding of the proto-oncogen nRTK c-Src is mediated by the phospholipid headgroups of the membrane.

c-Src membrane binding has been extensively characterized, being a two-prong association requiring the burial of its N-terminal myristoyl moiety and the electrostatic attachment of the cluster of basic residues in the SH4 domain to the anionic lipids. Membrane binding of c-Src is mostly reversible, however our group and others have provided evidence for clustering and irreversible binding of a small fraction of c-Src molecules upon membrane anchoring (Le Roux et al., 2016a, 2016b; Smith et al., 2016; Owen et al., 2010). As reported by Dwivedi et al., (2017) all the elements required for c-Src self-association are found in the N-terminal myristoylated SH4 domain, specifically within the first 9 residues. In the present thesis, I have used SPR to probe the critical determinants for c-Src persistent clustering upon membrane binding. Performing first, individual and combined mutations of residues K^5 and S^6 by alanine in synthetic myrSH4 peptides, impairment in the dimer formation was observed by mutants bearing the K5A mutation. The same and additional residues mutations (i.e. S3A, N4A, K7A, P8A, K9A and D10A) introduced in the myrUSH3 c-Src construct (residues 2-150), completely unveiled the role of K^5, K^7 and K^9 (K-motif) as the determinant residues of the SH4 domain for an effective c-Src self-association upon membrane binding.

The positive charge of the K-cluster is essential to guarantee self-association, as inferred from the lysine to acetylysine mutations, which is rather counterintuitive, since self-association driven by the positively charged SH4 domain should entail strong electrostatic repulsion. While the interaction with negatively charged lipids may partially redress this repulsion, the observation of c-Src dimers or higher order clusters in lipid bilayers composed by a homogeneous neutral lipid (DOPC), suggests a more specific interaction. In fact, replacement of the lysines in K-motif with arginine residues greatly enhances oligomerization, although the formal charge is retained. Guanidinium groups form strong non-covalent interaction with phosphate groups (Schug and Lindner, 2005) including those of zwitterionic phosphatidylcholine (Li et al., 2013), leading to the assumption that c-Src self-association is mediated by the phosphate groups of the lipids composing the membrane. Indeed, hitherto dimerization mediated by the SH4 domain have not been detected in solution (i.e. non-membrane context).

Scheidt et al., (2009) using NMR demonstrated that the interfacial insertion of the SH4 domain (myrSH4 peptide (residues 2-19)) was deeper in a negatively charged membrane compared to a neutral one. Consistently, we have detected a lower c-Src dimer formation on the neutral DOPC membrane compared to a negatively charged lipid bilayer, despite

the protein being at similar surface densities as in the negatively charged membrane. This suggests that c-Src dimerization is not driven solely by a protein-protein interactions but requires the interaction of the K-motif (^{5}KxKxK^9) with the lipids at the membrane interface, thus an effective insertion of the K-motif towards the lipid headgroup region comes up to be a necessary step.

Kooijman et al., (2007) proposed the electrostatic/hydrogen bond switch mechanism, from the interaction of effector proteins (with PA (Phosphatidic acid) binding domains) to membranes containing PA. The feature shared by the known PA binding domains is the presence of basic residues (K or R). These domains would initiate an electrostatic interaction (reversible) with the membrane and subsequently form a hydrogen bond between lysine/arginine residue(s) and PA, locking the protein on the lipid bilayer. The switch occurs upon change in the ionization properties of PA (from -1 to -2 net charge caused by deprotonation), immediately after the side chain of K or R interacts with PA's headgroup. We observe a similar phenomenon, excluding that c-Src self-association is not exclusive to PA, it also occurs on PC and PG[35] and thus hydrogen bond formation might not be dependent on the modification of lipid headgroup's ionization properties. Additionally, in our case, what would cause the c-Src "switch" from a monomeric to dimeric state on the membrane?

Hädicke and Blume, (2017) reported the formation of anti-parallel β-sheet by peptides with alternating lysine and not charged residues ((KX)$_4$K) bound to anionic lipid bilayers. The K-motif, responsible of c-Src membrane clustering, matches the alternating sequence and the perturbations observed upon altering the SH4 domain suggests that this β-sheet-like conformation could exist in the c-Src dimer interface. Furthermore, Sinthuvanich et al., (2012) engineered a cationic peptide SVS-1 (KVKVKVKV^{D}P^{L}PTKVKVKVK-NH$_2$), with anticancer activity, that in solution presents a random coil conformation but folds into a β-hairpin structure on the negatively charged membrane surface. Although this further provides evidence that a lysine residue altering (KX)$_4$ motif leads to a β-sheet like structuration, it also illustrates the feasible transition of the same lysine motif from a random-coil to a folded state.

Returning to the question on what triggers c-Src "switch" from a monomeric to a dimeric state on the membrane, keeping in mind the latter observations, one could contemplate a model where an intermediary c-Src specie is formed (IV) (*Figure 3.24.*, whose SH4 domain embeds deeper in the lipid headgroup region upon membrane binding, enabling hydrogen bond formation of K-motif with the lipid phosphate moieties, overall changing the structure of the SH4 domain (e.g. allosteric modulation). At the encounter of two c-Src intermediate species (IV), the SH4 domains of both biomolecules (that now have a particular conformation due to the positioning of the K-motif residues by the lipid phosphate groups) fold into a β-sheet structure, triggering c-Src dimerization on the membrane. An effective binding of the K-motif to the lipid head-groups would be first required so a direct SH4

---

[35] Indeed, when DOPG was substituted by DOPA in the lipid bilayer no significant increase in the self-associated fraction was detected.

domain – SH4 domain (protein-protein) interaction could occur, which could account for the overall lower amount of c-Src dimer formed, in contrast to the monomeric fraction.

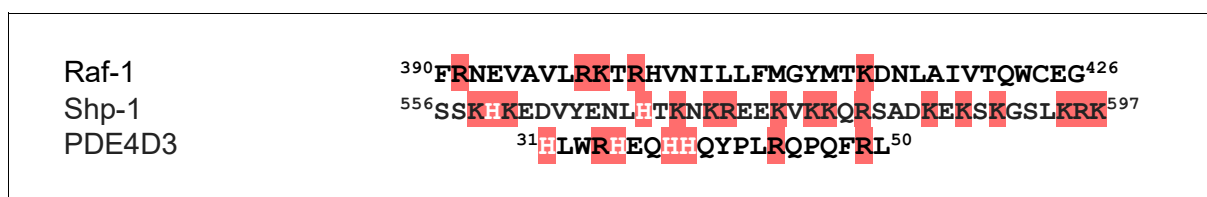**Figure 3.24.** Putative c-Src dimer formation mechanism.
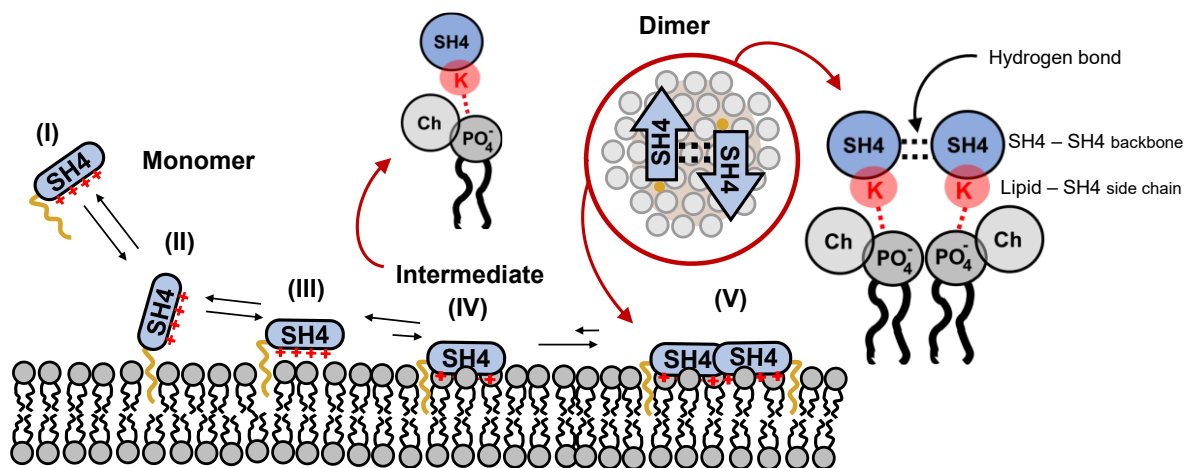
An analogous mechanism can be inferred in the membrane-dependent dimerization of Btk (Bruton's tyrosine kinase) reported by Chung et al., (2019) Btk is a member of the Tec family of tyrosine kinases that binds the membrane via a PH-TH module[36] interacting with phosphatidylinositol (3-5)-trisphosphate (PIP_3). The dimer interface of Btk interface comprises a direct protein-protein interaction involving hydrophobic residues (I^{92}, I^{95}, Y^{42} and F^{44}), but binding of additional PIP_3 outside the canonical site of the PH-TH module is required for dimerization to occur. It is suggested that binding of the second PIP_3 molecule, allosterically changes the structure to allow dimerization (Chung et al., 2019; Wang et al., 2019). The distinction with c-Src could be that the allosteric site and dimerization interface would be found in the same region (i.e. N-terminal region of the myristoylated SH4 domain), which is not surprising under the light of evolution.

The K-motif in the SH4 domain of c-Src apparently has a dual role, it provides myrSrc enhanced electrostatic interactions on binding to negatively charged lipids and independently, as confirmed from the neutral lipid bilayers measurements and the point mutations within the SH4 domain, it is responsible for c-Src self-association upon membrane anchoring. As earlier discussed, a similar dual role has been previously described by the clusters of basic residues forming PA binding domains (i.e. the electrostatic/hydrogen switch mechanism). Heretofore, the PA binding domains do not display homology in their sequences (*Figure 3.25.* A) (Andresen et al., 2002; Testerink and Munnik, 2005), yet show specificity for PA, thus a particular disposition of the K/R residues (i.e. tertiary structure) towards the lipid membrane might define the way to select PA.
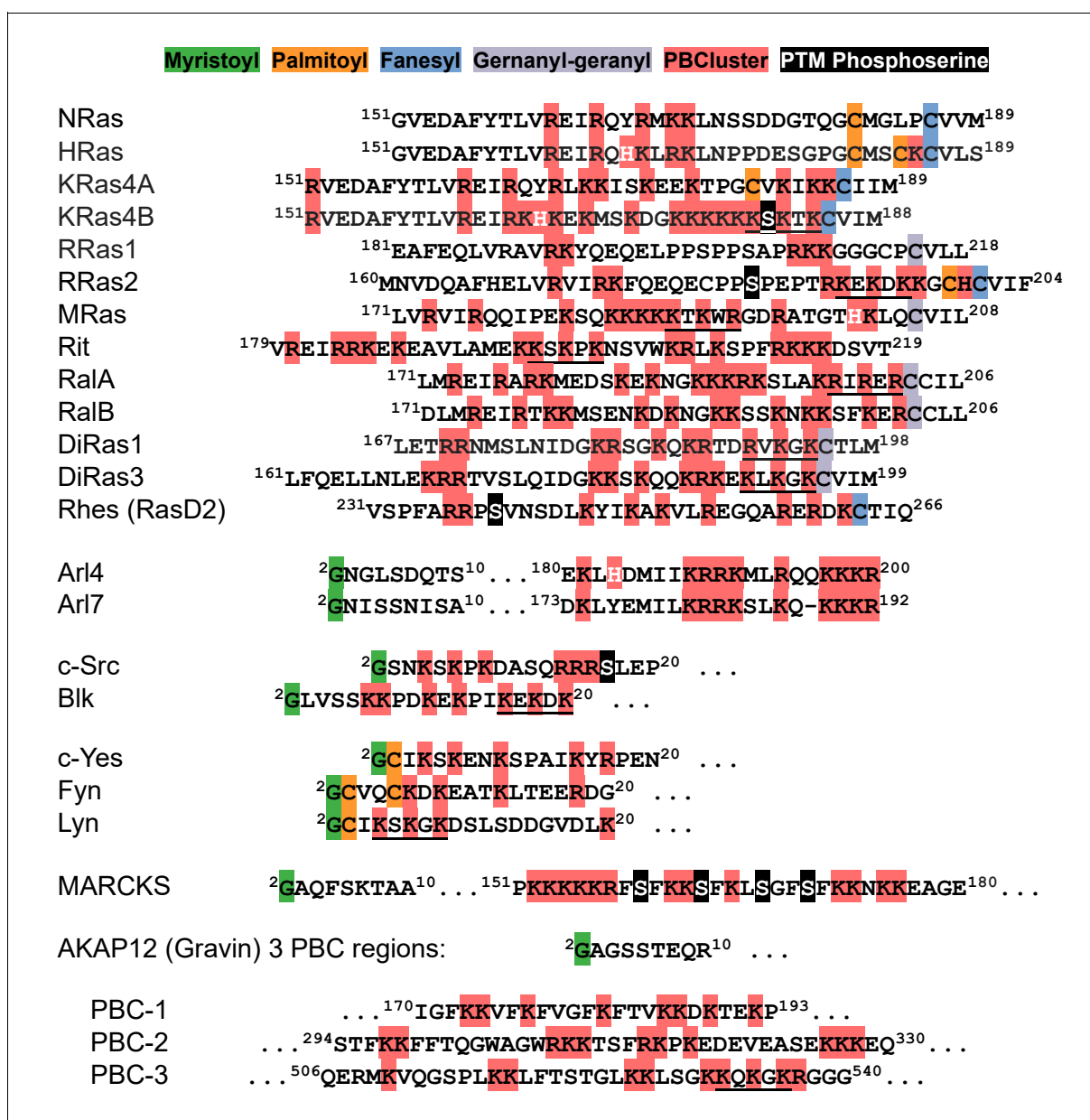
---

[36] PH: Pleckstrin homology domain and TH: Tec homology domain.

Figure 3.25. Sequences of (A) Phosphatidic Acid binding domains (B) Membrane binding proteins with polybasic domains.

A. Phosphatidic acid binding sequences

Raf-1	[390]FRNEVAVLRKTRHVNILLFMGYMTKDNLAIVTQWCEG[426]
Shp-1	[556]SSKHKEDVYENLHTKNKREEKVKKQRSADKEKSKGSLKRK[597]
PDE4D3	[31]HLWRHEQHHQYPLRQPQFRL[50]

B. Membrane binding proteins with poly-basic domains

Myristoyl Palmitoyl Fanesyl Gernanyl-geranyl PBCluster PTM Phosphoserine

NRas	[151]GVEDAFYTLVREIRQYRMKKLNSSDDGTQGCMGLPCVVM[189]
HRas	[151]GVEDAFYTLVREIRQHKLRKLNPPDESGPGCMSCKCVLS[189]
KRas4A	[151]RVEDAFYTLVREIRQYRLKKISKEEKTPGCVKIKKCIIM[189]
KRas4B	[151]RVEDAFYTLVREIRKHKEKMSKDGKKKKKKSKTKCVIM[188]
RRas1	[181]EAFEQLVRAVRKYQEQELPPSPPSAPRKKGGGCPCVLL[218]
RRas2	[160]MNVDQAFHELVRVIRKFQEQECPPSPEPTRKEKDKKGCHCVIF[204]
MRas	[171]LVRVIRQQIPEKSQKKKKKTKWRGDRATGTHKLQCVIL[208]
Rit	[179]VREIRRKEKEAVLAMEKKSKPKNSVWKRLKSPFRKKKDSVT[219]
RalA	[171]LMREIRARKMEDSKEKNGKKKRKSLAKRIRERCCIL[206]
RalB	[171]DLMREIRTKKMSENKDKNGKKSSKNKKSFKERCCLL[206]
DiRas1	[167]LETRRNMSLNIDGKRSGKQKRTDRVKGKCTLM[198]
DiRas3	[161]LFQELLNLEKRRTVSLQIDGKKSKQQKRKEKLKGKCVIM[199]
Rhes (RasD2)	[231]VSPFARRPSVNSDLKYIKAKVLREGQARERDKCTIQ[266]

Arl4	[2]GNGLSDQTS[10]...[180]EKLHDMIIKRRKMLRQQKKKR[200]
Arl7	[2]GNISSNISA[10]...[173]DKLYEMILKRRKSLKQ-KKKR[192]

c-Src	[2]GSNKSKPKDASQRRRSLEP[20] ...
Blk	[2]GLVSSKKPDKEKPIKEKDK[20] ...

c-Yes	[2]GCIKSKENKSPAIKYRPEN[20] ...
Fyn	[2]GCVQCKDEATKLTEERDG[20] ...
Lyn	[2]GCIKSKGKDSLSDDGVDLK[20] ...

MARCKS	[2]GAQFSKTAA[10]...[151]PKKKKKRFSFKKSFKLSGFSFKKNKKEAGE[180]...

AKAP12 (Gravin) 3 PBC regions:	[2]GAGSSTEQR[10] ...

PBC-1	...[170]IGFKKVFKFVGFKFTVKKDKTEKP[193]...
PBC-2	...[294]STFKKFFTQGWAGWRKKTSFRKPKEDEVEASEKKKEQ[330]...
PBC-3	...[506]QERMKVQGSPLKKLFTSTGLKKLSGKKQKGKRGGG[540]...

Conversely, the alternate distribution in the K-motif it is seemingly key to yield a β-sheet formation upon interaction with lipids (and a second molecule). Indeed, when the adjacent

residue D^{10} to the K-motif (^{5}KSKPKDA^{11} → ^{5}KSKPKRA^{11}) was mutated to R^{10}, on the negatively charged membrane, myrSrc self-association was not enhanced, although the apparent affinity of the protein was stronger. This evidence the exclusive dual role of the K-motif in the SH4 domain and that dimerization does not result from a non-specific electrostatic interaction with the membrane. Nonetheless, the K-motif is not sufficient to enable the dimerization function as suggested by our results, an efficient membrane interfacial insertion (i.e. lipid head-group region) of this motif is needed. In fact, Le Roux et al., (2016a) showed that c-Src construct bearing a lauroyl group instead of myristoyl on a negatively charge lipid bilayers failed to self-associate. myrSrc dimerization is observed in lower extent on neutral DOPC membranes, where the SH4 domain insertion toward the membrane interface is not favorable. Thereby the presence and nature of hydrophobic residues and/or moieties (i.e. myristoyl, farnesyl, etc.) along the K-motif might provide an efficient contact with the lipid head-group region, ultimately modulating the dimerization function of this motif. Additionally, membrane anatomy and biophysics could also regulate the K-motif, for instance Gorman et al. (2020) recently demonstrated that presence of cholesterol would increase the penetration of lysine residues (of poly-lysine peptides) depending on the PC:PS ratio in the composing membranes. Similarly, curvature promoted a deeper insertion and consequently β-hairpin formation of the cited peptide SVS-1 on zwitterionic DPPC membranes (Reid et al., 2018).

Broad diversity is observed in the arrangement of the basic residues in plasma membrane binding proteins (*Figure 3.25.*B) with poly-basic domains (PBD). However, the K-motif is found in various proteins not directly related to the SFKs. Is this just a mere coincidence? One of these proteins is the K-Ras 4B. This small GTPase K-Ras 4B shares some similarities with c-Src, it is one of the members of the Ras superfamily that is modified with a single acyl moiety (i.e. farnesyl) and holds a PBD (in the disordered Hyper-Variable Region (HVR)) as a second signal for effective membrane binding. K-Ras 4B is able to form nanoclusters on the plasma membrane (Zhou et al., 2014). In their extensive work Zhou et al., (2017) showed that the specific arrangement and nature of the basic residues composing the HVR of K-Ras 4B would determine the anionic lipids sequestered by the protein nanoclusters (lipid sorting) and consequently modulate the protein function. This lipid sorting could not be explained by simple electrostatic interaction since similar global net charge HVRs with different distribution of the basic residues yielded a different lipid sorting. In their words:

> *" [..] The precise amino acid sequence and prenyl group define a combinatorial code for lipid binding that extends beyond simple electrostatics. [...] "*

The authors suggested that the "lipid selection" encrypted in the HVR, was accomplished via disordered to ordered transitions of the HVR. Although their work did not breakdown the K-Ras 4B "basic residues code" and thus it is not clear what the K-motif in K-Ras 4B is specifically accountable for.

All the SFKs members are targeted to the plasma membrane, while the multiple acylated members (myristoylated and palmitoylated) such as Fyn and c-Yes are targeted to lipid rafts (Dubois et al., 2015; Simons and Toomre, 2000). c-Src solely myristoylated is distributed in both rafts and non-rafts regions (Martin et al., 2011; Seong et al., 2009). Intriguingly, impairment of the palmitoylation sites in Lck, re-localized the kinase in the cytoplasm in the presence of the myristoyl moiety alone and addition of six lysines in the Lck SH4 domain (like in the SH4 domain of c-Src) although was sufficient to restore the membrane binding of Lck, did not directed the protein to the lipid raft microdomains (Kwong and Lublin, 1995), raising up the question on why c-Src can be targeted to lipid raft domains.

Dwivedi et al., (2017) showed that a c-Src myristoylated peptide corresponding to the first residues of the SH4 domain (residues 2-9) formed lipid nano-platforms (in sense of lipid raft like features) on heterogeneous membranes containing liquid ordered and disordered phases. The c-Src nano-platform was reported to be established through lipid sorting and causing "phase mixing" in the heterogeneous membrane. Their work asserted that because of the ability of the myrSrc peptide to oligomerize itself on the lipid bilayer, the altogether packed myristoyl groups would provoke a mismatch in the membrane causing the recruitment of lipid molecules around the peptide oligomers. We provide evidence that membrane mediation is required for c-Src clustering on the lipid bilayer, therefore taking into account our observations, we interpret that c-Src dimerization could readily seed the lipid nano-raft generation without the need of specific lipids, through the direct interaction of the K-motif with the phosphate group of the lipids (*Figure 3.26.*).

Figure 3.26. Proposed model for c-Src lipid nanoraft generation.
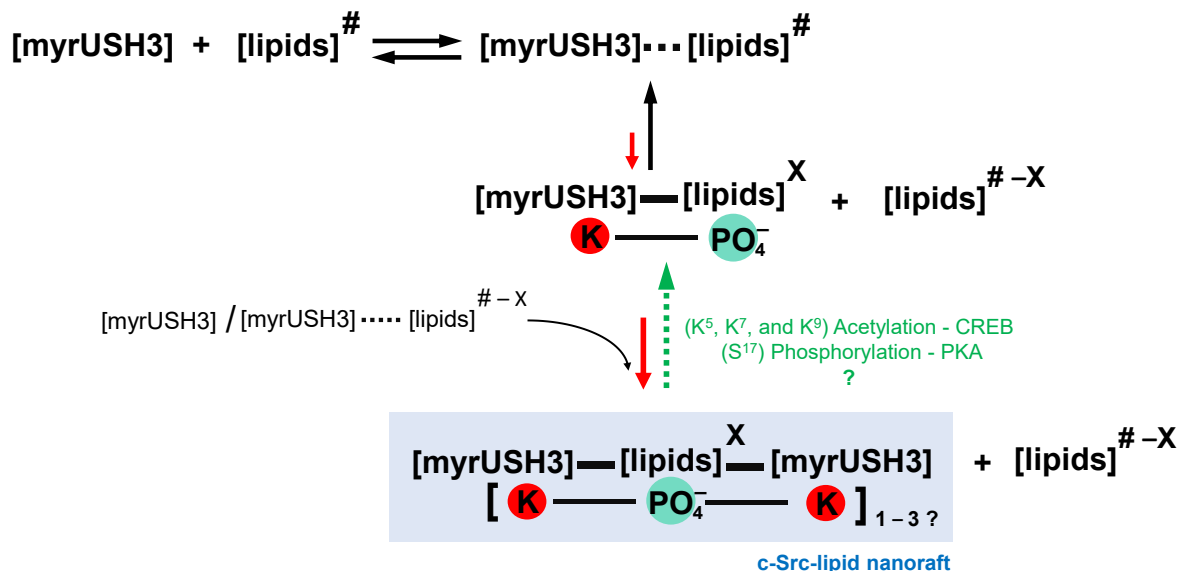
Consistent with Dwivedi et al., (2017)'s work, the model we suggest is that the source of a hydrophobic mismatch in the membrane results from the restricted mobility of the lipids interacting with the K-motif in c-Src dimer conformation, which enables the recruitment of lipids in the surroundings to compensate this packing defect, though the two myristoyl

groups might also contribute. Interestingly, de Kruijff et al., (1985) reported that upon polyLysine association to cardiolipin liposomes, the lipid acyl chains exhibited a more restricted motion structurally reorganizing the lipid vesicles, an effect not observed in the absence of the peptide. These results considerably support our model. It is not deniable that presence of other lipid types (such as in a heterogeneous membrane) could influence in the size of the resulting nano-platform, as reported by the results of Dwivedi et al., (2017), that showed formation of large lipid-myrSrc clusters when the membrane was heterogeneous.

In consonance with the K-Ras 4B case (Zhou et al., 2017), where singularity of the membrane anchoring domain could trigger specific lipid sorting yielding a distinct membrane platform, c-Src self-association might impel generation of specific lipid nano-platforms recruiting or being targeted by multi-protein complex induced for a particular signaling response. Interestingly, the serine-threonine kinase Akt has been shown to have different degree of activation depending on its localization, giving a greater and rapid response after stimuli in raft regions than in non-raft (Gao and Zhang, 2008). Similarly, a model with two types of response could be speculated for c-Src, where the long lived self-associated c-Src species on the membrane (lipid raft regions) would constitute fixed target sites readily prepared to initiate downstream signaling, while the fast diffusing reversible c-Src species would efficiently explore the membrane until the target partner is located resulting in a delayed activation.

Early work by the Resh's group had identified the importance of lysine residues in positions 5, 7 and 9 of c-Src and similar lysine clusters in other Src family members (Silverman and Resh, 1992). By measuring the retention of membrane bound [^{35}S]methionine labeled c-Src in pellets subsequent to ultracentifugation, they observed that radioactive c-Src could be displaced by an excess of myrSrc peptides (residues 2-12) from the lipid-bound fraction. These experiments were interpreted in terms of a competitive binding to a yet unidentified c-Src membrane receptor. However, in the light of the present results, these experiments probably reflected the formation of persistently membrane bound c-Src dimers, dissolved by the competitive formation of heterodimers with the unlabeled myrSrc peptides. With this "heterodimer formation" idea in mind, one could contemplate the c-Src SH4 domain K-motif as a targeting/binding motif to either c-Src regulatory partners or substrates on the membrane. For instance, similar alternating lysine clusters are observed in other SFKs: Src ^{5}KSKPKD^{10}, Lyn ^{5}KSKGKD^{10}, Yes ^{5}KSKENK^{10}, Fyn ^{7}KDKEATK^{13}. Except c-Src, the other SFK are palmitoylated, as well as myristoylated, so lipid anchoring $a\ priori$ would be efficient even without that positively charged residues, which could suggest a role of the conserved positively charged cluster as to enable the association with other membrane anchored molecules of the same kind (e.g. c-Src homodimers) or different (e.g. SFK heterodimers). Another putative example could be the positive cluster, containing lysine and arginine residues (^{51}YARKRNGQM^{59}) located in the small cytoplasmic tail extending from the small integral membrane protein SMIM30 encoded by lncRNA LINC0998[37]**.

---

[37] lncRNA = long non-coding RNA, LINC0998 = long intergenic non-protein coding RNA 998 (located in chromosome 7).

SMIM30 induces c-Src/Yes membrane anchoring promoting hepatocellular carcinoma (Pang et al. 2020). Although the binding mode has not been demonstrated, it is known to involve the N-terminal region of c-Src. In the light of the above results, we could hypothesize lipid-mediated hetero-dimerization/oligomerization involving SMIM30 C-terminal tail and one or more c-Src molecules through their SH4 domain. c-Src homo/hetero-dimer formation may restrict or confer a particular orientation to the overall protein modulating its specificity, additionally substrates of the protein forming the heterodimer with c-Src, could be phosphorylated by c-Src, altogether justifying for the broad spectrum of c-Src substrates and its engagement in multiple crucial signaling pathways.

While a hypothetical hetero-dimer regulation would depend on either c-Src or the partner protein, thereby increasing the factors that potentially could trigger the formation/dissociation, self-association of c-Src would only rely on factors affecting c-Src regulation (or the membrane). We have uncovered at least two post-traslational modifications, namely K-motif acetylation and phosphorylation of S17 in the SH4 domain, that impair c-Src self-association. Both modifications have been reported to occur *in vivo* (Huang et al., 2018; Walker et al., 1993), although a direct correlation with c-Src clustering regulation remains to be assessed. On the other hand, depletion of negatively charged lipids could decrease c-Src dimer formation, as suggested by our results self-association occurs in a lower extent in this type of membrane. Additionally, a positive curvature of the membrane induced a deeper insertion of the cationic peptide SVS-1 (KVKVKVKV$^\text{D}$P$^\text{L}$PTKVKVKVK-NH$_2$) towards the membrane interface, promoting the β-hairpin formation (Sinthuvanich et al., 2012). Thence, one could reason that a negative curvature of the membrane (towards extracellular matrix) would not favor c-Src self-association[38].

Unexpectedly, our membrane diffusion measurements for the myrUSH3 construct of c-Src revealed that accumulation of the self-associated species provoked membrane disruption, that likely derives from an increased lateral pressure alleviated through membrane bending (Stachowiak et al., 2012). Tournaviti et al., (2007) reported that overexpression of SFKs (c-Src, Yes, Fyn and Lck) SH4 domain containing constructs in CHO and HeLa cells induced membrane blebbing, although the mechanism was not clear, formation of the blebs correlated with greater cell invasion. In recent study, Ahler and coworkers (2019) similarly reported membrane blebbling in Src/Yes/Fyn (-/-/-) fibroblasts (SYFs) by full length c-Src and confirmed that an open global conformation and membrane binding was required, but not the kinase activity, this suggests that the membrane blebbing phenotype could be a function of c-Src self-association, as inferred from our observations.

In a nutshell, we have identified that the lysine motif (K-motif) in the SH4 domain of c-Src appears to play a dual function: a well-recognized role of enhancing binding through electrostatic forces complementing the hydrophobic insertion of myristoyl group, and a

---

[38] Nicely reviewed in Jarsch et al., (2016), there are a wide range of mechanisms involving membrane associated proteins, lipid compositions or the cytoskeleton to drive the membrane bending.

novel function triggering self-association by an allosteric modulation of the SH4 domain through lipid mediation. The presence of the K-motif in other membrane-associated proteins containing polybasic domains, raises the question whether this motif has a conserved function among these diverse membranes signaling proteins.

Chapter 4
Towards full-length c-Src

4.1. Context

4.2. Production of myristoylated myr-SH4-Unique-SH3-SH2 c-Src construct

4.3. Role of SH2 domain in the Src N-terminal Regulatory Element (SNRE)

      4.3.1. USH3SH2 resonance backbone assignment
      4.3.2. Mapping the effects on SH4-U domains induced by the SH2 domain
      4.3.3. Mapping the intramolecular interactions of SH3 domain in the USH3SH2 context
      4.3.4. Analysis of the intramolecular contacts in the putative myrUSH3HS2 context

4.4. Discussion

4.5. Materials and methods

4.1. Context

In c-Src, the SH3 and SH2 domains are known to regulate the kinase activity by stabilizing the inactive form of the enzyme. The compact inactive state of c-Src is achieved when the phosphorylated Y530 at the C-terminal tail binds the SH2 domain while the SH3 domain interacts with the polyproline motif of the SH2-SH1 linker region, altogether packing the SH3-SH2 domains against the (SH1) kinase domain.

The SH2-Kinase domain tandem is greatly conserved among cytoplasmic tyrosine kinases, so it is not surprising that with increasing organism complexity, the SH2 domain had evolved to regulate the kinase domain (Filippakopoulos et al., 2009). Another module that is frequently found along this SH2-SH1 unit is the one constituted by intrinsically disordered regions and SH3 domains (Arbesú and Pons, 2019), suggesting that another layer of regulation could exist on top of the SH2-SH1 domains. c-Src is based on this architecture, with an intrinsically disordered region (myrSH4-U domain) followed by the SH3-SH2-Kinase domains.

Auto-phosphorylation of c-Src Y419 in the kinase domain leads to an enhancement of the catalytic activity, completing the full activation of the protein kinase. Recently, Boczek et al., (2019) reported that key residues of the active center of c-Src kinase domain (K295, E310 & R409) showed different conformations when the Y419 phosphorylation occurred in the full-length construct in comparison to the kinase domain alone, indicating a crosstalk between the kinase domain and the regulatory domains. The authors used a full-length c-Src construct (SH4-U-SH3-SH2-SH1); however, it lacked myristoylation. Although this point may not seem important, Patwardhan and Resh, (2010) demonstrated reduced c-Src kinase activity in the non-myristoylated c-Src form (G2A mutant) in in $vitro$[39] assays.

Furthermore, Spassov et al., (2018) also testing in $vitro$ reported that deleting the Unique domain, the entire myristoylated SH4-Unique domains or just the myristoyl moiety had a negative impact on the kinase activity of c-Src due to reduced auto-phosphorylation (pY419), with the absence of myristoyl moiety having the greatest impact. Additionally, Bernadó et al. (2008) using a constitutive active c-Src mutant (Y530F) that only contained the globular SH3-SH2-Kinase domains, reported using SAXS experiments that the protein kinase conformation remains at an equilibrium 85% towards the closed form. So, are the myristoylated SH4-Unique domains necessary to achieve the state that favors the kinase activation?

Our group has described a novel functional role for the N-terminal region comprising the intrinsically disordered myrSH4-Unique domains and the SH3 domain, so that this entire region is referred as the c-Src N-terminal Regulatory Element (SNRE) (Maffei et al. 2015,

---

[39] While in $vivo$ experiments may not be straightforward to interpret, as the absence of myristoylation could change c-Src subcellular localization or consequent regulatory partners, in $vitro$ experiments reflect intrinsic molecular properties.

Arbesú et al. 2017). Previous results in the group, demonstrated that the c-Src N-terminal region involving the SH4 Unique and SH3 domains form an intramolecular fuzzy complex, where the IDR (SH4-U domains) maintains multiple weak contacts with the SH3 domain (Arbesú et al., 2017). The results in *Chapter 2*, have revealed that the myristoyl moiety would favor the fuzzy complex formation by adding cooperative transient interactions. Furthermore, "not defined/dynamic binding pockets" in the SH3 domain were found to harbor the myristoyl group. Additionally, the so-called Unique Lipid Binding Region (ULBR) (found in the Unique domain), exerts key roles in framing the myristoyl group interactions within the fuzzy interdomain complex. The role of the ULBR has been demonstrated to be biologically relevant (Arbesú et al., 2017), although the mechanisms of ULBR regulation remain not clear.

We hypothesize that among tyrosine kinases, the IDR-SH3 unit could have also evolved to modulate the kinase domain, as it may have the c-Src N-terminal Regulatory Element (SNRE). The long-range effects could be conveyed from the myr-IDR-SH3 module to the kinase domain via the SH2 domain. Therefore, following the *"divide and conquer"* approach, our next step is to characterize the SNRE with the adjacent SH2 domain.

4.2. Production of the myristoylated c-Src construct: myrSH4-U-SH3-SH2

Contribution statement: The production of myrUSH3SH2 was done in collaboration with Estefania Rusca as part of her Bsc. thesis under my practical supervision.

The aim was to produce the myristoylated N-terminal c-Src region including the SH2 domain (myrUSH3SH2), (ideally) fulfilling the protein sample standards for NMR studies (homogeneity and quantity). Thus, we kept recombinant protein expression in *Escherichia coli,* since it is the optimal system in terms of culturing times and protein product obtained. In addition, we have learned in *Chapter 2*, all the shortcomings associated to obtain the myrUSH3 construct of c-Src (residues 2-150). Besides the need to co-express the NMT enzyme to obtain the myristoylated protein, we have set the required measures to avoid side products (i.e. lauroylated protein) and the procedure to optimally purify myrUSH3. Nonetheless, as the size of myrUSH3SH2 construct is considerably larger (255 residues, ~27.9 kDa), additional problems such as misfolding or an overall lower protein yield are more likely to occur.

We leveraged the expression vector for myrUSH3 construct, by inserting the DNA encoding the SH2 domain of c-Src using the Gibson assembly (Gibson et al., 2009). The expression and purification of myrUSH3SH2 construct was carried out as per myrUSH3 protocol, however, as it can be observed in the SDS-PAGE gel (*Figure 4.1.*) monitoring myrUSH3SH2 throughout the multiple purification steps, this construct yields a large amount of truncated species that are difficult to separate and drastically reduce the yield of myristoylated protein.

Figure 4.1. SDS-PAGE gel of myrUSH3SH2 in the multiple purification steps.

MK = Protein marker
CL = Cell lysate (after sonication)
SN = Supernatant
FT = Flow Through Ni affinity chromatography
W(I) = 1st Wash fraction Ni affinity chromatography
W(II) = 2nd Wash fraction Ni affinity chromatography
E = Elution fraction Ni affinity chromatography
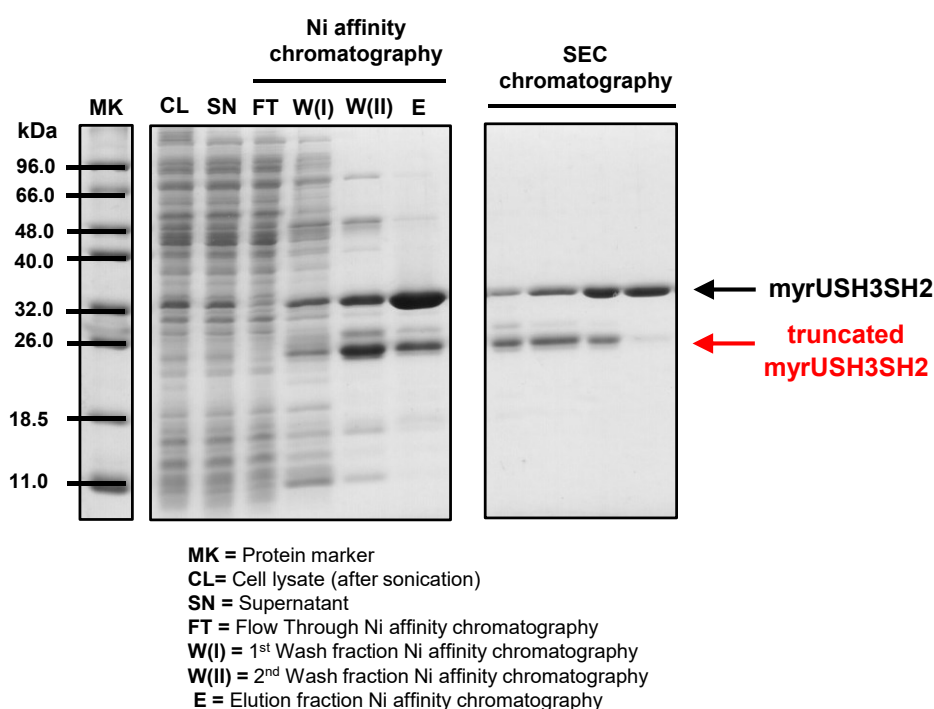
Before engaging an optimization process to obtain a pure myrUSH3SH2 sample which has been shown not to be an easy process in *Chapter 2*, we decided to adopt the same approach, which proved effective for the initial assessment of the SNRE (Maffei et al., (2015); Arbesú et al., (2017)). This approach consists in characterizing the c-Src construct in the absence of the myristoyl group. Afterwards, when the myristoylated construct becomes available, the additional myristoyl group effects will be identified. Thus, in this chapter we shall focus on the characterization of the non-myristoylated USH3SH2 c-Src construct.

As previously observed with the USH3 construct, in the absence of the myristoyl group, no large amount of truncated USH3SH2 was detected (*Figure 4.2.* A), suggesting that this unexpected truncation is directly related to myristoylation. The Marley method (*Figure 4.2.* B) was used to produce ^{13}C ^{15}N USH3SH2, obtaining higher amounts of labeled protein reducing the overall costs of the isotopic medium used[40] (i.e. ^{13}C glucose and ^{15}N ammonium chloride).

Figure 4.2. (A) SDS-PAGE gel of USH3SH2 in the multiple purification steps. (B) Marley's method outline.

---
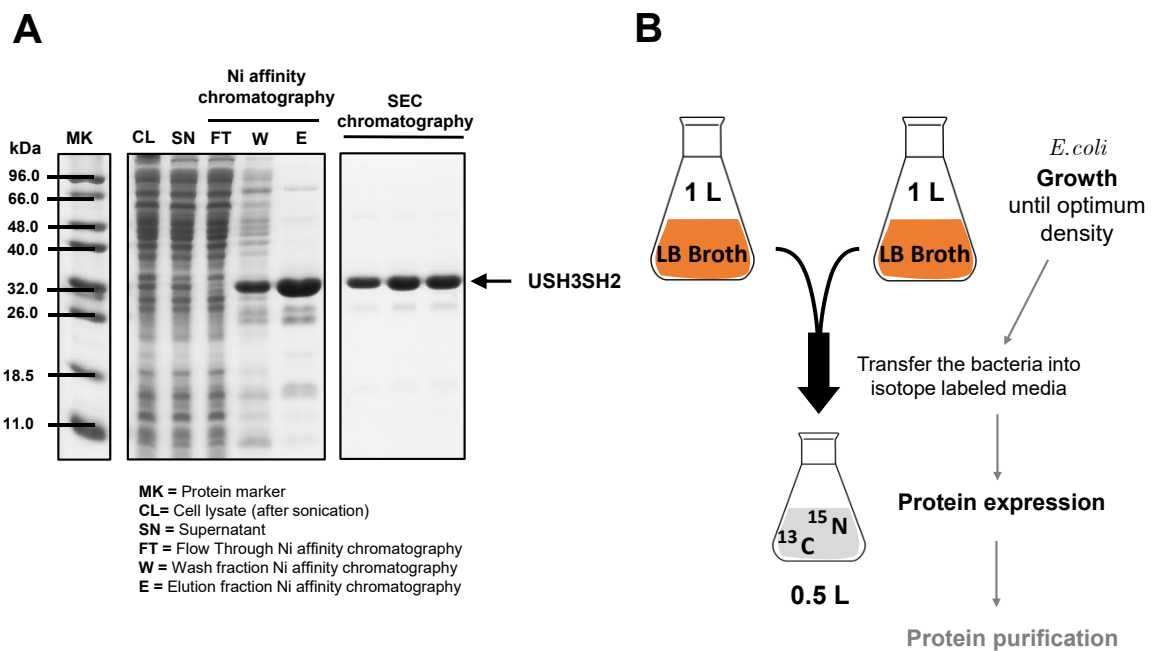
[40] Producing protein from 1 L of ^{15}N ^{13}C isotopic M9 medium can cost up to 600€.

4.3. Role of SH2 domain in the c-Src N-terminal Regulatory Element

4.3.1. c-Src USH3SH2 construct backbone resonance assignment

The intramolecular changes in the c-Src N-terminal fuzzy complex by the presence of SH2 domain are assessed by NMR through the analysis of chemical shift perturbations in the 2D ^{1}H ^{15}N – HSQC spectra. Thence, the USH3SH2 backbone resonance assignment was first performed. Although, resonance data was available for an SH3SH2 construct (chicken c-Src, Tessari et al., 1997) and the USH3 variant (Maffei et al., 2015), because of the presence of adjacent domains in USH3SH2, major changes in the residue nuclei resonances could occur and thus assignment just through comparison with previous data might lead to ambiguous peak assignment. We must verify the backbone resonances of all the residues.

The assignment of each peak (i.e. ^{1}H-^{15}N correlation) in the HSQC spectra of a protein is commonly achieved using 3D (^{1}H–^{15}N–^{13}C) pairs of experiments i) HNCO and HNcaCO ii) HNCA and HNcoCA iii) HNCACB and HNcoCACB. For given ^{1}H-^{15}N chemical shifts of the NH (amide backbone) of one amino-acid, the comparison of these 3D experiments provides the ^{13}C chemical shifts of Cα, Cβ & CO groups of this amino-acid plus the adjacent one. Knowing the protein sequence and the NMR *footprint* of each amino-acid plus the one that precedes it, allows to sequentially *walk* through the residues' ^{1}H-^{15}N chemical shifts in the HSQC spectra.

Since intrinsically disordered regions are more exposed to the aqueous solvent, the proton of the amide group easily exchanges with bulk solvent protons, strongly attenuating the NMR signals of the IDR residues in contrast to those of the folded domains. Working at lower temperatures solves this issue, as the amide proton exchange slows down. In addition, while IDRs remain dynamic at lower temperatures, the folded domains (e.g. SH3-SH2) tumble slowly because of a higher solvent viscosity, provoking almost complete loss of the signals of these domains residues and therefore the spectra will be less crowded in signals (*Figure 4.3.* A).

Figure 4.3. ^{1}H ^{15}N HSQC spectra for USH3SH2 at (A) 278K and (B) 298K.
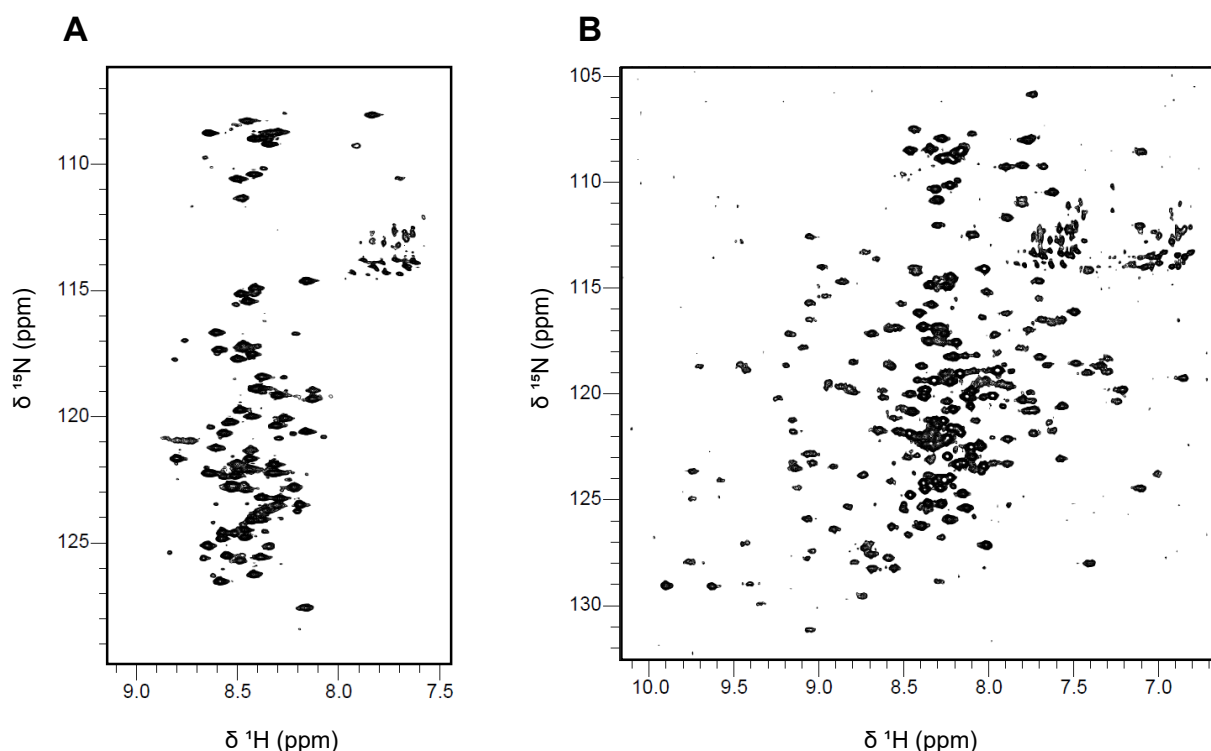
The NMR assignment of the SH4-Unique domains residues in USH3SH2 was performed at 278K, acquiring the experiments: 2D ^{1}H-^{15}N HSQC and the 3D HNCACB, CBCAcoNH, HNCO and HNcaCO. 83.5% of the residues of the SH4-Unique domains were unambiguously assigned. The remaining unassigned residues mostly included prolines (10/84 residues) that are not detected in these experiments, since they lack the amide proton.

The temperature was increased to 298K for assignment of the globular SH3-SH2 domains (*Figure 4.3* B). Standard 3D experiments were first attempted. However, due to the size of the USH3SH2 construct, signals in the 3D experiments corresponding to the well-ordered regions were not detected. For larger proteins >250 residues, the recorded NMR signal decays rapidly resulting in broader peak linewidths and thus a reduced signal-to-noise[41]. Thence, TROSY versions of the HNCA and HNcoCA experiments were tried. The TROSY approach was introduced by Pervushin et al., (1997) and allows to reduce the relaxation rate in larger molecules, therefore obtain sharp peaks in the NMR spectra of large proteins. However, the sensitivity was still very poor and not all the peaks corresponding to the SH3-SH2 domains residues were detected. Additionally, the sample amount was low, compounding to this non-optimal situation.

---

[41] Our USH3SH2 (255 residues) construct laid in the limit and had the peculiarity of a high dynamic disordered region (SH4-Unique domain). Deuterium labeling ^{2}H could alleviate this issue (Sattler and Fesik, 1996), however the costs of producing ^{2}H-^{15}N-^{13}C scale up greatly and the yield of protein obtained in ^{2}H labeled medium is known not to be good. Therefore, not quite convenient for our system.

We improved the USH3SH2 concentration in the NMR sample and we tried the BEST-TROSY version of the most sensitive experiments i) HNCO, ii) HNCA and HNcoCA using NUS (Non-Uniforming Sampling). BEST-TROSY pulse schemes have been shown to enhance sensitivity and spectral resolution in large (~270 residues) IDPs (Solyom et al., 2013). On the other hand, NUS allows to reduce the time of the overall experiment by reducing the signal sampling in the indirect dimensions (eg. ^{15}N, ^{13}C) (Kazimierczuk and Orekhov, 2015). This allows to either increment the accumulations within the experiment and thus enhance the sensitivity or improve the resolution by increasing the acquisition time in the indirect dimension. So, at this point we ended up with a relatively good set of ^{1}H–^{15}N–^{13}C chemical shifts data of the NH (amide backbone), CO and Cα groups of the SH3-SH2 domains residues in USH3SH2.

With the latter data and recurring to a comparative assignment using the data reported by Tessari et al. (1997) for residues in the SH3SH2 construct of (chicken) c-Src, we were able to complete the assignment the ^{1}H – ^{15}N HSQC peaks of the USH3SH2 construct residues.

4.3.2. Mapping the effects on SH4-U induced by the SH2 domain

The aim is to investigate how the N-terminal IDR:SH3 domain fuzzy complex is affected by the presence of the adjacent SH2 domain (USH3SH2 construct). Including this domain can induce direct or indirect effects on the IDR:SH3 fuzzy complex. While the direct effects could include IDR:SH2 interactions, the indirect effects could involve favoring or hampering preexisting IDR:SH3 interactions (observed in USH3) by modifying the SH3 domain environment. All these effects might not be exclusive.

First, the regions of the IDR (SH4-U domains) are examined using chemical shift perturbation (CSP) analysis to map the short-range interactions. USH3 was used as the reference state. The combined ^1H ^{15}N CSP of the IDR residues in USH3SH2, compared against USH3 are displayed in *Figure. 4.4.* (bottom plot). In the top panel of the same figure, I have included the previously CSP observed upon attachment of the SH3 domain to SH4-U, to have a reference of the magnitude of perturbations that could be expected, since the SH3 domain actively interacts with the SH4-U domains.

Figure 4.4. Combined ^1H ^{15}N CSP of (top) USH3 versus U (SH4-Unique) (both) in Buffer 50 mM NaH$_2$PO$_4$/Na$_2$HPO$_4$, pH 7 (bottom) USH3SH2 versus USH3 (both) in Buffer 50 mM Na$_2$HPO$_4$ 200 mM, Na$_2$SO$_4$, 10 mM DTT, pH 6.4. The red line represents the significant threshold defined as the mean CSP for the lowest decile (μ(lowest decile CSP)) plus five standard deviations (5σ). Prolines are marked with *. Experiments performed at 278K.
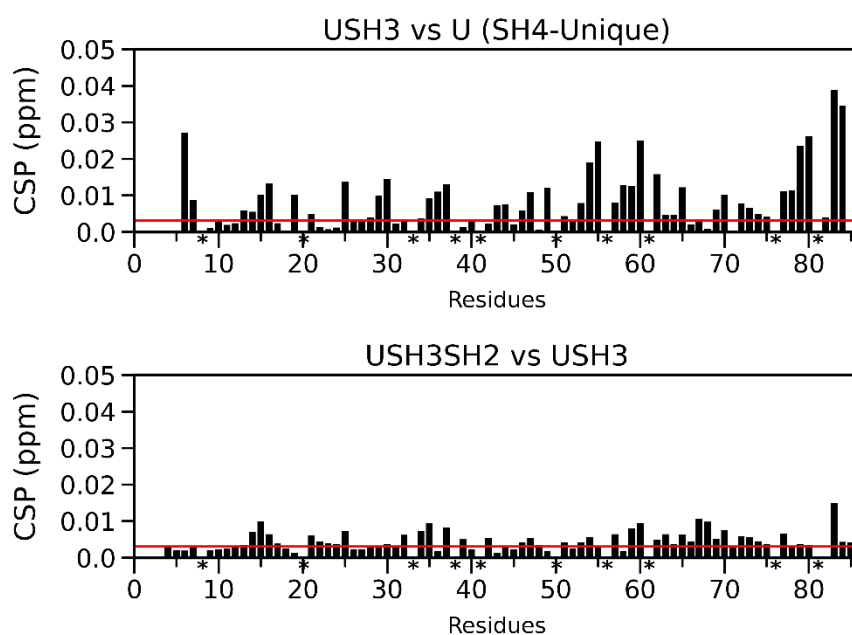

The overall effect of the SH2 domain on the chemical shifts of SH4-U (IDR) residues is lower than the direct effect of the SH3 domain. The chemical shifts of most of the IDR residues already perturbed by the SH3 domain are not affected by the presence of the SH2 domain, since the CSPs lay below the significance threshold. The larger SH2-induced perturbations are located in the second half of the SH4 domain ^{14}RRR^{16}, the ^{32}FPASQT^{37} segment and around the ULBR (^{59}AEPKLFGGFNSS^{70}). The observed SH2-induced

perturbations can be divided in two groups: (i) those that imply a modification of the chemical shift of residues previously affected by the SH3 domain, which may be interpreted as a modulation of a preexisting interaction and (ii) those that were not perturbed by the SH3 domain alone but are affected by the SH3-SH2 domains. The latter represent new direct interactions caused by the presence of the SH2 domain.

Peak intensity reduction (due to signal broadening) is also a measure of interaction that is sensitive to the dynamics, either through changes in the local correlation time, affecting relaxation, or through exchange broadening when inter/intra-molecular exchange regimes are slow or intermediate. Thus, to further assess changes in the SH4-U domains induced by the SH2 domain, we analyzed Intensity Perturbations (IP) (*See Materials and methods 4.4.7*) of the IDR (SH4-U) residues peak in a BT-HNCO spectra at 278K (*Figure 4.5.*).

Figure 4.5. Normalized Peak Intensity plots from ^{13}C-^{1}H-^{15}N HNCO experiments for (A) SH4-U in buffer 50 mM Na$_2$HPO$_4$/NaH$_2$PO$_4$, pH 7 (B) USH3 and (C) USH3SH2 both in buffer 50 mM Na$_2$HPO$_4$, 200 mM Na$_2$SO$_4$ 10mM DTT pH 6.4. Prolines are marked with *. All experiments performed at 278K.
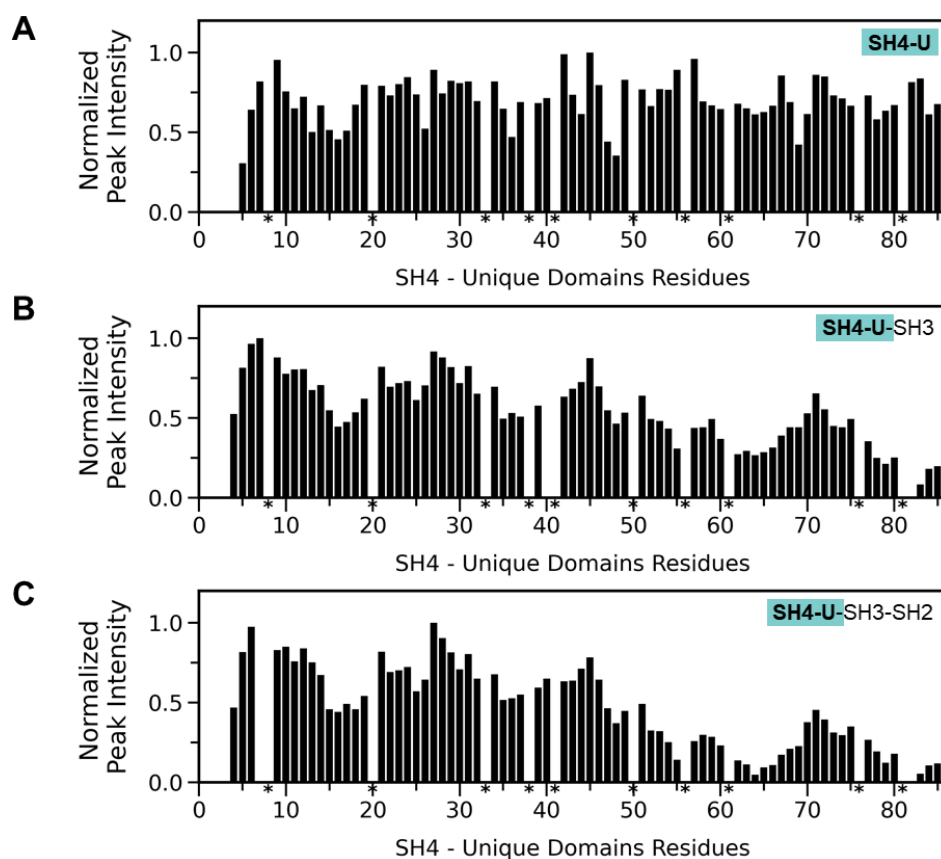

As displayed in *Figure 4.5.*, the IP profile for SH4-U (panel A) is rather flat, suggesting similar dynamics experienced through all the IDR (SH4-U), whereas the IDR in USH3 and USH3SH2 exhibits a similar pattern of intensity alterations, though the intensity is lower in the presence of the SH2 domain. It specially stands out the ULBR plus the prior region (^{53}AFAPAAAEPKLFGGNSS^{70}). Some of the residues showing the largest reduction in

124

intensity such as [55]A (next to [54]F) and [64]F show no chemical shift perturbation between USH3 and USH3SH2 (*Figure 4.4*), suggesting that the additional broadening observed in the USH3SH2 construct is not caused by chemical exchange but because of a conserved interaction with the SH3 domain sensing the increased correlation time in the presence of the neighbor SH2 domain.

SH3 binding to a high affinity peptide ligand with a canonical polyproline (PxxP) motif (i.e. synthetic peptide VSL12: Ac-VSLARRPLPPLP-OH) (Rickles et al., 1995) had been reported to impair most of (but not all) the IDR:SH3 interactions (Pérez et al., 2013). Upon SH3:PxxP interaction, the RT-loop becomes partially unavailable, therefore the IDR:SH3 interactions mediated by this loop are impaired.

Using VLS12 (PxxP peptide) as a tool to reduce the IDR:SH3 interactions, we further explored putative interactions of the IDR with the SH2 domain. We first used IP to map changes in the IDR when USH3SH2 and USH3 were complexed to PxxP (from now on referred as USH3^{PxxP}SH2 and USH3^{PxxP}). IP derived from the BT-HNCO spectra at 278K for USH3^{PxxP}SH2 and USH3^{PxxP} were compared respectively to the IP in absence of the ligand. Results of the IP plots are shown in *Figure 4.6*.

Figure 4.6. Comparative normalized Peak Intensity plots from ^{13}C-^{1}H-^{15}N HNCO experiments for USH3(SH2) isolated and PxxP complexed forms (A) USH3 vs USH3^{PxxP} (B) USH3SH2 vs USH3^{PxxP}SH2 and (C) USH3^{PxxP}SH2 vs USH3^{PxxP}. All constructs in buffer 50 mM Na$_2$HPO$_4$, 200 mM Na$_2$SO$_4$ 10mM DTT pH 6.4. Prolines are marked with *. All experiments performed at 278K.
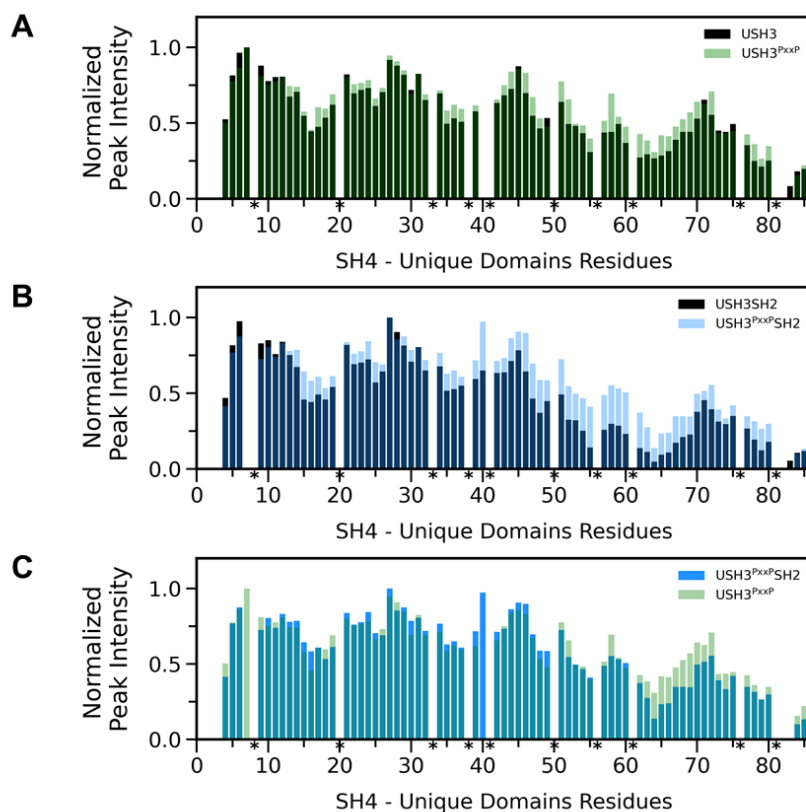
The IDR of the USH3^{PxxP} (*Figure 4.6.* A) exhibits a slight increase in the intensity profile compared to USH3, consistent with a weakening, but not a complete elimination of the interaction with the SH3 domain. The effect of the PxxP ligand is more pronounced in the USH3SH2 construct, although this could simply reflect that the changes in intensity caused by the presence of both SH3-SH2 domains are larger than those of the SH3 domain alone (i.e. increased correlation time). In panel C of *Figure 4.6*, we have compared the IP plots of USH3SH2^{PxxP} and USH3^{PxxP}. Both IP profiles match except for the C-terminal part of the ULBR, that shows a reduced peak intensity in USH3SH2^{PxxP}. This suggest that the SH4-U adopt a similar structure/dynamics upon PxxP peptide binding independent of the presence of the SH2 domain, except the ULBR.

The interaction of the ULBR with the SH3 domain is at least partially maintained in the presence of the PxxP ligand. The similar intensity profiles in USH3^{PxxP} and USH3^{PxxP}SH2 indicate that, in the presence of the PxxP ligand, the interaction of the IDR with the globular domains is restricted to the ULBR. The lower intensity in this region in the presence of the SH2 domain may be due to the higher molecular mass of the USH3SH2 construct or reflect additional direct contacts with the SH2 domain. So, we next calculated the CSP of USH3^{PxxP}SH2 vs USH3^{PxxP} (*Figure 4.7.*).

Figure 4.7. Combined ^{1}H ^{15}N CSP of USH3^{PxxP}SH2 vs USH3^{PxxP}. The red line represents the significant threshold defined as the mean CSP for the lowest decile (μ(lowest decile CSP)) plus five standard deviations (5σ). Prolines are marked with *. Experiments performed at 278K.
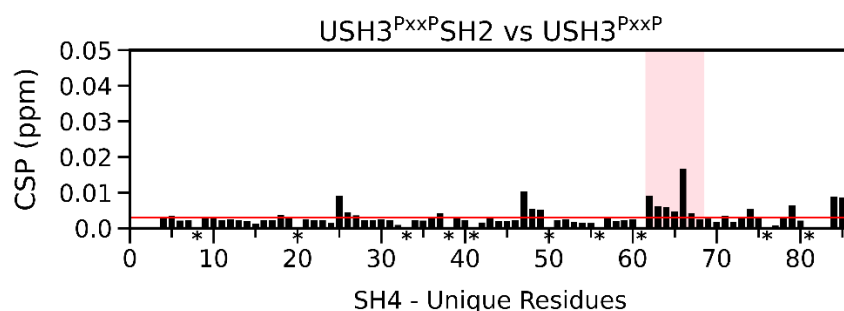

Almost complete absence of perturbations in the CSP plot (*Figure 4.7.*) is observed. This indicates that the IDR intramolecular interactions with the SH3-ligand bound form are similar even with the incorporation of the SH2 domain. The only significant difference in in the C-terminal part of the ULBR, the same in which intensity changes were observed between USH3^{PxxP} and USH3^{PxxP}SH2.

Although a direct ULBR:SH2 interaction is suggested, the minimal magnitude of the perturbations indicate that the main interaction of the ULBR is with the SH3 domain and the effect of the SH2 domain is either contribute some minor additional contacts or indirectly affect the regions of the SH3 domain where ULBR contacts, inducing a slightly different environment. This would be consistent with the results in *Chapter 2*, indicating that the ULBR would preferably interact with the β_1 strand and the C-terminal site of the SH3 domain, that now in the presence of the SH2 domain, both regions would be affected by the close presence of the SH3-SH2 linker.

We next compared the ^{1}H-^{15}N HSQC spectra of USH3^{PxxP}SH2 and USH3^{PxxP} using the respectively PxxP-unbound state as reference to calculate the CSP (*Figure. 4.8.*).

Figure 4.8. Combined ^{1}H ^{15}N CSP of (top) USH3^{PxxP} vs USH3 (bottom) USH3^{PxxP}SH2 vs USH3SH2. The red line represents the significant threshold defined as the mean CSP for the lowest decile (μ(lowest decile CSP)) plus five standard deviations (5σ). Prolines are marked with *. Experiments performed at 278K.
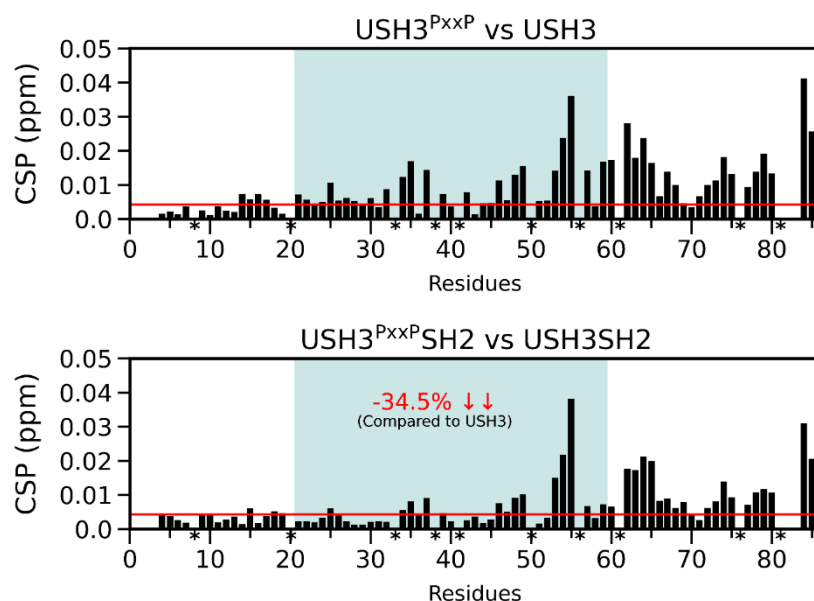
The addition of the PxxP ligand affects the chemical shifts of the SH4-U region differently in the presence or in the absence of the SH2 domain. The major differences are observed in the central region of the IDR, highlighted in *Figure 4.8.* (bottom), whose integrated CSP due to the PxxP:SH3 interaction are 34.5% lower in the presence of the SH2 domain. In particular, the changes in the environment of residues 30-50 caused by the binding of the PxxP to the SH3 domain are greatly reduced when the SH2 domain in present. The effect upon PxxP binding on the 70-80 region has also decreased with incorporation of the SH2. Since the effect of SH3 PxxP-ligand binding is the reduction of the IDR:SH3 contacts, the lower perturbations in the presence of the SH2 domain suggest that incorporation of this domain has already reduced the IDR:SH3 contacts; and thus, the PxxP-ligand binding would have a lesser effect in further affecting those contacts.

On the other hand, the higher perturbations on residues around ^{54}FA^{55} and ^{62}KLFG^{65} similarly occur independent of the presence of SH2 domain. This suggest that the direct interactions between the IDR and SH3 domains that are perturbed by the binding of the PxxP ligand, involves these two regions, each of them with a phenylalanine residue. However, in the presence of the SH2 domain, the pattern of perturbations around ^{62}KLFG^{65} (of the ULBR) is different, suggesting a slightly different interaction.

The results show that the presence of the SH2 domain modifies the preexisting IDR:SH3 interactions (i.e. the ones in USH3). These alterations induced by the SH2 domain cause

reduction of IDR:SH3 contacts in a similar manner as when the IDR partially detaches from SH3 domain upon PxxP ligand binding in USH3. To provide additional evidence, we chose USH3^{PxxP} state as reference and performed a CSP mapping of some IDR residues.

Figure 4.9. Chemical Shift mapping for residues in the SH4-U domains. $\Delta\delta$ ^{1}H (x axes) - $\Delta\delta$ ^{15}N (y axes) are calculated with respect to USH3^{PxxP} chemical shifts. Green cross represents 0.01 ppm.
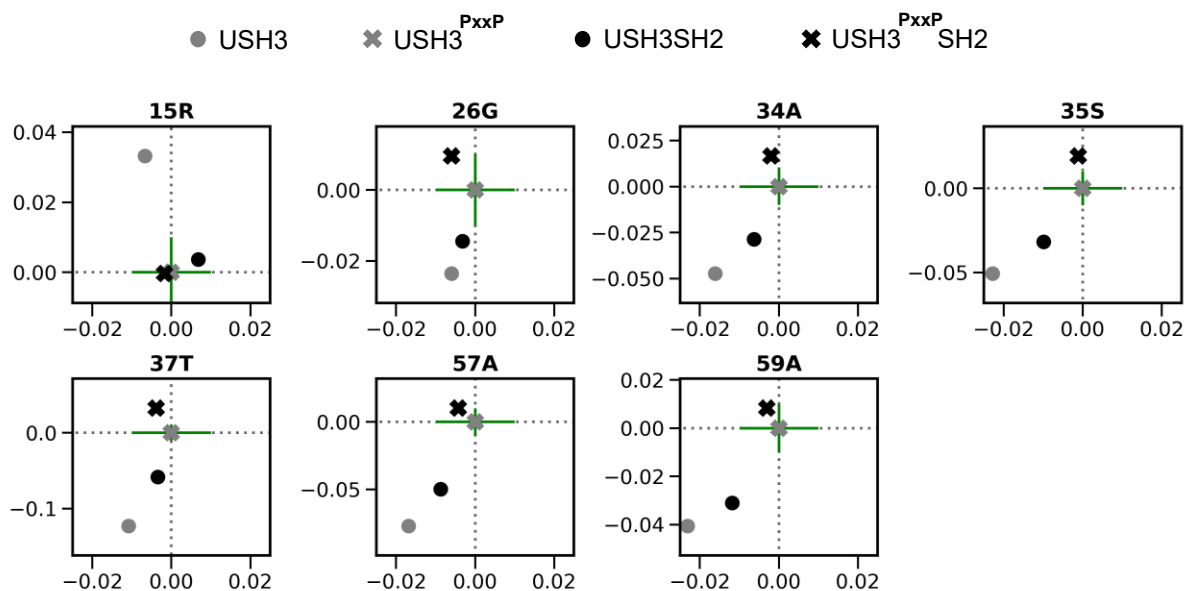

The SH4-U residues analyzed (R15, G26, A34, 35S, T37, A57 and A59) have been selected because they exhibit chemical shifts equivalent to those of the isolated IDR, upon SH3 PxxP-ligand binding in USH3 (Maffei et al., 2015). As shown in *Figure 4.9*, even in the absence of the PxxP-ligand, the USH3SH2 (black circle) residues' chemical shifts move towards those in USH3^{PxxP}. This clearly shows that the presence of the SH2 domain would partially decrease the preexisting IDR:SH3 interactions observed in the USH3 construct.

The results presented hitherto, do not provide enough support to establish that the SH4-U region interacts with the SH2 domain, although apparently it does affect the fuzzy interdomain IDR:SH3 complex. The lower extend of perturbations observed in the presence of the SH2 domain, suggest that IDR:SH3 interactions are mostly retained in USH3SH2, although some of these interactions are partially released. Moreover, the key ULBR is affected by the presence of the SH2 domain, presumably by indirect SH2 effects through the SH3 domain. In the following section we extended the analysis to the SH3 domain.

### 4.3.3. Mapping the intramolecular interactions of SH3 domain in the USH3SH2 context

The SH3-SH2 domains show minimal interdomain contacts beyond the SH32-linker region (residues 143-150). In an X-ray structure of the c-Src open state (PDB:1Y57, Cowan-Jacob et al., 2005) this region appears to form a short 3_{10}-helix. Structuration of this connector had also been demonstrated <u>in solution</u> by Tessari et al., (1997) through NMR measurements of an SH3SH2 (chicken) c-Src construct. Besides the SH32-linker region, Tessari et al., (1997) also concluded that no significant changes were observed when the SH3 and SH2 domains were bound together (in the dual-domain construct) as compared with the isolated domains.

Figure 4.10. Structure of the selected SH3-SH2 domains of c-Src in the open state (from PDB: 1Y57). Residues in the liker region are shown with intramolecular H-bond highlighted in blue.
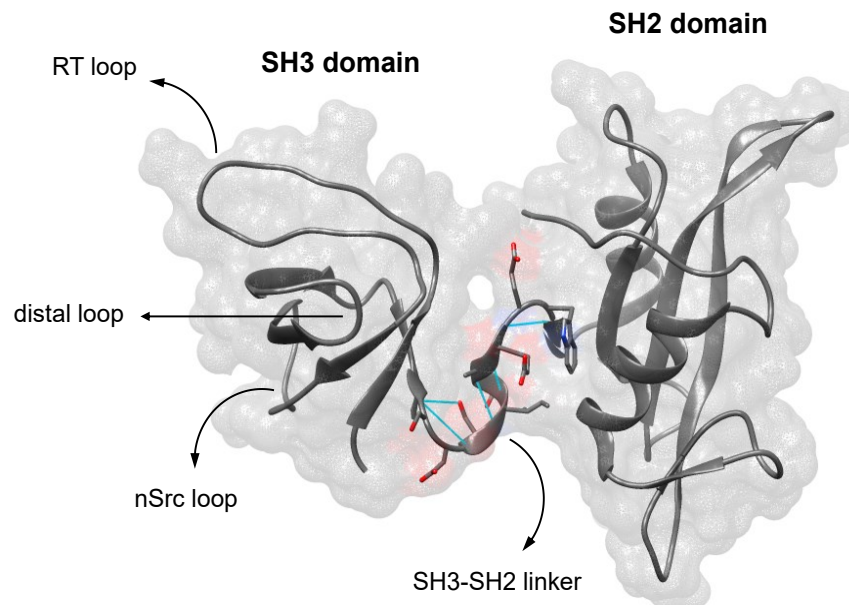
First, the CSP in the SH3 domain for USH3SH2 against USH3 are calculated (*Figure 4.11*). The CSP were also mapped on the crystal structure of SH3-SH2 domains to better discern the perturbations in the SH3 domain that likely could derive from direct contacts with the SH2 domain from those that could originate in a different IDR:SH3 interaction.

Figure 4.11. (top) Combined ^1H ^{15}N CSP of USH3SH2 vs USH3 mapped (bottom) over the c-Src selected SH2-SH3 domains crystal structure (PDB: 1Y57).
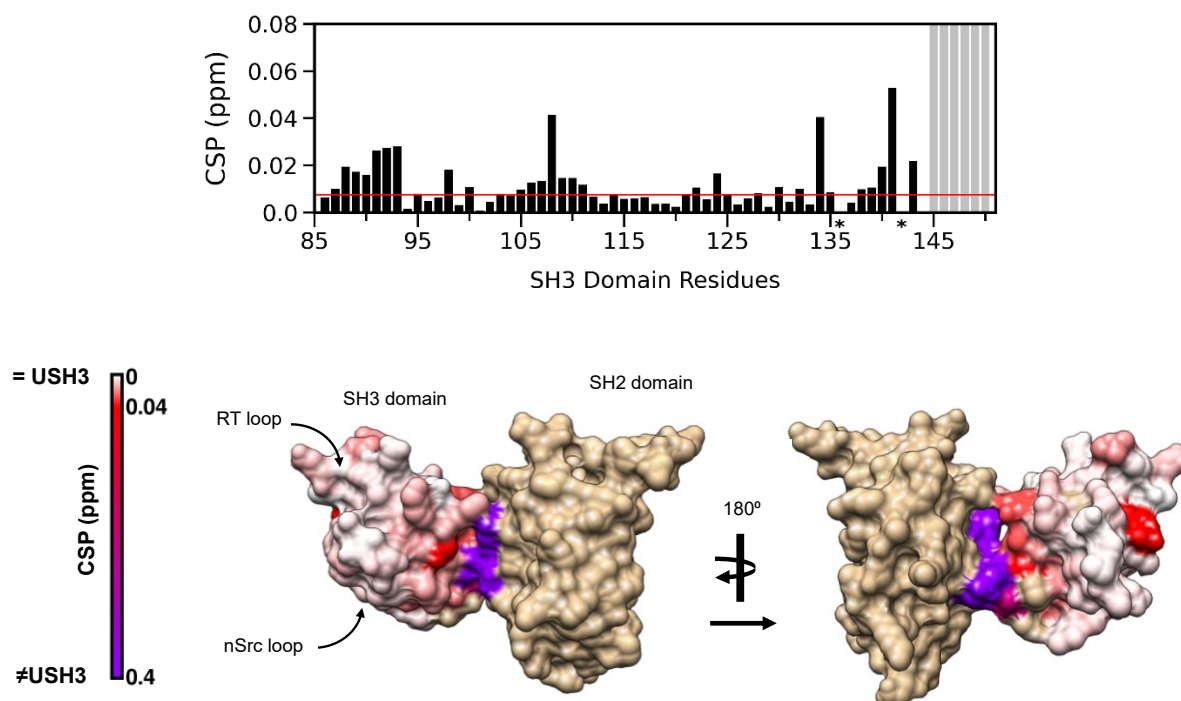
As expected, in USH3SH2 the SH3|2-linker region (^{144}DSIQAEE^{150}) is the most affected. The chemical shifts of the residues close to the SH3|2 interface region are also highly perturbed as observed in the X-ray structure. The disturbance of distant residues most likely reflects effects mediated by changes in the IDR (SH4-U) interactions, but even perturbations at the SH3|2 interface region could also originate from different SH4-U interactions, if the IDR interacts simultaneously with both domains or with SH3 regions affected by the close contact of the SH2 domain.

To try to differentiate these effects we performed a CSP mapping using the isolated SH3 as a reference state for the residues near the SH3-SH2 interface, namely the β_1 strand ^{86}VTTFVALY^{93} and the C-terminal part of the SH3 domain: ^{140}VAPS^{143} (highlighted in pink in *Figure 4.12*A).

Figure 4.12. (A) c-Src SH2-SH3 domains crystal structure (PDB: 1Y57) highlighting the SH3 domain residues at the SH3-SH2 interface region. (B) Chemical Shift mapping for residues in the SH3 domain. $\Delta\delta$ ^{1}H (x axes) - $\Delta\delta$ ^{15}N (y axes) are calculated with respect to isolated SH3 domain chemical shifts. Green cross represents 0.01 ppm.
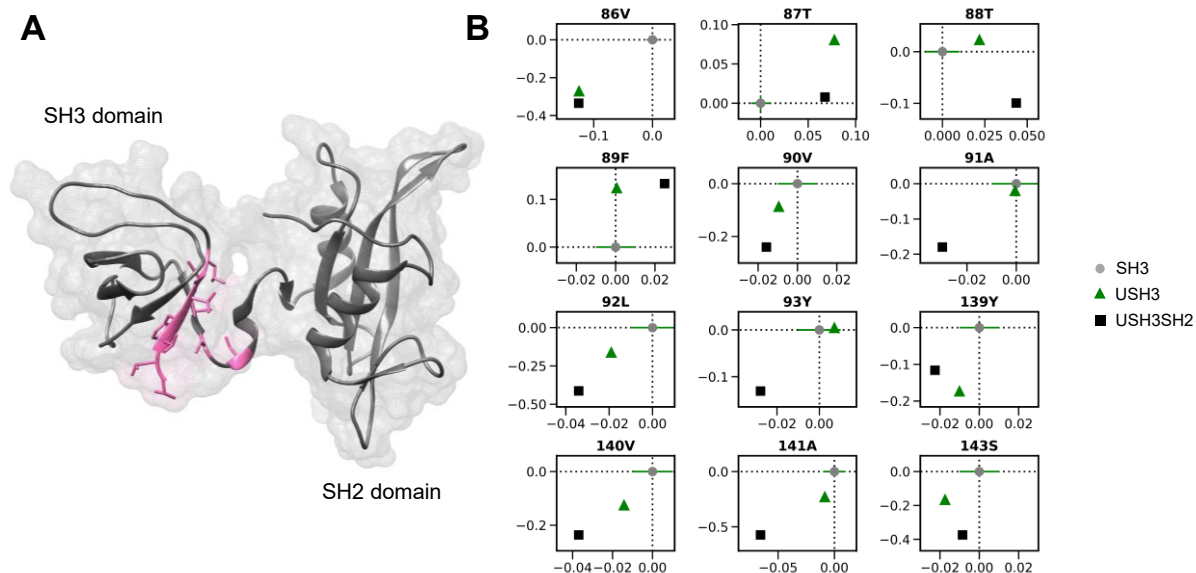
The nearly lineal progression of the chemical shifts from SH3, to USH3 and USH3SH2 for ^{90}V, ^{92}L, ^{140}V and ^{141}A residues, suggest that the SH2 domain could enhance preexisting interactions (i.e. in USH3) of the IDR with the SH3 domain in the SH3-SH2 interface region. Residue ^{91}A and ^{93}Y are affected by the SH2 domain, while they were hardly perturbed by the IDR (in USH3). Residue ^{86}V, that was strongly perturbed by the presence of the SH4-U is not further affected by the presence of the SH2 domain. The remaining residues analyzed show complex changes reflecting synergistic effects of the IDR and the SH2 domain. This suggests a possible modulation of the SH3-SH2 interface by the IDR.

The SH3 domain signals of USH3SH2, also showed perturbations in regions outside the SH3|2 interface. This could reflect changes in the IDR:SH3 interactions in the presence of the SH2 domain. To examine these effects, CSP are calculated against the isolated SH3 domain for USH3 and the USH3SH2 construct. The combined ^{1}H-^{15}N CSP plots are shown in *Figure 4.13.*

131

Figure 4.13. Combined ^{1}H ^{15}N CSP using the isolated SH3 domain as reference of (A) USH3 (B) USH3SH2. The red line represents the significant threshold defined as the mean CSP for the lowest decile (μ(lowest decile CSP)) plus five standard deviations (5σ). Prolines are marked with *. Experiments performed at 278K.
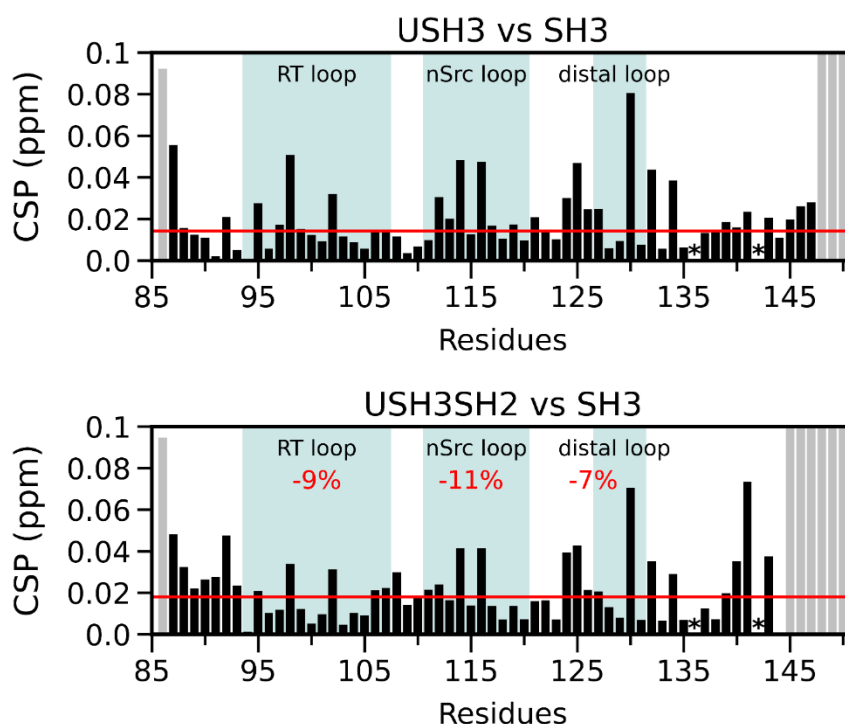
In both constructs, the residues with the highest CSP (gray bars) coincide with the different N/C-terminus of the compared constructs (eg. USH3$_{His6Tag}$ vs SH3). Therefore, it is not surprising, that the SH3|2-linker (^{143}SDSIQAEE^{150}) in USH3SH2 exhibits such higher perturbations, since the linker is structured in this construct. The β_1 strand: ^{87}TTFVALY^{93} and the β_5 strand: ^{139}YVAP^{142} (C-terminal part of the SH3 domain) are also more affected for USH3SH2. These regions are closer to the SH3|2 linker, but we earlier showed that the IDR has also a stronger interaction with these regions when the SH2 domain is present.

Most of the interactions in the fuzzy interdomain IDR:SH3 complex entail the three loops (RT, nSrc and distal) of the SH3 domain. The SH3 loops perturbations observed in the USH3SH2 are apparently comparable to those in USH3. Although, while the pattern of residues affected is similar, the magnitude of perturbations, obtained by integrating the CSP over the entire loop, are different. The percentage variation in integrated CSP in USH3 and USH3SH2 are indicated in *Figure 4.13*. The three SH3 loops showed slightly reduced perturbations in in USH3SH2 as compared to USH3, suggesting weaker interactions of the loops with the IDR in the presence of the SH2 domain. This would be consistent with the previous *subsection 4.3.2* results, showing that the presence of the SH2 domain provokes certain loss in the IDR contacts with the SH3 domain.

The results presented so far, have revealed that the intramolecular interactions of the SH3 domain in the fuzzy IDR:SH3 complex (USH3) are modified when the adjacent SH2 domain is present. The SH3 loops (RT, nSrc and distal) slightly lose intramolecular contacts with

the IDR, adopting an environment more similar to *free* SH3 domain. On the other hand, perturbation of the residues in the β_1 strand and the C-terminal part of the SH3 domain (close to the SH3-SH2 interface) suggest that the IDR interaction with these regions is enhanced (when the adjacent SH2 domain is present). The latter could explain the release of interactions from RT, nSrc and distal loops, if the β_1 strand and the C-terminal part of the SH3 domain compete with the SH3 loops for interactions with the IDR.

Upon SH3 ligand (PxxP peptide) binding, the fuzzy IDR:SH3 complex intramolecular interactions are *reshaped*. The IDR:RT loop (SH3 domain) interactions are impaired upon ligand binding and the remaining contacts occur through the nSrc plus distal loops and the C-terminal region of the SH3 domain. To recall, the IDR partially detaches from the SH3 domain upon ligand binding. We next explored if this *reshaping* was maintained in the presence of the SH2 domain.

The effects of the SH2 domain on the USH3:PxxP ligand bound form (USH3^{PxxP}), are determined using CSP. The CSP values for USH3^{PxxP}SH2 vs USH3^{PxxP} are also plotted on the c-Src crystal structure of SH3-SH2 domains in *Figure 4.14*.

Figure 4.14. Combined ^{1}H ^{15}N CSP of USH3^{PxxP}SH2 vs USH3^{PxxP} mapped over the c-Src selected SH2-SH3 domains crystal structure (PDB: 1Y57).
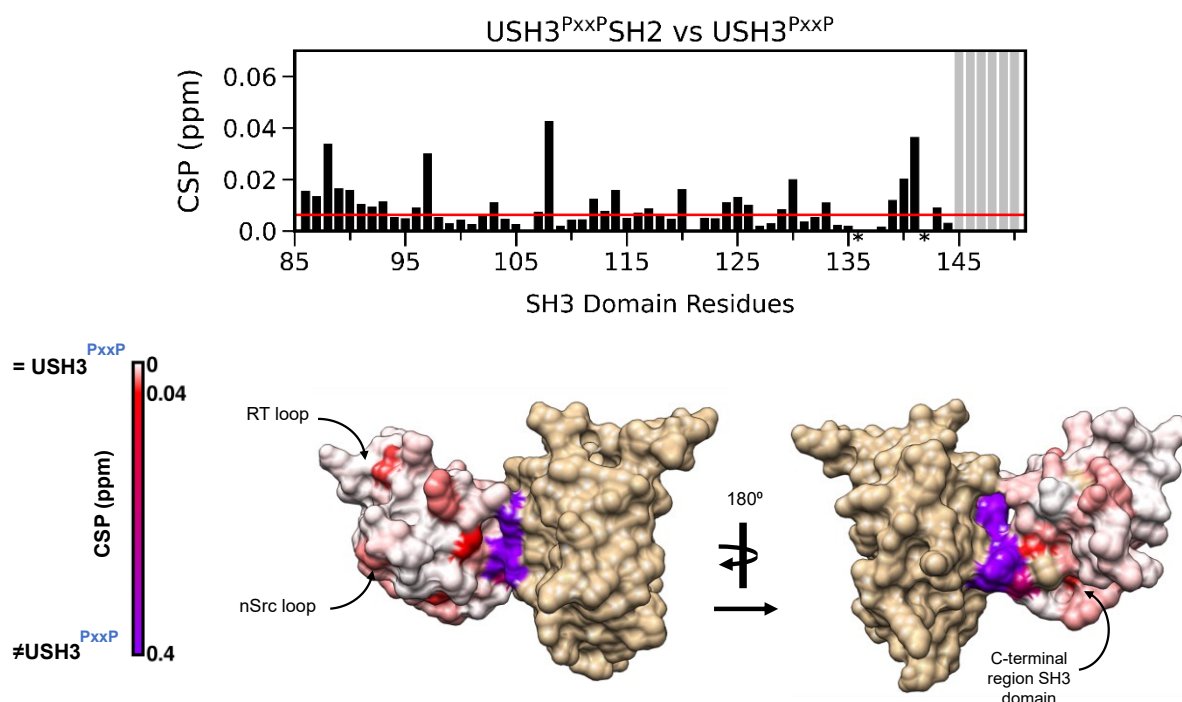
Besides the obvious perturbations at the SH3|2-linker region, small perturbations in the SH3 loops: RT (residue ^{97}S), nSrc (residue ^{120}D) and distal (residue ^{130}G) are observed in the presence of the SH2 domain (SH3-ligand bound state). Moreover, the β_1 strand ^{86}VTTFVALY^{93} and the C-terminal part of the SH3 domain: ^{140}VAPS^{143} are moderately perturbed. To note that in absence of the PxxP ligand, the latter regions were shown to increase the interactions with the IDR because of the SH2 domain incorporation. Thus,

using a CSP mapping (*Figure 4.15.*) with the isolated SH3-PxxP bound form as a reference state, we explored whether the IDR maintained the enhanced interaction with the β_1 strand and the C-terminal part of the SH3 (regions near the SH3|2 interface) when the SH2 domain was present even in the SH3-ligand bound state.

Figure 4.15. Chemical Shift mapping for residues in the SH3 domain. $\Delta\delta$ ^{1}H (x axes) - $\Delta\delta$ ^{15}N (y axes) are calculated with respect to isolated SH3 domain chemical shifts. Green cross represents 0.01 ppm.
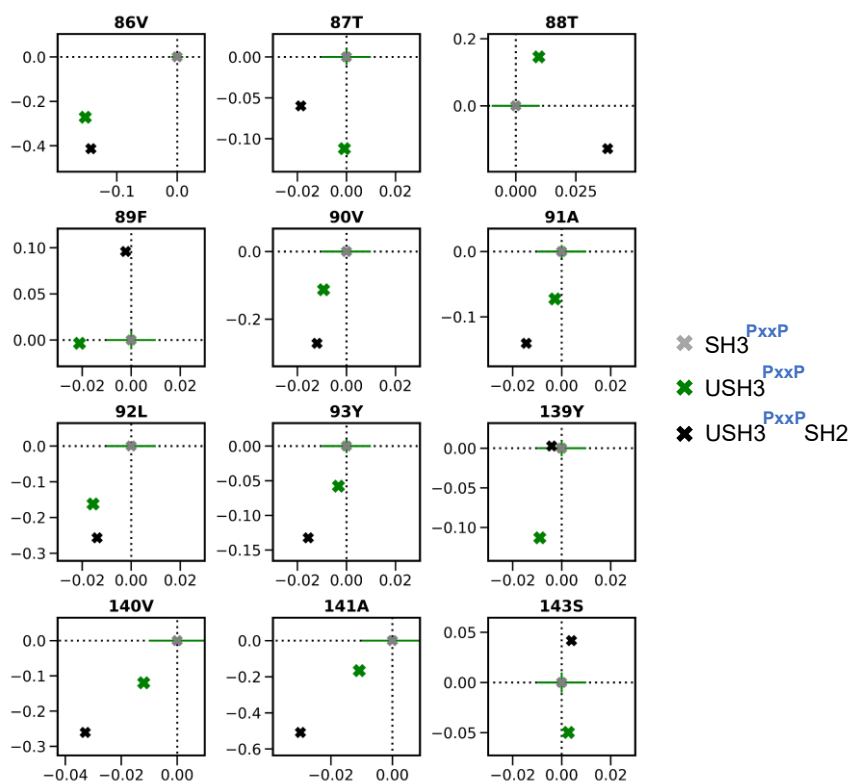
The almost linear change of the chemical shifts from SH3^{PxxP}, to USH3^{PxxP} and USH3^{PxxP}SH2 is shown for residues ^{90}V, ^{91}A, ^{93}Y, ^{140}V and ^{141}A, suggesting that even in the SH3-ligand bound state, the SH2 domain enhance preexisting interactions (i.e. in USH3^{PxxP}) of the IDR with the SH3 domain at the SH3|2 interface region. Residues ^{86}V and ^{92}L are likely affected by the presence of the IDR, but not the SH2 domain, whereas residue ^{139}Y in presence of the SH2 domain recovers the chemical shifts as in isolated SH3^{PxxP}. The remaining residues exhibit cooperative effects of the IDR and the SH2 domain when the SH3 is bound to the PxxP peptide.

Other alterations induced by the SH2 domain in USH3:PxxP ligand bound form included residues the SH3 loops. To further investigate the origin of these perturbations, we calculated CSP using the isolated SH3 complexed to PxxP ligand for USH3^{PxxP} and USH3^{PxxP}SH2 (*Figure 4.16.*).

Figure 4.16. Combined ^1H ^{15}N CSP of (top) USH3^{PxxP} versus SH3^{PxxP} (bottom) USH3^{PxxP}SH2 vs SH3^{PxxP}. The red line represents the significant threshold defined as the mean CSP for the lowest decile (μ(lowest decile CSP)) plus five standard deviations (5σ). Prolines are marked with *. Experiments performed at 298K.
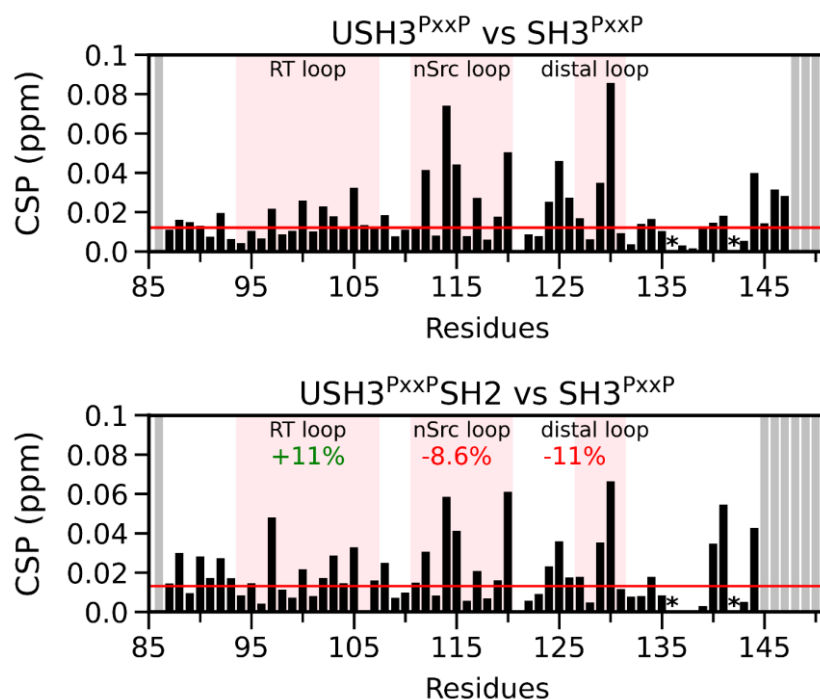
Using the isolated SH3^{PxxP} as reference, in absence (USH3$^{PxxP)}$ and presence of the SH2 domain (USH3^{PxxP}SH2) the major perturbations are found in the SH3 loops. The observed pattern of the residues affected is similar. This suggests that the origin of the perturbations could rely in the IDR (SH4-Unique domains) independent of the incorporation of the SH2 domain. Moreover, direct interaction between the SH2 domain and the SH3 loops are unlikely as inferred from the known X-ray structures, supporting that these effects probably reflect the perturbation with the IDR. However, the CSP magnitude of the SH3 loops is somewhat different in presence of the SH2 domain, thus suggesting that the IDR interactions might have slightly changed. Presence of the SH2 domain, seems to enhance (+11%) the intramolecular interactions in the RT loop (in comparison to the USH3^{PxxP}). Whereas the nSrc and distal loops partially lose contacts when the adjacent SH2 domain is present, as inferred from the integrated CSPs.

To confirm that the PxxP peptide binding induce the same perturbations to the SH3 domain of all c-Src constructs, we calculated the CSP of the PxxP complexed state using the *apo* form as the reference state.

Figure 4.17. Combined ^{1}H ^{15}N CSP of the native versus the PxxP-bound form for the (A) isolated SH3 domains (B) USH3 and (C) USH3SH2 constructs mapped over the c-Src selected domains of the crystal structure PDB: 1Y57 of c-Src.
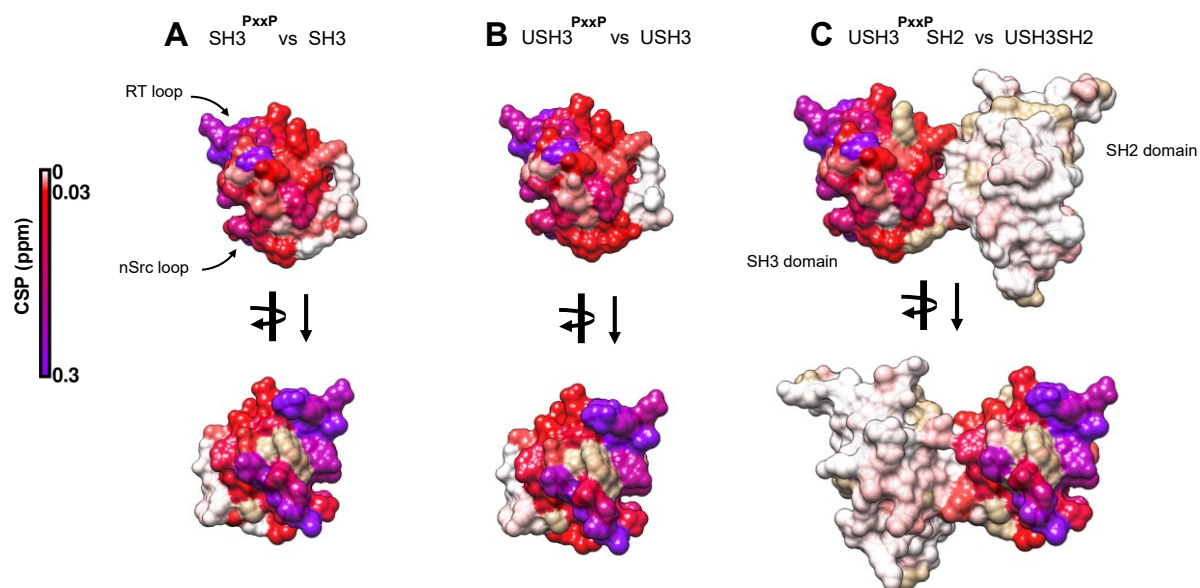

The very similar chemical shift effects caused in the SH3 domain by the PxxP (VSL12) peptide shown in *Figure 4.17*, indicate that its binds analogously in the SH3 domain of all the three c-Src constructs. Analyzing the PxxP-bound and *apo* forms of USH3SH2, shows that the SH2 domain is slightly perturbed upon ligand occupation of the SH3 domain. The effects are very small and spread all over the SH2 domain, though some of them are concentrated in the SH2 domain face directed towards the SH3-SH2 interdomain region. One hypothesis is that these alterations emerge from altered dynamics in SH3 domain upon PxxP peptide binding that are cross-communicated to the SH2 domain. Another explanation could be that the partial disengagement of the IDR (SH4-U) from the SH3 domain upon PxxP peptide binding, also impairs putative IDR:SH2 interactions. A third possibility, partially combining the previous two, is that the IDR, interacting with the SH3 and SH2 domains is an active element of the SH3-SH2 interface, and the perturbation caused by the peptide to the IDR:SH3 interaction is communicated to the SH3-SH2 interface. This would highlight a possible active role of the IDR in the cross-communication between the globular domains.

Finally, when the ^{1}H-^{15}N HSQC of USH3SH2 was measured, several residues in the SH3 and SH2 domains showed duplicated signals (*Figure 4.18*A). As sample purity was carefully assessed through SDS-PAGE and since the construct eluted as a single peak in the Size Exclusion Chromatography, duplicated signals probably arise from slow exchange between alternative conformations. On average the ratio between both peak intensities was < 1 indicating unequal populations of both conformations. The peak duplication pattern was different upon SH3 ligand binding. The high number of residues affected suggests a global effect. Moreover, Tessari et al. (1997) did not report such phenomena in their NMR analysis of the dual-domain SH3SH2 construct (i.e. absence of the IDR: SH4-U domains), thus the

IDR (SH4-Unique domains) may have a role, such as changing the domains dynamics due to its interaction with the SH3 domain or the SH3|2 interface region. However, this hypothesis needs further investigation.

Figure 4.18. (A) Structure of the SH3-SH2 domains of c-Src (from PDB: 1Y57) highlighting the residues that show signal duplication. Colored in red: residues that showed signal duplication in USH3SH2 and USH3PxxPSH2, in blue: residues exhibited signal duplication in USH3PxxPSH2 and in black: residues that showed signal duplication in USH3SH2 but not in USH3PxxPSH2. (B) Selected expansions of the USH3SH2 and USH3PxxPSH2 HSQC spectra displaying the residues presenting signal duplication.
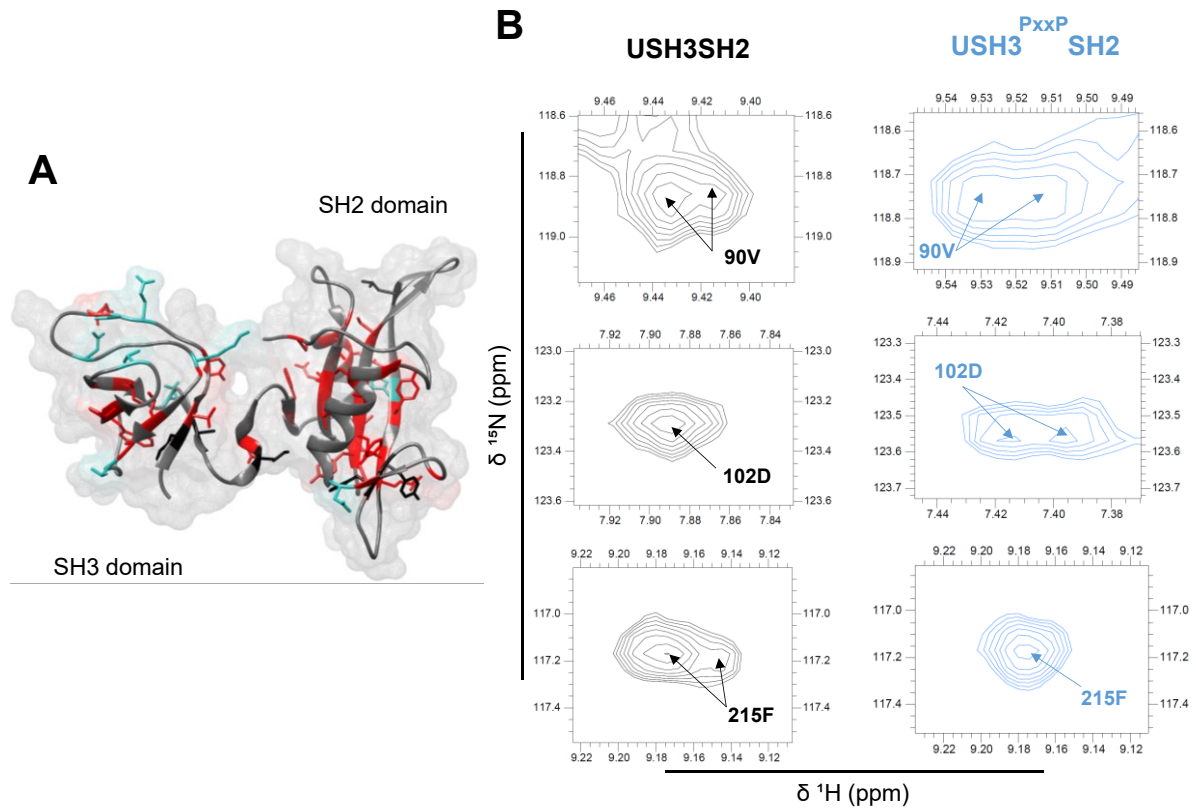
4.3.4. Analysis of the intramolecular contacts in the putative myrUSH3HS2 context

The results in *Chapter 2* revealed in the native myristoylated USH3 form (myrUSH3), the myristoyl group has binding sites within the SH3 domain in the proximity of the RT loop and the groove formed by the C-terminal region and β_1 strand (that is the SH3-SH2 interface region). The ULBR was required for an effective interaction of the myristoylated SH4 domain with the aforementioned SH3 binding sites. At the same time, the myristoyl moiety increased the local concentration of the IDR in the proximity of the SH3 domain by cooperatively favoring the preexisting interactions in absence of the myristoyl group. The overall consequence was multiple binding sites in the SH3 domain that harbored the myristoyl moiety.

In USH3SH2 (absence of myristoyl group) presumably the IDR interaction with the region close to the SH3-SH2 interface is enhanced and the results of the PxxP-binding, suggests that ULBR might be responsible of this promoted interaction. The presence of hydrophobic residues in both ULBR ⁶⁰EPKL<u>F</u>GG<u>F</u>NSS⁷⁰ and the SH3-SH2 interface (*Figure 4.19.*) could be the underlying reason of a stronger interaction.

Figure 4.19. Structure of the SH3-SH2 domains of c-Src (from PDB: 1Y57) highlighting hydrophobic residues at the SH3-SH2 interface region.
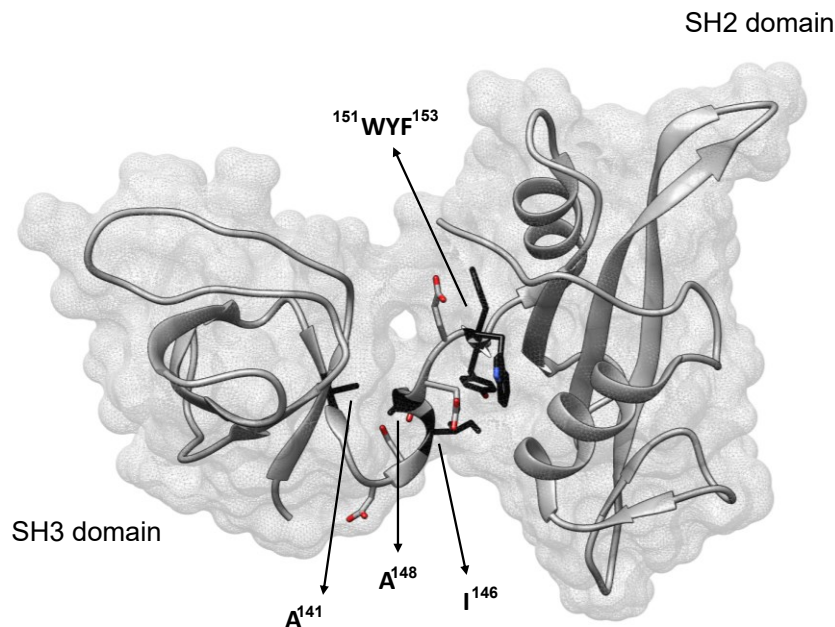
In the putative myrUSH3SH2 context, residues ¹⁵¹WYF¹⁵³ at the SH3-SH2 interface region would potentially flank the hydrophobic groove formed by the C-terminal region and β_1 strand where the myristoyl has been shown to interact in myrUSH3. Thence, in the myrUSH3SH2 context, it is likely that the affinity of the myristoyl group for SH3-SH2 interface region could be apparently stronger (due to increased hydrophobic interactions), with additional contribution of the ULBR. One consequent scenario is that this gives rise to a more "stable" hydrophobic pocket for the myristoyl group in the SH3-SH2 interface

region. So, if this ULBR – myrSH4 – SH3SH2 interface interaction is stronger, how is going to be the impact on the other intramolecular interactions that define the fuzzy IDR:SH3 complex? Results for the non myristoylated USH3SH2 have already revealed that some of the SH4-U:SH3 interactions are partially released in the presence of the SH2 domain and consistently the RT, nSrc and distal loop exhibited decreased perturbations (i.e. environment towards like the isolated SH3 domain), whereas presumably the interactions of the IDR (likely ULBR is accountable) with the regions close to the SH3-SH2 interface are enhanced. Will the presence of myristoyl group in myrUSH3SH2 will completely shift this behavior and restrict the SH4-U:SH3 interactions? Further questions related to the membrane binding of myrUSH3SH2 compared to myrUSH3 can be set out, considering that modulation of the myristoyl group might not be the same.

Particularly, the role of the ULBR has been demonstrated to be functionally relevant, although the regulation mechanisms are still poorly understood. In colon rectal cancer cells SW260 where deregulation of c-Src is observed, mutation of the ULBR reduced ~50% the invasive capacity of the cells (Arbesú et al., 2017; Maffei et al. 2015). Intramolecular interactions led by the myristoyl group that could regulate the ULBR through the regulatory domains are hypothesized in absence of the kinase domain i.e. myrUSH3SH2. Moreover, the myr:ULBR interactions in myrUSH3SH2 could also modulate the kinase activation, as presented in *subsection 4.1*. But further characterization of this myrUSH3SH2 c-Src construct will be required.

4.4. Discussion

The c-Src N-terminal Regulatory Element (SNRE) features a fuzzy complex formed by the myristoylated IDR (SH4 and Unique domains) with the globular SH3 domain (Maffei et al., 2015, Arbesú et al., 2017). The myristoyl moiety has been shown to enhance the formation of the fuzzy complex by favoring the IDR:SH3 contacts. Additionally, both the ULBR (in the Unique domain) and the myristoyl moiety have been proved to be key elements to maintain the conformational ensemble that defines the fuzzy complex (*Chapter 2*). In this chapter we have performed a preliminary characterization of the SNRE with the adjacent SH2 domain in the absence of the myristoyl group.

The initial results show that presence of the SH2 domain does affect the fuzzy interdomain IDR:SH3 complex. Nonetheless, the primary alterations do not indicate direct IDR:SH2 contacts but modification of the preexisting IDR:SH3 interactions (observed in USH3). Most of the effects imply that the IDR:SH3 interactions are partially released in presence of the SH2 domain. However, the key ULBR shows an opposite behavior. Although, a direct ULBR:SH2 interaction is suggested, the minimal magnitude of the perturbations indicate that the main interaction of the ULBR is with the SH3 domain and the effects are seemingly indirectly induced by the SH2 domain through the SH3|2 linker region. Potentially, the SH3 regions were the ULBR is known to interact (β_1 strand and C-terminal part of the SH3 domain) are now affected by the SH3|2 interface.

Consistently, the reduction of the IDR:SH3 contacts in presence of the SH2 domain is also observed in the SH3 domain. The SH3 loops (RT, nSrc and distal) that concentrate most of the fuzzy complex interactions (Arbesú et al. 2017), adopted an environment more similar to the isolated SH3 domain, indicating that the SH3:IDR contacts are reduced in USH3SH2. Nonetheless, at the SH3|2 interface region some residues showed cooperative effects by both the SH2 domain and the IDR. The results suggested that the SH2 domain incorporation enhanced preexisting IDR:SH3 interactions (i.e. in USH3) at the SH3|2 interface region, namely the β_1 strand and the C-terminal part of the SH3 domain. This could be compatible with the ULBR (in the IDR) having enhanced interactions with these SH3|2 interface regions. The presence of hydrophobic residues in both ULBR [60]EPK<u>L</u>FGG<u>F</u>NSS[70] and the SH3-SH2 interface region [143]SDS<u>I</u>QA<u>EEWYFKI</u>[155] could favor a stronger interaction.

Thus, in the USH3SH2 framework, the fuzzy IDR:SH3 complex interactions (in USH3) have been *re-balanced*. Most of the preexisting interactions now dwell at the SH3|2 interdomain region. This could suggest a possible modulation of the SH3|2 interface by the IDR and a probable specific role of the ULBR.

In combination with previous studies demonstrating the coupling of the ULBR and the RT loop in the SH3 domain, a scenario emerges with four main players in the SNRE: The SH3 RT loop, the SH3|2 interdomain region, the ULBR and the myristoylated SH4 N-terminal domain, as well as possible interactions of the SH3 domain with a polyproline segment in the SH2|1 linker or with external ligands.

Figure. 4.20. Domain architecture of c-Src illustrating the interactions involved in the activation mechanism of c-Src are shown. In black, the well-known interactions: SH2:pY530 (C-term tail) and the SH3:PxxP (SH2|1 linker). In red, the ULBR:SH3|2 linker, is hypothesized to participate in the activation mechanism.
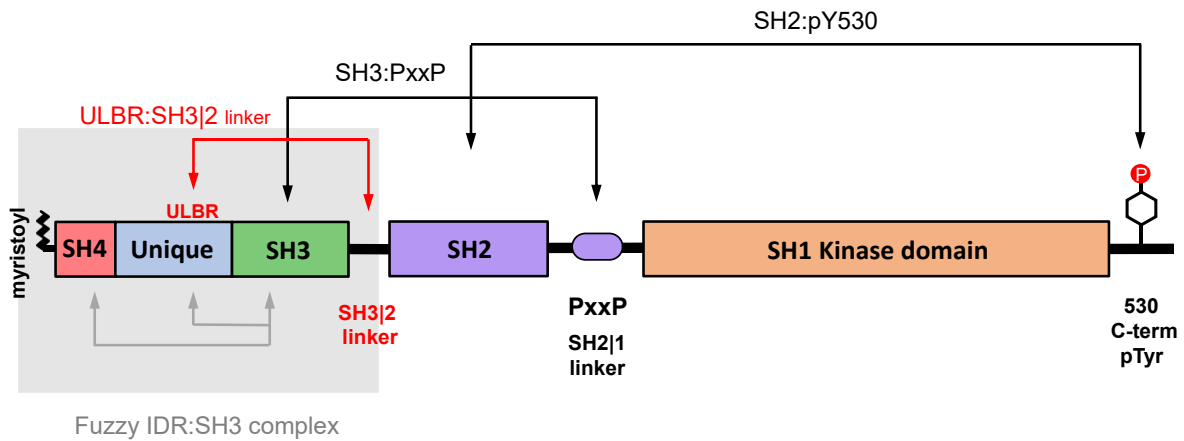
The linker region in the various SFKs is relatively well conserved (*Figure 4.21.*), featuring an enrichment in negatively charged residues, a conservation of side chain length (D/N and E/Q), and a conserved S/T. It precedes the start of the SH2 domain with three well conserved aromatic residues W-F/Y-F, followed by a less well-defined enrichment in positively charged residues.

Figure 4.21. Sequence conservation at the SH3|2-linker region for non-receptor SFKs: c-Src, Yes, Fyn, Fgr, Lyn, Lck, Blk and Hck. The conserved [151]W delimits the beginning of the SH2 domain.
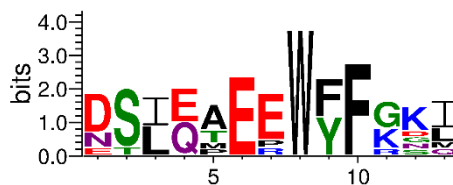
Simulations predict that replacement of Hck SH3|2 linker segment [140]VDSLETEE[147] with the one of Lck [140]ANSLEPEP[147] (both SFK members) results in different orientation between the SH3-SH2 domains and also leads to significant effects in the activation segment of the kinase domain of Hck (Meiselbach and Sticht, 2011). Additionally, Young et al., (2001) using molecular dynamics simulations with the globular domains of c-Src (SH3-SH2-SH1[Kinase]) described that the SH3|2 linker formed an "inducible snap lock". In the closed state, when the SH2 binds the phosphorylated Y530 in the tail, the SH3|2 linker possessed a rigid structure that dynamically coupled the SH3 and SH2 domain in the repressed state. Upon pY530 dephosphorylation and detachment of the SH2 domain, the SH3|2 linker gains certain flexibility. Mutation of the SH3|2 linker with glycines residues, resulted in uncorrelated motions between the SH3 and SH2 domains even when SH2-pY530 interaction existed. The same G mutations *in vivo* prompt the c-Src kinase activation (Young et al. 2001). This suggest that the SH3|2 linker could be a critical element in the activation mechanism of c-Src. Considering our results, we wonder on the consequences of

the IDR (particularly the ULBR) interaction with this "inducible snap lock" (SH3|2 linker), speculating that the myristoyl could also participate in this interaction.

Interestingly, Bernadó et al., (2008) found that the ensemble of the three globular domains, lacking the IDR adopts a closed conformation, even when the SH2 domain was disengaged from the C-terminal tail. Additionally, various *in vitro* assays (Patwardhan and Resh, 2010; Spassov et al., 2018) suggest an active role of the IDR and in particular the myristoyl moiety, in regulating the kinase activation. One can hypothesize that the IDR:SH3 fuzzy complex, with the key myr:ULBR:SH3|2 linker interaction, could be an additional factor to modulate the open-active state (*Figure 4.20.*). However, further characterization will be required. An evidence of myristoyl moiety involved in enzyme activation is found in myrGCAP1 (myristoylated guanylate cyclase-activating protein (GCAP)) that belongs to the group of Ca^{2+}-binding proteins related to the neuronal calcium sensors (NCS) family. Stephen et al., (2007) provided the crystal structure of myrGCAP1 and demonstrated that myristoyl moiety remained buried in GCAP1 protein in the Ca^{2+}-bound conformation, in contrast to recoverin (another NCS member), that exposes the myristoyl group upon binding of Ca^{2+} for membrane engagement. Structural details of myrGCAP1 revealed that the myristoyl moiety provided conformational stability and was required for full activation of the protein at signaling concentrations of Ca^{2+}.

Evidence for the interaction between the ULBR or the RT loop has been shown by the reciprocal effect of mutations in both regions (*Chapter 2*), indicating the preferred interaction between both regions. Evidence supporting this possible layer of regulation, could be deduced when comparing the different viral v-Src mutants (Maffei et al.,2015) (*Figure 4.22.*), concurrent mutations with hydrophobic residues in the RT loop and ULBR occur. Mutations would only survive the selection pressure if the conferred properties were convenient.

Figure. 4.22. Multiple sequence alignment for v-Src and c-Src. Sequences were fetched from Uniprot, entries: P12931, P63185, P25020 and P00526, corresponding to c-Src and v-Src from strains: Schmidt-Ruppin E, H-19 and Prague C respectively. Sequence alignment was performed with Clustal Omega (EMBL-EBI).

In this chapter we have studied in detail the effect of the VSL12, a synthetic high affinity polyproline SH3 binder. Binding of polyproline sequences is the canonical interaction expected for SH3 domains. The potential role of the SH3 domain connecting disordered regions and globular domains has been suggested by Arbesú and Pons (2019) on the basis of the widespread enrichment of non-canonical SH3 binding sequences (Teyra et al., 2017) in disordered regions adjacent to SH3 domains in a large number of human proteins. However, how particular SH3 domains recognizes specific polyproline sequences is still subject of investigation. Considering our results, whether a potential modulation of the RT loop of the SH3 domain through the ULBR could define or affect the PxxP ligand recognition, remains to be explored.

Binding of the VSL12 peptide to the SH3 domain reshapes the c-Src fuzzy IDR:SH3 complex. In addition, the presence of the SH2 domain causes a shift in the equilibrium of the intramolecular interactions involving the SH3 and the IDR. In the presence of the SH2 domain, the ULBR gains contacts with the SH3|2 interface, whereas in the interaction of the IDR with the SH3 domain increase at the RT loop and are reduced in the nSrc and distal loops. These compensating effects suggest a *"rewiring"* of the fuzzy complex. The increase of the intramolecular interactions (in USH3^{PxxP}SH2) involving the RT loop could stem from the increased availability of the ULBR due to its interaction with the SH3|2 interface.

The results presented in this chapter provided further insights on c-Src N-terminal Regulatory Element. However, the questions raised shall be investigated to allow further understanding on how tyrosine kinases with a similar domain architecture could exert such diverse cellular functions.

4.5. Material and methods

4.5.1. Cloning and mutagenesis

Using the Gibson assembly method (Gibson et al. 2009), the SH2 domain (residues 151-250) encoding was inserted in our previous vector pETDuet-1_USH3-Src_hNMT (Ampicillin resistance) containing the USH3 c-Src construct and the NMT. The required DNA fragments: 1) pETDuet-1_USH3-Src_hNMT linearized vector 2) SH2 domain (both with common overlapping regions) where amplified as per standard protocol using the Q5 High-Fidelity PCR Kit (New England Biolabs) and purified with the PCR Purification Kit (Qiagen). The assembly reaction of the fragments was carried out at 50C for 30min using Gibson assembly Kit from New England BioLabs. The reaction product plasmids were transformed and amplified in *E. coli* OmniMAX™, purified by miniprep procedure using QIAprep Spin Kit (Qiagen) and sequenced by Macrogen Inc. To obtain the non-myristoylated USH3SH2 construct, the mutation G2A was introduced using QuickChange II XL Kit (Agilent) or Q5 High-Fidelity Kit (New England BioLabs) by a standard site-directed mutagenesis procedure.

Plasmids of other c-Src constructs used in this section were previously prepared in our laboratory: USH3 (G2A) encoded in pETDuet-1_USH3-Src_hNMT (Ampicillin resistance) and SH3 encoded in pETM-30 (Kanamycin resistance).

4.5.2. Protein expression and purification

Plasmids were transformed in *Escherichia coli* Rosetta™ (DE3) pLysS (Novagen) and the bacteria cells were grown in 2x 1L Luria Broth (LB) medium supplemented with chloramphenicol (25 µg/mL) and ampicillin (100 µg/mL) (or 100 µg/mL kanamycin) at 37 °C until an OD_{600nm} of ~0.6 was reached. Then, cultures were harvested by centrifugation at 1000 g for 30 min and both resuspended in 0,5L of M9 medium containing 1 g/L ^{15}N NH_4Cl (Cambridge Isotope Laboratories). Before induction with 1mM of isopropyl-β-D-thiogalactopyranoside (IPTG) (Nzytech), 1,5 g/L of ^{13}C glucose (Cambridge Isotope Laboratories) (for ^{13}C carbon labeled samples, otherwise non-labeled glucose) was added to the media and the bacteria was additionally grown for 1h at 25°C. The protein expression was performed O/N at 25°C. In the case of myristoylated constructs preparation (myrUSH3 or myrUSH3SH2) before the induction with IPTG a freshly prepared solution of myristic and palmitic acid (Sigma) at 50 µM final concentration for each plus fatty acid free BSA (Sigma) at 600 µM final concentration was added to the cell culture. The lipid solution was prepared by adding one equivalent of NaOH, heating at 65 °C and adjusting the final pH to 8. The expression for myristoylated constructs was performed at 28°C for 5h and 1h after the induction had started 6g per culture L of glucose were added. Cells were harvested at 4000 rpm for 20 min and resuspended in lysis buffer (50 mM KH_2PO_4 /K_2HPO_4, 600 mM NaCl, 10 mM Imidazole, pH 7.5) supplemented with 1% v/v Triton X100, Protein Inhibitor Cocktail (Sigma) and 1 mM PMSF (Sigma), 25µg/mL lysozyme (Sigma) and 5µg/mL DNAse I (Roche). Cells were sonicated on ice and centrifuged at

25000 rpm for 45 min. Ni-NTA affinity chromatography was performed using a 1mL Ni-NTA cartridge (GE Healthcare). The protein was eluted with buffer containing 50 mM KH_2PO_4 /K_2HPO_4, 600 mM NaCl, 400 mM imidazole at pH 7.5 (plus 0.018 % Triton X100 (Sigma) for myristoylated constructs). The final purification step consisted of a size exclusion chromatography in a Superdex 75 26/60 (GE Healthcare), in phosphate buffer (NaH_2PO_4 /Na_2HPO_4, 150 mM NaCl, 0.2 mM EDTA, pH 7.5). For the NMR experiments buffer was exchanged to 50 mM Na_2HPO_4 200 mM, Na_2SO_4, 10 mM DTT, pH 6.4 using a size exclusion P10 column (GE Healthcare). The protein was concentrated either using Vivaspin of 5 or 10 kDa MWCO concentrators (Sigma Aldrich). For USH3SH2 c-Src constructs all the buffers contained at least 2 mM DTT.

The c-Src SH3 domain construct was expressed as a GST-fusion construct with a TEV cleavage site. In this case, after the Ni-NTA affinity chromatography, a PD-10 column (GE Healthcare) was used to remove the 400mM imidazole of the elution buffer. Then 1mM DTT, 0.5mM EDTA and 1:100 His-tagged TEV protease were added. TEV cleavage was left overnight at 4 °C rocking gently. The reaction product was then centrifuged for 10min at 3500 g. A "reverse" Ni-NTA affinity chromatography was performed, the collected flow-through contained the protein of interest, whereas the His$_6$-tagged GST and TEV were trapped onto the columns and subsequently discarded.

The VSL12 (Ac-VSLARRPLPPLP-OH) was synthesized by SynPeptide Co., Ltd (Shangai, China).

4.5.3. NMR Sample preparation

Samples were [15]N ^{13}C enriched for the backbone assignment of USH3SH2 or when 3D HNCO experiments were used otherwise samples were only[15]N labeled. The samples contained 0.25 – 0.48 mM protein concentration in buffer 50 mM Na_2HPO_4, 200 mM Na_2SO_4, 10 mM DTT, pH 6.4 plus 10 % of D_2O. The final samples volumes ranged from 250 – 300 μL. 5 mm Shigemi tubes (BMS-005-1T) were used.

For the 1:1 titration with VSL12 peptide, the sample was recovered from the Shigemi tube, the peptide was added from a concentrated stock solution in water that allowed to add volumes <1.5 μL and therefore not significantly altering the ionic strength.

4.5.4. NMR experiments for backbone assignment

For the backbone assignment of SH4-U domains of USH3SH2, 2D ^{1}H-^{15}N HSQC and the 3D HNCACB, CBCAcoNH, HNCO and HNcaCO experiments were acquired at 278K in a Bruker 850MHz equipped with CPTCI 1H/19F-13C/15N/DZ Gradient cryoprobe.

For the assignment of the SH3-SH2 domains of USH3SH2, the initial experiments including the TROSY scheme for HNCA and HNcoCA were acquired at 298K in a Bruker 950MHz equipped with 5mm CPTCI 1H-13C/15N/DZ Gradient cryoprobe. The subsequent experiments that contemplated BEST-TROSY and NUS schemes for the 3D experiments:

HNCO, HNCA and HNcoCA were acquired at 298K in Bruker 800 MHz Avance spectrometer equipped with a TCI CryoProbe. The 2D BEST-TROSY HSQC for USH3SH2 was also acquired at 298K in the latter spectrometer.

4.5.5. NMR experiments for CSP analysis

For the CSP analysis, 2D BEST-TROSY HSQC experiments were acquired for all the constructs used in this work in presence and absence of PxxP (VSL12) ligand, at 278K (for the IDR) and 298K (for SH3-SH2 domains) in a Bruker 600 MHz Avance III spectrometer equipped with a TCI CryoProbe.

4.5.6. NMR experiments for IP analysis

For the IP analysis of the SH4-U domains of USH3 and USH3SH2 in presence and absence of PxxP (VSL12) ligand, 3D BEST-TROSY HNCO experiments with NUS scheme were acquired at 278K in a Bruker 600 MHz Avance III spectrometer equipped with a TCI CryoProbe.

4.5.7. NMR Data processing and analysis

The USH3SH2 assignment experiments at 278K and 298K were processed using NMRPipe (Delaglio et al., 1995). The experiments that involved NUS schemes were processed using qMDD (Orekhov and Jaravine, 2011) and NMRPipe. The 2D ^{1}H ^{15}N HSQC spectra of all the samples used, were processed using Topspin 4.0.3.

The backbone assignment spectra and the subsequent sequential assignment of the USH3SH2 residues resonances were performed using CCPN Analysis 2.4 (Skinner et al. 2016).

For the CSP analysis, the spectra were analyzed using CCPN Analysis 2.4 and the resulting peaklists were exported to Farseer-NMR (Teixeira et al., 2018) for the CSP calculation, according to Chapter 2 equation 2.1. The statistical significant threshold line is defined as the mean CSP for the lowest decile (μ(lowest decile CSP)) plus five standard deviations (5σ). CSP were mapped over the SH3-SH2 domain crystal structures using UCSF Chimera (Pettersen et al., 2004).

For the IP analysis, the spectra were analyzed using CCPN Analysis 2.4. The relative peak intensities of the residues were calculated against the average peak intensity of all residues of the same spectra using the *equation 4.2*:

Equation 4.2. $$\text{Relative I}_{\text{residue i}} = \frac{\text{I}_{\text{residue i}}}{\text{I}_{\text{average}}}$$

To compare between samples, normalization (range 0-1) of the relative peak intensities of each sample was performed using the MinMaxScaler function from the Python scientific library Scikit-learn (Pedregosa et al., 2012).

PART (III) Conclusions

Chapter 5

The long read

5.1. Concluding remarks

Potential therapeutic targets in human cancers are of primordial importance for the scientific community. c-Src implication in cancer was discovered almost a century ago. c-Src oncogenic potential is rarely associated to mutations but results from deregulation of the multiple cellular signalling pathways in which c-Src intervenes.

The disclosure of c-Src structural architecture and subsequent regulatory function focused on the folded domains cassette SH3-SH2-SH1[Kinase], while the N-terminal domains myrSH4-Unique were assumed just to have a membrane-connecting function. Notwithstanding, close related tyrosine kinases (Src Family of tyrosine kinases (SFKs)) with a conserved domain architecture (SH3-SH2-SH1[Kinase]) exert significant diverse cellular functions, suggesting the presence of another layer of regulation to fine tune the modulation of the conserved SH3-SH2-SH1[Kinase] ensemble. The N-terminal domains (myrSH4-Unique) present high divergence among the SFKs. Besides the different degree of acylation at the N-terminus SH4 domain (myristoylation plus various palmitoylations), the Unique domain sequence is poorly conserved between the SFKs members. The paradigm shift that entailed the emergence of Intrinsically Disordered Proteins marked a turning point in the c-Src history.

Our group had experimentally demonstrated that c-Src N-terminal region (SH4-Unique) was an intrinsically disordered region (IDR) (Pérez et al., 2009) and subsequent studies, described a novel functional role for the N-terminal region comprising the intrinsically disordered SH4-Unique domains and the adjacent globular SH3 domain. This region has been named the c-Src N-terminal Regulatory Element (SNRE) (Maffei et al., 2015, Arbesú et al., 2017).

The (non-myristoylated) SNRE was shown to form an interdomain fuzzy complex, where the IDR (SH4-U domains) maintains multiple weak contacts with the SH3 domain (Arbesú et al., 2017). In *Chapter 2*, it is shown that the myristoyl group could have an additional role beyond membrane binding. The results reveal that the presence of the myristoyl moiety enhances the fuzzy complex formation by increasing the IDR concentration around the SH3 domain by adding cooperative transient interactions. As a consequence, multiple binding "pockets" in the SH3 domain harbor the myristoyl group when the protein is not bound to the membranes. The Unique Lipid Binding Region (ULBR) found in the Unique domain (Perez et al. 2013), exerts key roles in framing the myristoyl group interactions within the fuzzy interdomain complex. Mutation of the ULBR has been shown to reduce the oncogenic phenotype of colon rectal cancer cells (Arbesú et al., 2017, Aponte et al., 2021).

Various *in vitro* c-Src studies (Bernardó et al., 2008, Patwardhan and Resh 2010, Spassov et al., 2018, Boczek et al., 2019) suggest that complete kinase regulation is not achieved without the IDR and in particular the myristoyl moiety. The results in *Chapter 4* have shown that in the presence of the SH2 domain, the fuzzy IDR:SH3 complex interactions also contemplate the SH3|2 interdomain region. A possible modulation of the SH3|2 interface by the IDR with a probable specific role of the ULBR, is suggested. We hypothesize that the IDR:SH3 fuzzy complex modulates the kinase domain with long-range

effects conveyed through the SH3|2 interface. Further investigation of the fuzzy complex in a full-length c-Src construct, will open up a new avenue for the design of drugs modulating Src activity, potentially more specific than those based on direct tyrosine kinase inhibition, since targeting the IDR:SH3 fuzzy complex could indirectly affect the kinase activity, but directly targets a region with low homology to other kinases and is implicated in cell-specific responses.

On the other hand, we have determined (in *Chapter 3*) that the myristoylated SNRE dimerization upon membrane binding depends on its lysine cluster (^{5}KxKxK^9) located at the N-terminal part of the SH4 domain. The myristoylated N-terminal region of c-Src SH4 domain (residue 2-9) is enough to allow oligomerization (Dwivedi et al. 2017). Based on (i) perturbations observed upon modifying alternate residues in the SH4 domain and (ii) similarities with other peptides with alternating lysine and not charged residues ($(KX)_4K$) that are known to form β-sheet like structures upon binding to anionic lipid bilayers (Hädicke et al. 2017, Sinthuvanich et al. 2012), we hypothesize that the SH4 domains in the c-Src self-associated specie adopt a similar β-sheet like conformation. Interestingly, one of the mentioned peptides is the engineered cationic peptide SVS-1 (KVKVKVKV^{D}P^{L}PTKVKVKVK-NH$_2$) (Sinthuvanich et al. 2012) that has been shown to have anticancer activity. SVS-1 in solution presents a random coil conformation but folds into a β-hairpin structure on the negatively charged membrane surface. The biological significance of the c-Src membrane self-association has not been established yet. Thus, whether this SNRE feature is involved in the regulatory pathways of cancer cells remains to be investigated.

5.2. Conclusions

- In the membrane-free form of c-Src, the myristoyl moiety is harbored in its N-terminal fuzzy interdomain complex through multiple binding sites in the SH3 domain.

- The interaction of the myristoylated SH4 domain with the SH3 domain cooperatively favors the intramolecular interactions involving the entire intrinsically disordered region. This effect can be viewed as an increase of the local concentration around the SH3 domain of the residues that participate in the N-terminal fuzzy intramolecular interactions.

- The Unique Lipid Binding Region (in the Unique domain) and the myristoyl moiety have been proved to be key elements to maintain the conformational ensemble that defines the N-terminal fuzzy complex.

- The fuzzy interdomain IDR:SH3 complex is preserved in the c-Src membrane-bound form and consequently, the SH3 domain remains close to the membrane surface.

- The additional lipid binding regions found in the SNRE (ULBR, RT & nSrc loops of the SH3 domain) do not contribute to enhancing the c-Src membrane anchoring.

- A lysine motif (K-motif) with alternate lysine residues (positions 5, 7 and 9) in the myristoylated SH4 domain enables c-Src self-association upon membrane binding.

- It has been proposed that self-association of c-Src myristoylated SH4 domain occurs through an allosteric modulation of the K-motif ($^5KxKxK^9$) mediated by lipids.

- The c-Src N-terminal fuzzy interdomain complex also involves the interface region connecting the SH3 and SH2 domains.

Appendix

Figure A1. SPR responses (blue curves) after 60 s association of the myristoylated c-Src variants to DOPC LUVs. Best fit with the 1:1 Langmuir model (black curves) analyzed using the Biacore T200 3.0 Evaluation. The residuals plot shows the accuracy of the fit. Result plots are one representative experiment of the triplicate data.

Figure A2. SPR responses (blue curves) after 60 s association of the myristoylated c-Src variants to DOPC:DOPG (3:1) LUVs. Best fit with the 1:1 Langmuir model (black curves) analyzed using the Biacore T200 3.0 Evaluation. The residuals plot shows the accuracy of the fit. Result plots are one representative experiment of the triplicate data.
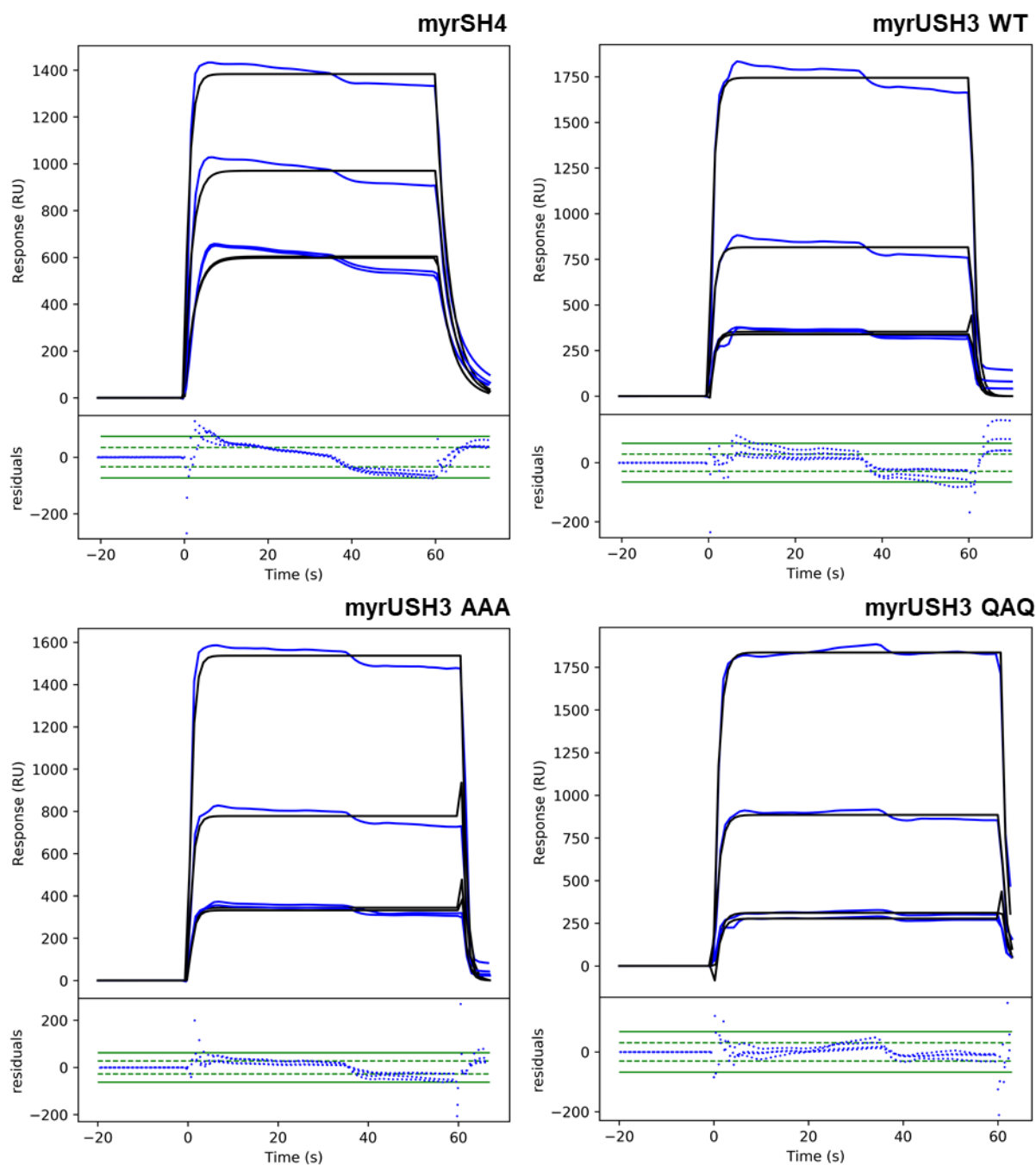
Figure A3. SPR responses (blue curves) after 60s association of the myristoylated c-Src variants to DOPC:DOPG (2:1) LUVs. Best fit with the 1:1 Langmuir model (black curves) analyzed using the Biacore T200 3.0 Evaluation. The residuals plot shows the accuracy of the fit. Result plots are one representative experiment of the triplicate data.
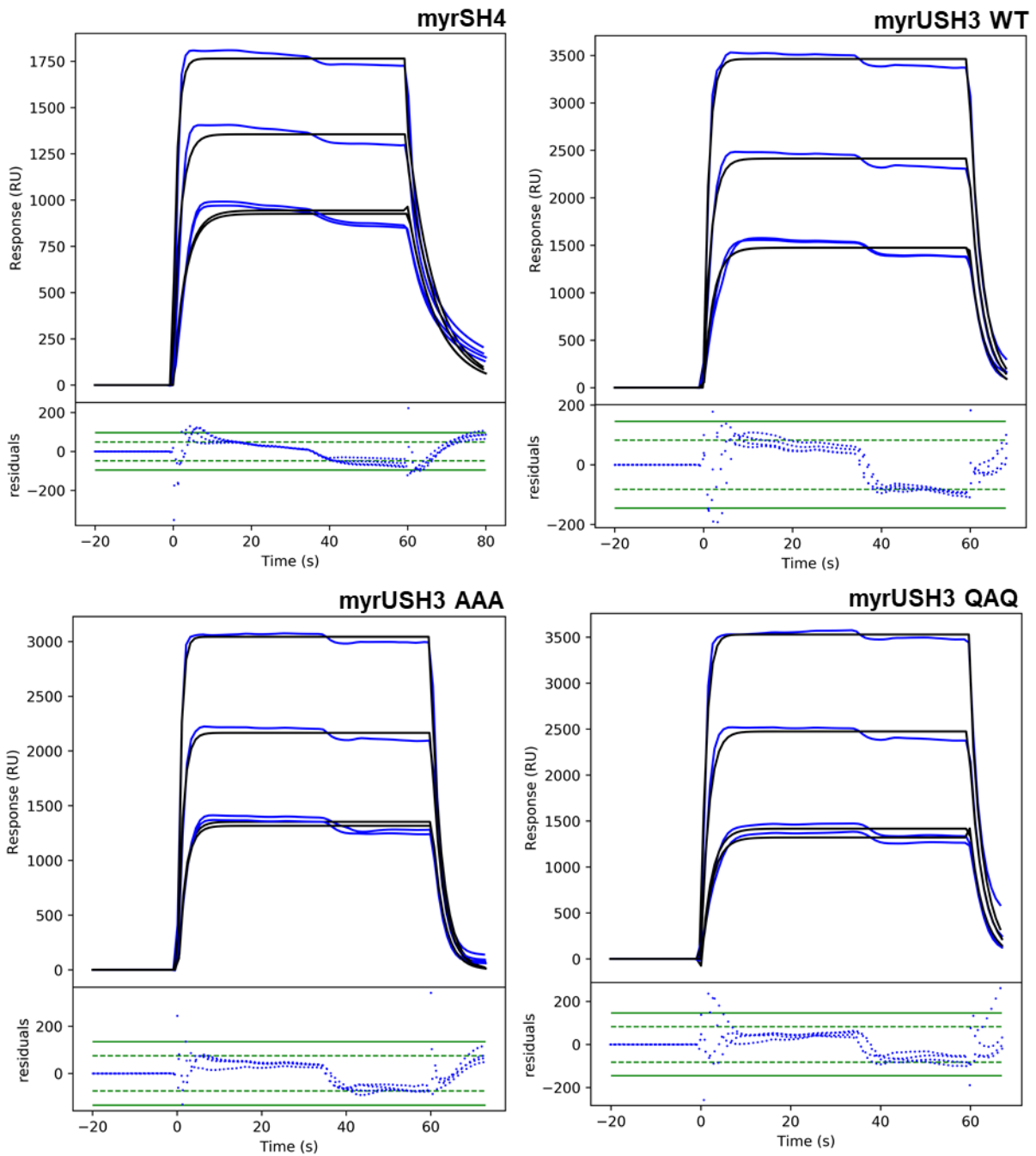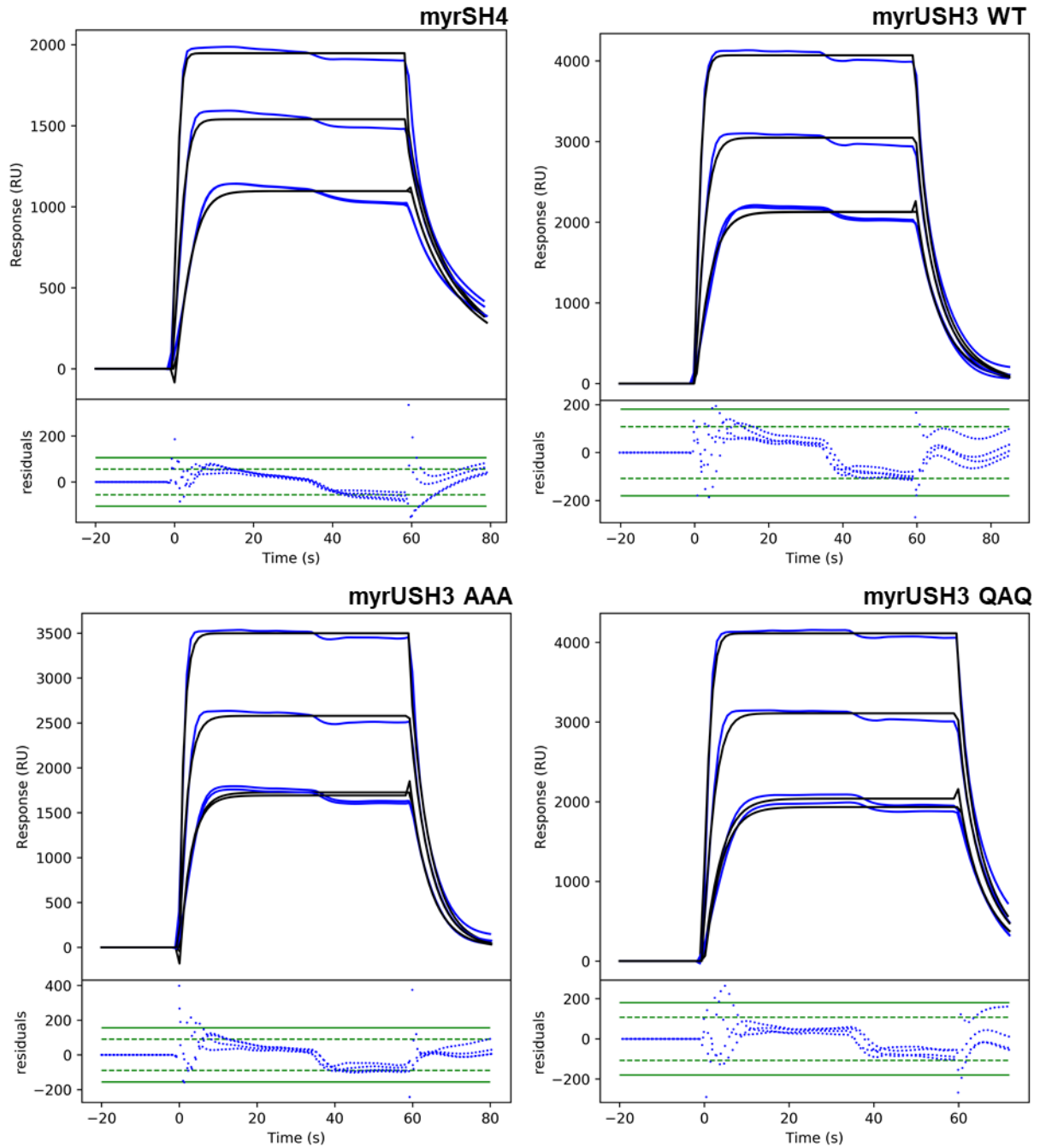
References

Adhyapak, P., and Kapoor, S. (2019). Membrane Dynamics in Health and Disease: Impact on Cellular Signalling. J. Membr. Biol. *252*, 213–226.

Ahler, E., Register, A.C., Chakraborty, S., Fang, L., Dieter, E.M., Sitko, K.A., Vidadala, R.S.R., Trevillian, B.M., Golkowski, M., Gelman, H., et al. (2019). A Combined Approach Reveals a Regulatory Mechanism Coupling Src's Kinase Activity, Localization, and Phosphotransferase-Independent Functions. Mol. Cell *74*, 393-408.e20.

Amata, I., Maffei, M., and Pons, M. (2014). Phosphorylation of unique domains of Src family kinases. Front. Genet. *5*, 1–6.

Ames, J.B., Ishima, R., and Tanaka, T. (1997). Molecular mechanics of calcium – myristoyl switches. *389*.

Andresen, B.T., Rizzo, M.A., Shome, K., and Romero, G. (2002). The role of phosphatidic acid in the regulation of the Ras/MEK/Erk signaling cascade. FEBS Lett. *531*, 65–68.

Aponte, E., Lafitte, M., Sirvent, A., and Simon, V. (2021). Regulation of Src tumor activity by its N-terminal intrinsically disordered region. bioRxiv 2021.05.10.443360; doi: https://doi.org/10.

Arbesú, M., and Pons, M. (2019). Integrating disorder in globular multidomain proteins: Fuzzy sensors and the role of SH3 domains. Arch. Biochem. Biophys. *677*, 108161.

Arbesú, M., Maffei, M., Cordeiro, T.N., Teixeira, J.M.C., Pérez, Y., Bernadó, P., Roche, S., and Pons, M. (2017). The Unique Domain Forms a Fuzzy Intramolecular Complex in Src Family Kinases. Structure 1–11.

Arold, S., Franken, P., Strub, M.-P., Hoh, F., Benichou, S., Benarous, R., and Dumas, C. (1997). The crystal structure of HIV-1 Nef protein bound to the Fyn kinase SH3 domain suggests a role for this complex in altered T cell receptor signaling. Structure *5*, 1361–1372.

Arold, S., O'Brien, R., Franken, P., Strub, M.P., Hoh, F., Dumas, C., and Ladbury, J.E. (1998). RT loop flexibility enhances the specificity of Src family SH3 domains for HIV-1 Nef. Biochemistry *37*, 14683–14691.

Bagrodia, S., Taylor, S.J., and Shalloway, D. (1993). Myristylation is required for Tyr-527 dephosphorylation and activation of pp60c-src in mitosis. Mol. Cell. Biol. *13*, 1464–1470.

Bakhtiar, R. (2013). Surface plasmon resonance spectroscopy: A versatile technique in a biochemist's toolbox. J. Chem. Educ. *90*, 203–209.

Bernadó, P., Pérez, Y., Svergun, D.I., and Pons, M. (2008). Structural Characterization of the Active and Inactive States of Src Kinase in Solution by Small-Angle X-ray Scattering. J. Mol. Biol. *376*, 492–505.

Bjorge, J.D., Jakymiw, A., and Fujita, D.J. (2000). Selected glimpses into the activation

and function of Src kinase. Oncogene *19*, 5620–5635.

Boczek, E.E., Luo, Q., Dehling, M., Röpke, M., Mader, S.L., Seidl, A., Kaila, V.R.I., and Buchner, J. (2019). Autophosphorylation activates c-Src kinase through global structural rearrangements. J. Biol. Chem. *294*, 13186–13197.

Boutin, J.A. (1997). Myristoylation. Cell. Signal. *9*, 15–35.

Broome, M.A., and Hunter, T. (1997). The PDGF receptor phosphorylates Tyr 138 in the c-Src SH3 domain in vivo reducing peptide ligand binding. Oncogene *14*, 17–34.

Brown, M.T., and Cooper, J.A. (1996). Regulation, substrates and functions of src. Biochim. Biophys. Acta - Rev. Cancer *1287*, 121–149.

Busch, D.J., Houser, J.R., Hayden, C.C., Sherman, M.B., Lafer, E.M., and Stachowiak, J.C. (2015). Intrinsically disordered proteins drive membrane curvature. Nat. Commun. *6*, 1–11.

Buser, C. a, Sigal, C.T., Resh, M.D., and McLaughlin, S. (1994). Membrane binding of myristylated peptides corresponding to the NH2 terminus of Src. Biochemistry *33*, 13093–13101.

Buss, J.E., Kamps, M.P., Gould, K., and Sefton, B.M. (1986). The absence of myristic acid decreases membrane binding of p60src but does not affect tyrosine protein kinase activity. J. Virol. *58*, 468–474.

Carvajal, F.J., Mattison, H.A., and Cerpa, W. (2016). Role of NMDA Receptor-Mediated Glutamatergic Signaling in Chronic and Acute Neuropathologies. Neural Plast. *2016*.

Chung, J.K., Nocka, L.M., Decker, A., Wang, Q., Kadlecek, T.A., Weiss, A., Kuriyan, J., and Groves, J.T. (2019). Switch-like activation of Bruton's tyrosine kinase by membrane-mediated dimerization. Proc. Natl. Acad. Sci. U. S. A. *166*, 10798–10803.

Cohen, P. (2002). The origins of protein phosphorylation. Nat. Cell Biol. *4*.

Constantine, R., Zhang, H., Gerstner, C.D., Frederick, J.M., and Baehr, W. (2012). Uncoordinated (UNC)119: Coordinating the trafficking of myristoylated proteins. Vision Res. *75*, 26–32.

Cooper, J.A., and Howell, B. (1993). The when and how of Src regulation. Cell *73*, 1051–1054.

Courtneidge, S.A., Levinson, A.D., and Bishop, J.M. (1980). The protein encoded by the transforming gene of avian sarcoma virus (pp60(src)) and a homologous protein in normal cells (pp60(proto-src)) are associated with the plasma membrane. Proc. Natl. Acad. Sci. U. S. A. *77*, 3783–3787.

Cowan-Jacob, S.W., Fendrich, G., Manley, P.W., Jahnke, W., Fabbro, D., Liebetanz, J., and Meyer, T. (2005). The crystal structure of a c-Src complex in an active conformation suggests possible steps in c-Src activation. Structure *13*, 861–871.

Delaglio, F., Grzesiek, S., Vuister, G.W., Zhu, G., Pfeifer, J., and Bax, A. (1995).

NMRPipe: A multidimensional spectral processing system based on UNIX pipes. J. Biomol. NMR *6*, 277–293.

Dionne, U., Chartier, F.J.M., López de los Santos, Y., Lavoie, N., Bernard, D.N., Banerjee, S.L., Otis, F., Jacquet, K., Tremblay, M.G., Jain, M., et al. (2018). Direct Phosphorylation of SRC Homology 3 Domains by Tyrosine Kinase Receptors Disassembles Ligand-Induced Signaling Networks. Mol. Cell *70*, 995-1007.e11.

Donepudi, M., and Resh, M.D. (2008). c-Src trafficking and co-localization with the EGF receptor promotes EGF ligand-independent EGF receptor activation and signaling. Cell. Signal. *20*, 1359–1367.

Dubois, F., Leroy, C., Simon, V., Benistant, C., and Roche, S. (2015). YES oncogenic activity is specified by its SH4 domain and regulates RAS/MAPK signaling in colon carcinoma cells. Am. J. Cancer Res. *5*, 1972–1987.

Dustin, C., M., R., Heppner, D.E., Lin, M.C.J., and van der Vliet, A. (2019). Redox regulation of tyrosine kinase signalling: more than meets the eye. J. Biochem. *167*, 151–163.

Dwivedi, M., Mejuch, T., Waldmann, H., and Winter, R. (2017). Lateral Organization of Host Heterogeneous Raft-like Membranes Altered by the Myristoyl Modification of Tyrosine Kinase c-Src. Angew. Chemie - Int. Ed. *56*, 10511–10515.

Erwin, N., Dwivedi, M., Mejuch, T., Waldmann, H., and Winter, R. (2018). Unc119a decreases the membrane binding of myristoylated c-src. ChemBioChem *19*, 1482–1487.

Fajer, M., Meng, Y., and Roux, B. (2017). The Activation of c-Src Tyrosine Kinase: Conformational Transition Pathway and Free Energy Landscape. J. Phys. Chem. B *121*, 3352–3363.

Filippakopoulos, P., Müller, S., and Knapp, S. (2009). SH2 domains: modulators of nonreceptor tyrosine kinase activity. Curr. Opin. Struct. Biol. *19*, 643–649.

Flamm, A.G., Le Roux, A.L., Mateos, B., Díaz-Lobo, M., Storch, B., Breuker, K., Konrat, R., Pons, M., and Coudevylle, N. (2016). N-Lauroylation during the Expression of Recombinant N-Myristoylated Proteins: Implications and Solutions. ChemBioChem *17*, 82–89.

Gaffarogullari, E.C., Masterson, L.R., Metcalfe, E.E., Traaseth, N.J., Balatri, E., Musa, M.M., Mullen, D., Distefano, M.D., and Veglia, G. (2011). A myristoyl/phosphoserine switch controls cAMP-dependent protein kinase association to membranes. J. Mol. Biol. *411*, 823–836.

Gahbauer, S., and Böckmann, R.A. (2016). Membrane-mediated oligomerization of G protein coupled receptors and its implications for GPCR function. Front. Physiol. *7*, 1–17.

Gao, X., and Zhang, J. (2008). Spatiotemporal Analysis of Differential Akt Regulation in Plasma Membrane Microdomains. Mol. Biol. Cell *19*, 4366–4373.

García-Martínez, J.M., Calcabrini, A., González, L., Martín-Forero, E., Agulló-Ortuño,

M.T., Simon, V., Watkin, H., Anderson, S.M., Roche, S., and Martín-Pérez, J. (2010). A non-catalytic function of the Src family tyrosine kinases controls prolactin-induced Jak2 signaling. Cell. Signal. *22*, 415–426.

Giannoni, E., Buricchi, F., Raugei, G., Ramponi, G., and Chiarugi, P. (2005). Intracellular Reactive Oxygen Species Activate Src Tyrosine Kinase during Cell Adhesion and Anchorage-Dependent Cell Growth. Mol. Cell. Biol. *25*, 6391–6403.

Gibson, D.G., Young, L., Chuang, R.Y., Venter, J.C., Hutchison, C.A., and Smith, H.O. (2009). Enzymatic assembly of DNA molecules up to several hundred kilobases. Nat. Methods *6*, 343–345.

Gingrich, J.R., Pelkey, K.A., Fam, S.R., Huang, Y., Petralia, R.S., Wenthold, R.J., and Salter, M.W. (2004). Unique domain anchoring of Src to synaptic NMDA receptors via the mitochondrial protein NADH dehydrogenase subunit 2. Proc. Natl. Acad. Sci. U. S. A. *101*, 6237–6242.

Gizachew, D., and Oswald, R. (2006). NMR structural studies of the myristoylated N-terminus of ADP ribosylation factor 6 (Arf6). FEBS Lett. *580*, 4296–4301.

Gonfloni, S., Weijland, A., Kretzschmar, J., and Superti-Furga, G. (2000). Crosstalk between the catalytic and regulatory domains allows bidirectional regulation of Src. Nat. Struct. Biol. *7*, 281–286.

Hädicke, A., and Blume, A. (2017). Binding of cationic model peptides (KX) 4 K to anionic lipid bilayers: Lipid headgroup size influences secondary structure of bound peptides. Biochim. Biophys. Acta - Biomembr. *1859*, 415–424.

Hansen, K., Johnell, M., Siegbahn, A., Rorsman, C., Engström, U., Wernstedt, C., Heldin, C.H., and Rönnstrand, L. (1996). Mutation of a Src phosphorylation site in the PDGF beta-receptor leads to increased PDGF-stimulated chemotaxis but decreased mitogenesis. EMBO J. *15*, 5299–5313.

Hantschel, O., Nagar, B., Guettler, S., Kretzschmar, J., Dorey, K., Kuriyan, J., and Superti-Furga, G. (2003). A myristoyl/phosphotyrosine switch regulates c-Abl. Cell *112*, 845–857.

Harrison, S.C. (2003). Variation on an Src-like theme. Cell *112*, 737–740.

Heppner, D.E., Dustin, C.M., Liao, C., Hristova, M., Veith, C., Little, A.C., Ahlers, B.A., White, S.L., Deng, B., Lam, Y.W., et al. (2018). Direct cysteine sulfenylation drives activation of the Src kinase. Nat. Commun. *9*, 1–11.

Homola, J., Yee, S.S., and Gauglitz, G. (1999). Surface plasmon resonance sensors: review. Sensors Actuators, B Chem. *54*, 3–15.

Hossain, M.I., Roulston, C.L., Kamaruddin, M.A., Chu, P.W.Y., Ng, D.C.H., Dusting, G.J., Bjorge, J.D., Williamson, N.A., Fujita, D.J., Cheung, S.N., et al. (2013). A truncated fragment of Src protein kinase generated by calpain-mediated cleavage is a mediator of neuronal death in excitotoxicity. J. Biol. Chem. *288*, 9696–9709.

Houser, J.R., Busch, D.J., Bell, D.R., Li, B., Ren, P., and Stachowiak, J.C. (2016). The

impact of physiological crowding on the diffusivity of membrane bound proteins. Soft Matter *12*, 2127–2134.

Huang, C., Zhang, Z., Chen, L., Lee, H.W., Ayrapetov, M.K., Zhao, T.C., Hao, Y., Gao, J., Yang, C., Mehta, G.U., et al. (2018). Acetylation within the N- and C-terminal domains of src regulates distinct roles of STAT3-mediated tumorigenesis. Cancer Res. *78*, 2825–2838.

Hubbard, S.R., and Till, J.H. (2000). Protein tyrosine kinase structure and function. Annu. Rev. Biochem. *69*, 373–398.

Huebner, R.J., and Todaro, G.J. (1969). Oncogenes of DNA Tumor Viruses as Determinants Of Cancer. Proc. Natl. Acad. Sci. U. S. A. *64*, 1087–1094.

Hunter, T., and Sefton, B.M. (1980). Transforming Gene Product of Rous Sarcoma Virus Phosphorylates Tyrosine. J. Biol. Chem. *77*, 1311–1315.

Huse, M., and Kuriyan, J. (2002). The conformational plasticity of protein kinases. Cell *109*, 275–282.

Irby, R., and Yeatman, T. (2000). Role of Src expression and activation in human cancer. Oncogene *19*, 5636–5642.

Irtegun, S., Wood, R.J., Ormsby, A.R., Mulhern, T.D., and Hatters, D.M. (2013). Tyrosine 416 Is Phosphorylated in the Closed , Repressed Conformation of c-Src. *8*.

Jarsch, I.K., Daste, F., and Gallop, J.L. (2016). Membrane curvature in cell biology: An integration of molecular mechanisms. J. Cell Biol. *214*, 375–387.

Kamps, M.P., Buss, J.E., and Sefton, B.M. (1985). Mutation of NH2-terminal glycine of p60(src) prevents both myristoylation and morphological transformation. Proc. Natl. Acad. Sci. U. S. A. *82*, 4625–4628.

Kato, J.Y., Takeya, T., Grandori, C., Iba, H., Levy, J.B., and Hanafusa, H. (1986). Amino acid substitutions sufficient to convert the nontransforming p60c-src protein to a transforming protein. Mol. Cell. Biol. *6*, 4155–4160.

Kazimierczuk, K., and Orekhov, V. (2015). Non-uniform sampling: Post-Fourier era of NMR data collection and processing. Magn. Reson. Chem. *53*, 921–926.

Kemble, D.J., and Sun, G. (2009). Direct and specific inactivation of protein tyrosine kinases in the Src and FGFR families by reversible cysteine oxidation. Proc. Natl. Acad. Sci. U. S. A. *106*, 5070–5075.

Kennedy, M.T., Brockman, H., and Rusnak, F. (1996). Contributions of Myristoylation to Calcineurin Structure / Function. *271*, 26517–26521.

Kim, J., Mosior, M., Chung, L.A., Wu, H., and McLaughlin, S. (1991). Binding of peptides with basic residues to membranes containing acidic phospholipids. Biophys. J. *60*, 135–148.

Kim, J., Shishidob, T., Jiangb, X., Aderemb, A., and Mclaughlinsn, S. (1994).

Phosphorylation, High Ionic Strength, and Calmodulin Reverse the Binding of MARCKS to Phospholipid Vesicles. *269*, 28214–28219.

Kim, Y., Ho, S.O., Gassman, N.R., Korlann, Y., Landorf, E. V., Collart, F.R., and Weiss, S. (2008). Efficient site-specific labeling of proteins via cysteines. Bioconjug. Chem. *19*, 786–791.

Konitsiotis, A.D., Roßmannek, L., Stanoev, A., Schmick, M., and Bastiaens, P.I.H. (2017). Spatial cycles mediated by UNC119 solubilisation maintain Src family kinases plasma membrane localisation. Nat. Commun. *8*, 1–16.

Kooijman, E.E., Tieleman, D.P., Testerink, C., Munnik, T., Rijkers, D.T.S., Burger, K.N.J., and De Kruijff, B. (2007). An electrostatic/hydrogen bond switch as the basis for the specific interaction of phosphatidic acid with proteins. J. Biol. Chem. *282*, 11356–11364.

Krueger, J.G., Wang, E., and Goldberg, A.R. (1980). Evidence that the src gene product of rous sarcoma virus is membrane associated. Virology *101*, 25–40.

de Kruijff, B., Rietveld, A., Telders, N., and Vaandrager, B. (1985). Molecular aspects of the bilayer stabilization induced by poly(l-lysines) of varying size in cardiolipin liposomes. BBA - Biomembr. *820*, 295–304.

Kuhlman, B., and Baker, D. (2004). Exploring folding free energy landscapes using computational protein design. Curr. Opin. Struct. Biol. *14*, 89–95.

Kwong, J., and Lublin, D.M. (1995). Amino-Terminal Palmitate or Polybasic Domain Can Provide Required Second Signal to Myristate for Membrane Binding of P56lck. Biochem. Biophys. Res. Commun. *207*, 868–876.

Van der Lee, R., Buljan, M., Lang, B., Weatheritt, R.J., Daughdrill, G.W., Dunker, A.K., Fuxreiter, M., Gough, J., Gsponer, J., Jones, D.T., et al. (2014). Classification of intrinsically disordered regions and proteins. Chem. Rev. *114*, 6589–6631.

Levinson, A.D., Courtneidge, S.A., and Bishop, J.M. (1981). Structural and functional domains of the Rous sarcoma virus transforming protein (pp60(src)). Proc. Natl. Acad. Sci. U. S. A. *78*, 1624–1628.

Li, L., Vorobyov, I., and Allen, T.W. (2013). The different interactions of lysine and arginine side chains with lipid membranes. J. Phys. Chem. B *117*, 11906–11920.

Liang, X., Lu, Y., Wilkes, M., Neubert, T.A., and Resh, M.D. (2004). The N-terminal SH4 Region of the Src Family Kinase Fyn Is Modified by Methylation and Heterogeneous Fatty Acylation. *279*, 8133–8139.

Maffei, M., Arbesú, M., Le Roux, A.L., Amata, I., Roche, S., and Pons, M. (2015). The SH3 Domain Acts as a Scaffold for the N-Terminal Intrinsically Disordered Regions of c-Src. Structure 893–902.

Malakauskas, S.M., and Mayo, S.L. (1998). Design, structure and stability of a Hyperthermophilic Protein Variant. Trends Biotechnol. *5*, 1–6.

Manning, G., Whyte, D.B., Martinez, R., Hunter, T., and Sudarsanam, S. (2002). The

protein kinase complement of the human genome. Science (80-.). *298*, 1912–1934.

Marianayagam, N.J., Sunde, M., and Matthews, J.M. (2004). The power of two: Protein dimerization in biology. Trends Biochem. Sci. *29*, 618–625.

Martin, G.S. (2001). The hunting of the Src. Nat. Rev. Mol. Cell Biol. *2*, 467–475.

Martin, G.S. (2004). The road to Src. Oncogene *23*, 7910–7917.

Martin, D.D.O., Beauchamp, E., and Berthiaume, L.G. (2011). Post-translational myristoylation: Fat matters in cellular life and death. Biochimie *93*, 18–31.

Maurer-Stroh, S., Eisenhaber, B., and Eisenhaber, F. (2002). N-terminal N-myristoylation of proteins: Refinement of the sequence motif and its taxon-specific differences. J. Mol. Biol. *317*, 523–540.

Mayer, B.J., Hamaguchi, M., and Hanafusa, H. (1988). A novel viral oncogene with structural similarity to phospholipase C. Nature *332*, 272–275.

McLaughlin, S., and Aderem, A. (1995). The myristoyl-electrostatic switch: a modulator of reversible protein-membrane interactions. Trends Biochem. Sci. *20*, 272–276.

Meiselbach, H., and Sticht, H. (2011). Effect of the SH3-SH2 domain linker sequence on the structure of Hck kinase. J. Mol. Model. *17*, 1927–1934.

Moran, M.F., Koch, C.A., Anderson, D., Ellis, C., England, L., Martin, G.S., and Pawson, T. (1990). Src homology region 2 domains direct protein-protein interactions in signal transduction. Proc. Natl. Acad. Sci. U. S. A. *87*, 8622–8626.

Müller, P., Schwille, P., and Weidemann, T. (2014). PyCorrFit-generic data evaluation for fluorescence correlation spectroscopy. Bioinformatics *30*, 2532–2533.

Murphy, S.M., Bergman, M., and Morgan, D.O. (1993). Suppression of c-Src activity by C-terminal Src kinase involves the c-Src SH2 and SH3 domains: analysis with Saccharomyces cerevisiae. Mol. Cell. Biol. *13*, 5290–5300.

Murray, D., Hermida-Matsumoto, L., Buser, C.A., Tsang, J., Sigal, C.T., Ben-Tal, N., Honig, B., Resh, M.D., and McLaughlin, S. (1998). Electrostatics and the membrane association of Src: Theory and experiment. Biochemistry *37*, 2145–2159.

Musafia, B., Buchner, V., and Arad, D. (1995). Complex salt bridges in proteins: Statistical analysis of structure and function. J. Mol. Biol. *254*, 761–770.

Nagar, B., Hantschel, O., Young, M.A., Scheffzek, K., Veach, D., Bornmann, W., Clarkson, B., Superti-Furga, G., and Kuriyan, J. (2003). Structural basis for the autoinhibition of c-Abl tyrosine kinase. Cell *112*, 859–871.

Nemeth, S.P., Fox, L.G., DeMarco, M., and Brugge, J.S. (1989). Deletions within the amino-terminal half of the c-src gene product that alter the functional activity of the protein. Mol. Cell. Biol. *9*, 1109–1119.

Obara, Y., Labudda, K., Dillon, T.J., and Stork, P.J.S. (2004). PKA phosphorylation of

Src mediates Rap1 activation in NGF and cAMP signaling in PC12 cells. J. Cell Sci. *117*, 6085–6094.

Okada, M. (2012). Regulation of the Src family kinases by Csk. Int. J. Biol. Sci. *8*, 1385–1397.

Oneyama, C., Hikita, T., Enya, K., Dobenecker, M.W., Saito, K., Nada, S., Tarakhovsky, A., and Okada, M. (2008). The Lipid Raft-Anchored Adaptor Protein Cbp Controls the Oncogenic Potential of c-Src. Mol. Cell *30*, 426–436.

Orekhov, V.Y., and Jaravine, V.A. (2011). Analysis of non-uniformly sampled spectra with multi-dimensional decomposition. Prog. Nucl. Magn. Reson. Spectrosc. *59*, 271–292.

Owen, D.M., Rentero, C., Rossy, J., Magenau, A., Williamson, D., Rodriguez, M., and Gaus, K. (2010). PALM imaging and cluster analysis of protein heterogeneity at the cell surface. J. Biophotonics *3*, 446–454.

Pan, Q., Qiao, F., Gao, C., Norman, B., Optican, L., and Zelenka, P.S. (2011). Cdk5 targets active Src for ubiquitin-dependent degradation by phosphorylating Src(S75). Cell. Mol. Life Sci. *68*, 3425–3436.

Parsons, S.J., and Parsons, J.T. (2004). Src family kinases, key regulators of signal transduction. Oncogene *23*, 7906–7909.

Patwardhan, P., and Resh, M.D. (2010). Myristoylation and membrane binding regulate c-Src stability and kinase activity. Mol Cell Biol *30*, 4094–4107.

Pedregosa, F., Varoquaux, G., Gramfort, A., Michel, V., Thirion, B., Grisel, O., Blondel, M., Müller, A., Nothman, J., Louppe, G., et al. (2012). Scikit-learn: Machine Learning in Python. J. Mach. Learn. Res. *12*, 2825–2830.

Peitzsch, R.M., and McLaughlin, S. (1993). Binding of Acylated Peptides and Fatty Acids to Phospholipid Vesicles: Pertinence to Myristoylated Proteins. Biochemistry *32*, 10436–10443.

Pérez, Y., Gairí, M., Pons, M., and Bernadó, P. (2009). Structural Characterization of the Natively Unfolded N-Terminal Domain of Human c-Src Kinase: Insights into the Role of Phosphorylation of the Unique Domain Supplementari Material. J. Mol. Biol. *391*, 136–148.

Pérez, Y., Maffei, M., Igea, A., Amata, I., Gairí, M., Nebreda, A.R., Bernadó, P., and Pons, M. (2013). Lipid binding by the Unique and SH3 domains of c-Src suggests a new regulatory mechanism. Sci. Rep. *3*, 1295.

Pervushin, K., Riek, R., Wider, G., and Wüthrich, K. (1997). Attenuated T2 relaxation by mutual cancellation of dipole-dipole coupling and chemical shift anisotropy indicates an avenue to NMR structures of very large biological macromolecules in solution. Proc. Natl. Acad. Sci. U. S. A. *94*, 12366–12371.

Pettersen, E.F., Goddard, T.D., Huang, C.C., Couch, G.S., Greenblatt, D.M., Meng, E.C., and Ferrin, T.E. (2004). UCSF Chimera - A visualization system for exploratory research

and analysis. J. Comput. Chem. *25*, 1605–1612.

Pluk, H., Dorey, K., and Superti-Furga, G. (2002). Autoinhibition of c-Abl. Cell *108*, 247–259.

Poincloux, R., Saati, T. Al, Maridonneau-Parini, I., and Le Cabec, V. (2009). The oncogenic activity of the Src family kinase Hck requires the cooperative action of the plasma membrane- and lysosome-associated isoforms. Eur. J. Cancer *45*, 321–327.

Pool, C.T., and Thompson, T.E. (1998). Chain length and temperature dependence of the reversible association of model acylated proteins with lipid bilayers. Biochemistry *37*, 10246–10255.

Rahman, M.A., Senga, T., Ito, S., Hyodo, T., Hasegawa, H., and Hamaguchi, M. (2010). S-nitrosylation at cysteine 498 of c-Src tyrosine kinase regulates nitric oxide-mediated cell invasion. J. Biol. Chem. *285*, 3806–3814.

Ralston, R., and Bishop, J.M. (1985). The Product of the Protooncogene C-Src is Modified during the Cellular Response to Platelet-Derived Growth Factor. *82*, 7845–7849.

Reid, K.A., Davis, C.M., Dyer, R.B., and Kindt, J.T. (2018). Binding, folding and insertion of a β-hairpin peptide at a lipid bilayer surface: Influence of electrostatics and lipid tail packing. Biochim. Biophys. Acta - Biomembr. *1860*, 792–800.

Ren, R., Mayer, B.J., Cicchetti, P., and Baltimoret, D. (1993). Identification of a Ten-Amino Acid Proline-Rich SH3 Binding Site. Science (80-.). *259*, 1157–1161.

Resh, M.D. (1999). Fatty acylation of proteins: New insights into membrane targeting of myristoylated and palmitoylated proteins. Biochim. Biophys. Acta - Mol. Cell Res. *1451*, 1–16.

Resh, M.D. (2006). Trafficking and signaling by fatty-acylated and prenylated proteins. Nat. Chem. Biol. *2*, 584–590.

Resh, M.D. (2013a). Lipid Modification of Proteins: Targeting to Membranes. Encycl. Biol. Chem. Second Ed. *2*, 736–740.

Resh, M.D. (2013b). Covalent lipid modifications of proteins. Curr. Biol. *23*, R431–R435.

Reynolds, A.B., Kanner, S.B., Bouton, A.H., Schaller, M.D., Weed, S.A., Flynn, D.C., and Parsons, J.T. (2014). SRChing for the substrates of Src. Oncogene *33*, 4537–4547.

Rickles, R.J., Botfield, M.C., Zhou, X.M., Henry, P.A., Brugge, J.S., and Zoller, M.J. (1995). Phage display selection of ligand residues important for Src homology 3 domain binding specificity. Proc. Natl. Acad. Sci. *92*, 10909–10913.

Robison, A.D., Sun, S., Poyton, M.F., Johnson, G.A., Pellois, J.P., Jungwirth, P., Vazdar, M., and Cremer, P.S. (2016). Polyarginine Interacts More Strongly and Cooperatively than Polylysine with Phospholipid Bilayers. J. Phys. Chem. B *120*, 9287–9296.

Roskoski, R. (2004). Src protein-tyrosine kinase structure and regulation. Biochem. Biophys. Res. Commun. *324*, 1155–1164.

Roskoski, R. (2005). Src kinase regulation by phosphorylation and dephosphorylation. Biochem. Biophys. Res. Commun. *331*, 1–14.

Rous, P. (1910). A transmissible avian neoplasm. (sarcoma of the common fowl.). J. Exp. Med. *12*, 696–705.

Rous, P. (1911). A Sarcoma of the Fowl Transmissible by an Agent Separable from the Tumor Cells. Am. J. Med. Sci. *142*, 312.

Le Roux, A.-L., Busquets, M.A., Sagués, F., and Pons, M. (2016a). Kinetics characterization of c-Src binding to lipid membranes: Switching from labile to persistent binding. Colloids Surfaces B Biointerfaces *138*, 17–25.

Le Roux, A.-L., Castro, B., Garbacik, E.T., Garcia Parajo, M.F., and Pons, M. (2016b). Single molecule fluorescence reveals dimerization of myristoylated Src N-terminal region on supported lipid bilayers. ChemistrySelect *1*, 642–647.

Sadowski, I., Stone, J.C., and Pawson, T. (1986). A noncatalytic domain conserved among cytoplasmic protein-tyrosine kinases modifies the kinase function and transforming activity of Fujinami sarcoma virus P130gag-fps. Mol. Cell. Biol. *6*, 4396–4408.

Santos, H.G.D., and Siltberg-Liberles, J. (2016). Paralog-Specific Patterns of Structural disorder and phosphorylation in the vertebrate SH3-SH2-Tyrosine kinase protein family. Genome Biol. Evol. *8*, 2806–2825.

Sasaki, H., Arai, H., Cocco, M.J., and White, S.H. (2009). pH dependence of sphingosine aggregation. Biophys. J. *96*, 2727–2733.

Sato, I., Obata, Y., Kasahara, K., Nakayama, Y., Fukumoto, Y., Yamasaki, T., Yokoyama, K.K., Saito, T., and Yamaguchi, N. (2009). Differential trafficking of Src, Lyn, Yes and Fyn is specified by the state of palmitoylation in the SH4 domain. J. Cell Sci. *122*, 965–975.

Sattler, M., and Fesik, S.W. (1996). Use of deuterium labeling in NMR: Overcoming a sizeable problem. Structure *4*, 1245–1249.

Scheidt, H.A., and Huster, D. (2009). Structure and dynamics of the myristoyl lipid modification of Src peptides determined by 2H solid-state NMR spectroscopy. Biophys. J. *96*, 3663–3672.

Schmitt, J.M., and Stork, P.J.S. (2002). PKA phosphorylation of Src mediates cAMP's inhibition of cell growth via Rap1. Mol. Cell *9*, 85–94.

Schug, K.A., and Lindner, W. (2005). Noncovalent Binding between Guanidinium and Anionic Groups: Focus on Biological- and Synthetic-Based Arginine/Guanidinium Interactions with Phosph[on]ate and Sulf[on]ate Residues. Chem. Rev. *105*, 67–114.

Sefton, B.M., Trowbridge, I.S., Cooper, J.A., and Scolnick, E.M. (1982). The transforming proteins of Rous sarcoma virus, Harvey sarcoma virus and Abelson virus contain tightly bound lipid. Cell *31*, 465–474.

Seong, J., Lu, S., Ouyang, M., Huang, H., Zhang, J., Frame, M.C., and Wang, Y. (2009).

Visualization of Src Activity at Different Compartments of the Plasma Membrane by FRET Imaging. Chem. Biol. *16*, 48–57.

Shahinian, S., and Silvius, J.R. (1995). Doubly-Lipid-Modified Protein Sequence Motifs Exhibit Long-Lived Anchorage to Lipid Bilayer Membranes. Biochemistry *34*, 3813–3822.

Shalloway, D., and Taylor, S.J. (1997). Src: more than the sum of its parts. Trend Cell Biol. *7*, 215–217.

Sharma, R., Raduly, Z., Miskei, M., and Fuxreiter, M. (2015). Fuzzy complexes: Specific binding without complete folding. FEBS Lett. *589*, 2533–2542.

Shenoy, S., Choi, J.K., Bagrodia, S., Copeland, T.D., Maller, J.L., and Shalloway, D. (1989). Purified maturation promoting factor phosphorylates pp60c-src at the sites phosphorylated during fibroblast mitosis. Cell *57*, 763–774.

Shenoy, S., Chackalaparampil, I., Bagrodia, S., Lin, P.H., and Shalloway, D. (1992). Role of p34cdc2-mediated phosphorylations in two-step activation of pp60c-src during mitosis. Proc. Natl. Acad. Sci. U. S. A. *89*, 7237–7241.

Sies, H. (2014). Role of metabolic H2O2 generation: Redox signaling and oxidative stress. J. Biol. Chem. *289*, 8735–8741.

Sigal, C.T., Zhou, W., Buser, C. a, McLaughlin, S., and Resh, M.D. (1994). Amino-terminal basic residues of Src mediate membrane binding through electrostatic interaction with acidic phospholipids. Proc. Natl. Acad. Sci. U. S. A. *91*, 12253–12257.

Silverman, L., and Resh, M.D. (1992). Lysine Residues Form an Integral Component of a Novel NH2-terminal Membrane Targeting Motif for Myristylated pp60 v-src. *119*, 415–425.

Silvius, J.R., and l'Heureux, F. (1994). Fluorimetric Evaluation of the Affinities of Isoprenylated Peptides for Lipid Bilayers. Biochemistry *33*, 3014–3022.

Simons, K., and Toomre, D. (2000). Lipid rafts and signal transduction. Nat. Rev. Mol. Cell Biol. *1*, 31–39.

Sinthuvanich, C., Veiga, A.S., Gupta, K., Gaspar, D., Blumenthal, R., and Schneider, J.P. (2012). Anticancer β-hairpin peptides: Membrane-induced folding triggers activityc. J. Am. Chem. Soc. *134*, 6210–6217.

Škerle, J., Humpolíčková, J., Johnson, N., Rampírová, P., Poláchová, E., Fliegl, M., Dohnálek, J., Suchánková, A., Jakubec, D., and Strisovsky, K. (2020). Membrane Protein Dimerization in Cell-Derived Lipid Membranes Measured by FRET with MC Simulations. Biophys. J. *118*, 1861–1875.

Skinner, S.P., Fogh, R.H., Boucher, W., Ragan, T.J., Mureddu, L.G., and Vuister, G.W. (2016). CcpNmr AnalysisAssign: a flexible platform for integrated NMR analysis. J. Biomol. NMR *66*, 111–124.

Smart, J.E., Oppermann, H., Czernilofsky, A.P., Purchio, A.F., Erikson, R.L., and Bishop, J.M. (1981). Characterization of sites for tyrosine phosphorylation in the transforming

protein of Rous sarcoma virus (pp60(v-src) and its normal cellular homologue (pp60(c-src). Proc. Natl. Acad. Sci. U. S. A. *78*, 6013–6017.

Smith, A.W., Huang, H.H., Endres, N.F., Rhodes, C., and Groves, J.T. (2016). Dynamic Organization of Myristoylated Src in the Live Cell Plasma Membrane. J. Phys. Chem. B *120*, 867–876.

Smith, M.T.J., Meissner, J., Esmonde, S., Wong, H.J., and Meiering, E.M. (2010). Energetics and mechanisms of folding and flipping the myristoyl switch in the β-trefoil protein, hisactophilin. Proc. Natl. Acad. Sci. U. S. A. *107*, 20952–20957.

Snyder, M.A., and Michael Bishop, J. (1984). A mutation at the major phosphotyrosine in pp60v-src alters oncogenic potential. Virology *136*, 375–386.

Solyom, Z., Schwarten, M., Geist, L., Konrat, R., Willbold, D., and Brutscher, B. (2013). BEST-TROSY experiments for time-efficient sequential resonance assignment of large disordered proteins. J. Biomol. NMR *55*, 311–321.

Sonnenburg, E.D., and Gordon, J.I. (2013). Protein N-Myristoylation (Elsevier Inc.).

Spassov, D.S., Ruiz-Saenz, A., Piple, A., and Moasser, M.M. (2018). A Dimerization Function in the Intrinsically Disordered N-Terminal Region of Src. Cell Rep. *25*, 449-463.e4.

Stachowiak, J.C., Schmid, E.M., Ryan, C.J., Ann, H.S., Sasaki, D.Y., Sherman, M.B., Geissler, P.L., Fletcher, D.A., and Hayden, C.C. (2012). Membrane bending by protein-protein crowding. Nat. Cell Biol. *14*, 944–949.

Stehelin, D., Varmus, H.E., Bishop, J.M., and Vogt, P.K. (1976a). DNA related to the transforming gene(s) of avian sarcoma viruses is present in normal avian DNA. Nature *260*, 170–173.

Stehelin, D., Guntaka, R. V., Varmus, H.E., and Bishop, J.M. (1976b). Purification of DNA complementary to nucleotide sequences required for neoplastic transformation of fibroblasts by avian sarcoma viruses. J. Mol. Biol. *101*, 349–365.

Stephen, R., Bereta, G., Golczak, M., Palczewski, K., and Sousa, M.C. (2007). Stabilizing Function for Myristoyl Group Revealed by the Crystal Structure of a Neuronal Calcium Sensor, Guanylate Cyclase-Activating Protein 1. Structure *15*, 1392–1402.

Stover, D.R., Liebetanz, J., and Lydon, N.B. (1994). Cdc2-mediated modulation of pp60(c-src) activity. J. Biol. Chem. *269*, 26885–26889.

Stover, D.R., Furet, P., and Lydon, N.B. (1996). Modulation of the SH2 binding specificity and kinase activity of Src by tyrosine phosphorylation within its SH2 domain. J. Biol. Chem. *271*, 12481–12487.

Sun, G., and Kemble, D.J. (2009). To C or not to C: Direct and indirect redox regulation of Src protein tyrosine kinase. Cell Cycle *8*, 2353–2355.

Tanaka, A., and Fujita, D.J. (1986). Expression of a molecularly cloned human c-src oncogene by using a replication-competent retroviral vector. Mol. Cell. Biol. *6*, 3900–3909.

Tanaka, T., Amest, J.B., Harvey, T.S., Stryer, L., and Lkura, M. (1995). Sequestration of the membrane-targeting myristoyl group of recoverin in the calcium-free state. Nature *376*, 444–447.

Tang, C., Loeliger, E., Luncsford, P., Kinde, I., Beckett, D., and Summers, M.F. (2004). Entropic switch regulates myristate exposure in the HIV-1 matrix protein. Proc. Natl. Acad. Sci. U. S. A. *101*, 517–522.

Teixeira, J.M.C., Skinner, S.P., Arbesú, M., Breeze, A.L., and Pons, M. (2018). Farseer-NMR: automatic treatment, analysis and plotting of large, multi-variable NMR data. J. Biomol. NMR *71*, 1–9.

Tessari, M., Gentile, L.N., Taylor, S.J., Shalloway, D.I., Nicholson, L.K., and Vuister, G.W. (1997). Heteronuclear NMR studies of the combined Src homology domains 2 and 3 of pp60 c-Src: Effects of phosphopeptide binding. Biochemistry *36*, 14561–14571.

Testerink, C., and Munnik, T. (2005). Phosphatidic acid: A multifunctional stress signaling lipid in plants. Trends Plant Sci. *10*, 368–375.

Teyra, J., Huang, H., Jain, S., Guan, X., Dong, A., Liu, Y., Tempel, W., Min, J., Tong, Y., Kim, P.M., et al. (2017). Comprehensive Analysis of the Human SH3 Domain Family Reveals a Wide Variety of Non-canonical Specificities. Structure *25*, 1598-1610.e3.

Thomas, S., and Brugge, J. (1997). Cellular functions regulated by Src family kinases. Annu Rev Cell Dev Biol *13*, 513–609.

Thomas, J.E., Soriano, P., and Brugge, J.S. (1991). Phosphorylation of c-Src on tyrosine 527 by another protein tyrosine kinase. Science (80-.). *254*, 568–571.

Timr, Š., Pleskot, R., Kadlec, J., Kohagen, M., Magarkar, A., and Jungwirth, P. (2017). Membrane Binding of Recoverin: From Mechanistic Understanding to Biological Functionality. ACS Cent. Sci. *3*, 868–874.

Tournaviti, S., Hannemann, S., Terjung, S., Kitzing, T.M., Stegmayer, C., Ritzerfeld, J., Walther, P., Grosse, R., Nickel, W., and Fackler, O.T. (2007). SH4-domain-induced plasma membrane dynamization promotes bleb-associated cell motility. J. Cell Sci. *120*, 3820–3829.

Towler, D.A., and Gordon, J.I. (1988). The biology and enzymology of eukaryotic protein acylation. Annu. Rev. Biochem. *57*, 69–99.

Vogel, A., Katzka, C.P., Waldmann, H., Arnold, K., Brown, M.F., and Huster, D. (2005). Lipid modifications of a ras peptide exhibit altered packing and mobility versus host membrane as detected by2H solid-state NMR. J. Am. Chem. Soc. *127*, 12263–12272.

Walker, F., DeBlaquiere, J., and Burgess, A.W. (1993). Translocation of pp60(c-src) from the plasma membrane to the cytosol after stimulation by platelet-derived growth factor. J. Biol. Chem. *268*, 19552–19558.

Wang, H.Y., Tao, J., Shumay, E., and Malbon, C.C. (2006). G-protein-coupled receptor-associated A-kinase anchoring proteins: AKAP79 and AKAP250 (gravin). Eur. J. Cell Biol.

85, 643–650.

Wang, Q., Pechersky, Y., Sagawa, S., Pan, A.C., and Shaw, D.E. (2019). Structural mechanism for Bruton's tyrosine kinase activation at the cell membrane. Proc. Natl. Acad. Sci. U. S. A. *116*, 9390–9399.

Wright, M.H., Heal, W.P., Mann, D.J., and Tate, E.W. (2010). Protein myristoylation in health and disease. J. Chem. Biol. *3*, 19–35.

Wu, Z., Cui, Q., and Yethiraj, A. (2013). Why do arginine and lysine organize lipids differently? Insights from coarse-grained and atomistic simulations. J. Phys. Chem. B *117*, 12145–12156.

Xu, W., Harrison, S.C., and Eck, M.J. (1997). Three-dimensional structure of the tyrosine kinase c-Src. Nature *385*, 595–602.

Xu, W., Doshi, A., Lei, M., Eck, M.J., and Harrison, S.C. (1999). Crystal structures of c-Src reveal features of its autoinhibitory mechanism. Mol. Cell *3*, 629–638.

Yeagle, P.L. (2014). Non-covalent binding of membrane lipids to membrane proteins. Biochim. Biophys. Acta - Biomembr. *1838*, 1548–1559.

Yeatman, T.J. (2004). A renaissance for SRC. Nat. Rev. Cancer *4*, 470–480.

Young, M.A., Gonfloni, S., Superti-Furga, G., Roux, B., and Kuriyan, J. (2001). Dynamic coupling between the SH2 and SH3 domains of c-Src and Hck underlies their inactivation by C-Terminal tyrosine phosphorylation. Cell *105*, 115–126.

Yu, X.M., Askalan, R., Keil, G.J., and Salter, M.W. (1997). NMDA channel regulation by channel-associated protein tyrosine kinase Src. Science (80-.). *275*, 674–678.

Zhang, H., Constantine, R., Vorobiev, S., Chen, Y., Seetharaman, J., Huang, Y.J., Xiao, R., Montelione, G.T., Gerstner, C.D., Davis, M.W., et al. (2011). UNC119 is required for G protein trafficking in sensory neurons. Nat. Neurosci. *14*, 874–880.

Zhou, Y., Liang, H., Rodkey, T., Ariotti, N., Parton, R.G., and Hancock, J.F. (2014). Signal Integration by Lipid-Mediated Spatial Cross Talk between Ras Nanoclusters. Mol. Cell. Biol. *34*, 862–876.

Zhou, Y., Prakash, P., Liang, H., Cho, K.J., Gorfe, A.A., and Hancock, J.F. (2017). Lipid-Sorting Specificity Encoded in K-Ras Membrane Anchor Regulates Signal Output. Cell *168*, 239-251.e16.

Zrihan-Licht, S., Lim, J., Keydar, I., Sliwkowski, M.X., Groopman, J.E., and Avraham, H. (1997). Association of Csk-homologous kinase (CHK) (formerly MATK) with HER-2/ErbB-2 in breast cancer cells. J. Biol. Chem. *272*, 1856–1863.